International Tables for Crystallography (2006). Vol. B, Chapter 2.5, pp. 276–345.

2.5. Electron diffraction and electron microscopy in structure determination

BY J. M. COWLEY, P. GOODMAN, B. K. VAINSHTEIN, B. B. ZVYAGIN AND D. L. DORSET

2.5.1. Foreword (J. M. COWLEY)

Given that electrons have wave properties and the wavelengths lie in a suitable range, the diffraction of electrons by matter is completely analogous to the diffraction of X-rays. While for X-rays the scattering function is the electron-density distribution, for electrons it is the potential distribution which is similarly peaked at the atomic sites. Hence, in principle, electron diffraction may be used as the basis for crystal structure determination. In practice it is used much less widely than X-ray diffraction for the determination of crystal structures but is receiving increasing attention as a means for obtaining structural information not readily accessible with X-ray- or neutron-diffraction techniques.

Electrons having wavelengths comparable with those of the X-rays commonly used in diffraction experiments have energies of the order of 100 eV. For such electrons, the interactions with matter are so strong that they can penetrate only a few layers of atoms on the surfaces of solids. They are used extensively for the study of surface structures by low-energy electron diffraction (LEED) and associated techniques. These techniques are not covered in this series of volumes, which include the principles and practice of only those diffraction and imaging techniques making use of high-energy electrons, having energies in the range of 20 keV to 1 MeV or more, in transmission through thin specimens.

For the most commonly used energy ranges of high-energy electrons, 100 to 400 keV, the wavelengths are about 50 times smaller than for X-rays. Hence the scattering angles are much smaller, of the order of 10^{-2} rad, the recording geometry is relatively simple and the diffraction pattern represents, to a useful first approximation, a planar section of reciprocal space.

The elastic scattering of electrons by atoms is several orders of magnitude greater than for X-rays. This fact has profound consequences, which in some cases are highly favourable and in other cases are serious hindrances to structure analysis work. On the one hand it implies that electron-diffraction patterns can be obtained from very small single-crystal regions having thicknesses equal to only a few layers of atoms and, with recently developed techniques, having diameters equivalent to only a few interatomic distances. Hence single-crystal patterns can be obtained from microcrystalline phases.

However, the strong scattering of electrons implies that the simple kinematical single-scattering approximation, on which most X-ray diffraction structure analysis is based, fails for electrons except for very thin crystals composed of light-atom materials. Strong dynamical diffraction effects occur for crystals which may be 100 Å thick, or less for heavy-atom materials. As a consequence, the theory of dynamical diffraction for electrons has been well developed, particularly for the particular special diffracting conditions relevant to the transmission of fast electrons (see Chapter 5.2), and observations of dynamical diffraction effects are commonly made and quantitatively interpreted. The possibility has thus arisen of using the observation of dynamical diffraction effects as the basis for obtaining crystal structure information. The fact that dynamical diffraction is dependent on the relative phases of the diffracted waves then implies that relative phase information can be deduced from the diffraction intensities and the limitations of kinematical diffraction, such as Friedel's law, do not apply. The most immediately practicable method for making use of this possibility is convergent-beam electron diffraction (CBED) as described in Section 2.5.3.

A further important factor, determining the methods for observing electron diffraction, is that, being charged particles, electrons can be focused by electromagnetic lenses. The irreducible aberrations of cylindrical magnetic lenses have, to date, limited the resolution of electron microscopes to the extent that the least resolvable distances (or 'resolutions') are about 100 times the electron wavelength. However, with microscopes having a resolution of better than 2 Å it is possible to distinguish the individual rows of atoms, parallel to the incident electron beam, in the principal orientations of many crystalline phases. Thus 'structure images' can be obtained, sometimes showing direct representation of projections of crystal structures [see *IT* C (1999), Section 4.3.8]. However, the complications of dynamical scattering and of the coherent imaging processes are such that the image intensities vary strongly with crystal thickness and tilt, and with the defocus or other parameters of the imaging system, making the interpretation of images difficult except in special circumstances. Fortunately, computer programs are readily available whereby image intensities can be calculated for model structures [see *IT* C (1999), Section 4.3.6] Hence the means exist for deriving the projection of the structure if only by a process of trial and error and not, as would be desirable, from a direct interpretation of the observations.

The accuracy with which the projection of a structure can be deduced from an image, or series of images, improves as the resolution of the microscope improves but is not at all comparable with the accuracy attainable with X-ray diffraction methods. A particular virtue of high-resolution electron microscopy as a structural tool is that it may give information on individual small regions of the sample. Structures can be determined of 'phases' existing over distances of only a few unit cells and the defects and local disorders can be examined, one by one.

The observation of electron-diffraction patterns forms an essential part of the technique of structure imaging in high-resolution electron microscopy, because the diffraction patterns are used to align the crystals to appropriate axial orientations. More generally, for all electron microscopy of crystalline materials the image interpretation depends on knowledge of the diffraction conditions. Fortunately, the diffraction pattern and image of any specimen region can be obtained in rapid succession by a simple switching of lens currents. The ready comparison of the image and diffraction data has become an essential component of the electron microscopy of crystalline materials but has also been of fundamental importance for the development of electron-diffraction theory and techniques.

The individual specimen regions giving single-crystal electron-diffraction patterns are, with few exceptions, so small that they can be seen only by use of an electron microscope. Hence, historically, it was only after electron microscopes were commonly available that the direct correlations of diffraction intensities with crystal size and shape could be made, and a proper basis was available for the development of the adequate dynamical diffraction theory.

For the complete description of a diffraction pattern or image intensities obtained with electrons, it is necessary to include the effects of inelastic scattering as well as elastic scattering. In contrast to the X-ray diffraction case, the inelastic scattering does not produce just a broad and generally negligible background. The average energy loss for an inelastic scattering event is about 20 eV, which is small compared with the energy of about 100 keV for the incident electrons. The inelastically scattered electrons have a narrow angular distribution and are diffracted in much the same way as the incident or elastically scattered electrons in a crystal. They therefore produce a highly modulated contribution to the diffraction pattern, strongly peaked about the Bragg spot positions (see Chapter 4.3). Also, as a result of the inelastic scattering processes, including thermal diffuse scattering, an effective

absorption function must be added in the calculation of intensities for elastically scattered electrons.

The inelastic scattering processes in themselves give information about the specimen in that they provide a measure of the excitations of both the valence-shell and the inner-shell electrons of the solid. The inner-shell electron excitations are characteristic of the type of atom, so that microanalysis of small volumes of specimen material (a few hundreds or thousands of atoms) may be achieved by detecting either the energy losses of the transmitted electrons or the emission of the characteristic X-ray [see *IT* C (1999), Section 4.3.4].

An adverse effect of the inelastic scattering processes, however, is that the transfer of energy to the specimen material results in radiation damage; this is a serious limitation of the application of electron-scattering methods to radiation-sensitive materials such as organic, biological and many inorganic compounds. The amount of radiation damage increases rapidly as the amount of information per unit volume, derived from the elastic scattering, is increased, *i.e.* as the microscope resolution is improved or as the specimen volume irradiated during a diffraction experiment is decreased. At the current limits of microscopic resolution, radiation damage is a significant factor even for the radiation-resistant materials such as semiconductors and alloys.

In the historical development of electron-diffraction techniques the progress has depended to an important extent on the level of understanding of the dynamical diffraction processes and this understanding has followed, to a considerable degree, from the availability of electron microscopes. For the first 20 years of the development, with few exceptions, the lack of a precise knowledge of the specimen morphology meant that diffraction intensities were influenced to an unpredictable degree by dynamical scattering and the impression grew that electron-diffraction intensities could not meaningfully be interpreted.

It was the group in the Soviet Union, led initially by Dr Z. G. Pinsker and later by Dr B. K. Vainshtein and others, which showed that patterns from thin layers of a powder of microcrystals could be interpreted reliably by use of the kinematical approximation. The averaging over crystal orientation reduced the dynamical diffraction effects to the extent that practical structure analysis was feasible. The development of the techniques of using films of crystallites having strongly preferred orientations, to give patterns somewhat analogous to the X-ray rotation patterns, provided the basis for the collection of three-dimensional diffraction data on which many structure analyses have been based [see Section 2.5.4 and *IT* C (1999), Section 4.3.5].

In recent years improvements in the techniques of specimen preparation and in the knowledge of the conditions under which dynamical diffraction effects become significant have allowed progress to be made with the use of high-energy electron diffraction patterns from thin single crystals for crystal structure analysis. Particularly for crystals of light-atom materials, including biological and organic compounds, the methods of structure analysis developed for X-ray diffraction, including the direct methods (see Section 2.5.7), have been successfully applied in an increasing number of cases. Often it is possible to deduce some structural information from high-resolution electron-microscope images and this information may be combined with that from the diffraction intensities to assist the structure analysis process [see *IT* C (1999), Section 4.3.8.8].

The determination of crystal symmetry by use of CBED (Section 2.5.3) and the accurate determination of structure amplitudes by use of methods depending on the observation of dynamical diffraction effects [*IT* C (1999), Section 4.3.7] came later, after the information on morphologies of crystals, and the precision electron optics associated with electron microscopes, became available.

In spite of the problem of radiation damage, a great deal of progress has been made in the study of organic and biological materials by electron-scattering methods. In some respects these materials are very favourable because, with only light atoms present, the scattering from thin films can be treated using the kinematical approximation without serious error. Because of the problem of radiation damage, however, special techniques have been evolved to maximize the information on the required structural aspects with minimum irradiation of the specimen. Image-processing techniques have been evolved to take advantage of the redundancy of information from a periodic structure and the means have been devised for combining information from multiple images and diffraction data to reconstruct specimen structure in three dimensions. These techniques are outlined in Sections 2.5.5 and 2.5.6. They are based essentially on the application of the kinematical approximation and have been used very effectively within that limitation.

For most inorganic materials the complications of many-beam dynamical diffraction processes prevent the direct application of these techniques of image analysis, which depend on having a linear relationship between the image intensity and the value of the projected potential distribution of the sample. The smaller sensitivities to radiation damage can, to some extent, remove the need for the application of such methods by allowing direct visualization of structure with ultra-high-resolution images and the use of microdiffraction techniques.

2.5.2. Electron diffraction and electron microscopy

(J. M. COWLEY)

2.5.2.1. *Introduction*

The contributions of electron scattering to the study of the structures of crystalline solids are many and diverse. This section will deal only with the scattering of high-energy electrons (in the energy range of 10^4 to 10^6 eV) in transmission through thin samples of crystalline solids and the derivation of information on crystal structures from diffraction patterns and high-resolution images. The range of wavelengths considered is from about 0.122 Å (12.2 pm) for 10 kV electrons to 0.0087 Å (0.87 pm) for 1 MeV electrons. Given that the scattering amplitudes of atoms for electrons have much the same form and variation with $(\sin\theta)/\lambda$ as for X-rays, it is apparent that the angular range for strong scattering of electrons will be of the order of 10^{-2} rad. Only under special circumstances, usually involving multiple elastic and inelastic scattering from very thick specimens, are scattering angles of more than 10^{-1} rad of importance.

The strength of the interaction of electrons with matter is greater than that of X-rays by two or three orders of magnitude. The single-scattering, first Born approximation fails significantly for scattering from single heavy atoms. Diffracted beams from single crystals may attain intensities comparable with that of the incident beam for crystal thicknesses of 10^2 Å, rather than 10^4 Å or more. It follows that electrons may be used for the study of very thin samples, and that dynamical scattering effects, or the coherent interaction of multiply scattered electron waves, will modify the diffracted amplitudes in a significant way for all but very thin specimens containing only light atoms.

The experimental techniques for electron scattering are largely determined by the possibility of focusing electron beams by use of strong axial magnetic fields, which act as electron lenses having focal lengths as short as 1 mm or less. Electron microscopes employing such lenses have been produced with resolutions approaching 1 Å. With such instruments, images showing individual isolated atoms of moderately high atomic number may be obtained. The resolution available is sufficient to distinguish neighbouring rows of adjacent atoms in the projected structures of thin crystals viewed in favourable orientations. It is therefore

possible in many cases to obtain information on the structure of crystals and of crystal defects by direct inspection of electron micrographs.

The electromagnetic electron lenses may also be used to form electron beams of very small diameter and very high intensity. In particular, by the use of cold field-emission electron guns, it is possible to obtain a current of 10^{-10} A in an electron beam of diameter 10 Å or less with a beam divergence of less than 10^{-2} rad, *i.e.* a current density of 10^4 A cm^{-2} or more. The magnitudes of the electron scattering amplitudes then imply that detectable signals may be obtained in diffraction from assemblies of fewer than 10^2 atoms. On the other hand, electron beams may readily be collimated to better than 10^{-6} rad.

The cross sections for inelastic scattering processes are, in general, less than for the elastic scattering of electrons, but signals may be obtained by the observation of electron energy losses, or the production of secondary radiations, which allow the analysis of chemical compositions or electronic excited states for regions of the crystal 100 Å or less in diameter.

On the other hand, the transfer to the sample of large amounts of energy through inelastic scattering processes produces radiation damage which may severely limit the applicability of the imaging and diffraction techniques, especially for biological and organic materials, unless the information is gathered from large specimen volumes with low incident electron beam densities.

Structure analysis of crystals can be performed using electron diffraction in the same way as with X-ray or neutron diffraction. The mathematical expressions and the procedures are much the same. However, there are peculiarities of the electron-diffraction case which should be noted.

(1) Structure analysis based on electron diffraction is possible for thin specimens for which the conditions for kinematical scattering are approached, *e.g.* for thin mosaic single-crystal specimens, for thin polycrystalline films having a preferred orientation of very small crystallites or for very extensive, very thin single crystals of biological molecules such as membranes one or a few molecules thick.

(2) Dynamical diffraction effects are used explicitly in the determination of crystal symmetry (with no Friedel's law limitations) and for the measurement of structure amplitudes with high accuracy.

(3) For many radiation-resistant materials, the structures of crystals and of some molecules may be determined directly by imaging atom positions in projections of the crystal with a resolution of 2 Å or better. The information on atom positions is not dependent on the periodicity of the crystal and so it is equally possible to determine the structures of individual crystal defects in favourable cases.

(4) Techniques of microanalysis may be applied to the determination of the chemical composition of regions of diameter 100 Å or less using the same instrument as for diffraction, so that the chemical information may be correlated directly with morphological and structural information.

(5) Crystal-structure information may be derived from regions containing as few as 10^2 or 10^3 atoms, including very small crystals and single or multiple layers of atoms on surfaces.

2.5.2.2. *The interactions of electrons with matter*

(1) The *elastic* scattering of electrons results from the interaction of the charged electrons with the electrostatic potential distribution, $\varphi(\mathbf{r})$, of the atoms or crystals. An incident electron of kinetic energy eW gains energy $e\varphi(\mathbf{r})$ in the potential field. Alternatively it may be stated that an incident electron wave of wavelength $\lambda = h/mv$ is diffracted by a region of variable refractive index

$$n(\mathbf{r}) = k/K_0 = \{[W + \varphi(\mathbf{r})]/W\}^{1/2} \simeq 1 + \varphi(\mathbf{r})/2W.$$

(2) The most important *inelastic* scattering processes are:

(*a*) thermal diffuse scattering, with energy losses of the order of 2×10^{-2} eV, separable from the elastic scattering only with specially devised equipment; the angular distribution of thermal diffuse scattering shows variations with $(\sin\theta)/\lambda$ which are much the same as for the X-ray case in the kinematical limit;

(*b*) bulk plasmon excitation, or the excitation of collective energy states of the conduction electrons, giving energy losses of 3 to 30 eV and an angular range of scattering of 10^{-4} to 10^{-3} rad;

(*c*) surface plasmons, or the excitation of collective energy states of the conduction electrons at discontinuities of the structure, with energy losses less than those for bulk plasmons and a similar angular range of scattering;

(*d*) interband or intraband excitation of valence-shell electrons giving energy losses in the range of 1 to 10^2 eV and an angular range of scattering of 10^{-4} to 10^{-2} rad;

(*e*) inner-shell excitations, with energy losses of 10^2 eV or more and an angular range of scattering of 10^{-3} to 10^{-2} rad, depending on the energy losses involved.

(3) In the original treatment by Bethe (1928) of the elastic scattering of electrons by crystals, the Schrödinger equation is written for electrons in the periodic potential of the crystal; *i.e.*

$$\nabla^2\psi(\mathbf{r}) + K_0^2[1 + \varphi(\mathbf{r})/W]\psi(\mathbf{r}) = 0, \qquad (2.5.2.1)$$

where

$$\begin{aligned}\varphi(\mathbf{r}) &= \int V(\mathbf{u}) \exp\{-2\pi i\mathbf{u}\cdot\mathbf{r}\}\, \mathrm{d}\mathbf{u} \\ &= \sum_{\mathbf{h}} V_{\mathbf{h}} \exp\{-2\pi i\mathbf{h}\cdot\mathbf{r}\}, \qquad (2.5.2.2)\end{aligned}$$

$\mathbf{K}_0$ is the wavevector in zero potential (outside the crystal) (magnitude $2\pi/\lambda$) and W is the accelerating voltage. The solutions of the equation are Bloch waves of the form

$$\psi(\mathbf{r}) = \sum_{\mathbf{h}} C_{\mathbf{h}}(\mathbf{k}) \exp\{-i(\mathbf{k}_0 + 2\pi\mathbf{h})\cdot\mathbf{r}\}, \qquad (2.5.2.3)$$

where $\mathbf{k}_0$ is the incident wavevector in the crystal and $\mathbf{h}$ is a reciprocal-lattice vector. Substitution of (2.5.2.2) and (2.5.2.3) in (2.5.2.1) gives the dispersion equations

$$(\kappa^2 - k_{\mathbf{h}}^2)C_{\mathbf{h}} + \sum_{\mathbf{g}}{}' V_{\mathbf{h}-\mathbf{g}} C_{\mathbf{g}} = 0. \qquad (2.5.2.4)$$

Here κ is the magnitude of the wavevector in a medium of constant potential V_0 (the 'inner potential' of the crystal). The refractive index of the electron in the average crystal potential is then

$$n = \kappa/K = (1 + V_0/W)^{1/2} \simeq 1 + V_0/2W. \qquad (2.5.2.5)$$

Since V_0 is positive and of the order of 10 V and W is 10^4 to 10^6 V, $n - 1$ is positive and of the order of 10^{-4}.

Solution of equation (2.5.2.4) gives the Fourier coefficients $C_{\mathbf{h}}^{(i)}$ of the Bloch waves $\psi^{(i)}(\mathbf{r})$ and application of the boundary conditions gives the amplitudes of individual Bloch waves (see Chapter 5.2).

(4) The experimentally important case of transmission of high-energy electrons through thin specimens is treated on the assumption of a plane wave incident in a direction almost perpendicular to an infinitely extended plane-parallel lamellar crystal, making use of the *small-angle scattering approximation* in which the forward-scattered wave is represented in the paraboloidal approximation to the sphere. The incident-beam direction, assumed to be almost parallel to the z axis, is unique and the z component of $\mathbf{k}$ is factored out to give

$$\nabla^2\psi + 2k\sigma\varphi\psi = \pm i2k\frac{\partial\psi}{\partial z}, \tag{2.5.2.6}$$

where $k = 2\pi/\lambda$ and $\sigma = 2\pi me\lambda/h^2$. [See Lynch & Moodie (1972), Portier & Gratias (1981), Tournarie (1962), and Chapter 5.2.]

This equation is analogous to the time-dependent Schrödinger equation with z replacing t. Retention of the $\pm$ signs on the right-hand side is consistent with both ψ and ψ^* being solutions, corresponding to propagation in opposite directions with respect to the z axis. The double-valued solution is of importance in consideration of reciprocity relationships which provide the basis for the description of some dynamical diffraction symmetries. (See Section 2.5.3.)

(5) The integral form of the wave equation, commonly used for scattering problems, is written, for electron scattering, as

$$\psi(\mathbf{r}) = \psi^{(0)}(\mathbf{r}) + (\sigma/\lambda)\int \frac{\exp\{-i\mathbf{k}|\mathbf{r}-\mathbf{r}'|\}}{|\mathbf{r}-\mathbf{r}'|}\varphi(\mathbf{r}')\psi(\mathbf{r}')\,\mathrm{d}\mathbf{r}'. \tag{2.5.2.7}$$

The wavefunction $\psi(\mathbf{r})$ within the integral is approximated by using successive terms of a Born series

$$\psi(\mathbf{r}) = \psi^{(0)}(\mathbf{r}) + \psi^{(1)}(\mathbf{r}) + \psi^{(2)}(\mathbf{r}) + \ldots. \tag{2.5.2.8}$$

The first Born approximation is obtained by putting $\psi(\mathbf{r}) = \psi^{(0)}(\mathbf{r})$ in the integral and subsequent terms $\psi^{(n)}(\mathbf{r})$ are generated by putting $\psi^{(n-1)}(\mathbf{r})$ in the integral.

For an incident plane wave, $\psi^{(0)}(\mathbf{r}) = \exp\{-i\mathbf{k}_0\cdot\mathbf{r}\}$ and for a point of observation at a large distance $\mathbf{R} = \mathbf{r} - \mathbf{r}'$ from the scattering object ($|\mathbf{R}| \gg |\mathbf{r}'|$), the first Born approximation is generated as

$$\psi^{(1)}(\mathbf{r}) = \frac{i\sigma}{\lambda R}\exp\{-i\mathbf{k}\cdot\mathbf{R}\}\int \varphi(\mathbf{r}')\exp\{i\mathbf{q}\cdot\mathbf{r}'\}\,\mathrm{d}\mathbf{r}',$$

where $\mathbf{q} = \mathbf{k} - \mathbf{k}_0$ or, putting $\mathbf{u} = \mathbf{q}/2\pi$ and collecting the pre-integral terms into a parameter μ,

$$\Psi(\mathbf{u}) = \mu\int\varphi(\mathbf{r})\exp\{2\pi i\mathbf{u}\cdot\mathbf{r}\}\,\mathrm{d}\mathbf{r}. \tag{2.5.2.9}$$

This is the Fourier-transform expression which is the basis for the *kinematical scattering approximation*. It is derived on the basis that all $\psi^{(n)}(\mathbf{r})$ terms for $n \neq 0$ are very much smaller than $\psi^{(0)}(\mathbf{r})$ and so is a weak scattering approximation.

In this approximation, the scattered amplitude for an atom is related to the atomic structure amplitude, $f(\mathbf{u})$, by the relationship, derived from (2.5.2.8),

$$\psi(\mathbf{r}) = \exp\{-i\mathbf{k}_0\cdot\mathbf{r}\} + i\frac{\exp\{-i\mathbf{k}\cdot\mathbf{r}\}}{R\lambda}\sigma f(\mathbf{u}),$$
$$f(\mathbf{u}) = \int\varphi(\mathbf{r})\exp\{2\pi i\mathbf{u}\cdot\mathbf{r}\}\,\mathrm{d}\mathbf{r}. \tag{2.5.2.10}$$

For centrosymmetrical atom potential distributions, the $f(\mathbf{u})$ are real, positive and monotonically decreasing with $|\mathbf{u}|$. A measure of the extent of the validity of the first Born approximation is given by the fact that the effect of adding the higher-order terms of the Born series may be represented by replacing $f(\mathbf{u})$ in (2.5.2.10) by the complex quantities $f(\mathbf{u}) = |\mathbf{f}|\exp\{i\eta(\mathbf{u})\}$ and for single heavy atoms the phase factor η may vary from 0.2 for $|\mathbf{u}| = 0$ to 4 or 5 for large $|\mathbf{u}|$, as seen from the tables of *IT* C (1999, Section 4.3.3).

(6) Relativistic effects produce appreciable variations of the parameters used above for the range of electron energies considered. The relativistic values are

$$m = m_0(1 - v^2/c^2)^{-1/2} = m_0(1-\beta^2)^{-1/2}, \tag{2.5.2.11}$$
$$\lambda = h[2m_0|e|W(1 + |e|W/2m_0c^2)]^{-1/2} \tag{2.5.2.12}$$
$$= \lambda_c(1-\beta^2)^{1/2}/\beta, \tag{2.5.2.13}$$

where λ_c is the Compton wavelength, $\lambda_c = h/m_0c = 0.0242$ Å, and

$$\sigma = 2\pi me\lambda/h^2 = (2\pi m_0 e/h^2)(\lambda_c/\beta)$$
$$= 2\pi/\{\lambda W[1 + (1-\beta^2)^{1/2}]\}. \tag{2.5.2.14}$$

Values for these quantities are listed in *IT* C (1999, Section 4.3.2). The variations of λ and σ with accelerating voltage are illustrated in Fig. 2.5.2.1. For high voltages, σ tends to a constant value, $2\pi m_0 e\lambda_c/h^2 = e/\hbar c$.

2.5.2.3. *Recommended sign conventions*

There are two alternative sets of signs for the functions describing wave optics. Both sets have been widely used in the literature. There is, however, a requirement for internal consistency within a particular analysis, independently of which set is adopted. Unfortunately, this requirement has not always been met and, in fact, it is only too easy at the outset of an analysis to make errors in this way. This problem might have come into prominence somewhat earlier were it not for the fact that, for centrosymmetric crystals (or indeed for centrosymmetric projections in the case of planar diffraction), only the signs used in the transmission and propagation functions can affect the results. It is not until the origin is set away from a centre of symmetry that there is a need to be consistent in every sign used.

Signs for electron diffraction have been chosen from two points of view: (1) defining as positive the sign of the exponent in the structure-factor expression and (2) defining the forward propagating free-space wavefunction with a positive exponent.

The second of these alternatives is the one which has been adopted in most solid-state and quantum-mechanical texts.

The first, or *standard crystallographic* convention, is the one which could most easily be adopted by crystallographers accustomed to retaining a positive exponent in the structure-factor equation. This also represents a consistent *International Tables* usage. It is, however, realized that both conventions will continue to be used in crystallographic computations, and that there are by now a large number of operational programs in use.

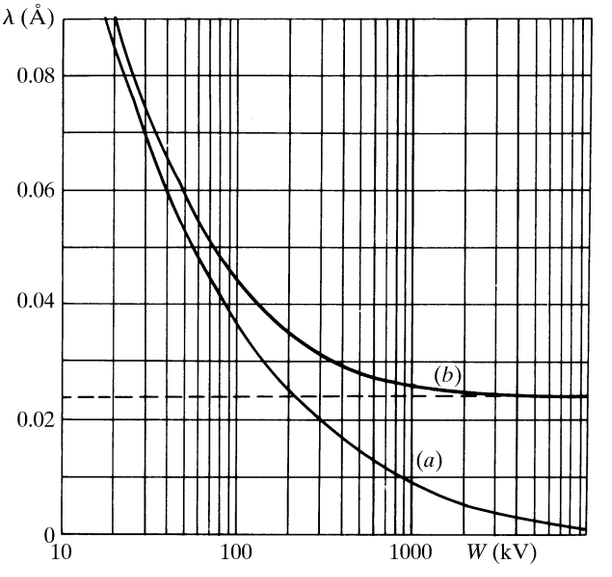

Fig. 2.5.2.1. The variation with accelerating voltage of electrons of (*a*) the wavelength, λ and (*b*) the quantity $\lambda[1 + (h^2/m_0^2c^2\lambda^2)] = \lambda_c/\beta$ which is proportional to the interaction constant σ [equation (2.5.2.14)]. The limit is the Compton wavelength λ_c (after Fujiwara, 1961).

Table 2.5.2.1. *Standard crystallographic and alternative crystallographic sign conventions for electron diffraction*

	Standard	Alternative
Free-space wave	$\exp[-i(\mathbf{k}\cdot\mathbf{r}-\omega t)]$	$\exp[+i(\mathbf{k}\cdot\mathbf{r}-\omega t)]$
Fourier transforming from real space to reciprocal space	$\int \psi(\mathbf{r})\exp[+2\pi i(\mathbf{u}\cdot\mathbf{r})]\,\mathrm{d}\mathbf{r}$	$\int \psi(\mathbf{r})\exp[-2\pi i(\mathbf{u}\cdot\mathbf{r})]\,\mathrm{d}\mathbf{r}$
Fourier transforming from reciprocal space to real space	$\psi(\mathbf{r}) = \int \Psi(\mathbf{u})\exp[-2\pi i(\mathbf{u}\cdot\mathbf{r})]\,\mathrm{d}\mathbf{u}$	$\int \Psi(\mathbf{u})\exp[+2\pi i(\mathbf{u}\cdot\mathbf{r})]\,\mathrm{d}\mathbf{u}$
Structure factors	$V(\mathbf{h}) = (1/\Omega)\sum_j f_j(\mathbf{h})\exp(+2\pi i\mathbf{h}\cdot\mathbf{r}_j)$	$(1/\Omega)\sum_j f_j(\mathbf{h})\exp(-2\pi i\mathbf{h}\cdot\mathbf{r}_j)$
Transmission function (real space)	$\exp[-i\sigma\varphi(x,y)\Delta z]$	$\exp[+i\sigma\varphi(x,y)\Delta z]$
Phenomenological absorption	$\sigma\varphi(\mathbf{r}) - i\mu(\mathbf{r})$	$\sigma\varphi(\mathbf{r}) + i\mu(\mathbf{r})$
Propagation function $P(h)$ (reciprocal space) within the crystal	$\exp(-2\pi i\zeta_{\mathbf{h}}\Delta z)$	$\exp(+2\pi i\zeta_{\mathbf{h}}\Delta z)$
Iteration (reciprocal space)	$\Psi_{n+1}(\mathbf{h}) = [\Psi_n(\mathbf{h})\cdot P(\mathbf{h})] * Q(\mathbf{h})$	
Unitarity test (for no absorption)	$T(\mathbf{h}) = Q(\mathbf{h}) * Q^*(-\mathbf{h}) = \delta(\mathbf{h})$	
Propagation to the image plane-wave aberration function, where $\chi(U) = \pi\lambda\Delta f U^2 + \frac{1}{2}\pi C_s\lambda^3 U^4$, $U^2 = u^2 + v^2$ and Δf is positive for overfocus	$\exp[i\chi(U)]$	$\exp[-i\chi(U)]$

σ = electron interaction constant $= 2\pi me\lambda/h^2$; m = (relativistic) electron mass; λ = electron wavelength; e = (magnitude of) electron charge; h = Planck's constant; $k = 2\pi/\lambda$; Ω = volume of the unit cell; $\mathbf{u}$ = continuous reciprocal-space vector, components u, v; $\mathbf{h}$ = discrete reciprocal-space coordinate; $\varphi(x,y)$ = crystal potential averaged along beam direction (positive); Δz = slice thickness; $\mu(\mathbf{r})$ = absorption potential [positive; typically $\leq 0.1\sigma\varphi(\mathbf{r})$]; Δf = defocus (defined as negative for underfocus); C_s = spherical aberration coefficient; $\zeta_{\mathbf{h}}$ = excitation error relative to the incident-beam direction and defined as negative when the point h lies outside the Ewald sphere; $f_j(\mathbf{h})$ = atomic scattering factor for electrons, f_e, related to the atomic scattering factor for X-rays, f_X, by the Mott formula $f_e = (e/\pi U^2)(Z - f_X)$. $Q(\mathbf{h})$ = Fourier transform of periodic slice transmission function.

It is therefore recommended (*a*) that a particular sign usage be indicated as either *standard crystallographic* or *alternative crystallographic* to accord with Table 2.5.2.1, whenever there is a need for this to be explicit in publication, and (*b*) that either one or other of these systems be adhered to throughout an analysis in a self-consistent way, even in those cases where, as indicated above, some of the signs appear to have no effect on one particular conclusion.

2.5.2.4. *Scattering of electrons by crystals; approximations*

The forward-scattering approximation to the many-beam dynamical diffraction theory outlined in Chapter 5.2 provides the basis for the calculation of diffraction intensities and electron-microscope image contrast for thin crystals. [See Cowley (1995), Chapter 5.2 and *IT* C (1999) Sections 4.3.6 and 4.3.8.] On the other hand, there are various approximations which provide relatively simple analytical expressions, are useful for the determination of diffraction geometry, and allow estimates to be made of the relative intensities in diffraction patterns and electron micrographs in favourable cases.

(*a*) *The kinematical approximation*, derived in Section 2.5.2.2 from the first Born approximation, is analagous to the corresponding approximation of X-ray diffraction. It assumes that the scattering amplitudes are directly proportional to the three-dimensional Fourier transform of the potential distribution, $\varphi(\mathbf{r})$.

$$V(\mathbf{u}) = \int \varphi(\mathbf{r})\exp\{2\pi i\mathbf{u}\cdot\mathbf{r}\}\,\mathrm{d}\mathbf{r}, \qquad (2.5.2.15)$$

so that the potential distribution $\varphi(\mathbf{r})$ takes the place of the charge-density distribution, $\rho(\mathbf{r})$, relevant for X-ray scattering.

The validity of the kinematical approximation as a basis for structure analysis is severely limited. For light-atom materials, such as organic compounds, it has been shown by Jap & Glaeser (1980) that the thickness for which the approximation gives reasonable accuracy for zone-axis patterns from single crystals is of the order of 100 Å for 100 keV electrons and increases, approximately as σ^{-1}, for higher energies. The thickness limits quoted for polycrystalline samples, having crystallite dimensions smaller than the sample thickness, are usually greater (Vainshtein, 1956). For heavy-atom materials the approximation is more limited since it may fail significantly for single heavy atoms.

(*b*) *The phase-object approximation* (POA), or high-voltage limit, is derived from the general many-beam dynamical diffraction expression, equation (5.2.13.1), Chapter 5.2, by assuming the Ewald sphere curvature to approach zero. Then the scattering by a thin sample can be expressed by multiplying the incoming wave amplitude by the transmission function

$$q(xy) = \exp\{-i\sigma\varphi(xy)\}, \qquad (2.5.2.16)$$

where $\varphi(xy) = \int \varphi(\mathbf{r})\,\mathrm{d}z$ is the projection of the potential distribution of the sample in the z direction, the direction of the incident beam. The diffraction-pattern amplitudes are then given by two-dimensional Fourier transform of (2.5.2.16).

This approximation is of particular value in relation to the electron microscopy of thin crystals. The thickness for its validity for 100 keV electrons is within the range 10 to 50 Å, depending on the accuracy and spatial resolution involved, and increases with accelerating voltage approximately as $\lambda^{-1/2}$. In computational work, it provides the starting point for the multi-slice method of dynamical diffraction calculations (*IT* C, 1999, Section 4.3.6.1).

(*c*) *The two-beam approximation* for dynamical diffraction of electrons assumes that only two beams, the incident beam and one diffracted beam (or two Bloch waves, each with two component amplitudes), exist in the crystal. This approximation has been adapted, notably by Hirsch *et al*. (1965), for use in the electron microscopy of inorganic materials.

It forms a convenient basis for the study of defects in crystals having small unit cells (metals, semiconductors *etc.*) and provides good preliminary estimates for the determination of crystal thicknesses and structure amplitudes for orientations well removed from principal axes, and for electron energies up to 200–500 keV, but it has decreasing validity, even for favourable cases, for higher energies. It has been used in the past as an 'extinction correction' for powder-pattern intensities (Vainshtein, 1956).

(*d*) *The Bethe second approximation*, proposed by Bethe (1928) as a means for correcting the two-beam approximation for the

effects of weakly excited beams, replaces the Fourier coefficients of potential by the 'Bethe potentials'

$$U_{\mathbf{h}} = V_{\mathbf{h}} - 2k_0\sigma \sum_{\mathbf{g}} \frac{V_{\mathbf{g}} \cdot V_{\mathbf{h}-\mathbf{g}}}{\kappa^2 - k_{\mathbf{g}}^2}. \qquad (2.5.2.17)$$

Use of these potentials has been shown to account well for the deviations of powder-pattern intensities from the predictions of two-beam theory (Horstmann & Meyer, 1965) and to predict accurately the extinctions of Kikuchi lines at particular accelerating voltages due to relativistic effects (Watanabe *et al*., 1968), but they give incorrect results for the small-thickness limit.

2.5.2.5. *Kinematical diffraction formulae*

(1) *Comparison with X-ray diffraction.* The relations of real-space and reciprocal-space functions are analogous to those for X-ray diffraction [see equations (2.5.2.2), (2.5.2.10) and (2.5.2.15)]. For diffraction by crystals

$$\varphi(\mathbf{r}) = \sum_{\mathbf{h}} V_{\mathbf{h}} \exp\{-2\pi i \mathbf{h}\cdot\mathbf{r}\},$$

$$V_{\mathbf{h}} = \int \varphi(\mathbf{r}) \exp\{2\varphi i \mathbf{h}\cdot\mathbf{r}\}\, \mathrm{d}\mathbf{r} \qquad (2.5.2.18)$$

$$= \frac{1}{\Omega}\sum_i f_i(\mathbf{h}) \exp\{2\pi i \mathbf{h}\cdot\mathbf{r}_i\}, \qquad (2.5.2.19)$$

where the integral of (2.5.2.18) and the summation of (2.5.2.19) are taken over one unit cell of volume (see Dawson *et al*., 1974).

Important differences from the X-ray case arise because

(*a*) the wavelength is relatively small so that the Ewald-sphere curvature is small in the reciprocal-space region of appreciable scattering amplitude;

(*b*) the dimensions of the single-crystal regions giving appreciable scattering amplitudes are small so that the 'shape transform' regions of scattering power around the reciprocal-lattice points are relatively large;

(*c*) the spread of wavelengths is small (10^{-5} or less, with no white-radiation background) and the degree of collimation is better (10^{-4} to 10^{-6}) than for conventional X-ray sources.

As a consequence of these factors, single-crystal diffraction patterns may show many simultaneous reflections, representing almost-planar sections of reciprocal space, and may show fine structure or intensity variations reflecting the crystal dimensions and shape.

(2) Kinematical diffraction-pattern intensities are calculated in a manner analogous to that for X-rays except that

(*a*) no polarization factor is included because of the small-angle scattering conditions;

(*b*) integration over regions of scattering power around reciprocal-lattice points cannot be assumed unless appropriate experimental conditions are ensured.

For a thin, flat, lamellar crystal of thickness H, the observed intensity is

$$I_{\mathbf{h}}/I_{\mathbf{0}} = |\sigma(V_{\mathbf{h}}/\Omega)(\sin\pi\zeta_{\mathbf{h}}H)/(\pi\zeta_{\mathbf{h}})|^2, \qquad (2.5.2.20)$$

where $\zeta_{\mathbf{h}}$ is the excitation error for the $\mathbf{h}$ reflection and Ω is the unit-cell volume.

For a single-crystal diffraction pattern obtained by rotating a crystal or from a uniformly bent crystal or for a mosaic crystal with a uniform distribution of orientations, the intensity is

$$I_{\mathbf{h}} = I_{\mathbf{0}} \frac{\sigma^2 |V_{\mathbf{h}}|^2 V_c d_{\mathbf{h}}}{4\pi^2\Omega^2}, \qquad (2.5.2.21)$$

where V_c is the crystal volume and $d_{\mathbf{h}}$ is the lattice-plane spacing.

For a polycrystalline sample of randomly oriented small crystals, the intensity per unit length of the diffraction ring is

$$I_{\mathbf{h}} = I_{\mathbf{0}} \frac{\sigma^2 |V_{\mathbf{h}}|^2 V_c d_{\mathbf{h}}^2 M_{\mathbf{h}}}{8\pi^2\Omega^2 L\lambda}, \qquad (2.5.2.22)$$

where $M_{\mathbf{h}}$ is the multiplicity factor for the $\mathbf{h}$ reflection and L is the camera length, or the distance from the specimen to the detector plane. The special cases of 'oblique texture' patterns from powder patterns having preferred orientations are treated in *IT* C (1999, Section 4.3.5).

(3) *Two-beam dynamical diffraction formulae: complex potentials including absorption.* In the two-beam dynamical diffraction approximation, the intensities of the directly transmitted and diffracted beams for transmission through a crystal of thickness H, in the absence of absorption, are

$$I_{\mathbf{0}} = (1+w^2)^{-1}\left[w^2 + \cos^2\left\{\frac{\pi H(1+w^2)^{1/2}}{\xi_{\mathbf{h}}}\right\}\right] \qquad (2.5.2.23)$$

$$I_{\mathbf{h}} = (1+w^2)^{-1}\sin^2\left\{\frac{\pi H(1+w^2)^{1/2}}{\xi_{\mathbf{h}}}\right\}, \qquad (2.5.2.24)$$

where $\xi_{\mathbf{h}}$ is the extinction distance, $\xi_{\mathbf{h}} = (2\sigma|V_{\mathbf{h}}|)^{-1}$, and

$$w = \xi_{\mathbf{h}}\zeta_{\mathbf{h}} = \Delta\theta/(2\sigma|V_{\mathbf{h}}|d_{\mathbf{h}}), \qquad (2.5.2.25)$$

where $\Delta\theta$ is the deviation from the Bragg angle.

For the case that $\zeta_{\mathbf{h}} = 0$, with the incident beam at the Bragg angle, this reduces to the simple *Pendellösung* expression

$$I_{\mathbf{h}} = 1 - I_{\mathbf{0}} = \sin^2\{2\pi\sigma|V_{\mathbf{h}}|H\}. \qquad (2.5.2.26)$$

The effects on the elastic Bragg scattering amplitudes of the inelastic or diffuse scattering may be introduced by adding an out-of-phase component to the structure amplitudes, so that for a centrosymmetric crystal, $V_{\mathbf{h}}$ becomes complex by addition of an imaginary component. Alternatively, an absorption function $\mu(\mathbf{r})$, having Fourier coefficients $\mu_{\mathbf{h}}$, may be postulated so that $\sigma V_{\mathbf{h}}$ is replaced by $\sigma V_{\mathbf{h}} + i\mu_{\mathbf{h}}$. The $\mu_{\mathbf{h}}$ are known as phenomenological absorption coefficients and their validity in many-beam diffraction has been demonstrated by, for example, Rez (1978).

The magnitudes $\mu_{\mathbf{h}}$ depend on the nature of the experiment and the extent to which the various inelastically or diffusely scattered electrons are included in the measurements being made. If measurements are made of purely elastic scattering intensities for Bragg reflections or of image intensity variations due to the interaction of the sharp Bragg reflections only, the main contributions to the absorption coefficients are as follows (Radi, 1970):

(*a*) from plasmon and single-electron excitations, μ_0 is of the order of 0.1 $V_{\mathbf{0}}$ and $\mu_{\mathbf{h}}$, for $\mathbf{h} \neq 0$, is negligibly small;

(*b*) from thermal diffuse scattering; $\mu_{\mathbf{h}}$ is of the order of 0.1 $V_{\mathbf{h}}$ and decreasing more slowly than $V_{\mathbf{h}}$ with scattering angle.

Including absorption effects in (2.5.2.26) for the case $\zeta_{\mathbf{h}} = 0$ gives

$$\begin{aligned} I_{\mathbf{0}} &= \tfrac{1}{2}\exp\{-\mu_0 H\}[\cosh\mu_{\mathbf{h}}H + \cos(2\pi\sigma V_{\mathbf{h}}H)], \\ I_{\mathbf{h}} &= \tfrac{1}{2}\exp\{-\mu_0 H\}[\cosh\mu_{\mathbf{h}}H - \cos(2\pi\sigma V_{\mathbf{h}}H)]. \end{aligned} \qquad (2.5.2.27)$$

The Borrmann effect is not very pronounced for electrons because $\mu_{\mathbf{h}} \ll \mu_{\mathbf{0}}$, but can be important for the imaging of defects in thick crystals (Hirsch *et al.*, 1965; Hashimoto *et al.*, 1961).

Attempts to obtain analytical solutions for the dynamical diffraction equations for more than two beams have met with few successes. There are some situations of high symmetry, with incident beams in exact zone-axis orientations, for which the many-beam solution can closely approach equivalent two- or three-beam

behaviour (Fukuhara, 1966). Explicit solutions for the three-beam case, which displays some aspects of many-beam character, have been obtained (Gjønnes & Høier, 1971; Hurley & Moodie, 1980).

2.5.2.6. *Imaging with electrons*

Electron optics. Electrons may be focused by use of axially symmetric magnetic fields produced by electromagnetic lenses. The focal length of such a lens used as a projector lens (focal points outside the lens field) is given by

$$f_p^{-1} = \frac{e}{8mW_r} \int_{-\infty}^{\infty} H_z^2(z)\, \mathrm{d}z, \qquad (2.5.2.28)$$

where W_r is the relativistically corrected accelerating voltage and H_z is the z component of the magnetic field. An expression in terms of experimental constants was given by Liebman (1955) as

$$\frac{1}{f} = \frac{A_0(NI)^2}{W_r(S+D)}, \qquad (2.5.2.29)$$

where A_0 is a constant, NI is the number of ampere turns of the lens winding, S is the length of the gap between the magnet pole pieces and D is the bore of the pole pieces.

Lenses of this type have irreducible aberrations, the most important of which for the paraxial conditions of electron microscopy is the third-order spherical aberration, coefficient C_s, giving a variation of focal length of $C_s\alpha^2$ for a beam at an angle α to the axis. Chromatic aberration, coefficient C_c, gives a spread of focal lengths

$$\Delta f = C_c\left(\frac{\Delta W_0}{W_0} + 2\frac{\Delta I}{I}\right) \qquad (2.5.2.30)$$

for variations ΔW_0 and ΔI of the accelerating voltage and lens currents, respectively.

The objective lens of an electron microscope is the critical lens for the determination of image resolution and contrast. The action of this lens in a conventional transmission electron microscope (TEM) is described by use of the Abbe theory for coherent incident illumination transmitted through the object to produce a wavefunction $\psi_0(xy)$ (see Fig. 2.5.2.2).

The amplitude distribution in the back focal plane of the objective lens is written

$$\Psi_0(u,v)\cdot T(u,v), \qquad (2.5.2.31)$$

where $\Psi_0(u,v)$ is the Fourier transform of $\psi_0(x,y)$ and $T(u,v)$ is the transfer function of the lens, consisting of an aperture function

$$A(u,v) = \begin{cases} 1 & \text{for } (u^2+v^2)^{1/2} \le A \\ 0 & \text{elsewhere} \end{cases} \qquad (2.5.2.32)$$

and a phase function $\exp\{i\chi(u,v)\}$ where the phase perturbation $\chi(uv)$ due to lens defocus Δf and aberrations is usually approximated as

$$\chi(uv) = \pi\cdot\Delta f\cdot\lambda(u^2+v^2) + \frac{\pi}{2}C_s\lambda^3(u^2+v^2)^2, \qquad (2.5.2.33)$$

and u, v are the reciprocal-space variables related to the scattering angles φ_x, φ_y by

$$u = (\sin\varphi_x)/\lambda,$$
$$v = (\sin\varphi_y)/\lambda.$$

The image amplitude distribution, referred to the object coordinates, is given by Fourier transform of (2.5.2.31) as

$$\psi(xy) = \psi_0(xy) * t(xy), \qquad (2.5.2.34)$$

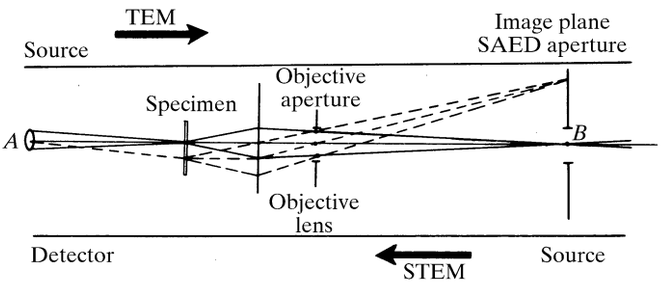

Fig. 2.5.2.2. Diagram representing the critical components of a conventional transmission electron microscope (TEM) and a scanning transmission electron microscope (STEM). For the TEM, electrons from a source A illuminate the specimen and the objective lens forms an image of the transmitted electrons on the image plane, B. For the STEM, a source at B is imaged by the objective lens to form a small probe on the specimen and some part of the transmitted beam is collected by a detector at A.

where $t(xy)$, given by Fourier transform of $T(u,v)$, is the spread function. The image intensity is then

$$I(xy) = |\psi(xy)|^2 = |\psi_0(xy) * t(xy)|^2. \qquad (2.5.2.35)$$

In practice the coherent imaging theory provides a good approximation but limitations of the coherence of the illumination have appreciable effects under high-resolution imaging conditions.

The variation of focal lengths according to (2.5.2.30) is described by a function $G(\Delta f)$. Illumination from a finite incoherent source gives a distribution of incident-beam angles $H(u_1,v_1)$. Then the image intensity is found by integrating incoherently over Δf and u_1, v_1:

$$I(xy) = \int\int G(\Delta f)\cdot H(u_1v_1) \times |\mathscr{F}\{\Psi_0(u-u_1, v-v_1)\cdot T_{\Delta f}(u,v)\}|^2\, \mathrm{d}(\Delta f)\cdot\, \mathrm{d}u_1\, \mathrm{d}v_1, \qquad (2.5.2.36)$$

where $\mathscr{F}$ denotes the Fourier-transform operation.

In the scanning transmission electron microscope (STEM), the objective lens focuses a small bright source of electrons on the object and directly transmitted or scattered electrons are detected to form an image as the incident beam is scanned over the object (see Fig. 2.5.2.2). Ideally the image amplitude can be related to that of the conventional transmission electron microscope by use of the 'reciprocity relationship' which refers to point sources and detectors for scalar radiation in scalar fields with elastic scattering processes only. It may be stated: 'The amplitude at a point B due to a point source at A is identical to that which would be produced at A for the identical source placed at B'.

For an axial point source, the amplitude distribution produced by the objective lens on the specimen is

$$\mathscr{F}[T(u,v)] = t(xy). \qquad (2.5.2.37)$$

If this is translated by the scan to X, Y, the transmitted wave is

$$\psi_0(xy) = q(xy)\cdot t(x-X, y-Y). \qquad (2.5.2.38)$$

The amplitude on the plane of observation following the specimen is then

$$\Psi(uv) = Q(u,v) * \{T(uv)\exp[2\pi i(uX+vY)]\}, \qquad (2.5.2.39)$$

and the image signal produced by a detector having a sensitivity function $H(u, v)$ is

$$I(X,Y) = \int H(u,v)|Q(u,v) * T(u,v) \times \exp\{2\pi i(uX + vY)\}|^2 \, du \, dv. \tag{2.5.2.40}$$

If $H(u, v)$ represents a small detector, approximated by a delta function, this becomes

$$I(x,y) = |q(xy) * t(xy)|^2, \tag{2.5.2.41}$$

which is identical to the result (2.5.2.35) for a plane incident wave in the conventional transmission electron microscope.

2.5.2.7. *Imaging of very thin and weakly scattering objects*

(*a*) *The weak-phase-object approximation.* For sufficiently thin objects, the effect of the object on the incident-beam amplitude may be represented by the transmission function (2.5.2.16) given by the phase-object approximation. If the fluctuations, $\varphi(xy) - \bar{\varphi}$, about the mean value of the projected potential are sufficiently small so that $\sigma[\varphi(xy) - \bar{\varphi}] \ll 1$, it is possible to use the *weak-phase-object approximation* (WPOA)

$$q(xy) = \exp\{-i\sigma\varphi(xy)\} = 1 - i\sigma\varphi(xy), \tag{2.5.2.42}$$

where $\varphi(xy)$ is referred to the average value, $\bar{\varphi}$. The assumption that only first-order terms in $\sigma\varphi(xy)$ need be considered is the equivalent of a single-scattering, or kinematical, approximation applied to the two-dimensional function, the projected potential of (2.5.2.16). From (2.5.2.42), the image intensity (2.5.2.35) becomes

$$I(xy) = 1 + 2\sigma\varphi(xy) * s(xy), \tag{2.5.2.43}$$

where the spread function $s(xy)$ is the Fourier transform of the imaginary part of $T(uv)$, namely $A(uv)\sin\chi(uv)$.

The optimum imaging condition is then found, following Scherzer (1949), by specifying that the defocus should be such that $|\sin\chi|$ is close to unity for as large a range of $U = (u^2 + v^2)^{1/2}$ as possible. This is so for a negative defocus such that $\chi(uv)$ decreases to a minimum of about $-2\pi/3$ before increasing to zero and higher as a result of the fourth-order term of (2.5.2.33) (see Fig. 2.5.2.3). This optimum, 'Scherzer defocus' value is given by

$$\frac{d\chi}{du} = 0 \quad \text{for} \quad \chi = -2\pi/3$$

or

$$\Delta f = -\left(\tfrac{4}{3}C_s\lambda\right)^{1/2}. \tag{2.5.2.44}$$

The resolution limit is then taken as corresponding to the value of $U = 1.51C_s^{-1/4}\lambda^{-3/4}$ when $\sin\chi$ becomes zero, before it begins to oscillate rapidly with U. The resolution limit is then

$$\Delta x = 0.66C_s^{1/4}\lambda^{3/4}. \tag{2.5.2.45}$$

For example, for $C_s = 1$ mm and $\lambda = 2.51 \times 10^{-2}$ Å (200 keV), $\Delta x = 2.34$ Å.

Within the limits of the WPOA, the image intensity can be written simply for a number of other imaging modes in terms of the Fourier transforms $c(\mathbf{r})$ and $s(\mathbf{r})$ of the real and imaginary parts of the objective-lens transfer function $T(\mathbf{u}) = A(\mathbf{u})\exp\{i\chi(\mathbf{u})\}$, where $\mathbf{r}$ and $\mathbf{u}$ are two-dimensional vectors in real and reciprocal space, respectively.

For dark-field TEM images, obtained by introducing a central stop to block out the central beam in the diffraction pattern in the back-focal plane of the objective lens,

$$I(\mathbf{r}) = [\sigma\varphi(\mathbf{r}) * c(\mathbf{r})]^2 + [\sigma\varphi(\mathbf{r}) * s(\mathbf{r})]^2. \tag{2.5.2.46}$$

Here, as in (2.5.2.42), $\varphi(\mathbf{r})$ should be taken to imply the difference from the mean potential value, $\varphi(\mathbf{r}) - \bar{\varphi}$.

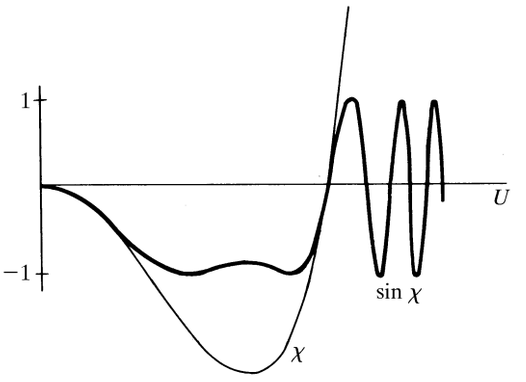

Fig. 2.5.2.3. The functions $\chi(U)$, the phase factor for the transfer function of a lens given by equation (2.5.2.33), and $\sin\chi(U)$ for the Scherzer optimum defocus condition, relevant for weak phase objects, for which the minimum value of $\chi(U)$ is $-2\pi/3$.

For bright-field STEM imaging with a very small detector placed axially in the central beam of the diffraction pattern (2.5.2.39) on the detector plane, the intensity, from (2.5.2.41), is given by (2.5.2.43).

For a finite axially symmetric detector, described by $D(\mathbf{u})$, the image intensity is

$$I(\mathbf{r}) = 1 + 2\sigma\varphi(\mathbf{r}) * \{s(\mathbf{r})[d(\mathbf{r}) * c(\mathbf{r})] - c(\mathbf{r})[d(\mathbf{r}) * s(\mathbf{r})]\}, \tag{2.5.2.47}$$

where $d(\mathbf{r})$ is the Fourier transform of $D(\mathbf{u})$ (Cowley & Au, 1978).

For STEM with an annular dark-field detector which collects all electrons scattered outside the central spot of the diffraction pattern in the detector plane, it can be shown that, to a good approximation (valid except near the resolution limit)

$$I(\mathbf{r}) = \sigma^2\varphi^2(\mathbf{r}) * [c^2(\mathbf{r}) + s^2(\mathbf{r})]. \tag{2.5.2.48}$$

Since $c^2(\mathbf{r}) + s^2(\mathbf{r}) = |t(\mathbf{r})|^2$ is the intensity distribution of the electron probe incident on the specimen, (2.5.2.48) is equivalent to the incoherent imaging of the function $\sigma^2\varphi^2(\mathbf{r})$.

Within the range of validity of the WPOA or, in general, whenever the zero beam of the diffraction pattern is very much stronger than any diffracted beam, the general expression (2.5.2.36) for the modifications of image intensities due to limited coherence may be conveniently approximated. The effect of integrating over the variables $\Delta f, u_1, v_1$, may be represented by multiplying the transfer function $T(u, v)$ by so-called 'envelope functions' which involve the Fourier transforms of the functions $G(\Delta f)$ and $H(u_1, v_1)$.

For example, if $G(\Delta f)$ is approximated by a Gaussian of width ε (at e^{-1} of the maximum) centred at Δf_0 and $H(u_1v_1)$ is a circular aperture function

$$H(u_1v_1) = \begin{cases} 1 & \text{if } u_1, v_1 < b \\ 0 & \text{otherwise,} \end{cases}$$

the transfer function $T_0(uv)$ for coherent radiation is multiplied by

$$\exp\{-\pi^2\lambda^2\varepsilon^2(u^2 + v^2)^2/4\} \cdot J_1(\pi B\eta)/(\pi B\eta)$$

where

$$\eta = f_0\lambda(u + v) + C_s\lambda^3(u^3 + v^3) + \pi i\varepsilon^2\lambda^2(u^3 + u^2v + uv^2 + v^3)/2. \tag{2.5.2.49}$$

(*b*) *The projected charge-density approximation.* For very thin specimens composed of moderately heavy atoms, the WPOA is

inadequate. Within the region of validity of the phase-object approximation (POA), more complicated relations analagous to (2.5.2.43) to (2.5.2.47) may be written. A simpler expression may be obtained by use of the two-dimensional form of Poisson's equation, relating the projected potential distribution $\varphi(xy)$ to the projected charge-density distribution $\rho(xy)$. This is the PCDA (projected charge-density approximation) (Cowley & Moodie, 1960),

$$I(xy) = 1 + 2\Delta f \cdot \lambda\sigma\rho(xy). \qquad (2.5.2.50)$$

This is valid for sufficiently small values of the defocus Δf, provided that the effects of the spherical aberration may be neglected, *i.e.* for image resolutions not too close to the Scherzer resolution limit (Lynch *et al.*, 1975). The function $\rho(xy)$ includes contributions from both the positive atomic nuclei and the negative electron clouds. For underfocus (Δf negative), single atoms give dark spots in the image. The contrast reverses with defocus.

2.5.2.8. *Crystal structure imaging*

(*a*) *Introduction.* It follows from (2.5.2.43) and (2.5.2.42) that, within the severe limitations of validity of the WPOA or the PCDA, images of very thin crystals, viewed with the incident beam parallel to a principal axis, will show dark spots at the positions of rows of atoms parallel to the incident beam. Provided that the resolution limit is less than the projected distances between atom rows (1–3 Å), the projection of the crystal structure may be seen directly.

In practice, theoretical and experimental results suggest that images may give a direct, although non-linear, representation of the projected potential or charge-density distribution for thicknesses much greater than the thicknesses for validity of these approximations, *e.g.* for thicknesses which may be 50 to 100 Å for 100 keV electrons for 3 Å resolutions and which increase for comparable resolutions at higher voltage but decrease with improved resolutions.

The use of high-resolution imaging as a means for determining the structures of crystals and for investigating the form of the defects in crystals in terms of the arrangement of the atoms has become a widely used and important branch of crystallography with applications in many areas of solid-state science. It must be emphasized, however, that image intensities are strongly dependent on the crystal thickness and orientation and also on the instrumental parameters (defocus, aberrations, alignment *etc.*). It is only when all of these parameters are correctly adjusted to lie within strictly defined limits that interpretation of images in terms of atom positions can be attempted [see *IT* C (1999, Section 4.3.8)].

Reliable interpretations of high-resolution images of crystals ('crystal structure images') may be made, under even the most favourable circumstances, only by the comparison of observed image intensities with intensities calculated by use of an adequate approximation to many-beam dynamical diffraction theory [see *IT* C (1999, Section 4.3.6)]. Most calculations for moderate or large unit cells are currently made by the multi-slice method based on formulation of the dynamical diffraction theory due to Cowley & Moodie (1957). For smaller unit cells, the matrix method based on the Bethe (1928) formulation is also frequently used (Hirsch *et al.*, 1965).

(*b*) *Fourier images.* For periodic objects in general, and crystals in particular, the amplitudes of the diffracted waves in the back focal plane are given from (2.5.2.31) by

$$\Psi_0(\mathbf{h}) \cdot T(\mathbf{h}). \qquad (2.5.2.51)$$

For rectangular unit cells of the projected unit cell, the vector $\mathbf{h}$ has components h/a and k/b. Then the set of amplitudes (2.5.2.34), and hence the image intensities, will be identical for two different sets of defocus and spherical aberration values $\Delta f_1, C_{s1}$ and $\Delta f_2, C_{s2}$ if, for an integer N,

$$\chi_1(h) = \chi_2(h) = 2N\pi;$$

i.e.

$$\pi\lambda\left(\frac{h^2}{a^2}+\frac{k^2}{b^2}\right)(\Delta f_1 - \Delta f_2) + \frac{1}{2}\pi\lambda^3\left(\frac{h^2}{a^2}+\frac{k^2}{b^2}\right)^2 (C_{s1} - C_{s2}) = 2\pi N.$$

This relationship is satisfied for all h, k if a^2/b^2 is an integer and

$$\Delta f_1 - \Delta f_2 = 2na^2/\lambda$$

and

$$C_{s1} - C_{s2} = 4ma^4/\lambda^3, \qquad (2.5.2.52)$$

where m, n are integers (Kuwabara, 1978). The relationship for Δf is an expression of the Fourier image phenomenon, namely that for a plane-wave incidence, the intensity distribution for the image of a periodic object repeats periodically with defocus (Cowley & Moodie, 1960). Hence it is often necessary to define the defocus value by observation of a non-periodic component of the specimen such as a crystal edge (Spence *et al.*, 1977).

For the special case $a^2 = b^2$, the image intensity is also reproduced exactly for

$$\Delta f_1 - \Delta f_2 = (2n+1)a^2/\lambda, \qquad (2.5.2.53)$$

except that in this case the image is translated by a distance $a/2$ parallel to each of the axes.

2.5.2.9. *Image resolution*

(1) *Definition and measurement.* The 'resolution' of an electron microscope or, more correctly, the 'least resolvable distance', is usually defined by reference to the transfer function for the coherent imaging of a weak phase object under the Scherzer optimum defocus condition (2.5.2.44). The resolution figure is taken as the inverse of the U value for which $\sin\chi(U)$ first crosses the axis and is given, as in (2.5.2.45), by

$$\Delta x = 0.66C_s^{1/4}\lambda^{3/4}. \qquad (2.5.2.45)$$

It is assumed that an objective aperture is used to eliminate the contribution to the image for U values greater than the first zero crossing, since for these contributions the relative phases are distorted by the rapid oscillations of $\sin\chi(U)$ and the corresponding detail of the image is not directly interpretable in terms of the projection of the potential distribution of the object.

The resolution of the microscope in practice may be limited by the incoherent factors which have the effect of multiplying the WPOA transfer function by envelope functions as in (2.5.2.49).

The resolution, as defined above, and the effects of the envelope functions may be determined by Fourier transform of the image of a suitable thin, weakly scattering amorphous specimen. The Fourier-transform operation may be carried out by use of an optical diffractometer. A more satisfactory practice is to digitize the image directly by use of a two-dimensional detector system in the microscope or from a photographic recording, and perform the Fourier transform numerically.

For the optical diffractometer method, the intensity distribution obtained is given from (2.5.2.43) as a radially symmetric function of U,

$$\begin{aligned} I(U) &= |\mathscr{F}I(xy)|^2 \\ &= \delta(U) + 4\sigma^2|\Phi(u)|^2 \cdot \sin^2\chi(U) \cdot E^2(U), \end{aligned} \qquad (2.5.2.54)$$

where $E(U)$ is the product of the envelope functions.

In deriving (2.5.2.54) it has been assumed that:

(*a*) the WPOA applies;

(*b*) the optical transmission function of the photographic record is linearly related to the image intensity, $I(xy)$;

(*c*) the diffraction intensity $|\Phi(U)|^2$ is a radially symmetric, smoothly varying function such as is normally produced by a sufficiently large area of the image of an amorphous material;

(*d*) there is no astigmatism present and no drift of the specimen; either of these factors would remove the radial symmetry.

From the form of (2.5.2.54) and a preknowledge of $|\Phi(U)|^2$, the zero crossings of $\sin\chi$ and the form of $E(U)$ may be deduced. Analysis of a through-focus series of images provides more complete and reliable information.

(2) Detail on a scale much smaller than the resolution of the electron microscope, as defined above, is commonly seen in electron micrographs, especially for crystalline samples. For example, lattice fringes, having the periodicity of the crystal lattice planes, with spacings as small as 0.6 Å in one direction, have been observed using a microscope having a resolution of about 2.5 Å (Matsuda *et al.*, 1978), and two-dimensionally periodic images showing detail on the scale of 0.5 to 1 Å have been observed with a similar microscope (Hashimoto *et al.*, 1977).

Such observations are possible because

(*a*) for periodic objects the diffraction amplitude $\Psi_0(uv)$ in (2.5.2.31) is a set of delta functions which may be multiplied by the corresponding values of the transfer function that will allow strong interference effects between the diffracted beams and the zero beam, or between different diffracted beams;

(*b*) the envelope functions for the WPOA, arising from incoherent imaging effects, do not apply for strongly scattering crystals; the more general expression (2.5.2.36) provides that the incoherent imaging factors will have much less effect on the interference of some sets of diffracted beams.

The observation of finely spaced lattice fringes provides a measure of some important factors affecting the microscope performance, such as the presence of mechanical vibrations, electrical interference or thermal drift of the specimen. A measure of the fineness of the detail observable in this type of image may therefore be taken as a measure of 'instrumental resolution'.

2.5.2.10. *Electron diffraction in electron microscopes*

Currently most electron-diffraction patterns are obtained in conjunction with images, in electron microscopes of one form or another, as follows.

(*a*) Selected-area electron-diffraction (SAED) patterns are obtained by using intermediate and projector lenses to form an image of the diffraction pattern in the back-focal plane of the objective lens (Fig. 2.5.2.2). The area of the specimen from which the diffraction pattern is obtained is defined by inserting an aperture in the image plane of the objective lens. For parallel illumination of the specimen, sharp diffraction spots are produced by perfect crystals.

A limitation to the area of the specimen from which the diffraction pattern can be obtained is imposed by the spherical aberration of the objective lens. For a diffracted beam scattered through an angle α, the spread of positions in the object for which the diffracted beam passes through a small axial aperture in the image plane is $C_s\alpha^3$, *e.g.* for $C_s = 1$ mm, $\alpha = 5 \times 10^{-2}$ rad (10,0,0 reflection from gold for 100 keV electrons), $C_s\alpha^3 = 1250$ Å, so that a selected-area diameter of less than about 2000 Å is not feasible. For higher voltages, the minimum selected-area diameter decreases with λ^2 if the usual assumption is made that C_s increases for higher-voltage microscopes so that $C_s\lambda$ is a constant.

(*b*) Convergent-beam electron-diffraction (CBED) patterns are obtained when an incident convergent beam is focused on the specimen, as in an STEM instrument or an STEM attachment for a conventional TEM instrument.

For a large, effectively incoherent source, such as a conventional hot-filament electron gun, the intensities are added for each incident-beam direction. The resulting CBED pattern has an intensity distribution

$$I(uv) = \int |\Psi_{u_1v_1}(uv)|^2 \, \mathrm{d}u_1 \, \mathrm{d}v_1, \qquad (2.5.2.55)$$

where $\Psi_{u_1v_1}(uv)$ is the Fourier transform of the exit wave at the specimen for an incident-beam direction u_1, v_1.

(*c*) Coherent illumination from a small bright source such as a field emission gun may be focused on the specimen to give an electron probe having an intensity distribution $|t(xy)|^2$ and a diameter equal to the STEM dark-field image resolution [equation (2.5.2.47)] of a few Å. The intensity distribution of the resulting microdiffraction pattern is then

$$|\Psi(uv)|^2 = |\Psi_0(uv) * T(uv)|^2, \qquad (2.5.2.56)$$

where $\Psi_0(uv)$ is the Fourier transform of the exit wave at the specimen. Interference occurs between waves scattered from the various incident-beam directions. The diffraction pattern is thus an in-line hologram as envisaged by Gabor (1949).

(*d*) Diffraction patterns may be obtained by using an optical diffractometer (or computer) to produce the Fourier transform squared of a small selected region of a recorded image. The optical diffraction-pattern intensity obtained under the ideal conditions specified under equation (2.5.2.54) is given, in the case of weak phase objects, by

$$I(uv) = \delta(uv) + 4\sigma^2|\Phi(uv)|^2 \cdot \sin^2\chi(uv) \cdot E^2(uv) \qquad (2.5.2.57)$$

or, more generally, by

$$I(uv) = c\delta(uv) + |\Psi(uv) \cdot T(uv) * \Psi^*(uv) \cdot T^*(uv)|^2,$$

where $\Psi(uv)$ is the Fourier transform of the wavefunction at the exit face of the specimen and c is a constant depending on the characteristics of the photographic recording medium.

2.5.3. Space-group determination by convergent-beam electron diffraction* (P. GOODMAN)

2.5.3.1. *Introduction*

2.5.3.1.1. *CBED*

Convergent-beam electron diffraction, originating in the experiments of Kossel and Möllenstedt (Kossel & Möllenstedt, 1938) has been established over the past two decades as a powerful technique for the determination of space group in inorganic materials, with particular application when only microscopic samples are available. Relatively recently, with the introduction of the analytical electron microscope, this technique – abbreviated as CBED – has become available as a routine, so that there is now a considerable accumulation of data from a wide range of materials. A significant extension of the technique in recent times has been the introduction of LACBED (large-angle CBED) by Tanaka & Terauchi (1985). This technique allows an extensive angular range of single diffraction orders to be recorded and, although this method cannot be used for microdiffraction (since it requires an extensive single-crystal area), new LACBED applications appear regularly, particularly in the field of semiconductor research (see Section 2.5.3.6).

The CBED method relies essentially on two basic properties of transmission electron diffraction, namely the radical departure from Friedel's law and the formation of characteristic extinction bands

* Questions related to this section may be addressed to Professor M. Tanaka, Research Institute for Scientific Measurements, Tohoku University, Sendai 980-8577, Japan.

within space-group-forbidden reflections. Departure from Friedel's law in electron diffraction was first noted experimentally by Miyake & Uyeda (1950). The prediction of space-group-forbidden bands (within space-group-forbidden reflections) by Cowley & Moodie (1959), on the other hand, was one of the first successes of *N*-beam theory. A detailed explanation was later given by Gjønnes & Moodie (1965). These are known variously as 'GM' bands (Tanaka *et al.*, 1983), or more simply and definitively as 'GS' (glide–screw) bands (this section). These extinctions have a close parallel with space-group extinctions in X-ray diffraction, with the reservation that only screw axes of order two are accurately extinctive under *N*-beam conditions. This arises from the property that only those operations which lead to identical *projections* of the asymmetric unit can have *N*-beam dynamical symmetries (Cowley *et al.*, 1961).

Additionally, CBED from perfect crystals produces high-order defect lines in the zero-order pattern, analogous to the defect Kikuchi lines of inelastic scattering, which provide a sensitive measurement of unit-cell parameters (Jones *et al.*, 1977; Fraser *et al.*, 1985; Tanaka & Terauchi, 1985).

The significant differences between X-ray and electron diffraction, which may be exploited in analysis, arise as a consequence of a much stronger interaction in the case of electrons (Section 2.5.2). Hence, thin, approximately parallel-sided crystal regions must be used in high-energy (100 kV–1 MV) electron transmission work, so that diffraction is produced from crystals effectively infinitely periodic in only two dimensions, leading to the relaxation of three-dimensional diffraction conditions known as 'excitation error' (Chapter 5.2). Also, there is the ability in CBED to obtain data from microscopic crystal regions of around 50 Å in diameter, with corresponding exposure times of several seconds, allowing a survey of a material to be carried out in a relatively short time.

In contrast, single-crystal X-ray diffraction provides much more limited symmetry information in a direct fashion [although statistical analysis of intensities (Wilson, 1949) will considerably supplement this information], but correspondingly gives much more direct three-dimensional geometric data, including the determination of unit-cell parameters and three-dimensional extinctions.

The relative strengths and weaknesses of the two techniques make it useful where possible to collect both convergent-beam and X-ray single-crystal data in a combined study. However, all parameters *can* be obtained from convergent-beam and electron-diffraction data, even if in a somewhat less direct form, making possible space-group determination from microscopic crystals and microscopic regions of polygranular material. Several reviews of the subject are available (Tanaka, 1994; Steeds & Vincent, 1983; Steeds, 1979). In addition, an atlas of characteristic CBED patterns for direct phase identification of metal alloys has been published (Mansfield, 1984), and it is likely that this type of procedure, allowing *N*-beam analysis by comparison with standard simulations, will be expanded in the near future.

2.5.3.1.2. *Zone-axis patterns from CBED*

Symmetry analysis is necessarily tied to examination of patterns near relevant zone axes, since the most intense *N*-beam interaction occurs amongst the zero-layer zone-axis reflections, with in addition a limited degree of upper-layer (higher-order Laue zone) interaction. There will generally be several useful zone axes accessible for a given parallel-sided single crystal, with the regions between axes being of little use for symmetry analysis. Only one such zone axis can be parallel to a crystal surface normal, and a microcrystal is usually chosen at least initially to have this as the principal symmetry axis. Other zone axes from that crystal may suffer mild symmetry degradation because the *N*-beam lattice component ('excitation error' extension) will not have the symmetry of the structure (Goodman, 1974; Eades *et al.*, 1983).

Upper-layer interactions, responsible for imparting three-dimensional information to the zero layer, are of two types: the first arising from 'overlap' of dynamic shape transforms and causing smoothly varying modulations of the zero-layer reflections, and the second, caused by direct interactions with the upper-layer, or higher-order Laue zone lines, leading to a sharply defined fine-line structure. These latter interactions are especially useful in increasing the accuracy of space-group determination (Tanaka *et al.*, 1983), and may be enhanced by the use of low-temperature specimen stages. The presence of these defect lines in convergent-beam discs, occurring especially in low-symmetry zone-axis patterns, allows symmetry elements to be related to the three-dimensional structure (Section 2.5.3.5; Fig. 2.5.3.4*c*).

To the extent that such three-dimensional effects can be ignored or are absent in the zero-layer pattern the *projection approximation* (Chapter 5.2) can be applied. This situation most commonly occurs in zone-axis patterns taken from relatively thin crystals and provides a useful starting point for many analyses, by identifying the projected symmetry.

2.5.3.2. *Background theory and analytical approach*

2.5.3.2.1. *Direct and reciprocity symmetries: types I and II*

Convergent-beam diffraction symmetries are those of Schrödinger's equation, *i.e.* of crystal potential, plus the diffracting electron. The appropriate equation is given in Section 2.5.2 [equation (2.5.2.6)] and Chapter 5.2 [equation (5.2.2.1)] in terms of the real-space wavefunction ψ. The symmetry elements of the crystal responsible for generating pattern symmetries may be conveniently classified as of two types (I and II) as follows.

I. The *direct* (type I: Table 2.5.3.1) symmetries imposed by this equation on the transmitted wavefunction given z-axis illumination ($\mathbf{k}_0$, the incident wavevector parallel to Z, the surface normal) are just the symmetries of φ whose operation leaves both crystal and z axis unchanged. These are also called 'vertical' symmetry elements, since they contain Z. These symmetries apply equally in real and reciprocal space, since the operator ∇^2 has circular symmetry in both spaces and does nothing to degrade the symmetry in

Table 2.5.3.1. *Listing of the symmetry elements relating to CBED patterns under the classifications of 'vertical' (I), 'horizontal' (II) and combined or roto-inversionary axes*

I. Vertical symmetry elements		
	International symbols	
	$2, 3, 4, 6$ $(2_1, 3_1, \ldots)$	
	m (c)	
	a, b (n)	
II. Horizontal symmetry elements		
	Diperiodic symbols	BESR symbols
	$2'$	m
	$2'_1$	
	m'	1_R
	a', b', n'	
	$\bar{1}'$	2_R
I + II	$\bar{4}'$	4_R
I × II	$\bar{3}' = 3 \times \bar{1}'$	$6_R = 3 \cdot 2_R$
	$\bar{6}' = 3 \times m'$	31_R

transmission. Hence, for high-symmetry crystals (zone axis parallel to z axis), and to a greater or lesser degree for crystals of a more general morphology, these zone-axis symmetries apply both to electron-microscope lattice images and to convergent-beam patterns under z-axis-symmetrical illumination, and so impact also on space-group determination by means of high-resolution electron microscopy (HREM). In CBED, these elements lead to *whole pattern* symmetries, to which every point in the pattern contributes, regardless of diffraction order and Laue zone (encompassing ZOLZ and HOLZ reflections).

II. Reciprocity-induced symmetries, on the other hand, depend upon ray paths and path reversal, and in the present context have relevance only to the diffraction pattern. Crystal-inverting or horizontal crystal symmetry elements combine with reciprocity to yield *indirect* pattern symmetries lacking a one-to-one real-space correspondence, within individual diffraction discs or between disc pairs. Type II elements are assumed to lie on the central plane of the crystal, midway between surfaces, as symmetry operators; this assumption amounts to a 'central plane' approximation, which has a very general validity in space-group-determination work (Goodman, 1984*a*).

A minimal summary of basic theoretical points, otherwise found in Chapter 5.2 and numerous referenced articles, is given here.

For a specific zero-layer diffraction order $g\ (= h, k)$ the incident and diffracted vectors are $\mathbf{k}_0$ and $\mathbf{k}_g$. Then the three-dimensional vector $\mathbf{K}_{0g} = \frac{1}{2}(\mathbf{k}_0 + \mathbf{k}_g)$ has the pattern-space projection, $\mathbf{K}_g = {}^{p}[\mathbf{K}_{0g}]$. The point $\mathbf{K}_g = \mathbf{0}$ gives the *symmetrical Bragg condition* for the associated diffraction disc, and $\mathbf{K}_g \neq \mathbf{0}$ is identifiable with the angular deviation of $\mathbf{K}_{0g}$ from the vertical z axis in three-dimensional space (see Fig. 2.5.3.1). $\mathbf{K}_g = \mathbf{0}$ also defines the symmetry centre within the two-dimensional disc diagram (Fig. 2.5.3.2); namely, the intersection of the lines S and G, given by the trace of excitation error, $\mathbf{K}_g = \mathbf{0}$, and the perpendicular line directed towards the reciprocal-space origin, respectively. To be definitive it is necessary to index diffracted amplitudes relating to a fixed crystal thickness and wavelength, with both crystallographic and momentum coordinates, as $\mathbf{u}_{g,K}$, to handle the continuous variation of $\mathbf{u}_g$ (for a particular diffraction order), with angles of incidence as determined by $\mathbf{k}_0$, and registered in the diffraction plane as the projection of $\mathbf{K}_{0g}$.

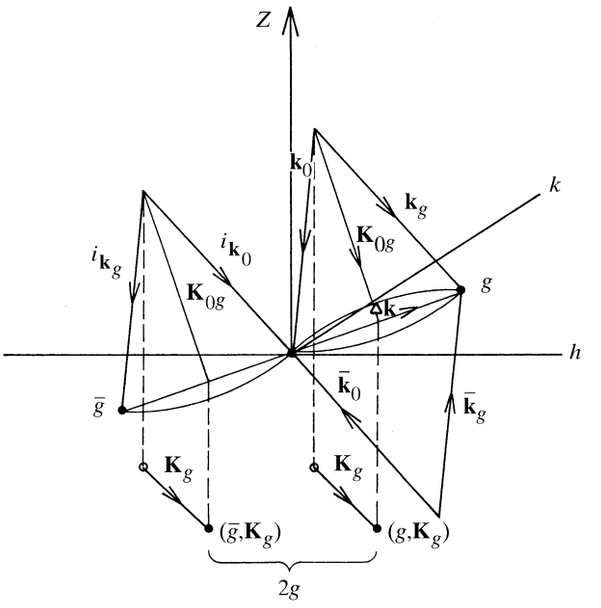

Fig. 2.5.3.1. Vector diagram in semi-reciprocal space, using Ewald-sphere constructions to show the 'incident', 'reciprocity' and 'reciprocity × centrosymmetry' sets of vectors. Dashed lines connect the full vectors $\mathbf{K}_{0g}$ to their projections $\mathbf{K}_g$ in the plane of observation.

2.5.3.2.2. *Reciprocity and Friedel's law*

Reciprocity was introduced into the subject of electron diffraction in stages, the essential theoretical basis, through Schrödinger's equation, being given by Bilhorn *et al.* (1964), and the N-beam diffraction applications being derived successively by von Laue (1935), Cowley (1969), Pogany & Turner (1968), Moodie (1972), Buxton *et al.* (1976), and Gunning & Goodman (1992).

Reciprocity represents a reverse-incidence configuration reached with the reversed wavevectors $\bar{\mathbf{k}}_0 = -\mathbf{k}_g$ and $\bar{\mathbf{k}}_g = -\mathbf{k}_0$, so that the scattering vector $\Delta\mathbf{k} = \mathbf{k}_g - \mathbf{k}_0 = \bar{\mathbf{k}}_0 - \bar{\mathbf{k}}_g$ is unchanged, but $\bar{\mathbf{K}}_{0g} = \frac{1}{2}(\bar{\mathbf{k}}_0 + \bar{\mathbf{k}}_g)$ is changed in sign and hence reversed (Moodie, 1972). The reciprocity equation,

$$\mathbf{u}_{g,\mathbf{K}} = \mathbf{u}^{*}_{g,\bar{\mathbf{K}}}, \tag{2.5.3.1}$$

is valid independently of crystal symmetry, but cannot contribute symmetry to the pattern unless a crystal-inverting symmetry element is present (since $\bar{\mathbf{K}}$ belongs to a reversed wavevector). The simplest case is centrosymmetry, which permits the right-hand side of (2.5.3.1) to be complex-conjugated giving the useful CBED pattern equation

$$\mathbf{u}_{g,\mathbf{K}} = \mathbf{u}_{\bar{g},\mathbf{K}}. \tag{2.5.3.2}$$

Since $\mathbf{K}$ is common to both sides there is a point-by-point identity between the related distributions, separated by $2g$ (the distance between g and $\bar{g}$ reflections). This invites an obvious analogy with *Friedel's law*, $F_g = F^{*}_{\bar{g}}$, with the reservation that (2.5.3.2) holds only for centrosymmetric crystals. This condition (2.5.3.2) constitutes what has become known as the $\pm H$ symmetry and, incidentally, is the only reciprocity-induced symmetry so general as to not depend upon a disc symmetry-point or line, nor on a particular zone axis (*i.e.* it is not a point symmetry but a translational symmetry of the pattern intensity).

2.5.3.2.3. *In-disc symmetries*

(*a*) *Dark-field (diffracted-beam) discs*. Other reciprocity-generated symmetries which are available for experimental observation relate to a single (zero-layer) disc and its origin $\mathbf{K}_g = \mathbf{0}$, and are summarized here by reference to Fig. 2.5.3.2, and given in operational detail in Table 2.5.3.2. The notation subscript R, for reciprocity-induced symmetries, introduced by Buxton *et al.* (1976) is now adopted (and referred to as BESR notation). Fig.

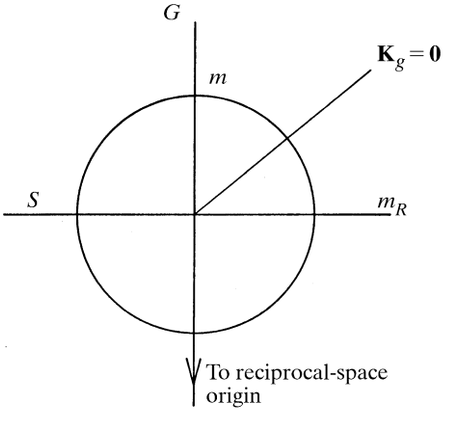

Fig. 2.5.3.2. Diagrammatic representation of a CBED disc with symmetry lines m, m_R (alternate labels G, S) and the central point $\mathbf{K}_g = 0$.

2.5.3.2 shows a disc crossed by reference lines m and m_R. These will be mirror lines of intensity if: (*a*) **g** is parallel to a vertical mirror plane; and (*b*) **g** is parallel to a horizontal diad axis, respectively. The third possible point symmetry, that of disc centrosymmetry (1_R in BESR notation) will arise from the presence of a horizontal mirror plane. Lines m and m_R become the GS extinction lines G and S when glide planes and screw axes are present instead of mirror planes and diad axes.

(*b*) *Bright-field (central-beam) disc*. The central beam is a special case since the point $\mathbf{K}_0 = \mathbf{0}$ is the centre of the whole pattern as well as of that particular disc. Therefore, both sets of rotational symmetry (types I and II) discussed above apply (see Table 2.5.3.3).

In addition, the central-beam disc is a source of three-dimensional lattice information from defect-line scattering. Given a sufficiently perfect crystal this fine-line structure overlays the more general intensity modulation, giving this disc a lower and more precisely recorded symmetry.

2.5.3.2.4. *Zero-layer absences*

Horizontal glides, a', n' (diperiodic, primed notation), generate zero-layer absent rows, or centring, rather than GS bands (see Fig. 2.5.3.3). This is an example of the projection approximation in its most universally held form, *i.e.* in application to absences. Other examples of this are: (*a*) appearance of both G and S extinction bands near their intersection irrespective of whether glide or screw axes are involved; and (*b*) suppression of the influence of vertical, non-primitive translations with respect to observations in the zero layer. It is generally assumed as a working rule that the zero-layer or ZOLZ pattern will have the rotational symmetry of the point-group component of the vertical screw axis (so that $2_1 \simeq 2$). Elements included in Table 2.5.3.1 on this pretext are given in parentheses. However, the presence of 2_1 rather than 2 (3_1 rather than 3 *etc.*) should be detectable as a departure from accurate twofold symmetry in the first-order-Laue-zone (FOLZ) reflection circle (depicted in Fig. 2.5.3.3). This has been observed in the cubic structure of $Ba_2Fe_2O_5Cl_2$, permitting the space groups $I23$ and $I2_13$ to be distinguished (Schwartzman *et al.*, 1996). A summary of all the symmetry components described in this section is given diagrammatically in Table 2.5.3.2.

2.5.3.3. *Pattern observation of individual symmetry elements*

The following guidelines, the result of accumulated experience from several laboratories, are given in an experimentally based sequence, and approximately in order of value and reliability.

(i) The value of X in an *X-fold rotation* axis is made immediately obvious in a zone-axis pattern, although a screw component is not detected in the pattern symmetry.

Roto-inversionary axes require special attention: $\bar{6}$ and $\bar{3}$ may be factorized, as in Tables 2.5.3.1, 2.5.3.3 and 2.5.3.4, to show better the additional CBED symmetries ($3/m'$ and $3 \times \bar{1}'$, respectively). $\bar{4}$ cannot be decomposed further (Table 2.5.3.1) and generates its own diffraction characteristics in non-projective patterns (see Section 2.5.3.5). This specific problem of observing the fourfold roto-

Table 2.5.3.2. *Diagrammatic illustrations of the actions of five types of symmetry elements (given in the last column in Volume A diagrammatic symbols) on an asymmetric pattern component, in relation to the centre of the pattern at* $\mathbf{K}_{00} = \mathbf{0}$*, shown as '* $\oplus$*', or in relation to the centre of a diffraction order at* $\mathbf{K}_{0g} = \mathbf{0}$*, shown as '+'*

Type	Symmetry element	Observation and action	In combination	Interpretation
Vertical	4			
	m; a	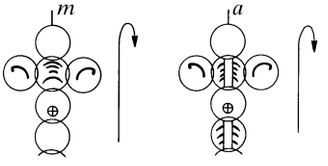	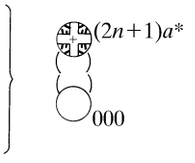	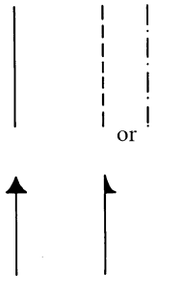
Horizontal	$2'$; $2'_1$	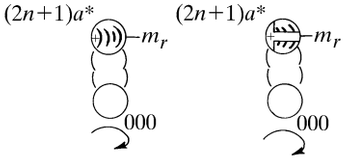		
	$i(\bar{1}')$	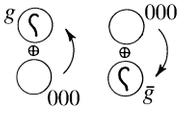		
	m'; a'	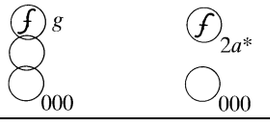		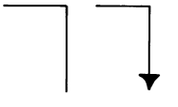

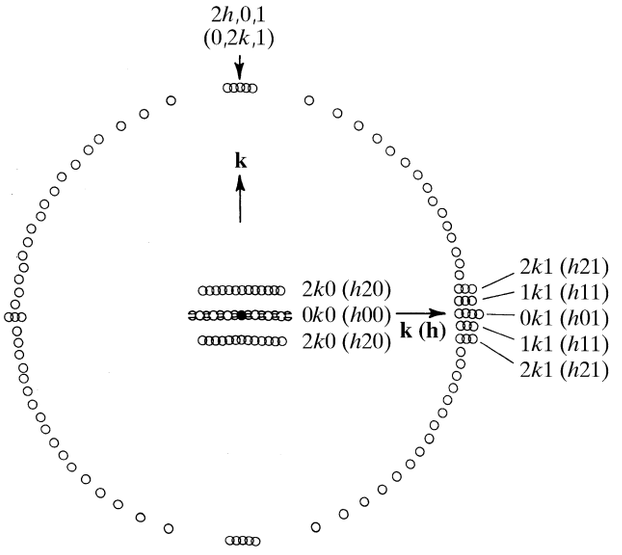

Fig. 2.5.3.3. Diagrammatic representation of the influence of non-symmorphic elements: (i) Alternate rows of the zero-layer pattern are absent owing to the horizontal glide plane. The pattern is indexed as for an '*a*' glide; the alternative indices (in parentheses) apply for a '*b*' glide. (ii) GS bands are shown along the central row of the zero layer, for odd-order reflections.

inversion symmetry has been resolved recently by Tanaka *et al.* (1994) using both CBED and LACBED techniques.

(ii) *Vertical mirror plane* determination may be the most accurate crystal point-symmetry test, given that it is possible to follow the symmetry through large crystal rotations (say 5 to 15°) about the mirror normal. It is also relatively unaffected by crystal surface steps as compared to (v) below.

(iii) *Horizontal glide planes* are determined unequivocally from zero-layer absences when the first Laue zone is recorded, either with the main pattern or by further crystal rotation; *i.e.* a section of this zone is needed to determine the lateral unit-cell parameters. This observation is illustrated diagrammatically in Fig. 2.5.3.3.

(iv) An extinction (GS) line or band through odd-order reflections of a zone-axis pattern indicates only a *projected glide line*. This is true because both $P2_1$ (No. 4) and *Pa* (No. 7) symmetries project into '*pg*' in two dimensions. However, the projection approximation has only limited validity in CBED. For all crystal rotations *around* the 2_1 axis, or alternatively *about the glide-plane 'a' normal*, dynamic extinction conditions are retained. This is summarized by saying that the diffraction vector $\mathbf{K}_{0g}$ should be either normal to a screw axis or contained within a glide plane for the generation of the *S* or *G* bands, respectively. Hence $P2_1$ and *Pa* may be distinguished by these types of rotations away from the zone axis with the consequence that the element 2_1 in particular is characterized by extinctions close to the Laue circle for the tilted ZOLZ pattern (Goodman, 1984*b*), and that the glide *a* will generate extinction bands through both ZOLZ and HOLZ reflections for all orientations maintaining Laue-circle symmetry about the *S* band (Steeds *et al.*, 1978).

As a supplement to this, in a refined technique not universally applicable, Tanaka *et al.* (1983) have shown that fine-line detail from HOLZ interaction can be observed which will separately identify *S*- (2_1) and *G*-band symmetry from a single pattern (see Fig. 2.5.3.6).

(v) The centre-of-symmetry (or $\pm H$) test can be made very sensitive by suitable choice of diffraction conditions but requires a reasonably flat crystal since it involves a pair of patterns (the angular beam shift involved is very likely to be associated with some lateral probe shift on the specimen). This test is best carried out at a low-symmetry zone axis, free from other symmetries, and preferably incorporating some fine-line HOLZ detail, in the following way. The hkl and $\bar{h}\bar{k}\bar{l}$ reflections are successively illuminated by accurately exchanging the central-beam aperture with the diffracted-beam apertures, having first brought the zone axis on to the electron-microscope optic axis. This produces the symmetrical $\pm H$ condition.

(vi) In seeking internal m_R symmetry as a test for a horizontal diad axis it is as well to involve some distinctive detail in the mirror symmetry (*i.e.* simple two-beam-like fringes should be avoided), and also to rotate the crystal about the supposed diad axis, to avoid an m_R symmetry due to projection [for examples see Fraser *et al.* (1985) and Goodman & Whitfield (1980)].

(vii) The presence or absence of the in-disc centrosymmetry element 1_R formally indicates the presence or absence of a horizontal mirror element m', either as a true mirror or as the mirror component of a horizontal glide plane g'. In this case the *absence* of symmetry provides more positive evidence than its presence, since absence is sufficient evidence for a lack of central-mirror crystal symmetry but an observed symmetry could arise from the operation of the projection approximation. If some evidence of the three-dimensional interaction is included in the observation or if three-dimensional interaction (from a large *c* axis parallel to the zone axis) is evident in the rest of the pattern, this latter possibility can be excluded. Interpretation is also made more positive by extending the angular aperture, especially by the use of LACBED.

These results are illustrated in Table 2.5.3.2 and by actual examples in Section 2.5.3.5.

2.5.3.4. *Auxiliary tables*

Space groups may very well be identified using CBED patterns from an understanding of the diffraction properties of real-space symmetry elements, displayed for example in Table 2.5.3.2. It is, however, of great assistance to have the symmetries tabulated in reciprocal space, to allow direct comparison with the pattern symmetries.

There are three generally useful ways in which this can be done, and these are set out in Tables 2.5.3.3 to 2.5.3.5. The simplest of these is by means of point group, following the procedures of Buxton *et al.* (1976). Next, the CBED pattern symmetries can be listed as diperiodic groups which are space groups in two dimensions, allowing identification with a restricted set of three-dimensional space groups (Goodman, 1984*b*). Finally, the dynamic extinctions (GS bands and zero-layer absences) can be listed for each non-symmorphic space group, together with the diffraction conditions for their observation (Tanaka *et al.*, 1983; Tanaka & Terauchi, 1985). Descriptions for these tables are given below.

Table 2.5.3.3. BESR symbols (Buxton *et al.*, 1976) incorporate the subscript *R* to describe reciprocity-related symmetry elements, *R* being the operator that rotates the disc pattern by 180° about its centre. The symbols formed in this way are $1_R, 2_R, 4_R, 6_R$, where X_R represents $2\pi/X$ rotation about the zone axis, followed by *R*. Of these, 2_R represents the $\pm H$ symmetry (two twofold rotations) described earlier [equation (2.5.3.2)] as a transformation of crystalline centrosymmetry; 6_R may be thought of as decomposing into $3 \cdot 2_R$ for purposes of measurement. The mirror line m_R (Fig. 2.5.3.2) is similarly generated by $m \cdot 1_R$.

Table 2.5.3.3 gives the BESR interrelation of pattern symmetries with point group (Buxton *et al.*, 1976; Steeds, 1983). Columns I and II of the table list the point symmetries of the whole pattern and bright-field pattern, respectively; column III gives the BESR diffraction groups. [*Note:* following the Pond & Vlachavas (1983) usage, '*' has been appended to the centrosymmetric groups.]

Table 2.5.3.3. *Diffraction point-group tables, giving whole-pattern and central-beam pattern symmetries in terms of BESR diffraction-group symbols and diperiodic group symbols*

I	II	III	IV	V	
				Cubic point groups	
Whole pattern	Bright field (central beam)	BESR group	Diperiodic group (point group)	[100]	[110]
1	1	1	1		
1	2	$\underline{1}_R$	m'		
2	2	2	2		
1	1	$^*2_R$	$\bar{1}'$		
2	2	$^*\underline{21}_R$	$2/m'$		
1	m	m_R	$2'$		23
m	m	m	m		
m	$2mm$	$\underline{m1}_R$	$2'mm'$		$\bar{4}3m$
2	$2mm$	$2m_Rm_R$	$2'2'2$	23	432
$2mm$	$2mm$	$2mm$	$mm2$		
m	m	$^*2_Rmm_R$	$2'/m$		$m\bar{3}$
$2mm$	$2mm$	$^*\underline{2mm1}_R$	mmm'	$m\bar{3}$	$m\bar{3}m$
4	4	4	4		
2	4	4_R	$\bar{4}'$		
4	4	$^*\underline{41}_R$	$4/m'$		
4	$4mm$	$4m_Rm_R$	$42'2'$	$\bar{4}32$	
$4mm$	$4mm$	$4mm$	$4mm$		
$2mm$	$4mm$	4_Rmm_R	$\bar{4}'m2'$	$\bar{4}3m$	
$4mm$	$4mm$	$^*\underline{4mm1}_R$	$4/m'mm$	$m\bar{3}m$	
3	3	3	3		
3	6	$\underline{31}_R$	$\bar{6}'$		
3	$3m$	$3m_R$	$32'$		
$3m$	$3m$	$3m$	$3m$		
$3m$	$6mm$	$\underline{3m1}_R$	$\bar{6}'m2'$		
6	6	6	6		
3	3	$^*6_R$	$\bar{3}'$		
6	6	$^*\underline{61}_R$	$6/m'$		
6	$6mm$	$6m_Rm_R$	$62'2'$		
$6mm$	$6mm$	$6mm$	$6mm$		
$3m$	$3m$	$^*6_Rmm_R$	$\bar{3}'m$		
$6mm$	$6mm$	$^*\underline{6mm1}_R$	$6/m'mm$		

Inspection of columns I and II shows that 11 of the 31 diffraction groups can be determined from a knowledge of the whole pattern and bright-field (central-beam disc) point symmetries alone. The remaining 10 pairs of groups need additional observation of the dark-field pattern for their resolution. Disc symmetries 1_R, m_R (Fig. 2.5.3.2; Table 2.5.3.2) are sought (*a*) in general zero-layer discs and (*b*) in discs having an m_R line perpendicular to a proposed twofold axis, respectively; the $\pm H$ test is applied for centrosymmetry, to complete the classification.

Column IV gives the equivalent diperiodic point-group symbol, which, unprimed, gives the corresponding three-dimensional symbol. This will always refer to a non-cubic point group. Column V gives the additional cubic point-group information indicating, where appropriate, how to translate the diffraction symmetry into [100] or [110] cubic settings, respectively.

Of the groups listed in column III, those representing the projection group of their class are underlined. These groups all contain 1_R, the BESR symbol for m'. When the projection approximation is applicable, only those groups underlined will apply. The effect of this approximation is to add a horizontal mirror plane to the symmetry group.

Table 2.5.3.4. This lists possible space groups for each of the classified zero-layer CBED symmetries. Since the latter constitute the 80 diperiodic groups, it is first necessary to index the pattern in diperiodic nomenclature; the set of possible space groups is then given by the table.

A basic requirement for diperiodic group nomenclature has been that of compatibility with *IT* A and I. This has been met by the recent Pond & Vlachavas (1983) tabulation. For example, DG: $(^*)pban'$, where * indicates centrosymmetry, becomes space group *Pban* when, in Seitz matrix description, the former group matrix is multiplied by the third primitive translation, a_3. Furthermore, in textual reference the prime can be optionally omitted, since the lower-case lattice symbol is sufficient indication of a two-dimensional periodicity (as *pban*).

The three sections of Table 2.5.3.4 are:

I. Point-group entries, given in H–M and BESR symbols.

II. Pattern symmetries, in diperiodic nomenclature, have three subdivisions: (i) symmorphic groups: patterns without zero-layer absences or extinctions. Non-symmorphic groups are then given in two categories: (ii) patterns with zero-layer GS bands, and (iii) patterns with zero-layer absences resulting from a horizontal glide plane; where the pattern *also* contains dynamic extinctions (GS bands) and so is listed in column (ii), the column (iii) listing is given in parentheses.

The 'short' (Pond & Vlachavas) symbol has proved an adequate description for all but nine groups for which the screw-axis content was needed: here $(2'_1)$, or $(2'_12'_1)$, have been added to the symbol.

III. Space-group entries are given in terms of *IT* A numbers. The first column of each row gives the same-name space group as illustrated by the example $pban' \rightarrow Pban$ above. The groups following in the same row (which have the same zero-layer symmetry) complete an exhaustive listing of the II*b* subgroups, given in *IT* A. Cubic space groups are underlined for the sake of clarity; hence, those giving rise to the zero-layer symmetry of the diffraction group in the [100] (cyclic) setting have a single underline: these are type I minimal supergroups in *IT* A nomenclature. The cubic groups are also given in the [110] setting, in underlined italics, since this is a commonly encountered high-symmetry setting. (*Note*: these then are no longer *minimal* supergroups and the relationship has to be found through a series of *IT* A listings.)

The table relates to maximal-symmetry settings. For monoclinic and orthorhombic systems there are three equally valid settings. For monoclinic groups, the oblique and rectangular settings appear separately; where rectangular *C*-centred groups appear in a second setting this is indicated by superscript '2'. For orthorhombic groups, superscripts correspond to the 'incident-beam' system adopted in Table 2.5.3.5, as follows: no superscript: [001] beam direction; superscript 1: [100] beam direction; superscript 2: [010] beam direction. The cubic system is treated specially as described above.

Table 2.5.3.5. This lists conditions for observation of GS bands for the 137 space groups exhibiting these extinctions. These are entered as '*G*', '*S*', or '*GS*', indicating whether a glide plane, screw axis, or both is responsible for the GS band. All three possibilities will lead to a glide line (and hence to both extinction bands) in projection, and one of the procedures (*a*), (*b*), or (*c*) of Section 2.5.3.3(iv) above is needed to complete the three-dimensional interpretation. In addition, the presence of horizontal glide planes, which result in systematic absences in these particular cases in the zero-layer pattern, is indicated by the symbol '–'. Where these occur at the site of prospective '*G*' or '*S*' bands from other glide or

screw elements the symbol of that element is given and the '*G*' or '*S*' symbol is omitted.

The following paragraphs give information on the real-space interpretation of GS band formation, and their specific extinction rules, considered useful in structural interpretation.

Real-space interpretation of extinction conditions. Dynamic extinctions (GS bands) are essentially a property of symmetry in reciprocal space. However, since diagrams from *IT* I and A are used there is a need to give an equivalent real-space description. These bands are associated with the half-unit-cell-translational glide planes and screw axes represented in these diagrams. Inconsistencies between 'conventional' and 'physical' real-space descriptions, however, become more apparent in dynamical electron diffraction, which is dependent upon three-dimensional scattering physics, than in X-ray diffraction. Also, the distinction between general (symmorphic) and specific (non-symmorphic) extinctions is more basic (in the former case). This is clarified by the following points:

(i) Bravais lattice centring restricts the conditions for observation of GS bands. For example, in space group *Abm*2 (No. 39), '*A*' centring prevents observation of the GS bands associated with the '*b*' glide at the [001] zone-axis orientation; this observation, and hence verification of the *b* glide, must be made at the lower-symmetry zone axes [0*vw*] (see Table 2.5.3.5). In the exceptional cases of space groups $I2_12_12_1$ and $I2_13$ (Nos. 24 and 199), conditions for the observation of the relevant GS bands are completely prevented by body centring; here the screw axes of the symmorphic groups *I*222 and *I*23 are parallel to the screw axes of their non-symmorphic derivatives. However, electron crystallographic methods also include direct structure imaging by HREM, and it is important to note here that while the indistinguishability encountered in data sets acquired in Fourier space applies to both X-ray diffraction and CBED (notwithstanding possible differences in HOLZ symmetries), this limitation does not apply to the HREM images (produced by dynamic scattering) yielding an approximate structure image for the (zone-axis) *projection*. This technique then becomes a powerful tool in space-group research by supplying phase information in a different form.

(ii) A different complication, relating to nomenclature, occurs in the space groups $P\bar{4}3n$, *Pn*3*n* and *Pm*3*n* (Nos. 218, 222 and 223) where '*c*' glides parallel to a diagonal plane of the unit cell occur as primary non-symmorphic elements (responsible for reciprocal-space extinctions) but are not used in the Hermann–Maugin symbol; instead the derivative '*n*' glide planes are used as characters, resulting in an *apparent* lack of correspondence between the conventionally given real-space symbols and the reciprocal-space extinctions.

(*Note*: In *IT* I non-symmorphic reflection rules which duplicate rules given by lattice centring, or those which are a consequence of more general rules, are given in parentheses; in *IT* A this clarification by parenthesizing, helpful for electron-diffraction analysis, has been removed.)

(iii) Finally, diamond glides (symbol '*d*') require special consideration since they are associated with translations $\frac{1}{4}, \frac{1}{4}, \frac{1}{4}$, and so would appear not to qualify for GS bands; however, this translation is a result of the conventional cell being defined in real rather than reciprocal space where the extinction symmetry is formed. Hence '*d*' glides occur only in *F*-centred lattices (most obviously Nos. 43, 70, 203, 277 and 228). These have correspondingly an *I*-centred reciprocal lattice for which the zero-layer two-dimensional unit cell has an edge of $a^{*\prime\prime} = 2a^*$. Consequently, the first-order row reflection along the diamond glide retains the reciprocal-space anti-symmetry on the basis of this physical unit cell (halved in real space), and leads to the labelling of odd-order reflections as $4n + 2$ (instead of $2n + 1$ when the cell is not halved). Additionally, although seven space groups are *I*-centred in real space with the conventional unit cell (Nos. 109, 110, 122, 141, 142, 220 and 230), these space groups are *F*-centred with the transformation $a'' = [110]$, $b'' = [1\bar{1}0]$, and correspondingly *I*-centred in the reciprocal-space cell as before, but the directions [100], [010] and reflection rows *h*00, 0*k*0 become replaced by directions [110] (or [1$\bar{1}$0]) and rows *hh*0, *h*$\bar{h}$0, in the entries of Table 2.5.3.5.

Extinction rules for symmetry elements appearing in Table 2.5.3.5. Reflection indices permitting observation of *G* and *S* bands follow [here 'zero-layer' and 'out-of-zone' (*i.e.* HOLZ or alternative zone) serve to emphasize that these are zone-axis observations].

(i) *Vertical glide planes* lead to '*G*' bands in reflections as listed ('*a*', '*b*', '*c*' and '*n*' glides):

*h*0*l*, *hk*0, 0*kl* out-of-zone reflections (for glide planes having normals [010], [001] and [100]) having $h + l$, $h + k$, $k + l = 2n + 1$, respectively, in the case of '*n*' glides, or *h*, *k*, *l* odd in the case of '*a*', '*b*' or '*c*' glides, respectively;

*h*00, 0*k*0, 00*l* zero-layer reflections with *h*, *k* or *l* odd.

Correspondingly for '*d*' glides:

(*a*) In *F*-centred cells:

*h*0*l*, *hk*0, 0*kl* out-of-zone reflections (for glide planes having normals [010], [100] and [001], having $h + l$, $k + l$, or $h + k = 4n + 2$, respectively, with *h*, *k* and *l* even; and (space group No. 43 only) zero-layer reflections *h*00, 0*k*0 with *h*, *k* even and $= 4n + 2$.

(*b*) In *I*-centred cells:

hhl (cyclic on *h*, *k*, *l* for cubic groups) out-of-zone reflections having $2h + l = 4n + 2$, with *l* even; and zero-layer reflections *hh*0, *h*$\bar{h}$0 (cyclic on *h*, *k*, *l* for cubic groups) having *h* odd.

(ii) *Horizontal screw axes*, namely 2_1 or the 2_1 component of screw axes 4_1, 4_3, 6_1, 6_3, 6_5, lead to '*S*' bands in reflection rows parallel to the screw axis, *i.e.* either *h*00, 0*k*0 or 00*l*, with conventional indexing, for *h*, *k* or *l* odd.

(iii) *Horizontal glide planes* lead to zero-layer absences rather than GS bands. When these prevent observation of a specific GS band (by removing the two-dimensional conditions), the symbol '−' indicates a situation where, in general, there will simply be absences for the odd-order reflections. However, Ishizuka & Taftø (1982) were the first to observe finite-intensity narrow bands under these conditions, and it is now appreciated that with a sufficient crystal thickness and a certain minimum for the *z*-axis repeat distance, GS bands can be recorded by violating the condition for horizontal-mirror-plane (m') extinction while satisfying the condition for *G* or *S*, achieved by appropriate tilts away from the exact zone-axis orientation [see Section 2.5.3.3(iv)].

2.5.3.5. *Space-group analyses of single crystals; experimental procedure and published examples*

2.5.3.5.1. *Stages of procedure*

(i) *Zone-axis patterns*. The first need is to record a principal zone-axis pattern. From this, the rotational order *X* of the vertical axis and associated mirror (including glide-line) components are readily observed (see all examples).

This pattern may include part of the higher-order Laue zone; in particular the closest or first-order Laue zone (FOLZ) should be included in order to establish the presence or absence of horizontal glide planes, as illustrated in Fig. 2.5.3.3. The projection approximation frequently applies to the zone-axis pattern, particularly when this is obtained from thin crystals (although this cannot apply by definition to the FOLZ). This is indicated by the absence of fine-line detail in the central beam particularly; identification of the projected symmetry is then straightforward.

(ii) *Laue circle patterns*. Next, it is usual to seek patterns in which discs around the Laue circle include the line m_R (Fig.

2.5.3.2). The internal disc symmetries observed together with those from the zone-axis pattern will determine a diffraction group, classifying the zero-layer symmetry. [Fig. 6(*c*) of Goodman & Whitfield (1980) gives an example of Laue-circle symmetries.]

(iii) *Alternative zone axes or higher-order Laue zones*. Finally, alternative zone or higher-order Laue-zone patterns may be sought for additional three-dimensional data: (*a*) to determine the three-dimensional extinction rules, (*b*) to test for centrosymmetry, or (*c*) to test for the existence of mirror planes perpendicular to the principal rotation axis. These procedures are illustrated in the following examples.

2.5.3.5.2. *Examples*

(1) *Determination of centrosymmetry; examples from the hexagonal system*. Fig. 2.5.3.4(*a*) illustrates the allocation of planar point groups from [0001] zone-axis patterns of β-Si_3N_4 (left-hand side) and β-GaS (right-hand side); the patterns exhibit point symmetries of 6 and 6*mm*, respectively, as indicated by the accompanying geometric figures, permitting point groups 6 or $6/m$, and 6*mm* or $6/mmm$, in three dimensions. Alternative zone axes are required to distinguish these possibilities, the actual test used (testing for the element m' or the centre of symmetry) being largely determined in practice by the type of crystal preparation.

Fig. 2.5.3.4(*b*) shows the CBED pattern from the $[11\bar{2}0]$ zone axis of β-Si_3N_4 (Bando, 1981), using a crystal with the corresponding cleavage faces. The breakdown of Friedel's law between reflections 0002 and $000\bar{2}$ rules out the point group $6/m$ (the element m' from the first setting is not present) and establishes 6 as the correct point group.

Also, the GS bands in the 0001 and $000\bar{1}$ reflections are consistent with the space group $P6_3$. [*Note*: screw axes 6_1, 6_3 and 6_5 are not distinguished from these data alone (Tanaka *et al.*, 1983).]

Fig. 2.5.3.4(*c*) shows CBED patterns from the vicinity of the $[1\bar{1}02]$ zone axis of β-GaS, only 11.2° rotated from the [0001] axis and accessible using the same crystal as for the previous [0001] pattern. This shows a positive test for centrosymmetry using a conjugate reflection pair $1\bar{1}01/\bar{1}10\bar{1}$, and establishes the centrosymmetric point group $\bar{6}/mmm$, with possible space groups Nos. 191, 192, 193 and 194. Rotation of the crystal to test the extinction rule for $hh2\bar{h}l$ reflections with l odd (Goodman & Whitfield, 1980) establishes No. 194 ($P6_3/mmc$) as the space group.

Comment: These examples show two different methods for testing for centrosymmetry. The $\pm H$ test places certain requirements on the specimen, namely that it be reasonably accurately parallel-sided – a condition usually met by easy-cleavage materials like GaS, though not necessarily by the wedge-shaped refractory Si_3N_4 crystals. On the other hand, the 90° setting, required for direct observation of a possible perpendicular mirror plane, is readily available in these fractured samples, but not for the natural cleavage samples.

(2) *Point-group determination in the cubic system, using Table 2.5.3.3*. Fig. 2.5.3.5 shows [001] (cyclic) zone-axis patterns from two cubic materials, which serve to illustrate the ability to distinguish cubic point groups from single zone-axis patterns displaying detailed central-beam structures. The left-hand pattern, from the mineral gahnite (Ishizuka & Taftø, 1982) has 4*mm* symmetry in *both* the whole pattern and the central (bright-field) beam, permitting only the BESR group $4mm1_R$ for the cubic system (column III, Table 2.5.3.3); this same observation establishes the crystallographic point group as $m3m$ (column V of Table 2.5.3.3). The corresponding pattern for the χ-phase precipitate of stainless steel (Steeds & Evans, 1980) has a whole-pattern symmetry of only 2*mm*, lower than the central-beam (bright-field) symmetry of 4*mm* (this lower symmetry is made clearest from the innermost reflections bordering the central beam). This combination leads to the BESR group 4_Rmm_R (column III, Table 2.5.3.3), and identifies the cubic point group as $\bar{4}3m$.

(3) *Analysis of data from FeS_2 illustrating use of Tables 2.5.3.4 and 2.5.3.5*. FeS_2 has a cubic structure for which a complete set of data has been obtained by Tanaka *et al*. (1983); the quality of the data makes it a textbook example (Tanaka & Terauchi, 1985) for demonstrating the interpretation of extinction bands.

Figs. 2.5.3.6(*a*) and (*b*) show the [001] (cyclic) exact zone-axis pattern and the pattern with symmetrical excitation of the 100 reflection, respectively (Tanaka *et al.*, 1983).

(i) Using Table 2.5.3.4, since there are GS bands, the pattern group must be listed in column II(ii); since a horizontal '*b*' glide plane is present (odd rows are absent in the b^* direction), the symbol must contain a 'b'' (or 'a'') (*cf.* Fig. 2.5.3.3). The only possible cubic group from Table 2.5.3.4 is No. 205.

(ii) Again, a complete GS cross, with both *G* and *S* arms, is present in the 100 reflection (central in Fig. 2.5.3.6*b*), confirmed by mirror symmetries across the *G* and *S* lines. From Table 2.5.3.5 only space group No. 205 has the corresponding entry in the column for '[100] cyclic' with *GS* in the cubic system (space groups Nos. 198–230). Additional patterns for the [110] setting, appearing in the original paper (Tanaka *et al.*, 1983), confirm the cubic system, and also give additional extinction characteristics for 001 and $1\bar{1}0$ reflections (Tanaka *et al.*, 1983; Tanaka & Terauchi, 1985).

(4) *Determination of centrosymmetry and space group from extinction characteristics*. Especially in working with thin crystals used in conjunction with high-resolution lattice imaging, it is sometimes most practical to determine the point group (*i.e.* space-group class) from the dynamic extinction data. This is exemplified in the Moodie & Whitfield (1984) studies of orthorhombic materials. Observations on the zero-layer pattern for Ge_3SbSe_3 with a point symmetry of 2*mm*, and with GS extinction bands along odd-order *h*00 reflections, together with missing reflection rows in the 0*k*0 direction, permit identification from Table 2.5.3.4. This zone-axis pattern has the characteristics illustrated in Figs. 2.5.3.3 and hence (having both missing rows and GS bands) should be listed in both II(ii) and II(iii). Hence the diffraction group must be either No. 40 or 41. Here, the class *mmm*, and hence centrosymmetry, has been identified through non-symmorphic elements.

This identification leaves seven possible space groups, Nos. 52, 54, 56, 57, 60, 61 and 62, to be distinguished by *hkl* extinctions.

The same groups are identified from Table 2.5.3.5 by seeking the entry *GS* '−' in one of the [001] (cyclic) entries for the orthorhombic systems. With the assumption that no other principal zone axis is readily available from the same sample (which will generally be true), Table 2.5.3.5, in the last three columns, indicates which *minor* zone axes should be sought in order to identify the space group, from the glide-plane extinctions of '*G*' bands. For example, space group 62 has no *h*0*l* extinctions, but will give 0*kl* extinction bands '*G*' according to the rules for an '*n*' glide, *i.e.* in reflections for which $k + l = 2n + 1$. Again, if the alternative principal settings *are* available (from the alternative cleavages of the sample) the correct space group can be found from the first three columns of Table 2.5.3.5.

From the above discussions it will be clear that Tables 2.5.3.4 and 2.5.3.5 present information in a complementary way: in Table 2.5.3.4 the specific pattern group is indexed first with the possible space groups following, while in Table 2.5.3.5 the space group is indexed first, and the possible pattern symmetries are then given, in terms of the standard *International Tables* setting.

2.5.3.6. *Use of CBED in study of crystal defects, twins and non-classical crystallography*

(i) Certain crystal defects lend themselves to analysis by CBED and LACBED. In earlier work, use was made of the high sensitivity

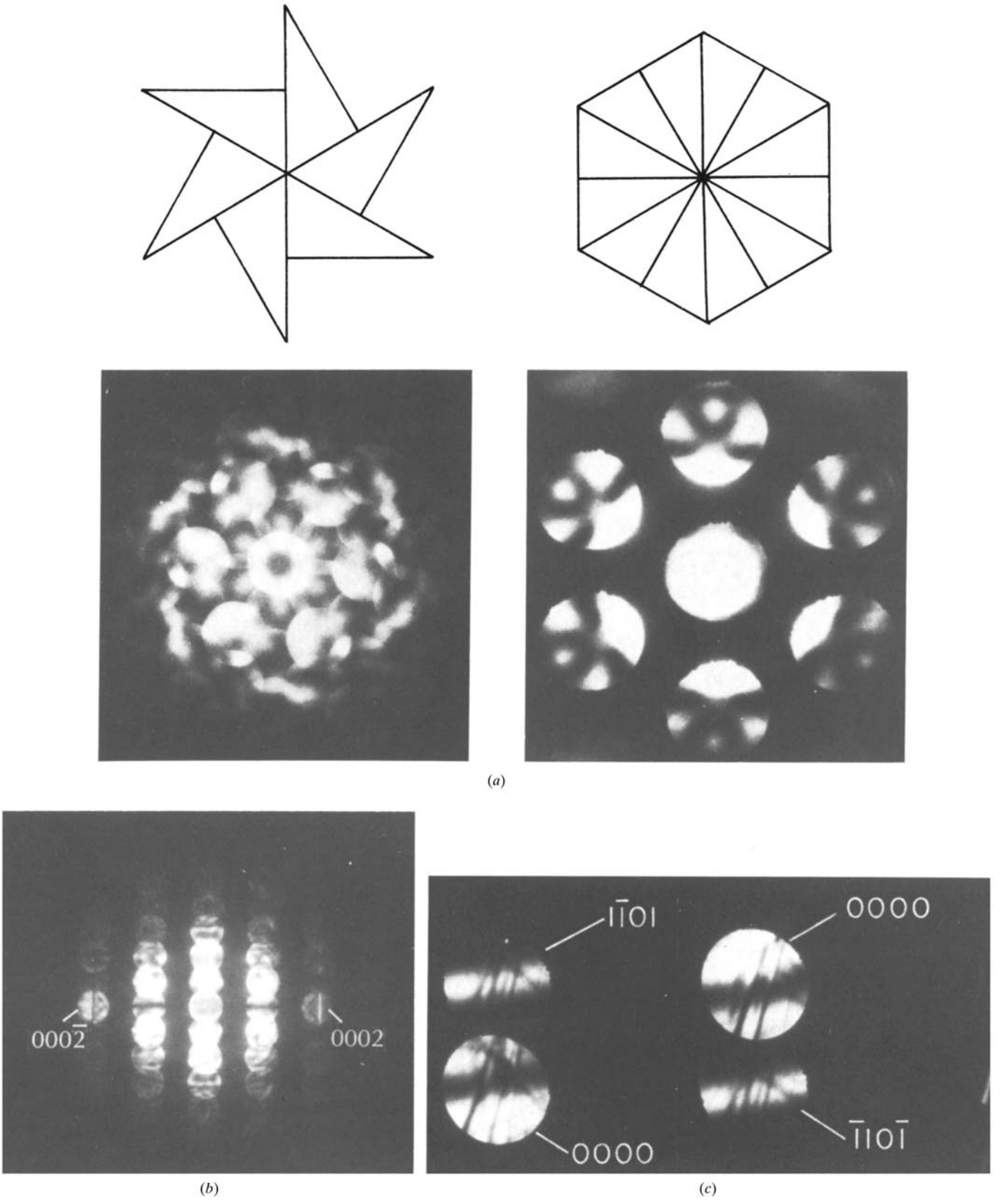

Fig. 2.5.3.4. (*a*) Zone-axis patterns from hexagonal structures β-Si_3N_4 (left) and β-GaS (right) together with the appropriate planar figures for point symmetries 6 and 6*mm*, respectively. (*b*) $[12\bar{1}0]$ zone-axis pattern from β-Si_3N_4, showing Friedel's law breakdown in symmetry between 0002 and $000\bar{2}$ reflections (Bando, 1981). (*c*) Conjugate pair of $1\bar{1}01/\bar{1}101$ patterns from β-GaS, taken near the $[1102]$ zone axis, showing a translational symmetry associated with structural centrosymmetry.

of HOLZ line geometry to unit-cell parameters (Jones *et al.*, 1977). A computer program (Tanaka & Terauchi, 1985) is available for simulating relative line positions from lattice geometry, assuming kinematical scattering, which at least provides a valid starting point since these spacings are mainly determined from geometric considerations. Fraser *et al.* (1985), for example, obtained a sensitivity of 0.03% in measurements of cubic-to-tetragonal distortions in this way, although the absolute accuracy was not established.

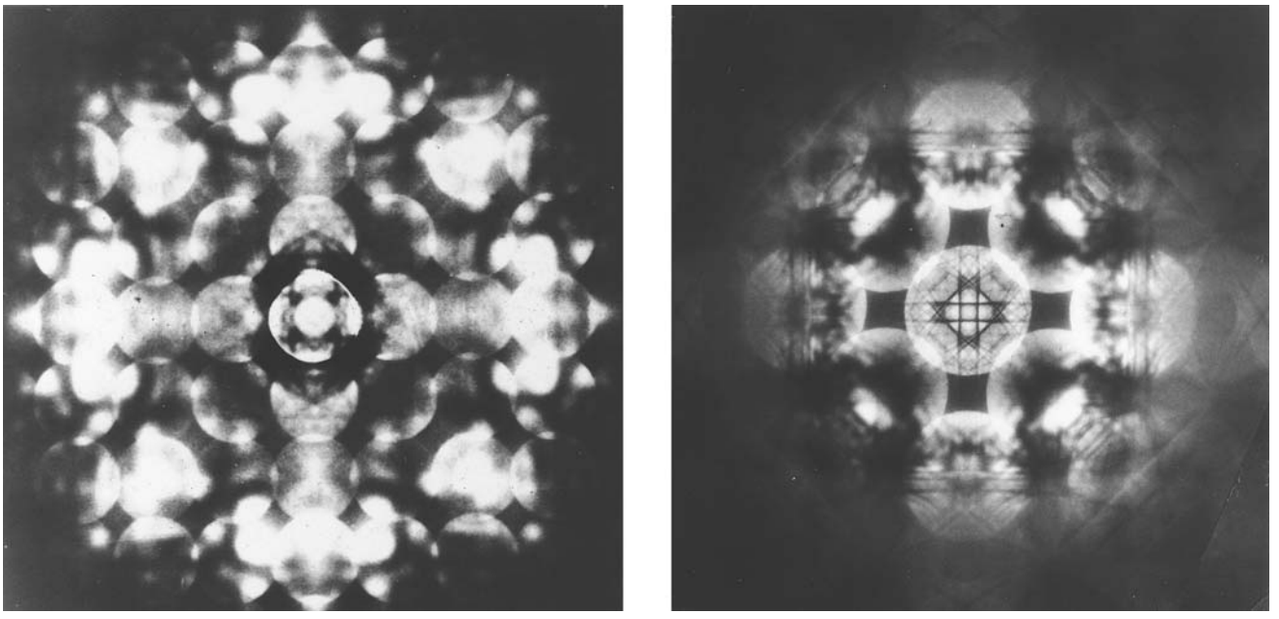

Fig. 2.5.3.5. Zone-axis patterns from cubic structures gahnite (left) (Ishizuka & Taftø, 1982) and χ-phase precipitate (right) (Steeds & Evans, 1980).

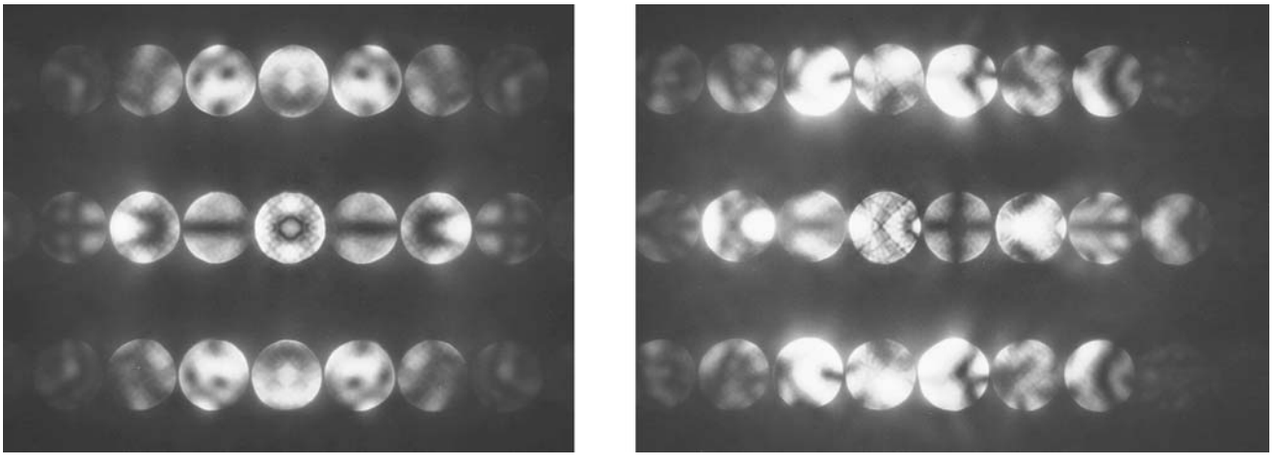

Fig. 2.5.3.6. (*a*) CBED pattern from the exact [001] (cyclic) zone-axis orientation of FeS_2. (*b*) Pattern from the [001] zone axis oriented for symmetrical excitation of the 100 reflection (central in the printed pattern) [from the collection of patterns presented in Tanaka *et al.* (1983); originals kindly supplied by M. Tanaka].

(ii) By contrast, techniques have been devised for evaluating Bragg-line splitting caused by the action of a strain field within the single crystal. One method depends upon the observation of splitting in HOLZ lines (Carpenter & Spence, 1982). More recently, the use of LACBED has allowed quantitative evaluation of lattice distortions in semiconductor heterostructures (*e.g.* containing GaAs–InGaAs interfaces). This technique has been reviewed by Chou *et al.* (1994).

(iii) Quite distinct from this is the analysis of stacking faults between undistorted crystal domains (Johnson, 1972). Coherent twin boundaries with at least a two-dimensional coincidence site lattice can be considered in a similar fashion (Schapink *et al.*, 1983). In marked contrast to electron-microscopy image analysis these boundaries need to be parallel (or nearly so) to the crystal surfaces rather than inclined or perpendicular to them for analysis by CBED or LACBED.

The term 'rigid-body displacement' (RBD) is used when it is assumed that no strain field develops at the boundary. A classification of the corresponding bi-crystal symmetries was developed by Schapink *et al.* (1983) for these cases. Since experimental characterization of grain boundaries is of interest in metallurgy, this represents a new area for the application of LACBED and algorithms invoking reciprocity now make routine *N*-beam analysis feasible.

The original investigations, of a mid-plane stacking fault in graphite (Johnson, 1972) and of a mid-plane twin boundary in gold (Schapink *et al.*, 1983), represent classic examples of the influence of bi-crystal symmetry on CBED zone-axis patterns, whereby the changed central-plane symmetry is transformed through reciprocity into an exact diffraction symmetry. (*a*) In the graphite ($P6_3/mmc$) example, the hexagonal pattern of the unfaulted graphite is replaced by a trigonal pattern with mid-plane faulting. Here a mirror plane at

the centre of the perfect crystal (*A–B–A* stacking) is replaced by an inversion centre at the midpoint of the single rhombohedral cell *A–B–C*; the projected symmetry is also reduced from hexagonal to trigonal: both whole pattern and central beam then have the symmetry of $3m1$. The $2H$ polytype of TaS_2 ($P6_3/mmc$) (Tanaka & Terauchi, 1985) gives a second clear example. (*b*) In the case of a [111] gold crystal, sectioning the f.c.c. structure parallel to [111] preparatory to producing the twin already reduces the finite crystal symmetry to $R\bar{3}m$, *i.e.* a trigonal space group for which the central beam, and the HOLZ reflections in particular, exhibit the trigonal symmetry of $31m$ (rather than the $3m1$ of trigonal graphite). A central-plane twin boundary with no associated translation introduces a central horizontal mirror plane into the crystal. For the zone-axis pattern the only symmetry change will be in the central beam, which will become centrosymmetric, increasing its symmetry to $6mm$. Using diffraction-group terminology these cases are seen to be relative inverses. Unfaulted graphite has the BESR group $6mm1_R$ (central beam and whole pattern hexagonal); central-plane faulting results in a change to the group 6_Rmm_R. Unfaulted [111] gold correspondingly has the BESR group symmetry 6_Rmm_R; central-plane twinning results in the addition of the element 1_R (for a central mirror plane), leading to the group $6mm1_R$.

(iv) Finally, no present-day discussion of electron-crystallographic investigations of symmetry could be complete without reference to two aspects of non-classical symmetries widely discussed in the literature in recent years. The recent discovery of noncrystallographic point symmetries in certain alloys (Shechtman *et al.*, 1984) has led to the study of quasi-crystallinity. An excellent record of the experimental side of this subject may be found in the book *Convergent-beam electron diffraction III* by Tanaka *et al.* (1994), while the appropriate space-group theory has been developed by Mermin (1992). It would be inappropriate to comment further on this new subject here other than to state that this is clearly an area of study where combined HREM, CBED and selected-area diffraction (SAD) evidence is vital to structural elucidation.

The other relatively new topic is that of modulated structures. From experimental evidence, two distinct structural phenomena can be distinguished for structures exhibiting incommensurate superlattice reflections. Firstly, there are 'Vernier' phases, which exist within certain composition ranges of solid solutions and are composed of two extensive substructures, for which the superspace-group nomenclature developed by de Wolff *et al.* (1981) is structurally valid (*e.g.* Withers *et al.*, 1993). Secondly, there are structures essentially composed of random mixtures of two or more substructures existing as microdomains within the whole crystal (*e.g.* Grzinic, 1985). Here the SAD patterns will contain superlattice reflections with characteristic profiles and/or irregularities of spacings. A well illustrated review of incommensurate-structure analysis in general is given in the book by Tanaka *et al.* (1994), while specific discussions of this topic are given by Goodman *et al.* (1992), and Goodman & Miller (1993).

2.5.3.7. *Present limitations and general conclusions*

The list of examples given here must necessarily be regarded as unsatisfactory considering the vastness of the subject, although some attempt has been made to choose a diverse range of problems which will illustrate the principles involved. Some particular aspects, however, need further mention.

One of these concerns the problem of examining large-unit-cell materials with a high diffraction-pattern density. This limits the possible convergence angle, if overlap is to be avoided, and leaves numerous but featureless discs [for example Goodman (1984*b*)]. Technical advances which have been made to overcome this problem include the beam-rocking technique (Eades, 1980) and LACBED (Tanaka *et al.*, 1980), both of which are reviewed by Tanaka & Terauchi (1985) and Eades *et al.* (1983). The disadvantage of these latter methods is that they both require a significantly larger area of specimen than does the conventional technique, and it may be that more sophisticated methods of handling the crowded conventional patterns are still needed.

Next, the matter of accuracy must be considered. There are two aspects of the subject where this is of concern. Firstly, there is a very definite limit to the sensitivity with which symmetry can be detected. In a simple structure of medium-light atoms, displacements of say 0.1 Å or less from a pseudomirror plane could easily be overlooked. An important aspect of CBED analysis, not mentioned above, is the *N*-beam computation of patterns which is required when something approaching a refinement (in the context of electron diffraction) is being attempted. Although this quantitative aspect has a long history [for example see Johnson (1972)], it has only recently been incorporated into symmetry studies as a routine (Creek & Spargo, 1985; Tanaka, 1994). Multi-slice programs which have been developed to produce computer-simulated pattern output are available (Section 2.5.3.8).

Next there is concern as to the allocation of a space group to structures which microscopically have a much lower symmetry (Goodman *et al.*, 1984). This arises because the volume sampled by the electron probe necessarily contains a large number of unit cells. Reliable microscopic interpretation of certain nonstoichiometric materials requires that investigations be accompanied by high-resolution microscopy. Frequently (especially in mineralogical samples), nonstoichiometry implies that a space group exists only on average, and that the concept of absolute symmetry elements is inapplicable.

From earlier and concluding remarks it will be clear that combined X-ray/CBED and CBED/electron-microscopy studies of inorganic materials represents the standard ideal approach to space-group analysis at present; given this approach, all the space-group problems of classical crystallography appear soluble. As has been noted earlier, it is important that HREM be considered jointly with CBED in determining space group by electron crystallography, and that only by this joint study can the so-called 'phase problem' be completely overcome. The example of the space-group pairs $I222/I2_12_12_1$ and $I23/I2_13$ has already been cited. Using CBED, it might be expected that FOLZ lines would show a break from twofold symmetry with the incident beam aligned with a 2_1 axis. However, a direct distinction should be made apparent from high-resolution electron micrographs. Other less clear-cut cases occur where the HREM images allow a space-group distinction to be made between possible space groups of the same arithmetic class, especially when only one morphology is readily obtained (*e.g.* $P222_1$, $P22_12_1$, $P2_12_12_1$).

The slightly more subtle problem of distinguishing enantiomorphic space-group pairs can be solved by one of two approaches: either the crystal must be rotated around an axis by a known amount to obtain two projections, or the required three-dimensional phase information can be deduced from specific three-beam-interaction data. This problem is part of the more general problem of solving handedness in an asymmetric structure, and is discussed in detail by Johnson & Preston (1994).

2.5.3.8. *Computer programs available*

(1) A FORTRAN source listing of program *TCBED* for simulating three-dimensional convergent-beam patterns with absorption by the Bloch-wave method: Zuo *et al.* (1989) [see also *Electron microdiffraction* (Spence & Zuo, 1992) for other useful programs and worked examples for the analysis of these diffraction

(*continued on page* 306)

Table 2.5.3.4. *Tabulation of principal-axis CBED pattern symmetries against relevant space groups given as IT A numbers*

Three columns of diperiodic groups (central section) correspond to (i) symmorphic groups, (ii) non-symmorphic groups (GS bands) and (iii) non-symmorphic groups (zero-layer absences arising from horizontal glide planes). Cubic space groups are given underlined in the right-hand section with the code: underlining = [001](cyclic) setting; italics + underlining = [110](cyclic) setting. Separators ';' and ':' indicate change of Bravais lattice type and change of crystal system, respectively.

	I Point groups		II Diperiodic groups				III Space groups
DG	H–M	BESR	(i)	(ii)	(iii)	SG	Subgroups II*b* (Subgroups 1)
Oblique						Triclinic	
1	1	1	$p1$			1	
2*	$\bar{1}$	2_R	$p\bar{1}'$			2	
						Monoclinic (Oblique)	
3	12	2	$p2$			3	4, 5
4	$1m$	1_R	pm'			6	8
5	$1m$				pb'	7	9
6*	$2/m$	21_R	$p2/m'$			10	11, 12
7*	$2/m$	21_R			$p2/b'$	13	14, 15
Rectangular						(Rectangular)	
8	21	m_R	$p2'$			3	5^2: *195*; *197*, *199*
9	21	m_R		$p2_1'$		4	*198*
10	21	m_R	$c2'$			5	*196*
11	$m1$	m	pm			6^2	7, 8^2
12	$m1$	m		pa		7^2	9^2
13	$m1$	m	cm			8	9
14*	$12/m$	2_Rmm_R	$p2'/m$			10	13, 12^2: *200*, *201*; *204*
15*	$12/m$	2_Rmm_R		$p2_1'/m$		11	14
16*	$12/m$	2_Rmm_R		$p2'/a$		13^2	15^2: *206*
17*	$12/m$	2_Rmm_R		$p2_1'/m$		14^2	*205*
18*	$12/m$	2_Rmm_R	$c2'/m$			12	15: *202*, *203*
						Orthorhombic	
19	222	$2m_Rm_R$	$p2'2'2$			16	17; 21^2; 22: 195; 196, *207*, *206*; *211*, *214*
20	222	$2m_Rm_R$		$p2_1'2'2$		17^2	18^2; 20^2: *212*, *213*
21	222	$2m_Rm_R$		$p2_1'2_1'2$		18	19: 198
22	222	$2m_Rm_R$	$c2'2'2$			21	20; 23, 24: 197, 199, *209*, *210*
23	$mm2$	$2mm$	$pmm2$			25	26, 27; 38, 39; 42
24	$mm2$	$2mm$		$pbm2$		28	29, 30, 31^2; 40, 41
25	$mm2$	$2mm$		$pba2$		32	33, 34; 43
26	$mm2$	$2mm$	$cmm2$			35	36, 37; 44, 45, 46
27	$mm2$	$m1_R$	$p2'mm'$			25^2	28^1; 35^2, 42^2; 38^2, 39^2: *215*; *217*
28	$mm2$	$m1_R$		$p2_1'm'a$		26^1	31^1; 36^1
29	$mm2$	$m1_R$		$p2_1'ab'$	$(p2_1'ab')$	29^2	33^2
30	$mm2$	$m1_R$			$p2_1'ma'$	26^2	29^1; 36^2
31	$mm2$	$m1_R$			$p2_1'mn'$	31^2	33^2
32	$mm2$	$m1_R$			$p2'mb'$	28^2	32^2, 40^2, 41^2
33	$mm2$	$m1_R$			$p2'aa'$	27^2	30^2; 37^2
34	$mm2$	$m1_R$			$pb2'n'$	30^1	34^2; 43^2: *218*; *219*
35	$mm2$	$m1_R$	$c2'mm'$			38^1	40^1; 44^2, 46^1: *216*; *220*
36	$mm2$	$m1_R$			$c2'mb'$	39^1	41^1; 45^2, 46^2
37*	mmm	$2mm1_R$	$pmmm'$			47	49, 51^1; 65^2, 67^2; 69: *200*; *202*, *221*, *224*, *226*, *228*, *229*
38*	mmm	$2mm1_R$		$pbmm'$ $(2_1')$		51^2	53^1, 57, 59^2; 63^1, 64^1
39*	mmm	$2mm1_R$		$pbam'$ $(2_1'2_1')$		55	58, 62^2
40*	mmm	$2mm1_R$		$pmab'$ $(2_1'2_1')$	$(pmab')$	57^1	60^2, 61, 62: 205
41*	mmm	$2mm1_R$		$pbaa'$ $(2_1')$	$(pbaa')$	54^2	52, 56^2, 60^1

Table 2.5.3.4. *Tabulation of principal-axis CBED pattern symmetries against relevant space groups given as IT A numbers* (*cont.*)

	I Point groups		II Diperiodic groups				III Space groups
DG	H–M	BESR	(i)	(ii)	(iii)	SG	Subgroups II*b* (Subgroups 1)
42*	*mmm*	$2mm1_R$			$pmma'$ $(2'_1)$	51	54, 55^2, 57^2; 63^2, 64^2
43*	*mmm*	$2mm1_R$			$pmmn'$ $(2'_12'_1)$	59	56, 62^1
44*	*mmm*	$2mm1_R$			$pbmn'$ $(2'_1)$	53^2	52^1, 58^1, 60
45*	*mmm*	$2mm1_R$			$pmaa'$	49^2	50^2, 53, 54^1; 66^2, 68^1: 222, 223
46*	*mmm*	$2mm1_R$			$pban'$	50	52^2, 48; 70: 201; 203, 230
47*	*mmm*	$2mm1_R$	$cmmm'$			65	63, 66; 72, 74^2, 71: 204, 225, 227
48*	*mmm*	$2mm1_R$			$cmma'$	67	64, 68; 72^1, 74, 73: 206
Square						Tetragonal	
49	4	4	$p4$			75	77, 76, 78; 79, 80
50	$4/m$	41_R	$p4/m'$			83	84; 87
51	$4/m$	41_R			$p4/n'$	85	86, 88
52	422	$4m_Rm_R$	$p42'2'$			89	93, 91, 95; 97, 98: 207, 208; 209, 210; 211, 214
53	422	$4m_Rm_R$		$p42'_12'$		90	94, 92, 96: 212, 213
54	$4mm$	$4mm$	$p4mm$			99	101, 103, 105; 107, 108
55	$4mm$	$4mm$		$p4bm$		100	102, 104, 106; 109, 110
56*	$4/mmm$	$4mm1_R$	$p4/m'mm$			123	124, 131, 132; 139, 140; 221, 223; 225, 226; 229
57*	$4/mmm$	$4mm1_R$		$p4/m'bm$ $(2'_1)$		127	128, 135, 136
58*	$4/mmm$	$4mm1_R$			$p4/n'bm$	125	126, 133, 134; 141, 142: 222, 224; 227, 228; 230
59*	$4/mmm$	$4mm1_R$			$p4/n'mm$ $(2'_1)$	129	130, 137, 138
60	$\bar{4}$	4_R	$p\bar{4}'$			81	82
61	$\bar{4}2m$	4_Rmm_R	$p\bar{4}'m\bar{2}'$			115	116; 119, 120
62	$\bar{4}2m$	4_Rmm_R		$p\bar{4}b2'$		117	118; 122: 220
63	$\bar{4}2m$	4_Rmm_R	$p\bar{4}'2'm$			111	112; 121: 215; 216; 217; 218; 219
64	$\bar{4}2m$	4_Rmm_R		$p4'2'_1m$		113	114
Hexagonal						Trigonal	
65	3	3	$p3$			143	144, 145; 146
66	$\bar{3}$	6_R	$p\bar{3}'$			147	148
67	32	$3m_R$	$p312'$			149	151, 153
68	32	$3m_R$	$p32'1$			150	152, 154; 155
69	$3m$	$3m$	$p31m$			157	159
70	$3m$	$3m$	$p3m1$			156	158; 160, 161
71*	$\bar{3}m$	6_Rmm_R	$p\bar{3}'1m$			162	163
72*	$\bar{3}m$	6_Rmm_R	$p\bar{3}'m1$			164	165; 166, 167
						Hexagonal	
73	6	6	$p6$			168	171, 172, 173, 169, 170
74	$\bar{6}$	31_R	$p3/m'$ $(p\bar{6}')$			174	
75	622	$6m_Rm_R$	$p62'2'$			177	180, 181, 182, 178, 179
76	$6mm$	$6mm$	$p6mm$			183	184, 185, 186
77*	$6/m$	61_R	$p6/m'$			175	176
78*	$6/mmm$	$6mm1_R$	$p6/m'mm$			191	192, 193, 194
79	$\bar{6}m2$	$3m1_R$	$p3/m'2'm$ $(p\bar{6}'m2')$			189	190
80	$\bar{6}m2$	$3m1_R$	$p3/m'm2'$ $(p\bar{6}'2'm)$			187	188

Table 2.5.3.5. *Conditions for observation of GS bands for the 137 space groups exhibiting these extinctions*

Point groups 2, *m*, 2/*m* (2nd setting unique axis $\|b$)

Space group		Incident-beam direction [$u0w$]
4	$P2_1$	$0k0$ 2_1 S
7	Pc	$h0l$ c G
9	Cc	$h0l$ c G
11	$P2_1/m$	$0k0$ 2_1 S
13	$P2/c$	$h0l$ c G
14	$P2_1/c$	$0k0$ 2_1 S $h0l$ c G
15	$C2/c$	$h0l$ c G

Point groups 222, *mm*2

Space group		Incident-beam direction					
		[100]	[010]	[001]	[$uv0$]	[$0vw$]	[$u0w$]
17	$P222_1$	$00l$ 2_1 S	$00l$ 2_1 S		$00l$ 2_1 S		
18	$P2_12_12$	$0k0$ 2_1 S	$h00$ 2_1 S	$h00$, $0k0$ 2_1 S		$h00$ 2_1 S	$0k0$ 2_1 S
19	$P2_12_12_1$	$0k0$, $00l$ 2_1 S	$h00$, $00l$ 2_1 S	$h00$, $0k0$ 2_1 S	$00l$ 2_1 S	$h00$ 2_1 S	$0k0$ 2_1 S
20	$C222_1$	$00l$ 2_1 S	$00l$ 2_1 S		$00l$ 2_1 S		
26	$Pmc2_1$	$00l$ $c+2_1$ GS	$00l$ 2_1 $c'-$		$00l$ 2_1 S		$h0l$ c G
27	$Pcc2$	$00l$ c $c'-$	$00l$ c $c'-$			$0kl$ c G	$h0l$ c G
28	$Pma2$			$h00$ a G			$h0l$ a G
29	$Pca2_1$	$00l$ 2_1 $c'-$	$00l$ $c+2_1$ GS	$h00$ a G	$00l$ 2_1 S	$0kl$ c G	$h0l$ a G
30	$Pnc2$	$00l$ c $n'-$	$00l$ n $c'-$	$0k0$ n G		$0kl$ n G	$h0l$ c G
31	$Pmn2_1$	$00l$ $n+2_1$ GS	$00l$ 2_1 $n'-$	$h00$ n G	$00l$ 2_1 S		$h0l$ n G
32	$Pba2$			$h00$, $0k0$ a b G		$0kl$ b G	$h0l$ a G

Table 2.5.3.5. *Conditions for observation of GS bands for the 137 space groups exhibiting these extinctions* (*cont.*)

Space group		Incident-beam direction					
		[100]	[010]	[001]	[uv0]	[0vw]	[u0w]
33	$Pna2_1$	00l 2_1 $n'-$	00l $n+2_1$ GS	h00, 0k0 a b G	00l 2_1 S	0kl n G	h0l a G
34	$Pnn2$	00l n $n'-$	00l n $n'-$	h00, 0k0 n G		0kl n G	h0l n G
36	$Cmc2_1$	00l $c+2_1$ GS	00l 2_1 $c'-$		00l 2_1 S		h0l c G
37	$Ccc2$	00l c $c'-$	00l c $c'-$			0kl c G	h0l c G
39	$Abm2$					0kl b G	
40	$Ama2$			h00 a G			h0l a G
41	$Aba2$			h00 a G		0kl b G	h0l a G
43	$Fdd2$	00l $d'-$	00l d $d'-$	h00, 0k0 d G		0kl d G	h0l d G
45	$Iba2$	$b'-$	$a'-$			0kl b G	h0l a G
46	$Ima2$		$a'-$				h0l a G

Point group *mmm*

Space group		Incident-beam direction					
		[100]	[010]	[001]	[uv0]	[0vw]	[u0w]
48	$P\,2/n\,2/n\,2/n$	00l, 0k0 n $n'-$	00l, h00 n $n'-$	0k0, h00 n $n'-$	hk0 n G	0kl n G	h0l n G
49	$P\,2/c\,2/c\,2/m$	00l c $c'-$	00l c $c'-$			0kl c G	h0l c G
50	$P\,2/b\,2/a\,2/n$	0k0 n $b'-$	h00 n $a'-$	0k0, h00 b a $n'-$	hk0 n G	0kl b G	h0l a G
51	$P\,2_1/m\,2/m\,2/a$		h00 $a+2_1$ GS	h00 2_1 $a'-$	hk0 a G	h00 2_1 S	
52	$P\,2/n\,2_1/n\,2/a$	00l, 0k0 n 2_1 $a'-$	00l, h00 n a $n'-$	0k0 $n+2_1$ GS h00 n $n'-$	hk0 a G	0kl n G	h0l n G 0k0 2_1 S
53	$P\,2/m\,2/n\,2_1/a$	00l $n+2_1$ GS	h00, 00l a 2_1 $a'-$	h00 n $a'-$	hk0 a G 00l 2_1 S		h0l n G

Table 2.5.3.5. *Conditions for observation of GS bands for the 137 space groups exhibiting these extinctions* (*cont.*)

Space group		Incident-beam direction					
		[100]	[010]	[001]	[*uv*0]	[0*vw*]	[*u*0*w*]
54	$P\,2_1/c\,2/c\,2/a$	$00l$ c $c'-$	$h00$ $a+2_1$ *GS* $00l$ c $c'-$	$h00$ 2_1 $a'-$	$hk0$ a *G*	$0kl$ c *G* $h00$ 2_1 *S*	$h0l$ c *G*
55	$P\,2_1/b\,2_1/a\,2/m$	$0k0$ 2_1 $b'-$	$h00$ 2_1 $a'-$	$0k0, h00$ $b+2_1, a+2_1$ *GS*		$0kl$ b *G* $h00$ 2_1 *S*	$h0l$ a *G* $0k0$ 2_1 *S*
56	$P\,2_1/c\,2_1/c\,2/n$	$0k0$ $n+2_1$ *GS* $00l$ c $c'-$	$h00$ $n+2_1$ *GS* $00l$ c $c'-$	$0k0, h00$ 2_1 $n'-$	$hk0$ n *G*	$0kl$ c *G* $h00$ 2_1 *S*	$h0l$ c *G* $0k0$ 2_1 *S*
57	$P\,2/b\,2_1/c\,2_1/m$	$00l$ $c+2_1$ *GS* $0k0$ 2_1 $b'-$	$00l$ 2_1 $c'-$	$0k0$ $b+2_1$ *GS*	$00l$ 2_1 *S*	$0kl$ b *G*	$h0l$ c *G* $0k0$ 2_1 *S*
58	$P\,2_1/n\,2_1/n\,2/m$	$00l, 0k0$ $n\quad 2_1$ $n'-$	$00l, h00$ $n\quad 2_1$ $n'-$	$0k0, h00$ $n+2_1$ *GS*		$0kl$ n *G* $h00$ 2_1 *S*	$h0l$ n *G* $0k0$ 2_1 *S*
59	$P\,2_1/m\,2_1/m\,2/n$	$0k0$ $n+2_1$ *GS*	$h00$ $n+2_1$ *GS*	$0k0, h00$ 2_1 $n'-$	$hk0$ n *G*	$h00$ 2_1 *S*	$0k0$ 2_1 *S*
60	$P\,2_1/b\,2/c\,2_1/n$	$00l$ $c+2_1$ *GS* $0k0$ n $b'-$	$h00$ $n+2_1$ *GS* $00l$ 2_1 $c'-$	$0k0, h00$ $b\quad 2_1$ $n'-$	$hk0$ n *G* $00l$ 2_1 *S*	$0kl$ b *G* $h00$ 2_1 *S*	$h0l$ c *G*
61	$P\,2_1/b\,2_1/c\,2_1/a$	$00l$ $c+2_1$ *GS* $0k0$ 2_1 $b'-$	$h00$ $a+2_1$ *GS* $00l$ 2_1 $c'-$	$0k0$ $b+2_1$ *GS* $h00$ 2_1 $a'-$	$hk0$ a *G* $00l$ 2_1 *S*	$0kl$ b *G* $h00$ 2_1 *S*	$h0l$ c *G* $0k0$ 2_1 *S*
62	$P\,2_1/n\,2_1/m\,2_1/a$	$0k0, 00l$ 2_1 $n'-$	$00l$ $n+2_1$ *GS* $h00$ $a+2_1$	$0k0$ $n+2_1$ *GS* $h00$ 2_1 $a'-$	$hk0$ a *G* $00l$ 2_1 *S*	$0kl$ n *G* $h00$ 2_1 *S*	$0k0$ 2_1 *S*
63	$C\,2/m\,2/c\,2_1/m$	$00l$ $c+2_1$ *GS*	$00l$ 2_1 $c'-$		$00l$ 2_1 *S*		$h0l$ c *G*
64	$C\,2/m\,2/c\,2_1/a$	$00l$ $c+2_1$ *GS*	$00l$ 2_1 $c'-$		$hk0$ a *G* $00l$ 2_1 *S*		$h0l$ c *G*
66	$C\,2/c\,2/c\,2/m$	$00l$ c $c'-$	$00l$ c $c'-$			$0kl$ c *G*	$h0l$ c *G*
67	$C\,2/m\,2/m\,2/a$				$hk0$ a *G*		

Table 2.5.3.5. *Conditions for observation of GS bands for the 137 space groups exhibiting these extinctions* (*cont.*)

Space group		Incident-beam direction											
		[100]		[010]		[001]		[*uv*0]		[0*vw*]		[*u*0*w*]	
68	*C* 2/*c* 2/*c* 2/*a*	00*l* *c*	*c*′–	00*l* *c*	*c*′–			*hk*0 *a*	*G*	0*kl* *c*	*G*	*h*0*l* *c*	*G*
70	*F* 2/*d* 2/*d* 2/*d*	00*l*, 0*k*0 *d*	*d*′–	*h*00, 00*l* *d*	*d*′–	0*k*0, *h*00 *d*	*d*′–	*hk*0 *d*	*G*	0*kl* *d*	*G*	*h*0*l* *d*	*G*
72	*I* 2/*b* 2/*a* 2/*m*		*b*′–		*a*′–					0*kl* *b*	*G*	*h*0*l* *a*	*G*
73	*I* 2/*b* 2/*c* 2/*a*		*b*′–		*c*′–		*a*′–	*hk*0 *a*	*G*	0*kl* *b*	*G*	*h*0*l* *c*	*G*
74	*I* 2/*m* 2/*m* 2/*a*							*hk*0 *a*	*G*				

Point groups 4, $\bar{4}$, 4/*m*

Space group		Incident-beam direction	
		[*uv0*]	
76	$P4_1$	00*l* 4_1	*S*
78	$P4_3$	00*l* 4_3	*S*
85	$P4/n$	*hk*0 *n*	*G*
86	$P4_2/n$	*hk*0 *n*	*G*
88	$I4_1/a$	*hk*0 *a*	*G*

Point group 422

Space group		Incident-beam direction			
		[*uv0*]		[0*vw*]	
90	$P42_12$			*h*00 2_1	*S*
91	$P4_122$	00*l* 4_1	*S*		
92	$P4_12_12$	00*l* 4_1	*S*	*h*00 2_1	*S*
94	$P4_22_12$			*h*00 2_1	*S*
95	$P4_322$	00*l* 4_3	*S*		
96	$P4_32_12$	00*l* 4_3	*S*	*h*00 2_1	*S*

Point group 4*mm*

Space group		Incident-beam direction									
		[100]		[001]		[110]		[*u*0*w*] and [0*vw*]*		[*uūw*]	
100	*P*4*bm*			*h*00, 0*k*0 *a* *b*	*G*			*h*0*l*, 0*kl* *a* *b*	*G*		
101	$P4_2cm$	00*l* *c*	*c*′–					*h*0*l*, 0*kl* *c*	*G*		
102	$P4_2nm$	00*l* *n*	*n*′–	*h*00, 0*k*0 *n*	*G*			*h*0*l*, 0*kl* *n*	*G*		
103	*P*4*cc*	00*l* *c*	*c*′–			00*l* *c*	*c*′–	*h*0*l*, 0*kl* *c*	*G*	*hhl* *c*	*G*
104	*P*4*nc*	00*l* *n*	*n*′–	*h*00, 0*k*0 *n*	*G*	00*l* *c*	*c*′–	*h*0*l*, 0*kl* *n*	*G*	*hhl* *c*	*G*
105	$P4_2mc$					00*l* *c*	*c*′–			*hhl* *c*	*G*

Table 2.5.3.5. *Conditions for observation of GS bands for the 137 space groups exhibiting these extinctions* (*cont.*)

Space group	Incident-beam direction				
	[100]	[001]	[110]	[*u*0*w*] and [0*vw*]*	[*uūw*]
106 $P4_2bc$		*h*00, 0*k*0 *a* *b* *G*	00*l* *c* *c*′−	*h*0*l*, 0*kl* *a* *b* *G*	*hhl* *c* *G*
108 $I4cm$				*h*0*l*, 0*kl* *c* *G*	
109 $I3_1md$		*hh*0 $\bar{h}h$0 *G* *d*	00*l* *d* *d*′−		*hhl* *G* *d*
110 $I4_1cd$		*hh*0 $\bar{h}h$0 *G* *d*	00*l* *d* *d*′−	*h*0*l*, 0*kl* *G* *c*	*hhl* *G* *d*

* Conditions in this column are cyclic on *h* and *k*.

Point groups $\bar{4}2m$, 4/*mmm*

Space group	Incident-beam direction					
	[100]	[001]	[110]	[*u*0*w*] and [0*vw*]*	[*uuw*]	[*uv*0]
112 $P\bar{4}2c$			00*l* *c* *c*′−		*hhl* *c* *G*	
113 $P\bar{4}2_1m$	0*k*0 2_1 *S*	*h*00, 0*k*0 2_1 *S*		0*k*0, *h*00 2_1 *S*		
114 $P\bar{4}2_1c$	0*k*0 2_1 *S*	*h*00, 0*k*0 2_1 *S*	00*l* *c* *c*′−	0*k*0, *h*00 2_1 *S*	*hhl* *c* *G*	
116 $P\bar{4}c2$	00*l* *c* *c*′−			*h*0*l*, 0*kl* *c* *G*		
117 $P\bar{4}b2$		*h*00, 0*k*0 *a* *b* *G*		*h*0*l*, 0*kl* *a* *b* *G*		
118 $P\bar{4}n2$	00*l* *n* *n*′−	*h*00, 0*k*0 *n* *G*		*h*0*l*, 0*kl* *n* *G*		
120 $I\bar{4}c2$				*h*0*l*, 0*kl* *c* *G*		
122 $I\bar{4}2d$		*hh*0 $\bar{h}h$0 *G* *d*	00*l* *d* *d*′−		*hhl* *G* *d*	
124 $P\,4/m\,2/c\,2/c$	00*l* *c* *c*′−		00*l* *c* *c*′−	*h*0*l*, 0*kl* *c* *G*	*hhl* *c* *G*	
125 $P\,4/n\,2/b\,2/m$	0*k*0 *n* *b*′−	*h*00, 0*k*0 *a* *b* *n*′−		*h*0*l*, 0*kl* *a* *b* *G*		*hk*0 *n* *G*
126 $P\,4/n\,2/n\,2/c$	0*k*0 *n* 00*l* *n* *n*′−	*h*00, 0*k*0 *n* *n*′−	00*l* *c* *c*′−	*h*0*l*, 0*kl* *n* *G*	*hhl* *c* *G*	*hk*0 *n* *G*
127 $P\,4/m\,2_1/b\,2/m$	0*k*0 2_1 *b*′−	*h*00 $a+2_1$ *GS* 0*k*0 $b+2_1$		*h*0*l*, 0*kl* *a* *b* *G* 0*k*0, *h*00 2_1 *S*		

Table 2.5.3.5. *Conditions for observation of GS bands for the 137 space groups exhibiting these extinctions* (*cont.*)

Space group		Incident-beam direction					
		[100]	[001]	[110]	[$u0w$] and [$0vw$]*	[uuw]	[$uv0$]
128	$P\,4/m\,2_1/n\,2/c$	$00l$, $0k0$ n 2_1 $n'-$	$h00$, $0k0$ $n+2_1$ *GS*	$00l$ c $c'-$	$h0l$, $0kl$ n *G* $0k0$, $h00$ 2_1 *S*	hhl c *G*	
129	$P\,4/n\,2_1/m\,2/m$	$0k0$ $n+2_1$ *GS*	$h00$, $0k0$ 2_1 $n'-$		$0k0$, $h00$ 2_1 *S*		$hk0$ n *G*
130	$P\,4/n\,2_1/c\,2/c$	$0k0$ $n+2_1$ *GS* $00l$ c $c'-$	$h00$, $0k0$ 2_1 $n'-$	$00l$ c $c'-$	$h0l$, $0kl$ c *G* $0k0$, $h00$ 2_1 *S*	hhl c *G*	$hk0$ n *G*
131	$P\,4_2/m\,2/m\,2/c$			$00l$ c $c-$		hhl c *G*	
132	$P\,4_2/m\,2/c\,2/m$	$00l$ c $c'-$			$h0l$, $0kl$ c *G*		
133	$P\,4_2/n\,2/b\,2/c$	$0k0$ n $b'-$	$h00$, $0k0$ a b $n'-$	$00l$ c $c'-$	$h0l$, $0kl$ a b *G*	hhl c *G*	$hk0$ n *G*
134	$P\,4_2/n\,2/n\,2/m$	$0k0$, $00l$ n $n'-$	$h00$, $0k0$ n $n'-$		$h0l$, $0kl$ n *G*		$hk0$ n *G*
135	$P\,4_2/m\,2_1/b\,2/c$	$0k0$ 2_1 $b'-$	$h00$, $0k0$ $a+2_1$ $b+2_1$ *GS*	$00l$ c $c'-$	$h0l$, $0kl$ a b *G* $0k0$, $h00$ 2_1 *S*	hhl c *G*	
136	$P\,4_2/m\,2_1/n\,2/m$	$00l$, $0k0$ n 2 $n'-$	$h00$, $0k0$ $n+2_1$ *GS*		$h0l$, $0kl$ n *G* $0k0$, $h00$ 2_1 *S*		
137	$P\,4_2/n\,2_1/m\,2/c$	$0k0$ $n+2_1$ *GS*	$h00$, $0k0$ 2_1 $n'-$	$00l$ c $c'-$	$0k0$, $h00$ 2_1 *S*	hhl c *G*	$hk0$ n *G*
138	$P\,4_2/n\,2_1/c\,2/m$	$0k0$ $n+2_1$ *GS* $00l$ c $c'-$	$h00$, $0k0$ 2_1 $n'-$		$h0l$, $0kl$ c *G* $0k0$, $h00$ 2_1 *S*		$hk0$ n *G*
140	$I\,4/m\,2/c\,2/m$				$h0l$, $0kl$ c *G*		
141	$I\,4_1/a\,2/m\,2/d$		$hh0$ $\bar{h}h0$ d $a'-$	$00l$, $\bar{h}h0$ d a $d'-$		hhl d *G*	$hk0$ a *G*
142	$I\,4_1/a\,2/c\,2/d$		$hh0$ $\bar{h}h0$ d $a'-$	$00l$, $\bar{h}h0$ d a $d'-$	$h0l$, $0kl$ c *G*	hhl d *G*	$hk0$ a *G*

* Conditions in this column are cyclic on h and k.

Table 2.5.3.5. *Conditions for observation of GS bands for the 137 space groups exhibiting these extinctions* (*cont.*)

Point groups 3*m*, $\bar{3}m$, 6, 6/*m*, 622, 6*mm*, $\bar{6}m2$, 6/*mmm*

Space group		Incident-beam direction			
		[100]	[210]	[2*u u w*]	[*v*0*w*]
158	$P3c1$		$000l$ c G	$hh2\bar{h}l$ c G	
159	$P31c$	$000l$ c G			$h\bar{h}0l$ c G
161	$R3c$		$000l$ $l = 6n + 3$ G c	$hh2\bar{h}l$ G c	
163	$P\bar{3}1c$	$000l$ c G			$h\bar{h}0l$ c G
165	$P\bar{3}c1$		$000l$ c G	$hh2\bar{h}l$ c G	
167	$R\bar{3}c$		$000l$ $l = 6n + 3$ G c	$hh2\bar{h}l$ G c	
169	$P6_1$	$000l$ 6_1 S	$000l$ 6_1 S		
170	$P6_5$	$00l$ 6_5 S	$00l$ 6_5 S		
173	$P6_3$	$000l$ 6_3 S	$000l$ 6_3 S		
176	$P6_3/m$	$000l$ 6_3 S	$000l$ 6_3 S		
178	$P6_122$	$000l$ 6_1 S	$000l$ 6_1 S		
179	$P6_522$	$000l$ 6_5 S	$000l$ 6_5 S		
182	$P6_322$	$000l$ 6_3 S	$000l$ 6_3 S		
184	$P6cc$	$000l$ c $c'-$	$000l$ c $c'-$	$hh2\bar{h}l$ c G	$h\bar{h}0l$ c G
185	$P6_3cm$	$000l$ 6_3 $c'-$	$000l$ $c + 6_3$ GS	$hh2\bar{h}l$ c G	
186	$P6_3mc$	$000l$ $c + 6_3$ GS	$000l$ 6_3 $c'-$		$h\bar{h}0l$ c G
188	$P\bar{6}c2$		$000l$ c G	$hh2\bar{h}l$ c G	
190	$P\bar{6}c2$	$000l$ c G			$h\bar{h}0l$ c G
192	$P6/mcc$	$000l$ c $c'-$	$000l$ c $c'-$	$hh2\bar{h}l$ c G	$h\bar{h}0l$ c G
193	$P6_3/mcm$	$00l$ 6_3 $c'-$	$000l$ $c + 6_3$ GS	$hh2\bar{h}l$ c G	
194	$P6_3/mmc$	$000l$ $c + 6_3$ GS	$000l$ 6_3 $c'-$		$h\bar{h}0l$ c G

Table 2.5.3.5. *Conditions for observation of GS bands for the 137 space groups exhibiting these extinctions* (*cont.*)

Point groups 23, *m*3, 432, *m*3*m*

Space group		Incident-beam direction			
		[100] (cyclic)	[110] (cyclic)	[*uv*0] (cyclic)	[*uuw*] (cyclic)
198	$P2_13$	$00l$, $0k0$ 2_1 S	$00l$ 2_1 S	$00l$ 2_1 S	
201	$Pn\bar{3}$ $P2/n\bar{3}$	$00l$, $0k0$ n $n'-$		$\bar{k}h0$ n G	
203	$Pd\bar{3}$ $F2/d\bar{3}$	$00l$, $0k0$ d $d'-$		$\bar{k}h0$ d G	
205	$Pa\bar{3}$ $P2_1/a\bar{3}$	$00l$ $c+2_1$ GS $0k0$ 2_1 $b'-$	$00l$ 2_1 S $\bar{h}h0$ a G	$00l$ 2_1 S $\bar{k}h0$ a G	
206	$Ia\bar{3}$ $I2_1/a\bar{3}$		$\bar{h}h0$ a G	$\bar{k}h0$ a G	
212	$P4_332$			$00l$ 4_3 S	
213	$P4_132$			$00l$ 4_1 S	
218	$P\bar{4}3n$		$00l$ c $n-$	hhl c G	
219	$F\bar{4}3c$			hhl c G	
220	$I\bar{4}3d$	$0kk$ $0\bar{k}k$ d G	$00l$ d $d-$	hhl d G	
222	$Pn\bar{3}n$	$00l$, $0k0$ n $n'-$	$00l$ c $n-$	$hk0$ n G	hhl c G
223	$Pm\bar{3}n$		$00l$ c $n'-$		hhl c G
224	$Pn\bar{3}m$	$00l$, $0k0$ n $n'-$		$hk0$ n G	
226	$Fm\bar{3}c$				hhl c G
227	$Fd\bar{3}m$	$00l$, $0k0$ d $d'-$		$hk0$ d G	
228	$Fd\bar{3}c$	$00l$, $0k0$ d $d'-$		$hk0$ d G	hhl c G
230	$Ia\bar{3}d$	$0kk$ $0\bar{k}k$ d $b'-$	$00l$, $\bar{h}h0$ $d\quad a$ $d'-$	$hk0$ a G	hhl d G

patterns]. Contact J. M. Zuo or J. C. H. Spence, Physics Department, Arizona State University, Tempe, Arizona, USA.

(2) A package for CBED pattern simulation by both Bloch-wave and multi-slice methods is available from P. Stadelmann (pierre.stadelmann@cime.uhd.edfl.ch), Lausanne, Switzerland, in UNIX for workstations [Silicon Graphics, Dec Alpha (OSF), IBM RISC 6000, SUN and HP-9000].

(3) HOLZ line simulations: Listing for PC 8801 (NEC): Tanaka & Terauchi (1985, pp. 174–175).

2.5.4. Electron-diffraction structure analysis (EDSA)

(B. K. VAINSHTEIN AND B. B. ZVYAGIN)

2.5.4.1. *Introduction*

Electron-diffraction structure analysis (EDSA) (Vainshtein, 1964) based on electron diffraction (Pinsker, 1953) is used for the investigation of the atomic structure of matter together with X-ray and neutron diffraction analysis. The peculiarities of EDSA, as compared with X-ray structure analysis, are defined by a strong interaction of electrons with the substance and by a short wavelength λ. According to the Schrödinger equation (see Section 5.2.2) the electrons are scattered by the electrostatic field of an object. The values of the atomic scattering amplitudes, f_e, are three orders higher than those of X-rays, f_x, and neutrons, f_n. Therefore, a very small quantity of a substance is sufficient to obtain a diffraction pattern. EDSA is used for the investigation of very thin single-crystal films, of ~5–50 nm polycrystalline and textured films, and of deposits of finely grained materials and surface layers of bulk specimens. The structures of many ionic crystals, crystal hydrates and hydro-oxides, various inorganic, organic, semiconducting and metallo-organic compounds, of various minerals, especially layer silicates, and of biological structures have been investigated by means of EDSA; it has also been used in the study of polymers, amorphous solids and liquids.

Special areas of EDSA application are: determination of unit cells; establishing orientational and other geometrical relationships between related crystalline phases; phase analysis on the basis of d_{hkl} and I_{hkl} sets; analysis of the distribution of crystallite dimensions in a specimen and inner strains in crystallites as determined from line profiles; investigation of the surface structure of single crystals; structure analysis of crystals, including atomic position determination; precise determination of lattice potential distribution and chemical bonds between atoms; and investigation of crystals of biological origin in combination with electron microscopy (Vainshtein, 1964; Pinsker, 1953; Zvyagin, 1967; Pinsker *et al.*, 1981; Dorset, 1976; Zvyagin *et al.*, 1979).

There are different kinds of electron diffraction (ED) depending on the experimental conditions: high-energy (HEED) (above 30–200 kV), low-energy (LEED) (10–600 V), transmission (THEED), and reflection (RHEED). In electron-diffraction studies use is made of special apparatus – electron-diffraction cameras in which the lens system located between the electron source and the specimen forms the primary electron beam, and the diffracted beams reach the detector without aberration distortions. In this case, high-resolution electron diffraction (HRED) is obtained. ED patterns may also be observed in electron microscopes by a selected-area method (SAD). Other types of electron diffraction are: MBD (microbeam), HDD (high-dispersion), CBD (convergent-beam), SMBD (scanning-beam) and RMBD (rocking-beam) diffraction (see Sections 2.5.2 and 2.5.3). The recent development of electron diffractometry, based on direct intensity registration and measurement by scanning the diffraction pattern against a fixed detector (scintillator followed by photomultiplier), presents a new improved level of EDSA which provides higher precision and reliability of structural data (Avilov *et al.*, 1999; Tsipursky & Drits, 1977; Zhukhlistov *et al.*, 1997, 1998; Zvyagin *et al.*, 1996).

Electron-diffraction studies of the structure of molecules in vapours and gases is a large special field of research (Vilkov *et al.*, 1978). See also *Stereochemical Applications of Gas-Phase Electron Diffraction* (1988).

2.5.4.2. *The geometry of ED patterns*

In HEED, the electron wavelength λ is about 0.05 Å or less. The Ewald sphere with radius λ^{-1} has a very small curvature and is approximated by a plane. The ED patterns are, therefore, considered as plane cross sections of the reciprocal lattice (RL) passing normal to the incident beam through the point 000, to scale $L\lambda$ (Fig. 2.5.4.1). The basic formula is

$$r = |\mathbf{h}|L\lambda, \text{ or } rd = L\lambda, \qquad (2.5.4.1)$$

where r is the distance from the pattern centre to the reflection, $\mathbf{h}$ is the reciprocal-space vector, d is the appropriate interplanar distance and L is the specimen-to-screen distance. The deviation of the Ewald sphere from a plane at distance h from the origin of the coordinates is $\delta_h = h^2\lambda/2$. Owing to the small values of λ and to the rapid decrease of f_e depending on $(\sin\theta)/\lambda$, the diffracted beams are concentrated in a small angular interval (≤ 0.1 rad).

Single-crystal ED patterns image one plane of the RL. They can be obtained from thin ideal crystalline plates, mosaic single-crystal films, or, in the RHEED case, from the faces of bulk single crystals. Point ED patterns can be obtained more easily owing to the following factors: the small size of the crystals (increase in the dimension of RL nodes) and mosaicity – the small spread of crystallite orientations in a specimen (tangential tension of the RL nodes). The crystal system, the parameters of the unit cell and the Laue symmetry are determined from point ED patterns; the probable space group is found from extinctions. Point ED patterns may be used for intensity measurements if the kinematic approximation holds true or if the contributions of the dynamic and secondary scattering are not too large.

The indexing of reflections and the unit-cell determination are carried out according to the formulae relating the RL to the DL (direct lattice) (Vainshtein, 1964; Pinsker, 1953; Zvyagin, 1967).

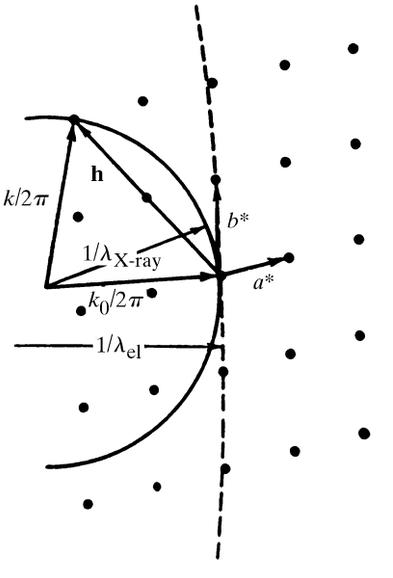

Fig. 2.5.4.1. Ewald spheres in reciprocal space. Dotted line: electrons, solid line: X-rays.

Under electron-diffraction conditions crystals usually show a tendency to lie down on the substrate plane on the most developed face. Let us take this as (001). The vectors a and b are then parallel, while vector c^* is normal to this plane, and the RL points are considered as being disposed along direct lines parallel to the axis c^* with constant hk and variable l.

The interpretation of the point patterns as respective RL planes is quite simple in the case of orthogonal lattices. If the lattice is triclinic or monoclinic the pattern of the crystal in the position with the face (001) normal to the incident beam does not have to contain $hk0$ reflections with non-zero h and k because, in general, the planes ab and a^*b^* do not coincide. However, the intersection traces of direct lines hk with the plane normal to them (plane ab) always form a net with periods

$$(a\sin\gamma)^{-1}, (b\sin\gamma)^{-1}, \text{and angle } \gamma' = \pi - \gamma \qquad (2.5.4.2a)$$

(Fig. 2.5.4.2). The points hkl along these directions hk are at distances

$$\eta = ha^*\cos\beta^* + kb^*\cos\alpha^* + lc^* \qquad (2.5.4.3)$$

from the ab plane.

By changing the crystal orientation it is possible to obtain an image of the a^*b^* plane containing $hk0$ reflections, or of other RL planes, with the exception of planes making a small angle with the axis c^*.

In the general case of an arbitrary crystal orientation, the pattern is considered as a plane section of the system of directions hk which makes an angle φ with the plane ab, intersecting it along a direction $[uv]$. It is described by two periods along directions $0h$, $0k$;

$$(a\sin\gamma\cos\psi_h)^{-1}, (b\sin\gamma\cos\psi_k)^{-1}, \qquad (2.5.4.2b)$$

with an angle γ'' between them satisfying the relation

$$\cos\gamma'' = \sin\psi_h\sin\psi_k - \cos\psi_h\cos\psi_k\cos\gamma, \qquad (2.5.4.2c)$$

and by a system of parallel directions

$$p_h h + p_k k = l; \quad l = 0, \pm 1, \pm 2, \ldots. \qquad (2.5.4.4)$$

The angles ψ_h, ψ_k are formed by directions $0h$, $0k$ in the plane of the pattern with the plane ab. The coefficients p_h, p_k depend on the unit-cell parameters, angle φ and direction $[uv]$. These relations are used for the indexing of reflections revealed near the integer positions hkl in the pattern and for unit-cell calculations (Vainshtein, 1964; Zvyagin, 1967; Zvyagin *et al.*, 1979).

In RED patterns obtained with an incident beam nearly parallel to the plane ab one can reveal all the RL planes passing through c^* which become normal to the beam at different azimuthal orientations of the crystal.

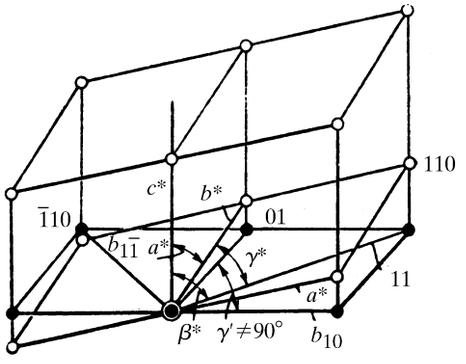

Fig. 2.5.4.2. Triclinic reciprocal lattice. Points: open circles, projection net: black circles.

With the increase of the thickness of crystals (see below, Chapter 5.1) the scattering becomes dynamical and Kikuchi lines and bands appear. Kikuchi ED patterns are used for the estimation of the degree of perfection of the structure of the surface layers of single crystals for specimen orientation in HREM (*IT* C, 1999, Section 4.3.8). Patterns obtained with a convergent beam contain Kossel lines and are used for determining the symmetry of objects under investigation (see Section 5.1.2).

Texture ED patterns are a widely used kind of ED pattern (Pinsker, 1953; Vainshtein, 1964; Zvyagin, 1967). Textured specimens are prepared by substance precipitation on the substrate, from solutions and suspensions, or from gas phase in vacuum. The microcrystals are found to be oriented with a common (developed) face parallel to the substrate, but they have random azimuthal orientations. Correspondingly, the RL also takes random azimuthal orientations, having c^* as the common axis, *i.e.* it is a rotational body of the point RL of a single crystal. Thus, the ED patterns from textures bear a resemblance, from the viewpoint of their geometry, to X-ray rotation patterns, but they are less complicated, since they represent a plane cross section of reciprocal space.

If the crystallites are oriented by the plane (hkl), then the axis $[hkl]^*$ is the texture axis. For the sake of simplicity, let us assume that the basic plane is the plane (001) containing the axes a and b, so that the texture axis is $[001]^*$, *i.e.* the axis c^*. The matrices of appropriate transformations will define a transition to the general case (see *IT* A, 1995). The RL directions hk = constant, parallel to the texture axis, transform to cylindrical surfaces, the points with η_{hkl} = constant are in planes perpendicular to the texture axis, while any 'tilted' lines transform to cones or hyperboloids of rotation. Each point hkl transforms to a ring lying on these surfaces. In practice, owing to a certain spread of c^* axes of single crystals, the rings are blurred into small band sections of a spherical surface with the centre at the point 000; the oblique cross section of such bands produces reflections in the form of arcs. The main interference curves for texture patterns are ellipses imaging oblique plane cross sections of the cylinders hk (Fig. 2.5.4.3).

At the normal electron-beam incidence (tilting angle $\varphi = 0°$) the ED pattern represents a cross section of cylinders perpendicular to the axis c^*, *i.e.* a system of rings.

On tilting the specimen to an angle φ with respect to its normal position (usually $\varphi \simeq 60°$) the patterns image an oblique cross section of the cylindrical RL, and are called oblique-texture (OT)

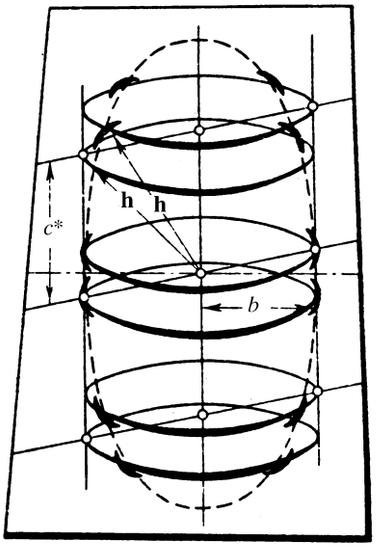

Fig. 2.5.4.3. Formation of ellipses on an electron-diffraction pattern from an oblique texture.

ED patterns. The ellipses (hk = constant) and layer lines (l = constant) for orthogonal lattices are the main characteristic lines of ED patterns along which the reflections are arranged. The shortcoming of oblique-texture ED patterns is the absence of reflections lying inside the cone formed by rotation of the straight line coming from the point 000 at an angle $(90^\circ - \varphi)$ around the axis c^* and, in particular, of reflections 00l. However, at $\varphi \lesssim 60$–70° the set of reflections is usually sufficient for structural determination.

For unit-cell determination and reflection indexing the values d (*i.e.* $|\mathbf{h}|$) are used, and the reflection positions defined by the ellipses hk to which they belong and the values η are considered. The periods a^*, b^* are obtained directly from h_{100} and h_{010} values. The period c^*, if it is normal to the plane a^*b^* (γ^* being arbitrary), is calculated as

$$c^* = \eta/l = (h_{hkl}^2 - h_{hk0}^2)^{1/2}/l. \qquad (2.5.4.5a)$$

For oblique-angled lattices

$$c^* = [(h_{l_1+l}^2 + h_{l_1-l}^2 - 2h_l^2)/2]^{1/2}/l. \qquad (2.5.4.5b)$$

In the general case of oblique-angled lattices the coaxial cylinders hk have radii

$$b_{hk} = (1/\sin\gamma)[(h^2/a^2) + (k^2/b^2) - (2hk\cos\gamma/ab)]^{1/2} \qquad (2.5.4.6)$$

and it is always possible to use the measured or calculated values b_{hk} in (2.5.4.5a) instead of h_{hk0}, since

$$\eta = (h_{hkl}^2 - b_{hk}^2)^{1/2}. \qquad (2.5.4.7)$$

In OT patterns the b_{hk} and η values are represented by the lengths of the small axes of the ellipses $B_{hk} = L\lambda b_{hk}$ and the distances of the reflections hkl from the line of small axes (equatorial line of the pattern)

$$D_{hkl} = L\lambda\eta/\sin\varphi = hp + ks + lq. \qquad (2.5.4.8)$$

Analysis of the B_{hk} values gives a, b, γ, while p, s and q are calculated from the D_{hkl} values. It is essential that the components of the normal projections c_n of the axis c on the plane ab measured in the units of a and b are

$$\begin{aligned} x_n &= (c/a)(\cos\beta - \cos\alpha\cos\gamma)/\sin^2\gamma \\ &= -p/q, \\ y_n &= (c/b)(\cos\alpha - \cos\beta\cos\gamma)/\sin^2\gamma \\ &= -s/q. \end{aligned} \qquad (2.5.4.9)$$

Obtaining x_n, y_n one can calculate

$$c_n = [(x_n a)^2 + (y_n b)^2 + 2x_n y_n ab\cos\gamma]^{1/2}.$$

Since

$$\begin{aligned} d_{001} &= L\lambda/q\sin\varphi, \\ c &= (c_n^2 + d_{001}^2)^{1/2}. \end{aligned} \qquad (2.5.4.10)$$

The α, β values are then defined by the relations

$$\begin{aligned} \cos\alpha &= (x_n a\cos\gamma + y_n b)/c, \\ \cos\beta &= (x_n a + y_n b\cos\gamma)/c. \end{aligned} \qquad (2.5.4.11)$$

Because of the small particle dimensions in textured specimens, the kinematic approximation is more reliable for OT patterns, enabling a more precise calculation of the structure amplitudes from the intensities of reflections.

Polycrystal ED patterns. In this case, the RL is a set of concentric spheres with radii h_{hkl}. The ED pattern, like an X-ray powder pattern, is a set of rings with radii

$$r_{hkl} = h_{hkl}L\lambda. \qquad (2.5.4.12)$$

2.5.4.3. *Intensities of diffraction beams*

The intensities of scattering by a crystal are determined by the scattering amplitudes of atoms in the crystal, given by (see also Section 5.2.1)

$$\begin{aligned} f_e^{\rm abs}(s) &= 4\pi K\int \varphi(r)r^2\frac{\sin sr}{sr}\,{\rm d}r; \\ K &= \frac{2\pi me}{h^2};\ f_e = K^{-1}f_e^{\rm abs}, \end{aligned} \qquad (2.5.4.13)$$

where $\varphi(r)$ is the potential of an atom and $s = 4\pi(\sin\theta)/\lambda$. The absolute values of $f_e^{\rm abs}$ have the dimensionality of length L. In EDSA it is convenient to use f_e without K. The dimensionality of f_e is [potential L^3]. With the expression of f_e in V Å^3 the value K^{-1} in (2.5.4.13) is 47.87 V Å^2.

The scattering atomic amplitudes $f_e(s)$ differ from the respective $f_x(s)$ X-ray values in the following: while $f_x(0) = Z$ (electron shell charge), the atomic amplitude at $s = 0$

$$f_e(0) = 4\pi\int\varphi(r)r^2\,{\rm d}r \qquad (2.5.4.14)$$

is the 'full potential' of the atom. On average, $f_e(0) \simeq Z^{1/3}$, but for small atomic numbers Z, owing to the peculiarities in the filling of the electron shells, $f_e(0)$ exhibits within periods of the periodic table of elements 'reverse motion', *i.e.* they decrease with Z increasing (Vainshtein, 1952, 1964). At large $(\sin\theta)/\lambda$, $f_e \simeq Z$. The atomic amplitudes and, consequently, the reflection intensities, are recorded, in practice, up to values of $(\sin\theta)/\lambda \simeq 0.8$–$1.2$ Å^{-1}, *i.e.* up to $d_{\min} \simeq 0.4$–0.6 Å.

The structure amplitude Φ_{hkl} of a crystal is determined by the Fourier integral of the unit-cell potential (see Chapter 1.2),

$$\Phi_{hkl} = \int_\Omega \varphi(\mathbf{r})\exp\{2\pi i(\mathbf{r}\cdot\mathbf{h})\}\,{\rm d}v_r, \qquad (2.5.4.15)$$

where Ω is the unit-cell volume. The potential of the unit cell can be expressed by the potentials of the atoms of which it is composed:

$$\varphi(\mathbf{r}) = \sum_{{\rm cell},\,i}\varphi_{{\rm at}\,i}(\mathbf{r} - \mathbf{r}_i). \qquad (2.5.4.16)$$

The thermal motion of atoms in a crystal is taken into account by the convolution of the potential of an atom at rest with the probability function $w(\mathbf{r})$ describing the thermal motion:

$$\varphi_{\rm at} = \varphi_{\rm at}(\mathbf{r}) * w(\mathbf{r}). \qquad (2.5.4.17)$$

Accordingly, the atomic temperature factor of the atom in a crystal is

$$f_{eT}[(\sin\theta)/\lambda] = f_e f_T = f_e[(\sin\theta)/\lambda]\exp\{-B[(\sin\theta)/\lambda]^2\}, \qquad (2.5.4.18)$$

where the Debye temperature factor is written for the case of isotropic thermal vibrations. Consequently, the structure amplitude is

$$\Phi_{hkl} = \sum_{{\rm cell},\,i} f_{eT_i}\exp\{2\pi i(hx_i + ky_i + lz_i)\}. \qquad (2.5.4.19)$$

This general expression is transformed (see *IT* I, 1952) according to the space group of a given crystal.

To determine the structure amplitudes in EDSA experimentally, one has to use specimens satisfying the kinematic scattering condition, *i.e.* those consisting of extremely thin crystallites. The

limit of the applicability of the kinematic approximation (Blackman, 1939; Vainshtein, 1964) can be estimated from the formula

$$A = \lambda\left|\frac{\langle\Phi_{\mathbf{h}}\rangle}{\Omega}\right| t \lesssim 1, \qquad (2.5.4.20)$$

where $\langle\Phi_{\mathbf{h}}\rangle$ is the averaged absolute value of $\Phi_{\mathbf{h}}$ (see also Section 5.2.1). Since $\langle\Phi_{\mathbf{h}}\rangle$ are proportional to $Z^{0.8}$, condition (2.5.4.20) is better fulfilled for crystals with light and medium atoms. Condition (2.5.4.20) is usually satisfied for textured and polycrystalline specimens. But for mosaic single crystals as well, the kinematic approximation limit is, in view of their real structure, substantially wider than estimated by (2.5.4.20) for ideal crystals. The fulfillment of the kinematic law for scattering can be, to a greater or lesser extent, estimated by comparing the decrease of experimental intensity $I_h[(\sin\theta)/\lambda]$ averaged over definite angular intervals, and sums $\sum f^2_{\rm obs}[(\sin\theta)/\lambda]$ calculated for the same angular intervals.

For mosaic single-crystal films the integral intensity of reflection is

$$I_{\mathbf{h}} = j_0 S\lambda^2\left|\frac{\Phi_{\mathbf{h}}}{\Omega}\right|^2 \frac{t d_{\mathbf{h}}}{\alpha} \simeq \Phi^2_{\mathbf{h}} d_{\mathbf{h}}; \qquad (2.5.4.21)$$

for textures

$$I_{\mathbf{h}} = j_0 S\lambda^2\left|\frac{\Phi_{\mathbf{h}}}{\Omega}\right|^2 \frac{tL\lambda p}{2\pi R'\sin\varphi} \simeq \Phi^2_{\mathbf{h}} p/R'. \qquad (2.5.4.22)$$

Here j_0 is the incident electron-beam density, S is the irradiated specimen area, t is the thickness of the specimen, α is the average angular spread of mosaic blocks, R' is the horizontal coordinate of the reflection in the diffraction pattern and p is the multiplicity factor. In the case of polycrystalline specimens the local intensity in the maximum of the ring reflection

$$I_{\mathbf{h}} = j_0 S\lambda^2\left|\frac{\Phi_{\mathbf{h}}}{\Omega}\right|^2 \frac{t d^2_{\mathbf{h}} p\Delta S}{4\pi L\lambda} \simeq \Phi^2_{\mathbf{h}} d^2_{\mathbf{h}} p \qquad (2.5.4.23)$$

is measured, where ΔS is the measured area of the ring.

The transition from kinematic to dynamic scattering occurs at critical thicknesses of crystals when $A \geq 1$ (2.5.4.20). Mosaic or polycrystalline specimens then result in an uneven contribution of various crystallites to the intensity of the reflections. It is possible to introduce corrections to the experimental structure amplitudes of the first strong reflections most influenced by dynamic scattering by applying in simple cases the two-wave approximation (Blackman, 1939) or by taking into account multibeam theories (Fujimoto, 1959; Cowley, 1981; Avilov *et al.* 1984; see also Chapter 5.2).

The application of kinematic scattering formulae to specimens of thin crystals (5–20 nm) or dynamic corrections to thicker specimens (20–50 nm) permits one to obtain reliability factors between the calculated $\Phi^{\rm calc}$ and observed $\Phi^{\rm obs}$ structure amplitudes of $R = 5$–15%, which is sufficient for structural determinations.

With the use of electron diffractometry techniques, reliability factors as small as $R = 2$–3% have been reached and more detailed data on the distribution of the inner-crystalline potential field have been obtained, characterizing the state and bonds of atoms, including hydrogen (Zhukhlistov *et al.*, 1997, 1998; Avilov *et al.*, 1999).

The applicability of kinematics formulae becomes poorer in the case of structures with many heavy atoms for which the atomic amplitudes also contain an imaginary component (Shoemaker & Glauber, 1952). The experimental intensity measurement is made by a photo method or by direct recording (Avilov, 1979). In some cases the amplitudes Φ_{hkl} can be determined from dynamic scattering patterns – the bands of equal thickness from a wedge-shaped crystal (Cowley, 1981), or from rocking curves.

2.5.4.4. *Structure analysis*

The unit cell is defined on the basis of the geometric theory of electron-diffraction patterns, and the space group from extinctions. It is also possible to use the method of converging beams (Section 5.2.2). The structural determination is based on experimental sets of values $|\Phi_{hkl}|^2$ or $|\Phi_{hkl}|$ (Vainshtein, 1964).

The trial-and-error method may be used for the simplest structures. The main method of determination is the construction of the Patterson functions

$$P(xyz) = \frac{1}{\Omega}\left[\Phi^2_{000} + 2\sum_{hkl=-\infty}^{hkl=+\infty}|\Phi_{hkl}|^2\cos 2\pi(hx+ky+lz)\right] \qquad (2.5.4.24)$$

and their analysis on the basis of heavy-atom methods, superposition methods and so on (see Chapter 2.3). Direct methods are also used (Dorset *et al.*, 1979). Thus the phases of structure factors are calculated and assigned to the observed moduli

$$\Phi_{\mathbf{h}} = |\Phi_{\mathbf{h},\,\rm obs}|\exp\{i\alpha_{\rm calc}\}. \qquad (2.5.4.25)$$

The distribution of the potential in the unit cell, and, thereby, the arrangement in it of atoms (peaks of the potential) are revealed by the construction of three-dimensional Fourier series of the potential (see also Chapter 1.3)

$$\varphi(xyz) = \frac{1}{\Omega}\sum_{\mathbf{h}}\Phi_{hkl}\exp\{-2\pi i(hx+ky+lz)\} \qquad (2.5.4.26a)$$

or projections

$$\varphi'(xy) = \frac{1}{S}\sum_{\mathbf{h}}\Phi_{hk0}\exp\{-2\pi i(hx+ky)\}. \qquad (2.5.4.26b)$$

The general formulae (2.5.4.26*a*) and (2.5.4.26*b*) transform, according to known rules, to the expressions for each space group (see *IT* I, 1952). If Φ_{hkl} are expressed in V Å^3 and the volume Ω or the cell area S in Å^3 and Å^2, respectively, then the potential φ is obtained directly in volts, while the projection of the potential φ' is in V Å. The amplitudes $|\Phi_{hkl}|$ are reduced to an absolute scale either according to a group of strong reflections

$$\sum|\Phi_{\mathbf{h}}|^{\rm calc} = \sum|\Phi_{\mathbf{h}}|^{\rm obs} \qquad (2.5.4.27)$$

or using the Parseval equality

$$\sum_{\mathbf{h}=-\infty}^{+\infty}|\Phi_{\mathbf{h}}|^2 = \Omega^2\langle\varphi^2\rangle = \Omega\sum_{i(\rm cell)}\frac{1}{2\pi^2}\int_0^\infty f^2_{eT_i}(s)s^2\,{\rm d}s \qquad (2.5.4.28)$$

or Wilson's statistical method

$$\langle\Phi^2[(\sin\theta)/\lambda]\rangle = \sum_i f^2_{eT_i}[(\sin\theta)/\lambda]. \qquad (2.5.4.29)$$

The term Φ_{000} defines the mean inner potential of a crystal, and is calculated from $f_e(0)$ [(2.5.4.13), (2.5.4.19)]

$$\langle\varphi_{\rm cr}\rangle = \Phi_{000}/\Omega = \frac{1}{\Omega}\sum f_e(0). \qquad (2.5.4.30)$$

The Fourier series of the potential in EDSA possess some peculiarities (Vainshtein, 1954, 1964) which make them different from the electron-density Fourier series in X-ray analysis. Owing to the peculiarities in the behaviour of the atomic amplitudes (2.5.4.13), which decrease more rapidly with increasing $(\sin\theta)/\lambda$ compared with f_x, the peaks of the atomic potential

$$\varphi_{\rm at}(r) = \frac{1}{2\pi^2}\int f_{eT}(s)\frac{\sin sr}{sr}s^2\ {\rm d}s \qquad (2.5.4.31)$$

are more 'blurred' and exhibit a larger half-width than the electron-density peaks $\rho_{\rm at}(r)$. On average, this half-width corresponds to the 'resolution' of an electron-diffraction pattern – about 0.5 Å or better. The potential in the maximum ('peak height') does not depend as strongly on the atomic number as in X-ray analysis:

$$\varphi(0) = \frac{1}{2\pi^2}\int f_{eT}(s)s^2\ {\rm d}s \sim Z^{0.75}, \qquad (2.5.4.32)$$

while in X-ray diffraction $\rho(0) \sim Z^{1.2}$. In such a way, in EDSA the light atoms are more easily revealed in the presence of heavy atoms than in X-ray diffraction, permitting, in particular, hydrogen atoms to be revealed directly without resorting to difference syntheses as in X-ray diffraction. Typical values of the atomic potential $\varphi(0)$ (which depend on thermal motion) in organic crystals are: H ~ 35, C ~ 165, O 215 V; in Al crystals 330 V, in Cu crystals 750 V.

The EDSA method may be used for crystal structure determination, depending on the types of electron-diffraction patterns, for crystals containing up to several tens of atoms in the unit cell. The accuracy in determination of atomic coordinates in EDSA is about 0.01–0.005 Å on average. The precision of EDSA makes it possible to determine accurately the potential distribution, to investigate atomic ionization, to obtain values for the potential between the atoms and, thereby, to obtain data on the nature of the chemical bond.

If the positions in the cell are occupied only partly, then the measurement of $\varphi_i(0)$ gives information on population percentage.

There is a relationship between the nuclear distribution, electron density and the potential as given by the Poisson equation

$$\nabla^2\varphi(\mathbf{r}) = -4\pi e[\rho_+(\mathbf{r}) - \rho_-(\mathbf{r})]. \qquad (2.5.4.33)$$

This makes it possible to interrelate X-ray diffraction, EDSA and neutron-diffraction data. Thus for the atomic amplitudes

$$f_e(s) = 4\pi Ke[Z - f_x(s)]s^{-2}, \qquad (2.5.4.34)$$

where Z is the nuclear charge and f_x the X-ray atomic scattering amplitude, and for structure amplitudes

$$\Phi_{hkl} = \pi Ke[Z_{hkl} - F_{hkl}]|\mathbf{h}|^{-2}, \qquad (2.5.4.35)$$

where F_{hkl} is the X-ray structure amplitude of the electron density of a crystal and Z_{hkl} is the amplitude of scattering from charges of nuclei in the cell taking into account their thermal motion. The values Z_{hkl} can be calculated easily from neutron-diffraction data, since the charges of the nuclei are known and the experiment gives the parameters of their thermal motion.

In connection with the development of high-resolution electron-microscopy methods (HREM) it has been found possible to combine the data from direct observations with EDSA methods. However, EDSA permits one to determine the atomic positions to a greater accuracy, since practically the whole of reciprocal space with 1.0–0.4 Å resolution is used and the three-dimensional arrangement of atoms is calculated. At the same time, in electron microscopy, owing to the peculiarities of electron optics and the necessity for an objective aperture, the image of the atoms in a crystal $\varphi'(\mathbf{x}) * A(\mathbf{x})$ is a convolution, with the aperture function blurring the image up to 1.5–2 Å resolution. In practice, in TEM one obtains only the images of the heaviest atoms of an object. However, the possibility of obtaining a direct image of a structure with all the defects in the atomic arrangement is the undoubted merit of TEM.

2.5.5. Image reconstruction* (B. K. VAINSHTEIN)

2.5.5.1. *Introduction*

In many fields of physical measurements, instrumental and informative techniques, including electron microscopy and computational or analogue methods for processing and transforming signals from objects investigated, find a wide application in obtaining the most accurate structural data. The signal may be radiation from an object, or radiation transmitted through the object, or reflected by it, which is transformed and recorded by a detector.

The image is the two-dimensional signal $I(xy)$ on the observation plane recorded from the whole three-dimensional volume of the object, or from its surface, which provides information on its structure. In an object this information may change owing to transformation of the scattered wave inside an instrument. The real image $J(xy)$ is composed of $I(xy)$ and noise $N(xy)$ from signal disturbances:

$$J(xy) = I(xy) + N(xy). \qquad (2.5.5.1)$$

Image-reconstruction methods are aimed at obtaining the most accurate information on the structure of the object; they are subdivided into two types (*Picture Processing and Digital Filtering*, 1975; Rozenfeld, 1969):

(*a*) Image restoration – separation of $I(xy)$ from the image by means of compensation of distortions introduced in it by an image-forming system as well as by an account of the available quantitative data reflecting its structure.

(*b*) Image enhancement – maximum exclusion from the observed image $J(xy)$ (2.5.5.1) of all its imperfections $N(xy)$ from both accidental distortions in objects and various 'noise' in signals and detector, and obtaining $I(xy)$ as the result.

These two methods may be used separately or in combination.

The image should be represented in the form convenient for perception and analysis, *e.g.* in digital form, in lines of equal density, in points of different density, in half-tones or colour form and using, if necessary, a change or reversal of contrast.

Reconstructed images may be used for the three-dimensional reconstruction of the spatial structure of an object, *e.g.* of the density distribution in it (see Section 2.5.6).

This section is connected with an application of the methods of image processing in transmission electron microscopy (TEM). In TEM (see Section 2.5.2), the source-emitted electrons are transmitted through an object and, with the aid of a system of lenses, form a two-dimensional image subject to processing.

Another possibility for obtaining information on the structure of an object is structural analysis with the aid of electron diffraction – EDSA. This method makes use of information in reciprocal space – observation and measurement of electron-diffraction patterns and calculation from them of a two-dimensional projection or three-dimensional structure of an object using the Fourier synthesis. To do this, one has to find the relative phases of the scattered beams.

The wavefunction of an electron-microscopic image is written as

$$\psi_I = \mathscr{F}^{-1}T\mathscr{F}q\psi_0. \qquad (2.5.5.2)$$

Here ψ_0 is the incident plane wave. When the wave is transmitted through an object, it interacts with the electrostatic potential $\varphi(\mathbf{r})$ [$\mathbf{r}(xyz)$ is the three-dimensional vector in the space of the object]; this process is described by the Schrödinger equation (Section 2.5.2.1). As a result, on the exit surface of an object the wave takes the form $q\psi_0(\mathbf{x})$ where q is the transmission function and $\mathbf{x}$ is the two-dimensional vector $\mathbf{x}(xy)$. The diffraction of the wave $q\psi_0$ is

* Questions related to this section may be addressed to Dr D. L. Dorset (see list of contributing authors). Dr Dorset kindly checked the proofs of this section.

described by the two-dimensional Fourier operator:

$$\mathscr{F}q = Q(\mathbf{u}) = \int q(\mathbf{x}) \exp[2\pi i(\mathbf{xu})]\ \mathrm{d}\mathbf{x}. \qquad (2.5.5.3)$$

Here, we assume the initial wave amplitude to be equal to unity and the initial phase to be zero, so that $q\psi_0 = q$, which defines, in this case, the wavefunction in the back focal plane of an objective lens with the reciprocal-space coordinates $\mathbf{u}(u, v)$. The function Q is modified in reciprocal space by the lens transfer function $T(\mathbf{u})$. The scattered wave transformation into an image is described by the inverse Fourier operator $\mathscr{F}^{-1}TQ$.

The process of the diffraction $\mathscr{F}q\psi_0 = Q$, as seen from (2.5.5.1), is the same in both TEM and EDSA. Thus, in TEM under the lens actions $\mathscr{F}^{-1}TQ$ the image formation from a diffraction pattern takes place with an account of the phases, but these phases are modified by the objective-lens transfer function. In EDSA, on the other hand, there is no distorting action of the transfer function and the 'image' is obtained by computing the operation $\mathscr{F}^{-1}Q$.

The computation of projections, images and Fourier transformation is made by discretization of two-dimensional functions on a two-dimensional network of points – pixels in real space $\mathbf{x}(x_j, y_k)$ and in reciprocal space $\mathbf{u}(u_m, v_n)$.

2.5.5.2. *Thin weak phase objects at optimal defocus*

The intensity distribution $I(xy) \sim |\psi_I|^2$ of an electron wave in the image plane depends not only on the coherent and inelastic scattering, but also on the instrumental functions. The electron wave transmitted through an object interacts with the electrostatic potential $\varphi(\mathbf{r})$ which is produced by the nuclei charges and the electronic shells of the atoms. The scattering and absorption of electrons depend on the structure and thickness of a specimen, and the atomic numbers of the atoms of which it is composed. If an object with the three-dimensional distribution of potential $\varphi(\mathbf{r})$ is sufficiently thin, then the interaction of a plane electron wave ψ_0 with it can be described as the interaction with a two-dimensional distribution of potential projection $\varphi(\mathbf{x})$,

$$\varphi(\mathbf{x}) = \int_0^b \varphi(\mathbf{r})\ \mathrm{d}z, \qquad (2.5.5.4)$$

where b is the specimen thickness. It should be noted that, unlike the three-dimensional function of potential $\varphi(\mathbf{r})$ with dimension $[M^{1/2}L^{3/2}T^{-1}]$, the two-dimensional function of potential projection $\varphi(\mathbf{x})$ has the potential-length dimension $[M^{1/2}L^{1/2}T^{-1}]$ which, formally, coincides with the charge dimension. The transmission function, in the general case, has the form $q(\mathbf{x}) = \exp[-i\sigma\varphi(\mathbf{x})]$ (2.5.2.42), and for weak phase objects the approximation $[\sigma\varphi \ll 1]$

$$q(\mathbf{x}) = 1 - i\sigma\varphi(\mathbf{x}) \qquad (2.5.5.5)$$

is valid.

In the back focal plane of the objective lens the wave has the form

$$Q(uv) \cdot T(U) \qquad (2.5.5.6)$$

$$T = A(U) \exp(i\chi U) \qquad (2.5.5.7a)$$

$$\chi(U) = \pi\Delta f \lambda U^2 + \frac{\pi}{2} C_s \lambda^3 U^4, \qquad (2.5.5.7b)$$

where $U = (u^2 + v^2)^{1/2}$; $\exp[i\chi(U)]$ is the Scherzer phase function (Scherzer, 1949) of an objective lens (Fig. 2.5.5.1), $A(U)$ is the aperture function, C_s the spherical aberration coefficient, and Δf the defocus value [(2.5.2.32)–(2.5.2.35)].

The bright-field image intensity (in object coordinates) is

$$I(xy) = |\psi_I(xy) * t(xy)|^2, \qquad (2.5.5.8)$$

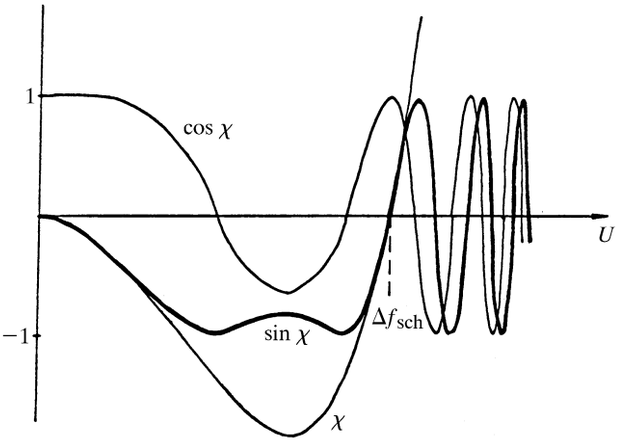

Fig. 2.5.5.1. The χ function and two components of the Scherzer phase function $\sin\chi(U)$ and $\cos\chi(U)$.

where $t = \mathscr{F}^{-1}[T]$. The phase function (2.5.5.7) depends on defocus, and for a weak phase object (Cowley, 1981)

$$I(xy) = 1 + 2\sigma\varphi(xy) * s(xy), \qquad (2.5.5.9)$$

where $s = \mathscr{F}^{-1}[A(U)\sin\chi]$, which includes only an imaginary part of function (2.5.5.6). While selecting defocus in such a way that under the Scherzer defocus conditions [(2.5.2.44), (2.5.2.45)] $|\sin\chi| \simeq 1$, one could obtain

$$I(xy) = 1 + 2\sigma\varphi(xy) * a(xy). \qquad (2.5.5.10)$$

In this very simple case the image reflects directly the structure of the object – the two-dimensional distribution of the projection of the potential convoluted with the spread function $a = \mathscr{F}^{-1}A$. In this case, no image restoration is necessary. Contrast reversal may be achieved by a change of defocus.

At high resolution, this method enables one to obtain an image of projections of the atomic structure of crystals and defects in the atomic arrangement – vacancies, replacements by foreign atoms, amorphous structures and so on; at resolution worse than atomic one obtains images of dislocations as continuous lines, inserted phases, inclusions *etc.* (Cowley, 1981). It is also possible to obtain images of thin biological crystals, individual molecules, biological macromolecules and their associations.

Image restoration. In the case just considered (2.5.5.10), the projection of potential $\varphi(xy)$, convoluted with the spread function, can be directly observed. In the general case (2.5.5.9), when the aperture becomes larger, the contribution to image formation is made by large values of spatial frequencies U, in which the function $\sin\chi$ oscillates, changing its sign. Naturally, this distorts the image just in the region of appropriate high resolution. However, if one knows the form of the function $\sin\chi$ (2.5.5.7), the true function $\varphi(xy)$ can be restored.

This could be carried out experimentally if one were to place in the back focal plane of an objective lens a zone plate transmitting only one-sign regions of $\sin\chi$ (Hoppe, 1971). In this case, the information on $\varphi(xy)$ is partly lost, but not distorted. To perform such a filtration in an electron microscope is a rather complicated task.

Another method is used (Erickson & Klug, 1971). It consists of a Fourier transformation $\mathscr{F}^{-1}$ of the measured intensity distribution TQ (2.5.5.6) and division of this transform, according to (2.5.5.7*a*,*b*), by the phase function $\sin\chi$. This gives

$$\frac{TQ}{\sin\chi} = Q(uv)A(U). \qquad (2.5.5.11a)$$

Then, the new Fourier transformation $\mathscr{F}QA$ yields (in the weak-phase-object approximation) the true distribution

$$\varphi(xy) * a(xy). \qquad (2.5.5.11b)$$

The function $\sin\chi$ depending on defocus Δf should be known to perform this procedure. The transfer function can also be found from an electron micrograph (Thon, 1966). It manifests itself in a circular image intensity modulation of an amorphous substrate or, if the specimen is crystalline, in the 'noise' component of the image. The analogue method (optical Fourier transformation for obtaining the image $\sin\chi$) can be used (optical diffraction, see below); digitization and Fourier transformation can also be applied (Hoppe *et al.*, 1973).

The thin crystalline specimen implies that in the back focal objective lens plane the discrete kinematic amplitudes Φ_{hk} are arranged and, by the above method, they are corrected and released from phase distortions introduced by the function $\sin\chi$ (see below) (Unwin & Henderson, 1975).

For the three-dimensional reconstruction (see Section 2.5.6) it is necessary to have the projections of potential of the specimen tilted at different angles α to the beam direction (normal beam incidence corresponds to $\alpha = 0$). In this case, the defocus Δf changes linearly with increase of the distance l of specimen points from the rotation axis $\Delta f_\alpha = \Delta f_0(1 + l\sin\alpha)$. Following the above procedure for passing on to reciprocal space and correction of $\sin\chi$, one can find $\varphi_\alpha(xy)$ (Henderson & Unwin, 1975).

2.5.5.3. *An account of absorption*

Elastic interaction of an incident wave with a weak phase object is defined on its exit surface by the distribution of potential projection $\varphi(xy)$; however, in the general case, the electron scattering amplitude is a complex one (Glauber & Schomaker, 1953). In such a way, the image itself has the phase and amplitude contrast. This may be taken into account if one considers not only the potential projection $\varphi(xy)$, but also the 'imaginary potential' $\mu(xy)$ which describes phenomenologically the absorption in thin specimens. Then, instead of (2.5.5.5), the wave on the exit surface of a specimen can be written as

$$q(xy) = 1 - i\sigma\varphi(xy) - \mu(xy) \qquad (2.5.5.12)$$

and in the back focal plane if $\Phi = \mathscr{F}\varphi$ and $M = \mathscr{F}\mu$

$$Q(uv) = \delta(uv) - i\sigma\Phi(uv) - M(uv). \qquad (2.5.5.13)$$

Usually, μ is small, but it can, nevertheless, make a certain contribution to an image. In a sufficiently good linear approximation, it may be assumed that the real part $\cos\chi$ of the phase function (2.5.5.7*a*) affects $M(uv)$, while $\Phi(xy)$, as we know, is under the action of the imaginary part $\sin\chi$.

Thus, instead of (2.5.5.6), one can write

$$Q(\exp i\chi) = \delta(\mathbf{u}) - i\sigma\Phi(\mathbf{u})\sin\chi - M(\mathbf{u})\cos\chi, \qquad (2.5.5.14)$$

and as the result, instead of (2.5.5.10),

$$I(xy) = 1 + 2\sigma\varphi(xy) * \mathscr{F}^{-1}(\sin\chi) * a(U) - 2\mu(xy) * \mathscr{F}^{-1}(\cos\chi) * a(U). \qquad (2.5.5.15)$$

The functions $\varphi(xy)$ and $\mu(xy)$ can be separated by object imaging using the through-focus series method. In this case, using the Fourier transformation, one passes from the intensity distribution (2.5.5.15) in real space to reciprocal space. Now, at two different defocus values Δf_1 and Δf_2 [(2.5.5.6), (2.5.5.7*a*,*b*)] the values $\Phi(\mathbf{u})$ and $M(\mathbf{u})$ can be found from the two linear equations (2.5.5.14). Using the inverse Fourier transformation, one can pass on again to real space which gives $\varphi(\mathbf{x})$ and $\mu(\mathbf{x})$ (Schiske, 1968). In practice, it is possible to use several through-focus series and to solve a set of equations by the least-squares method.

Another method for processing takes into account the simultaneous presence of noise $N(\mathbf{x})$ and transfer function zeros (Kirkland *et al.*, 1980). In this method the space frequencies corresponding to small values of the transfer function modulus are suppressed, while the regions where such a modulus is large are found to be reinforced.

2.5.5.4. *Thick crystals*

When the specimen thickness exceeds a certain critical value ($\sim$50–100 Å), the kinematic approximation does not hold true and the scattering is dynamic. This means that on the exit surface of a specimen the wave is not defined as yet by the projection of potential $\varphi(xy) = \int\varphi(\mathbf{r})\,\mathrm{d}z$ (2.5.5.3), but one has to take into account the interaction of the incident wave ψ_0 and of all the secondary waves arising in the whole volume of a specimen.

The dynamic scattering calculation can be made by various methods. One is the multi-slice (or phase-grating) method based on a recurrent application of formulae (2.5.5.3) for n thin layers Δz_i thick, and successive construction of the transmission functions q_i (2.5.5.4), phase functions $Q_i = \mathscr{F}q_i$, and propagation function $p_k = [k/2\pi i\Delta z]\exp[ik(x^2 + y^2)/2\Delta z]$ (Cowley & Moodie, 1957).

Another method – the scattering matrix method – is based on the solution of equations of the dynamic theory (Chapter 5.2). The emerging wave on the exit surface of a crystal is then found to diffract and experience the transfer function action [(2.5.5.6), (2.5.5.7*a*,*b*)].

The dynamic scattering in crystals may be interpreted using Bloch waves:

$$\Psi^j(\mathbf{r}) = \sum_H C_H^j \exp(-2\pi i\mathbf{k}_H^j\cdot\mathbf{r}). \qquad (2.5.5.16)$$

It turns out that only a few (bound and valence Bloch waves) have strong excitation amplitudes. Depending on the thickness of a crystal, only one of these waves or their linear combinations (Kambe, 1982) emerges on the exit surface. An electron-microscopic image can be interpreted, at certain thicknesses, as an image of one of these waves [with a correction for the transfer function action (2.5.5.6), (2.5.5.7*a*,*b*)]; in this case, the identical images repeat with increasing thickness, while, at a certain thickness, the contrast reversal can be observed. Only the first Bloch wave which arises at small thickness, and also repeats with increasing thickness, corresponds to the projection of potential $\varphi(xy)$, *i.e.* the atom projection distribution in a thin crystal layer.

An image of other Bloch waves is defined by the function $\varphi(\mathbf{r})$, but their maxima or minima do not coincide, in the general case, with the atomic positions and cannot be interpreted as the projection of potential. It is difficult to reconstruct $\varphi(xy)$ from these images, especially when the crystal is not ideal and contains imperfections. In these cases one resorts to computer modelling of images at different thicknesses and defocus values, and to comparison with an experimentally observed pattern.

The imaging can be performed directly in an electron microscope not by a photo plate, but using fast-response detectors with digitized intensity output on line. The computer contains the necessary algorithms for Fourier transformation, image calculation, transfer function computing, averaging, and correction for the observed and calculated data. This makes possible the interpretation of the pattern observed directly in experiment (Herrmann *et al.*, 1980).

2.5.5.5. *Image enhancement*

The real electron-microscope image is subdivided into two components:

$$J(xy) = I(xy) + N(xy). \tag{2.5.5.17}$$

The main of these, $I(xy)$, is a two-dimensional image of the 'ideal' object obtained in an electron microscope with instrumental functions inherent to it. However, in the process of object imaging and transfer of this information to the detector there are various sources of noise. In an electron microscope, these arise owing to emission-current and accelerating-voltage fluctuations, lens-supplying current (temporal fluctuations), or mechanical instabilities in a device, specimen or detector (spatial shifts). The two-dimensional detector (*e.g.* a photographic plate) has structural inhomogeneities affecting a response to the signal. In addition, the specimen is also unstable; during preparation or imaging it may change owing to chemical or some other transformations in its structure, thermal effects and so on. Biological specimens scatter electrons very weakly and their natural state is moist, while in the electron-microscope column they are under vacuum conditions. The methods of staining (negative or positive), *e.g.* of introducing into specimens substances containing heavy atoms, as well as the freeze-etching method, somewhat distort the structure of a specimen. Another source of structure perturbation is radiation damage, which can be eliminated at small radiation doses or by using the cryogenic technique. The structure of stained specimens is affected by stain graininess. We assume that all the deviations $\Delta I_k(xy)$ of a specimen image from the 'ideal' image $I_k(xy)$ are included in the noise term $N_k(xy)$. The substrate may also be inhomogeneous. All kinds of perturbations cannot be separated and they appear on an electron microscope image as the full noise content $N(xy)$.

The image enhancement involves maximum noise suppression $N(xy)$ and hence the most accurate separation of a useful signal $I(xy)$ from the real image $J(xy)$ (2.5.5.1). At the signal/noise ratio $I/N \simeq 1$ such a separation appears to be rather complicated. But in some cases the real image reflects the structure sufficiently well, *e.g.* during the atomic structure imaging of some crystals ($I/N > 10$). In other cases, especially of biological specimen imaging, the noise N distorts substantially the image, $(I/N) \sim 5$–10. Here one should use the methods of enhancement. This problem is usually solved by the methods of statistical processing of sets of images J_k $(k = 1, \ldots, n)$. If one assumes that the informative signal $I_k(xy)$ is always the same, then the noise error $N(xy)$ may be reduced.

The image enhancement methods are subdivided into two classes:

(*a*) image averaging in real space *xy*;

(*b*) Fourier analysis and filtration in reciprocal space.

These methods can be used separately or in combination. The enhancement can be applied to both the original and the restored images; there are also methods of simultaneous restoration and enhancement.

The image can be enhanced by analogue (mainly optical and photographic) methods or by computational methods for processing digitized functions in real and reciprocal space.

The cases where the image has translational symmetry, rotational symmetry, and where the image is asymmetric will be considered.

Periodic images. An image of the crystal structure with atomic or molecular resolution may be brought to self-alignment by a shift by a and b periods in a structure projection. This can be performed photographically by printing the shifted image on the same photographic paper or, *vice versa*, by shifting the paper (McLachlan, 1958).

The Fourier filtration method for a periodic image I_p with noise N is based on the fact that in Fourier space the components $\mathscr{F}I_p$ and $\mathscr{F}N$ are separated. Let us carry out the Fourier transformation of the periodic signal I_p with the periods a, b and noise N:

$$\begin{aligned}\mathscr{F}J &= \mathscr{F}[I_p(xy) + N(xy)] \\ &= \textstyle\int I_p(xy)\exp[2\pi i(hx+ky)]\,\mathrm{d}x\,\mathrm{d}y + \mathscr{F}N \\ &= \textstyle\sum \Phi_{hk}\delta(\mathbf{u}-\mathbf{u}_{hk}) + \mathscr{F}N; \\ \mathbf{u}_{hk} &= h\mathbf{a}^* + k\mathbf{b}^*.\end{aligned} \tag{2.5.5.18}$$

The left part of (2.5.5.18) represents the Fourier coefficients Φ_{hk} distributed discretely with periods a^* and b^* in the plane $\mathbf{u}(uv)$. This is the two-dimensional reciprocal lattice. The right-hand side of (2.5.5.18) is the Fourier transform $\mathscr{F}N$ distributed continuously in the plane. Thus these parts are separated. Let us 'cut out' from distribution (2.5.5.18) only Φ_{hk} values using the 'window' function $w(uv)$. The window should match each of the real peaks Φ_{hk} which, owing to the finite dimensions of the initial periodic image, are not points, as this is written in an idealized form in (2.5.5.18) with the aid of δ functions. In reality, the 'windows' may be squares of about $a^*/10$, $b^*/10$ in size, or a circle. Performing the Fourier transformation of product (2.5.5.18) without $\mathscr{F}N$, and set of windows $w(\mathbf{u}) = w(uv) * \sum_{h,k}\delta(\mathbf{u} - h\mathbf{a}^* - k\mathbf{b}^*)$, we obtain:

$$\begin{aligned}J(xy) &= \mathscr{F}^{-1}\{w(\mathbf{u})\textstyle\sum\limits_{h,k}\Phi_{h,k}\delta(\mathbf{u}-\mathbf{u}_{h,k})\} \\ &= W(xy) * I_p(\mathbf{x}),\end{aligned} \tag{2.5.5.19}$$

the periodic component without the background, $W(xy) = \mathscr{F}^{-1}w(\mathbf{u})$. The zero coefficient Φ_{00} in (2.5.5.19) should be decreased, since it is due, in part, to the noise. When the window w is sufficiently small, I_p in (2.5.5.19) represents the periodic distribution $\langle I\rangle$ (average over all the unit cells of the projection) included in I_p (2.5.5.18). Nevertheless, some error from noise in an image does exist, since with Φ_{hk} we also introduced into the inverse Fourier transformation the background transform values $\mathscr{F}^{-1}N_{hk}$ which are within the 'windows'.

This approach is realized by an analogue method [optical diffraction and filtering of electron micrographs in a laser beam (Klug & Berger, 1964)] and can also be carried out by computing.

As an example, Fig. 2.5.5.2(*b*) shows an electron micrograph of the periodic structure of a two-dimensional protein crystal, while Fig. 2.5.5.2(*c*) represents optical diffraction from this layer. In order to dissect the aperiodic component $\mathscr{F}N$ in a diffraction plane, according to the scheme in Fig. 2.5.5.2(*a*), one places a mask with windows covering reciprocal-lattice points. After such a filtration, only the I_p component makes a contribution during the image formation by means of a lens, while the component $\mathscr{F}N$ diffracted by the background is delayed. As a result, an optical pattern of the periodic structure is obtained (Fig. 2.5.5.2*d*).

Optical diffractometry also assists in determining the parameters of a two-dimensional lattice and its symmetry.

Using the same method, one can separate the superimposed images of two-dimensional structures with different periodicity and in different orientation, the images of the 'near' and 'far' sides of tubular periodic structures with monomolecular walls (Klug & DeRosier, 1966; Kiselev *et al.*, 1971), and so on.

Computer filtering involves measuring the image optical density $J_{\rm obs}$, digitization, and Fourier transformation (Crowther & Amos, 1971). The sampling distance usually corresponds to one-third of the image resolution. When periodic weak phase objects are investigated, the transformation (2.5.5.18) yields the Fourier coefficients. If necessary, we can immediately make corrections in them using the microscope transfer function according to (2.5.5.6), (2.5.5.7*a*,*b*) and (2.5.5.11*a*), and thereby obtain the true kinematic amplitudes Φ_{hk}. The inverse transformation (2.5.5.16) gives a projection of the structure (Unwin & Henderson, 1975; Henderson & Unwin, 1975).

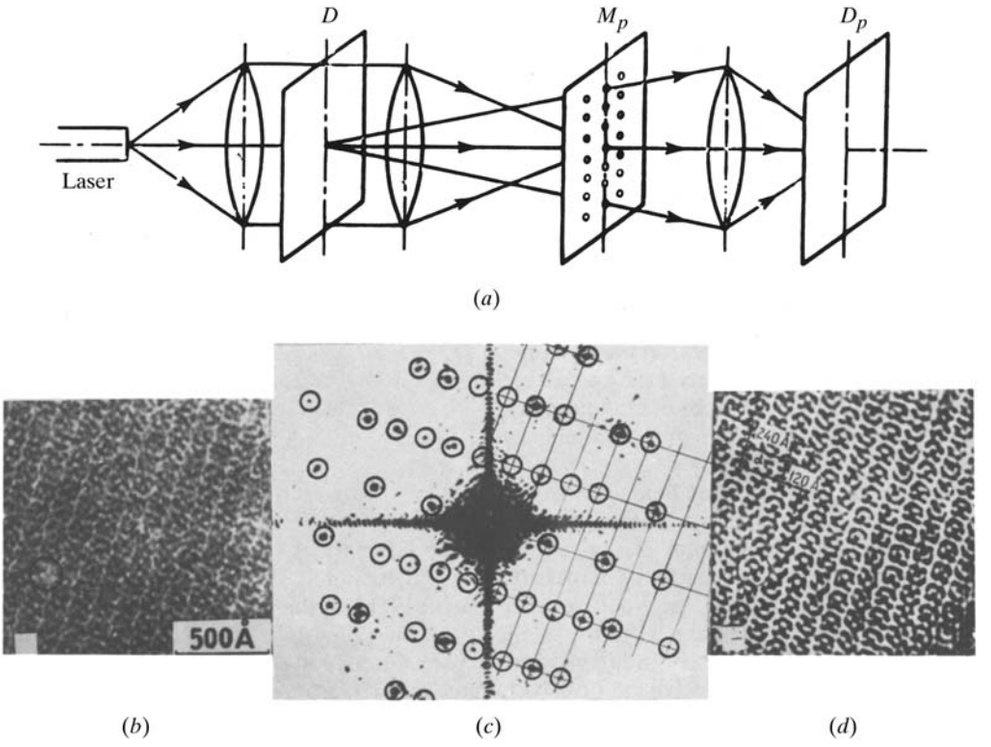

Fig. 2.5.5.2. (*a*) Diagram of an optical diffractometer. *D* is the object (an electron micrograph), M_p is the diffraction plane and a mask that transmits only Φ_{hk}, D_p is the plane of the (filtered) image; (*b*) an electron micrograph of a crystalline layer of the protein phosphorylase *b*; (*c*) its optical diffraction pattern (the circles correspond to the windows in the mask that transmits only the Φ_{hk} diffracted beams from the periodic component of the image); (*d*) the filtered image. Parts (*b*)–(*d*) are based on the article by Kiselev *et al.* (1971).

Sometimes, an observed image $J(\mathbf{x})$ is 'noised' by the $N(\mathbf{x})$ to a great extent. Then, one may combine data on real and reciprocal space to construct a sufficiently accurate image. In this case, the electron-diffraction pattern is measured and structure-factor moduli from diffraction reflection intensities $I_{hk,\,\mathrm{obs}}$ are obtained:

$$|\Phi_{hk,\,\mathrm{obs}}| \sim \sqrt{I_{hk,\,\mathrm{obs}}}. \tag{2.5.5.20}$$

At the same time, the structure factors

$$\Phi_{hk,\,\mathrm{calc}} = |\Phi_{hk,\,\mathrm{calc}}| \exp(i\alpha_{hk,\,\mathrm{calc}}) \tag{2.5.5.21}$$

are calculated from the processed structure projection image by means of the Fourier transformation. However, owing to poor image quality we take from these data only the values of phases α_{hk} since they are less sensitive to scattering density distortions than the moduli, and construct the Fourier synthesis

$$I(xy) = \sum_{hk} |\Phi_{hk,\,\mathrm{obs}}| \exp(i\alpha_{hk,\,\mathrm{calc}}) \times \exp[2\pi i(hx + ky)]. \tag{2.5.5.22}$$

Here the possibilities of combining various methods open up, *e.g.* for obtaining the structure-factor moduli from X-ray diffraction, and phases from electron microscopy, and so on (Gurskaya *et al.*, 1971).

Images with point symmetry. If a projection of an object (and consequently, the object itself) has a rotational *N*-fold axis of symmetry, the structure coincides with itself on rotation through the angle $2\pi/N$. If the image is rotated through arbitrary angles and is aligned photographically with the initial image, then the best density coincidence will take place at a rotation through $\alpha = (k2\pi/N)$ $(k = 1, \ldots, N)$ which defines *N*. The pattern averaging over all the rotations will give the enhanced structure image with an $(N)^{1/2}$ times reduced background (Markham *et al.*, 1963).

Rotational filtering can be performed on the basis of the Fourier expansion of an image in polar coordinates over the angles (Crowther & Amos, 1971).

$$I(r, \psi) = \sum_{n=-\infty}^{+\infty} g_n(r) \exp(in\varphi). \tag{2.5.5.23}$$

The integral over the radius from azimuthal components g_n gives their power

$$p_n \sim \int_0^a |g_n|^2 r \, \mathrm{d}r, \tag{2.5.5.24}$$

where *a* is the maximum radius of the particle. A set p_n forms a spectrum, the least common multiple *N* of strong peaks defining the *N*-fold symmetry. The two-dimensional reconstructed image of a particle with rotational symmetry is defined by the synthesis (2.5.5.24) with $n = 0, N, 2N, 3N$.

Asymmetric images. In this case, a set of images is processed by computational or analogue methods. The initial selection of images involves the fulfillment of the maximum similarity condition.

The averaging of *n* images in real space gives

$$I_{\mathrm{enh}} = (1/n) \sum_{k=1}^{n} J_k(xy) = \langle I_k \rangle (xy) + (1/n) \sum N_k(xy). \tag{2.5.5.25}$$

The signal/noise ratio on an average image is $(n)^{1/2}$ times enhanced.

The degree of similarity and accuracy of superposition of two images with an account both of translational and angular shifts is estimated by a cross-correlation function* of two selected images J_1 and J_2 (Frank, 1975, 1980).

* At $I_j = I_k$ this is the autocorrelation function, an analogue of the Patterson function used in crystallography.

$$k(\mathbf{x}') = J_1 * J_2 = \int J_1(x)J_2(x+x')\ \mathrm{d}x$$
$$= k_{I_1I_2} + k_{I_1N_2} + k_{I_2N_1} + k_{N_1N_2}. \qquad (2.5.5.26)$$

The value $k(\mathbf{x}')$ is the measure of image similarity, the x' coordinate of the maximum indicates the shift of the images relative to each other. The first term of the resultant expression (2.5.5.26) is the cross-correlation function of noise-corrected images being compared, the second and third terms are approximately equal to zero, since the noise does not correlate with the signal; the last term is the autocorrelation function of the noise (Cramér, 1954; Frank, 1975, 1980).

The calculation of a correlation function is performed by means of Fourier transformation on the basis of the convolution theorem, since the Fourier transformation of the product of the Fourier transform of function J_1 and the conjugated Fourier transform function J_2 gives the cross-correlation function of the initial functions:

$$k = \mathscr{F}^{-1}[\mathscr{F}J_1 \cdot \mathscr{F}^*J_2]. \qquad (2.5.5.27)$$

The probability density of samples for images has the form

$$p(J_1J_2\ldots J_n) = \frac{1}{(\sigma\sqrt{2\pi})^n} \times \exp\left[\frac{-1}{2\sigma^2}\sum^n \int [J_k(\mathbf{x}+\mathbf{x}_k) - J(\mathbf{x})]^2\ \mathrm{d}x\right]. \qquad (2.5.5.28)$$

Here J is the tentative image (as such, a certain 'best' image can first be selected, while at the repeated cycle an average image is obtained), $J_k(\mathbf{x})$ is the image investigated, σ is the standard deviation of the normal distribution of noises and x_k the relative shift of the image. This function is called a likelihood function; it has maxima relative to the parameters $J(x)$, x_k, σ. The average image and dispersion are

$$J(\mathbf{x}) = (1/n)\sum^n [J_k(\mathbf{x}-\mathbf{x}_k)],$$
$$\sigma^2 = (1/n)\sum^n [J_k(\mathbf{x}-\mathbf{x}_k) - J(\mathbf{x})]^2. \qquad (2.5.5.29)$$

This method is called the maximum-likelihood method (Cramér, 1954; Kosykh *et al.*, 1983).

It is convenient to carry out the image alignment, in turn, with respect to translational and angular coordinates. If we start with an angular alignment we first use autocorrelation functions or power spectra, which have the maximum and the symmetry centre at the origin of the coordinates. The angular correlation maximum

$$f(\theta') = \int f_k(\theta-\theta')f_e(\theta)\ \mathrm{d}\theta \qquad (2.5.5.30)$$

gives the mutual angle of rotation of two images.

Then we carry out the translational alignment of rotationally aligned images using the translational correlation function (2.5.5.26) (Langer *et al.*, 1970).

In the iteration alignment method, the images are first translationally aligned and then an angular shift is determined in image space in polar coordinates with the centre at the point of the best translational alignment. After the angular alignment the whole procedure may be repeated (Steinkilberg & Schramm, 1980).

The average image obtained may have false high-frequency components. They can be excluded by multiplying its Fourier components by some function and suppressing high-space frequencies, for instance by an 'artificial temperature factor' $\exp\{-B|\mathbf{u}|^2\}$.

For a set of similar images the Fourier filtration method can also be used (Ottensmeyer *et al.*, 1977). To do this, one should prepare from these images an artificial 'two-dimensional crystal', *i.e.* place them in the same orientation at the points of the two-dimensional lattice with periods a, b.

$$J = \sum_{k=1}^{n} J_k(\mathbf{x}-\mathbf{t}_p);\ \mathbf{t} = p_1\mathbf{a} + p_2\mathbf{b}. \qquad (2.5.5.31)$$

The processing is then performed according to (2.5.5.18), (2.5.5.19); as a result one obtains $\langle I(xy)\rangle$ with reduced background. Some translational and angular errors in the arrangement of the images at the artificial lattice points act as an artificial temperature factor. The method can be realized by computing or by optical diffraction.

2.5.6. Three-dimensional reconstruction*

(B. K. VAINSHTEIN)

2.5.6.1. *The object and its projection*

In electron microscopy we obtain a two-dimensional image $\varphi_2(\mathbf{x}_\tau)$ – a projection of a three-dimensional object $\varphi_3(\mathbf{r})$ (Fig. 2.5.6.1):

$$\varphi_2(\mathbf{x}_\tau) = \int \varphi_3(\mathbf{r})\ \mathrm{d}\tau \quad \boldsymbol{\tau} \perp \mathbf{x}. \qquad (2.5.6.1)$$

The projection direction is defined by a unit vector $\boldsymbol{\tau}(\theta,\psi)$ and the projection is formed on the plane $\mathbf{x}$ perpendicular to $\boldsymbol{\tau}$. The set of various projections $\varphi_2(\mathbf{x}_{\tau_i}) = \varphi_{2i}(\mathbf{x}_i)$ may be assigned by a discrete or continuous set of points $\boldsymbol{\tau}_i(\theta_i,\psi_i)$ on a unit sphere $|\boldsymbol{\tau}| = 1$ (Fig. 2.5.6.2). The function $\varphi(\mathbf{x}_\tau)$ reflects the structure of an object, but gives information only on $\mathbf{x}_\tau$ coordinates of points of its projected density. However, a set of projections makes it possible to reconstruct from them the three-dimensional (3D) distribution $\varphi_3(xyz)$ (Radon, 1917; DeRosier & Klug, 1968; Vainshtein *et al.*, 1968; Crowther, DeRosier & Klug, 1970; Gordon *et al.*, 1970; Vainshtein, 1971*a*; Ramachandran & Lakshminarayanan, 1971; Vainshtein & Orlov, 1972, 1974; Gilbert, 1972*a*; Herman, 1980). This is the task of the three-dimensional reconstruction of the structure of an object:

$$\text{set } \varphi_2(\mathbf{x}_i) \rightarrow \varphi_3(\mathbf{r}). \qquad (2.5.6.2)$$

Besides electron microscopy, the methods of reconstruction of a structure from its projections are also widely used in various fields, *e.g.* in X-ray and NMR tomography, in radioastronomy, and in various other investigations of objects with the aid of penetrating, back-scattered or their own radiations (Bracewell, 1956; Deans, 1983; Mersereau & Oppenheim, 1974).

In the general case, the function $\varphi_3(\mathbf{r})$ (2.5.6.1) (the subscript indicates dimension) means the distribution of a certain scattering density in the object. The function $\varphi_2(\mathbf{x})$ is the two-dimensional projection density; one can also consider one-dimensional projections $\varphi_1(x)$ of two- (or three-) dimensional distributions. In electron microscopy, under certain experimental conditions, by functions $\varphi_3(\mathbf{r})$ and $\varphi_2(\mathbf{x})$ we mean the potential and the projection of the potential, respectively [the electron absorption function μ (see Section 2.5.4) may also be considered as 'density']. Owing to a very large depth of focus and practical parallelism of the electron beam passing through an object, in electron microscopy the vector $\boldsymbol{\tau}$ is the same over the whole area of the irradiated specimen – this is the case of parallel projection.

The 3D reconstruction (2.5.6.2) can be made in the real space of an object – the corresponding methods are called the methods of direct three-dimensional reconstruction (Radon, 1917; Vainshtein

* Questions related to this section may be addressed to Professor J. M. Cowley (see list of contributing authors). Professor Cowley kindly checked the proofs for this section.

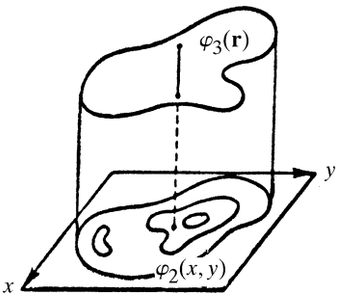

Fig. 2.5.6.1. A three-dimensional object φ_3 and its two-dimensional projection φ_2.

et al., 1968; Gordon *et al.*, 1970; Vainshtein, 1971*a*; Ramachandran & Lakshminarayanan, 1971; Vainshtein & Orlov, 1972, 1974; Gilbert, 1972*a*).

On the other hand, three-dimensional reconstruction can be carried out using the Fourier transformation, *i.e.* by transition to reciprocal space. The Fourier reconstruction is based on the well known theorem: the Fourier transformation of projection φ_2 of a three-dimensional object φ_3 is the central (*i.e.* passing through the origin of reciprocal space) two-dimensional plane cross section of a three-dimensional transform perpendicular to the projection vector (DeRosier & Klug, 1968; Crowther, DeRosier & Klug, 1970; Bracewell, 1956). In Cartesian coordinates a three-dimensional transform is

$$\mathscr{F}_3[\varphi_3(\mathbf{r})] = \Phi_3(uvw) = \iiint \varphi_3(xyz) \times \exp\{2\pi i(ux + vy + wz)\}\ \mathrm{d}x\ \mathrm{d}y\ \mathrm{d}z. \quad (2.5.6.3)$$

The transform of projection $\varphi_2(xy)$ along z is

$$\begin{aligned}\mathscr{F}_2[\varphi_2(xy)] = \Phi_3(uv0) &= \iiint \varphi_3(xyz) \times \exp\{2\pi i(ux + vy + 0z)\}\ \mathrm{d}x\ \mathrm{d}y\ \mathrm{d}z \\ &= \iiint \varphi_3(xyz)\ \mathrm{d}z \exp\{2\pi i(ux + vy)\}\ \mathrm{d}x\ \mathrm{d}y \\ &= \iint \varphi_2(xy) \exp\{2\pi i(ux + vy)\}\ \mathrm{d}x\ \mathrm{d}y \\ &= \Phi_2(uv). \end{aligned} \quad (2.5.6.4)$$

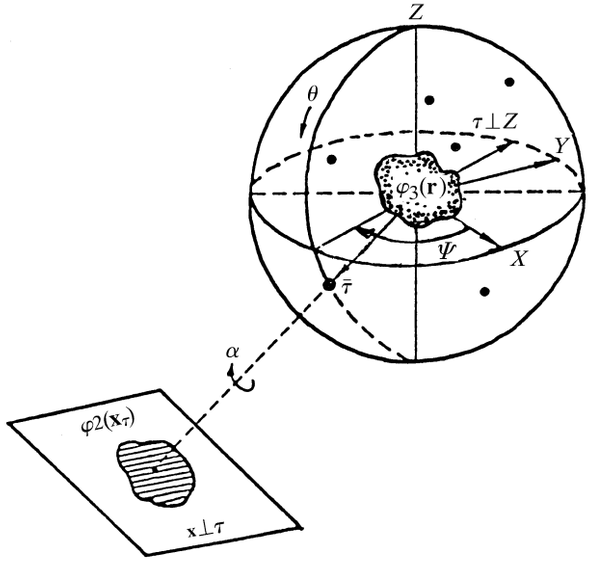

Fig. 2.5.6.2. The projection sphere and projection φ_2 of φ_3 along $\boldsymbol{\tau}$ onto the plane $\mathbf{x} \perp \boldsymbol{\tau}$. The case $\boldsymbol{\tau} \perp z$ represents orthoaxial projection. Points indicate a random distribution of $\boldsymbol{\tau}$.

In the general case (2.5.6.1) of projecting the plane $\mathbf{x}(xy) \| \mathbf{u}(uv) \perp \boldsymbol{\tau}$ along the vector $\boldsymbol{\tau}$

$$\mathscr{F}_2[\varphi_2(\mathbf{x}_\tau)] = \Phi_2(\mathbf{u}_\tau). \quad (2.5.6.5)$$

Reconstruction with Fourier transformation involves transition from projections φ_{2i} at various $\boldsymbol{\tau}_i$ to cross sections Φ_{2i}, then to construction of the three-dimensional transform $\Phi_3(\mathbf{u})$ by means of interpolation between φ_{2i} in reciprocal space, and transition by the inverse Fourier transformation to the three-dimensional distribution $\varphi_3(\mathbf{r})$:

$$\begin{aligned}&\text{set } \varphi_{2i}(\mathbf{x}_{\tau i}) \rightarrow \text{ set } \mathscr{F}_2(\varphi_2) \\ &\quad \equiv \text{ set } \Phi_{2i} \rightarrow \Phi_3 \rightarrow \mathscr{F}_3^{-1}(\Phi_3) \equiv \varphi_3(\mathbf{r}). \end{aligned} \quad (2.5.6.6)$$

Transition (2.5.6.2) or (2.5.6.6) from two-dimensional electron-microscope images (projections) to a three-dimensional structure allows one to consider the complex of methods of 3D reconstruction as three-dimensional electron microscopy. In this sense, electron microscopy is an analogue of methods of structure analysis of crystals and molecules providing their three-dimensional spatial structure. But in structure analysis with the use of X-rays, electrons, or neutrons the initial data are the data in reciprocal space $|\Phi_{2i}|$ in (2.5.6.6), while in electron microscopy this role is played by two-dimensional images $\varphi_{2i}(\mathbf{x})$ [(2.5.6.2), (2.5.6.6)] in real space.

In electron microscopy the 3D reconstruction methods are, mainly, used for studying biological structures (symmetric or asymmetric associations of biomacromolecules), the quaternary structure of proteins, the structures of muscles, spherical and rod-like viruses, bacteriophages, and ribosomes.

An exact reconstruction is possible if there is a continuous set of projections φ_τ corresponding to the motion of the vector $\boldsymbol{\tau}(\theta, \psi)$ over any continuous line connecting the opposite points on the unit sphere (Fig. 2.5.6.2). This is evidenced by the fact that, in this case, the cross sections $\mathscr{F}_2$ which are perpendicular to $\boldsymbol{\tau}$ in Fourier space (2.5.6.4) continuously fill the whole of its volume, *i.e.* give $\mathscr{F}_3(\varphi_3)$ (2.5.6.3) and thereby determine $\varphi_3(\mathbf{r}) = \mathscr{F}^{-1}(\Phi_3)$.

In reality, we always have a discrete (but not continuous) set of projections φ_{2i}. The set of φ_{2i} is, practically, obtained by the rotation of the specimen under the beam through various angles (Hoppe & Typke, 1979) or by imaging of the objects which are randomly oriented on the substrate at different angles (Kam, 1980; Van Heel, 1984). If the object has symmetry, one of its projections is equivalent to a certain number of different projections.

The object $\varphi_3(\mathbf{r})$ is finite in space. For function $\varphi_3(\mathbf{r})$ and any of its projections there holds the normalization condition

$$\Omega = \int \varphi_3(\mathbf{r})\ \mathrm{d}v_\mathbf{r} = \int \varphi_2(\mathbf{x})\ \mathrm{d}\mathbf{x} = \int \varphi_1(x)\ \mathrm{d}x, \quad (2.5.6.7)$$

where Ω is the total 'weight' of the object described by the density distribution φ_3. If one assumes that the density of an object is constant and that inside the object $\varphi = \text{constant} = 1$, and outside it $\varphi = 0$, then Ω is the volume of an object. The volume of an object, say, of molecules, viruses and so on, is usually known from data on the density or molecular mass.

2.5.6.2. *Orthoaxial projection*

In practice, an important case is where all the projection directions are orthogonal to a certain straight line: $\boldsymbol{\tau} \perp z$ (Fig. 2.5.6.3). Here the axis of rotation or the axis of symmetry of an object is perpendicular to an electron beam. Then the three-dimensional problem is reduced to the two-dimensional one, since each cross section $\varphi_{2i}(\mathbf{x}, z = \text{constant})$ is represented by its one-dimensional projections. The direction of vector $\boldsymbol{\tau}$ is defined by the rotational angle ψ of a specimen:

$$\varphi_1(x_{\psi_i}) \equiv L^i(\psi_i) = \int \varphi_2(\mathbf{x})\ \mathrm{d}\tau_\psi;\ x_i \perp \boldsymbol{\tau}_\psi. \quad (2.5.6.8)$$

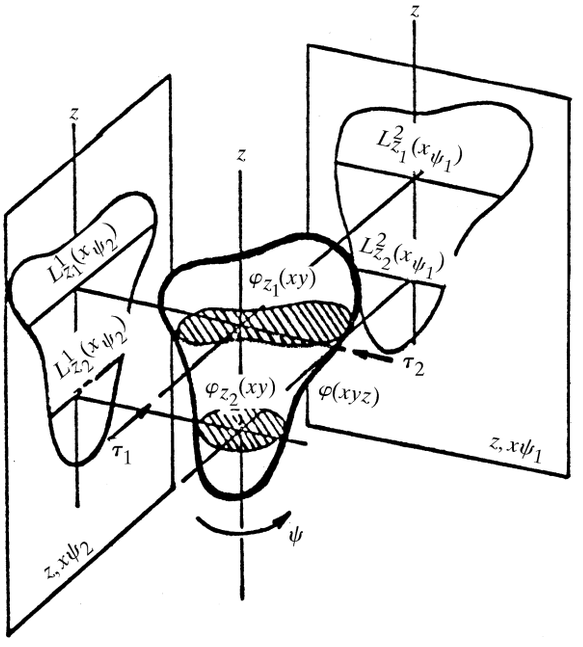

Fig. 2.5.6.3. Orthoaxial projection.

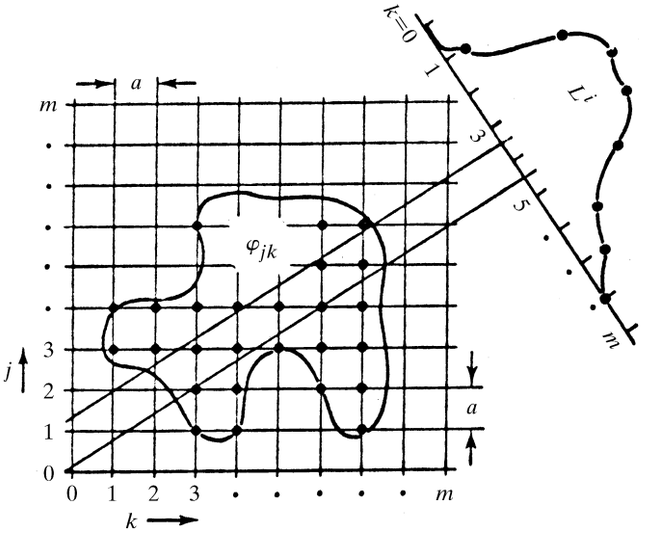

Fig. 2.5.6.4. Discretization and oblique projection.

In this case, the reconstruction is carried out separately for each level z_l:

$$\text{set } \varphi_{1,\,z_l}(x_\psi) \equiv \text{ set } L^i_{z_l} \rightarrow \varphi_{2i}(xyz_l) \qquad (2.5.6.9)$$

and the three-dimensional structure is obtained by superposition of layers $\varphi_{2z_l}(xy)\Delta z$ (Vainshtein *et al.*, 1968; Vainshtein, 1978).

2.5.6.3. *Discretization*

In direct methods of reconstruction as well as in Fourier methods the space is represented as a discrete set of points $\varphi(\mathbf{x}_{jk})$ on a two-dimensional net or $\varphi(\mathbf{r}_{jkl})$ on a three-dimensional lattice. It is sometimes expedient to use cylindrical or spherical coordinates. In two-dimensional reconstruction the one-dimensional projections are represented as a set of discrete values L^i, at a certain spacing in x_ψ. The reconstruction (2.5.6.9) is carried out over the discrete net with m^2 nodes φ_{jk}. The net side A should exceed the diameter of an object D, $A > D$; the spacing $a = A/m$. Then (2.5.6.8) transforms into the sum

$$L^i = \sum_k \varphi_{jk}. \qquad (2.5.6.10)$$

For oblique projections the above sum is taken over all the points within the strips of width a along the axis $\boldsymbol{\tau}_{\psi_i}$ (Fig. 2.5.6.4).

The resolution δ of the reconstructed function depends on the number h of the available projections. At approximately uniform angular distribution of projections, and diameter equal to D, the resolution at reconstruction is estimated as

$$\delta \simeq 2D/h. \qquad (2.5.6.11)$$

The reconstruction resolution δ should be equal to or somewhat better than the instrumental resolution d of electron micrographs ($\delta < d$), the real resolution of the reconstructed structure being d. If the number of projections h is not sufficient, *i.e.* $\delta > d$, then the resolution of the reconstructed structure is δ (Crowther, DeRosier & Klug, 1970; Vainshtein, 1978).

In electron microscopy the typical instrumental resolution d of biological macromolecules for stained specimens is about 20 Å; at the object with diameter $D \simeq 200$ Å the sufficient number h of projections is about 20. If the projections are not uniformly distributed in projection angles, the resolution decreases towards $\mathbf{x} \perp \boldsymbol{\tau}$ for such $\boldsymbol{\tau}$ in which the number of projections is small.

Properties of projections of symmetric objects. If the object has an N-fold axis of rotation, its projection has the same symmetry. At orthoaxial projection perpendicular to the N-fold axis the projections which differ in angle at $j(2\pi/N)$ are identical:

$$\varphi_2(\mathbf{x}_\psi) = \varphi_2[\mathbf{x}_{\psi + j(2\pi/N)}] \quad (j = 1, 2, \ldots, N). \qquad (2.5.6.12)$$

This means that one of its projections is equivalent to N projections. If we have h independent projections of such a structure, the real number of projections is hN (Vainshtein, 1978). For a structure with cylindrical symmetry ($N = \infty$) one of its projections fully determines the three-dimensional structure.

Many biological objects possess helical symmetry – they transform into themselves by the screw displacement operation $s_{p/q}$, where p is the number of packing units in the helical structure per q turns of the continuous helix. In addition, the helical structures may also have the axis of symmetry N defining the pitch of the helix. In this case, a single projection is equivalent to $h = pN$ projections (Cochran *et al.*, 1952).

Individual protein molecules are described by point groups of symmetry of type N or $N/2$. Spherical viruses have icosahedral symmetry 532 with two-, three- and fivefold axes of symmetry. The relationship between vectors $\boldsymbol{\tau}$ of projections is determined by the transformation matrix of the corresponding point group (Crowther, Amos *et al.*, 1970).

2.5.6.4. *Methods of direct reconstruction*

Modelling. If several projections are available, and, especially, if the object is symmetric, one can, on the basis of spatial imagination, recreate approximately the three-dimensional model of the object under investigation. Then one can compare the projections of such a model with the observed projections, trying to draw them as near as possible. In early works on electron microscopy of biomolecules the tentative models of spatial structure were constructed in just this way; these models provide, in the case of the quaternary structure of protein molecules or the structure of viruses, schemes for the arrangement of protein subunits. Useful subsidiary information in this case can be obtained by the method of optical diffraction and filtration.

2.5.6.5. *The method of back-projection*

This method is also called the synthesis of projection functions. Let us consider a two-dimensional case and stretch along τ_{ψ_i} each one-dimensional projection L^i (Fig. 2.5.6.5) by a certain length b; thus, we obtain the projection function

$$L^i(\mathbf{x}) = \frac{1}{b} L^i(x_i) \cdot 1(\tau_i). \tag{2.5.6.13}$$

Let us now superimpose h functions L^i

$$\sum_{i=1}^{h} L^i(\mathbf{x}) = \Sigma_2(\mathbf{x}). \tag{2.5.6.14}$$

The continuous sum over the angles of projection synthesis is

$$\Sigma_2(\mathbf{x}) = \int_0^{\pi} L(\psi, \mathbf{x})\, \mathrm{d}\psi = \rho_2(\mathbf{x}) * |\mathbf{x}|^{-1}$$

$$\simeq \sum_{i=1}^{h} L^i = \rho_2(\mathbf{x}) + B(1); \tag{2.5.6.15}$$

this is the convolution of the initial function with a rapidly falling function $|\mathbf{x}|^{-1}$ (Vainshtein, 1971*b*). In (2.5.6.15), the approximation for a discrete set of h projections is also written. Since the function $|\mathbf{x}|^{-1}$ approaches infinity at $x = 0$, the convolution with it will reproduce the initial function $\rho(\mathbf{x})$, but with some background B decreasing around each point according to the law $|\mathbf{x}|^{-1}$. At orthoaxial projection the superposition of cross sections $\varphi_2(\mathbf{x}, z_k)$ arranged in a pile gives the three-dimensional structure φ_3.

Radon operator. Radon (1917; see also Deans, 1983) gave the exact solution of the problem of reconstruction. However, his mathematical work was for a long time unknown to investigators engaged in reconstruction of a structure from images; only in the early 1970s did some authors obtain results analogous to Radon's (Ramachandran & Lakshminarayanan, 1971; Vainshtein & Orlov, 1972, 1974; Gilbert, 1972*a*).

The convolution in (2.5.6.15) may be eliminated using the Radon integral operator, which modifies projections by introducing around each point the negative values which annihilate on superposition the positive background values. The one-dimensional projection modified with the aid of the Radon operator has the form

$$\tilde{L}(x_\psi) = \frac{1}{2\pi^2} \int_0^{\infty} \frac{2L(x_\psi) - L(x_\psi + x'_\psi) - L(x_\psi - x'_\psi)}{x'^2_\psi}\, \mathrm{d}x'_\psi. \tag{2.5.6.16}$$

Now $\varphi_2(\mathbf{x})$ is calculated analogously to (2.5.6.14), not from the initial projections L but from the modified projection $\tilde{L}$:

$$\varphi_2(\mathbf{x}) = \int_0^{\pi} \tilde{L}(\psi, \mathbf{x})\, \mathrm{d}\psi \simeq \sum_{i=1}^{k} \tilde{L}_i(\psi_i, \mathbf{x}). \tag{2.5.6.17}$$

The reconstruction of high-symmetry structures, in particular helical ones, by the direct method is carried out from one projection making use of its equivalence to many projections. The Radon formula in discrete form can be obtained using the double Fourier transformation and convolution (Ramachandran & Lakshminarayanan, 1971).

2.5.6.6. *The algebraic and iteration methods*

These methods have been derived for the two-dimensional case; consequently, they can also be applied to three-dimensional reconstruction in the case of orthoaxial projection.

Let us discretize $\varphi_2(\mathbf{x})$ by a net m^2 of points φ_{jk}; then we can construct the system of equations (2.5.6.10).

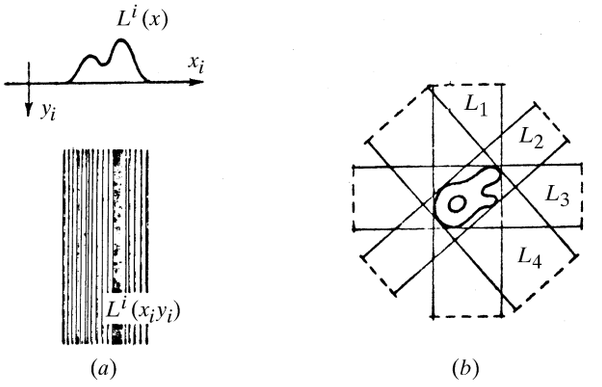

Fig. 2.5.6.5. (*a*) Formation of a projection function; (*b*) superposition of these functions.

When h projections are available the condition of unambiguous solution of system (2.5.6.10) is: $h \geq m$. At $m \simeq (3\text{–}5)h$ we can, in practice, obtain sufficiently good results (Vainshtein, 1978).

Methods of reconstruction by iteration have also been derived that cause some initial distribution to approach one $\varphi_2(\mathbf{x})$ satisfying the condition that its projection will resemble the set L^i. Let us assign on a discrete net φ_{jk} as a zero-order approximation the uniform distribution of mean values (2.5.6.7)

$$\varphi^0_{jk} = \langle \varphi \rangle = \Omega / m^2. \tag{2.5.6.18}$$

The projection of the qth approximation φ^q_{jk} at the angle φ_i (used to account for discreteness) is L^{iq}_n.

The next approximation φ^{q+1} for each point jk is given in the method of 'summation' by the formula

$$\varphi^{q+1}_{jk} = \max[\varphi^q_{jk} + (L^i_n - L^{i,q}_n)/N^i_{L_n};\, 0], \tag{2.5.6.19}$$

where N_{L^i} is the number of points in a strip of the projection L^i_n. One cycle of iterations involves running φ^q_{jk} around all of the angles ψ_j (Gordon *et al.*, 1970).

When carrying out iterations, we may take into account the contribution not only of the given projection, but also of all others. In this method the process of convergence improves. Some other iteration methods have been elaborated (Gordon & Herman, 1971; Gilbert, 1972*b*; Crowther & Klug, 1974; Gordon, 1974).

2.5.6.7. *Reconstruction using Fourier transformation*

This method is based on the Fourier projection theorem [(2.5.6.3)–(2.5.6.5)]. The reconstruction is carried out according to scheme (2.5.6.6) (DeRosier & Klug, 1968; Crowther, DeRosier & Klug, 1970; Crowther, Amos *et al.* 1970; DeRosier & Moore, 1970; Orlov, 1975). The three-dimensional Fourier transform $\mathscr{F}_3(\mathbf{u})$ is found from a set of two-dimensional cross sections $\mathscr{F}_2(\mathbf{u})$ on the basis of the Whittaker–Shannon interpolation. If the object has helical symmetry (which often occurs in electron microscopy of biological objects, *e.g.* on investigating bacteriophage tails, muscle proteins) cylindrical coordinates are used. Diffraction from such structures with c periodicity and scattering density $\varphi(r, \psi, z)$ is defined by the Fourier–Bessel transform:

$$\Phi(R, \Psi, Z) = \sum_{n=-\infty}^{+\infty} \exp\left[in\left(\Psi + \frac{\pi}{2}\right)\right] \int_0^{\infty} \int_0^{2\pi} \int_0^{l} \varphi(r, \psi, z)$$

$$\times J_n(2\pi r R) \exp[-i(n\psi + 2\pi z Z)] r\, \mathrm{d}r\, \mathrm{d}\psi\, \mathrm{d}z$$

$$= \sum_n G_n(R, Z) \exp\left[in\left(\Psi + \frac{\pi}{2}\right)\right]. \tag{2.5.6.20}$$

The inverse transformation has the form

$$\rho(r,\psi,z)=\sum_n \int g_n(r,Z)\exp(in\psi)\exp(2\pi izZ)\ \mathrm{d}Z, \qquad (2.5.6.21)$$

so that g_n and G_n are the mutual Bessel transforms

$$G_n(R,Z)=\int_0^\infty g_n(rZ)J_n(2\pi rR)2\pi r\ \mathrm{d}r \qquad (2.5.6.22)$$

$$g_n(r,Z)=\int_0^\infty G_n(R,Z)J_n(2\pi rR)2\pi R\ \mathrm{d}R. \qquad (2.5.6.23)$$

Owing to helical symmetry, (2.5.6.22), (2.5.6.23) contain only those of the Bessel functions which satisfy the selection rule (Cochran *et al.*, 1952)

$$l=mp+(nq/N), \qquad (2.5.6.24)$$

where N, q and p are the helix symmetry parameters, $m=0,\pm1,\pm2,\ldots$. Each layer l is practically determined by the single function J_n with the lowest n; the contribution of other functions is neglected. Thus, the Fourier transformation of one projection of a helical structure, with an account of symmetry and phases, gives the three-dimensional transform (2.5.6.23). We can introduce into this transform the function of temperature-factor type filtering the 'noise' from large spatial frequencies.

2.5.6.8. *Three-dimensional reconstruction in the general case*

In the general case of 3D reconstruction $\varphi_3(\mathbf{r})$ from projections $\varphi_2(\mathbf{x}_\tau)$ the projection vector $\boldsymbol{\tau}$ occupies arbitrary positions on the projection sphere (Fig. 2.5.6.2). Then, as in (2.5.6.15), we can construct the three-dimensional spatial synthesis. To do this, let us transform the two-dimensional projections $\varphi_{2i}[\mathbf{x},\boldsymbol{\tau}(\theta,\psi)_i]$ by extending them along $\boldsymbol{\tau}$ as in (2.5.6.13) into three-dimensional projection functions $\varphi_3(\mathbf{r}_{\tau_i})$.

Analogously to (2.5.6.15), such a three-dimensional synthesis is the integral over the hemisphere (Fig. 2.5.6.2)

$$\begin{aligned}\Sigma_3(\mathbf{r})&=\int_\omega \varphi_3(\mathbf{r},\boldsymbol{\tau}_i)\ \mathrm{d}\omega_\tau=\varphi(\mathbf{r})*|\mathbf{r}|^{-2}\\ &\simeq \Sigma\varphi_{3i}[\mathbf{r}_{\tau(\theta,\psi)_i}]\simeq\varphi_3(\mathbf{r})+B; \qquad (2.5.6.25)\end{aligned}$$

this is the convolution of the initial function with $|\mathbf{r}|^{-2}$ (Vainshtein, 1971*b*).

To obtain the exact reconstruction of $\varphi_3(\mathbf{r})$ we find, from each $\varphi_2(\mathbf{x}_{\boldsymbol{\tau}})$, the modified projection (Vainshtein & Orlov, 1974; Orlov, 1975)

$$\tilde{\varphi}_2(\mathbf{x}_\tau)=\int\frac{\varphi_2(\mathbf{x}_{\boldsymbol{\tau}})-\varphi_2(\mathbf{x}'_{\boldsymbol{\tau}})}{|\mathbf{x}_{\boldsymbol{\tau}}-\mathbf{x}'_{\boldsymbol{\tau}}|^3}\ \mathrm{d}s_{\mathbf{x}'}. \qquad (2.5.6.26)$$

By extending $\varphi_2(\mathbf{x}_{\boldsymbol{\tau}})$ along $\boldsymbol{\tau}$ we transform them into $\tilde{\varphi}_3(\mathbf{r}_{\boldsymbol{\tau}})$. Now the synthesis over the angles $\omega_\tau=(\theta,\psi,\alpha)_\tau$ gives the three-dimensional function

$$\varphi_3(\mathbf{r})=\frac{1}{4\pi^3}\int\tilde{\varphi}_3(\mathbf{r}_{\boldsymbol{\tau}})\ \mathrm{d}\omega_{\boldsymbol{\tau}}\simeq\sum_i\tilde{\varphi}_{3i}[\mathbf{r}_{\tau(\theta,\psi,\alpha)_i}]. \qquad (2.5.6.27)$$

The approximation for a discrete set of angles is written on the right. In this case we are not bound by the coaxial projection condition which endows the experiment with greater possibilities; the use of object symmetry also profits from this. To carry out the 3D reconstruction (2.5.6.25) or (2.5.6.27) one should know all three Euler's angles ψ, θ, α (Fig. 2.5.6.2).

The projection vectors $\boldsymbol{\tau}_i$ should be distributed more or less uniformly over the sphere (Fig. 2.5.6.2). This can be achieved by using special goniometric devices.

Another possibility is the investigation of particles which, during the specimen preparation, are randomly oriented on the substrate. This, in particular, refers to asymmetric ribosomal particles. In this case the problem of determining these orientations arises.

The method of spatial correlation functions may be applied if a large number of projections with uniformly distributed projection directions is available (Kam, 1980). The space correlation function is the averaged characteristic of projections over all possible directions which is calculated from the initial projections or the corresponding sections of the Fourier transform. It can be used to find the coefficients of the object density function expansion over spherical harmonics, as well as to carry out the 3D reconstruction in spherical coordinates.

Another method (Van Heel, 1984) involves the statistical analysis of image types, subdivision of images into several classes and image averaging inside the classes. Then, if the object is rotated around some axis, the 3D reconstruction is carried out by the iteration method.

If such a specimen is inclined at a certain angle with respect to the beam, then the images of particles in the preferred orientation make a series of projections inclined at an angle β and having a random azimuth. The azimuthal rotation is determined from the image having zero inclination.

If particles on the substrate have a characteristic shape, they may acquire a preferable orientation with respect to the substrate, their azimuthal orientation α being random (Radermacher *et al.*, 1987).

In the general case, the problem of determining the spatial orientations of randomly distributed identical three-dimensional particles $\varphi_3(\mathbf{r})$ with an unknown structure may be solved by measuring their two-dimensional projections $p(\mathbf{x}_\tau)$ (Fig. 2.5.6.1)

$$p(\mathbf{x}_{\tau_i})\equiv\varphi_2(\mathbf{x}_{\tau_i})\simeq\int\varphi_3(\mathbf{r})\ \mathrm{d}\tau_i\quad\mathbf{x}\perp\boldsymbol{\tau}_i; \qquad (2.5.6.1a)$$

if the number i of such projections is not less than three, $i\geq3$ (Vainshtein & Goncharov, 1986*a*,*b*; Goncharov *et al.* 1987; Goncharov, 1987). The direction of the vector $\boldsymbol{\tau}_i$ along which the projection $p(\boldsymbol{\tau}_i)$ is obtained is set by the angle $\omega_i(\theta_i,\psi_i)$ (Fig. 2.5.6.2).

The method is based on the analysis of one-dimensional projections q_α of two-dimensional projections $p(\mathbf{x}_{\tau_i})$

$$q(x_{\perp\alpha})=\int p(\mathbf{x}_{\tau_i})\ \mathrm{d}x_{\parallel\alpha}, \qquad (2.5.6.28)$$

where α is the angle of the rotation about vector $\boldsymbol{\tau}$ in the p plane.

Lemma 1. Any two projections $p_1(\mathbf{x}_{\tau_i})$ and $p_2(\mathbf{x}_{\tau_2})$ (Fig. 2.5.6.6) have common (identical) one-dimensional projections $q_{12}(x_{12})$:

$$q_{12}(x_{12})=q_{1,\alpha_1 j}(x_{\perp\alpha_1 j})=q_{2,\alpha_2 k}(x_{\perp\alpha_2 k}). \qquad (2.5.6.29)$$

Vectors $\boldsymbol{\tau}_1$ and $\boldsymbol{\tau}_2$ (Fig. 2.5.6.3) determine plane h in which they are both lying. Vector $m_{12}=\langle\tau_1\tau_2\rangle$ is normal to plane h and parallel to axis x_{12} of the one-dimensional projection q_{12}; both $x_{\perp\alpha_1 j}$ and $x_{\perp\alpha_2 j}$ axes along which the projections q_1 and q_2 are constructed are perpendicular to x_{12}.

The corresponding lemma in the Fourier space states:

Lemma 2. Any two plane transforms, $\Phi_2(\mathbf{u}_{\tau_1})=\mathscr{F}_2 p_1$ and $\Phi_2(\mathbf{u}_{\tau_2})=\mathscr{F}_2 p_2$ intersect along the straight line v_{12} (Fig. 2.5.6.7); the one-dimensional transform $Q(v_{12})$ is the transform of $q_{12}: Q(v_{12})=\mathscr{F}_1 g_{12}$.

Thus in order to determine the orientations $\omega_i(\theta_i,\psi_i,\alpha_i)$ of a three-dimensional particle $\varphi_{3,\omega_i}(\mathbf{r})$ it is necessary either to use projections p_i in real space or else to pass to the Fourier space (2.5.6.5).

Now consider real space. The projections p_i are known and can be measured but angles α_{ij} of their rotation about vector $\boldsymbol{\tau}_i$ (Fig. 2.5.6.8) are unknown and should be determined. Let us choose any two projections p_1 and p_2 and construct a set of one-dimensional projections $q_{1,\alpha_1 j}$ and $q_{2,\alpha_2 k}$ by varying angles α_{1j} and α_{2k}. In

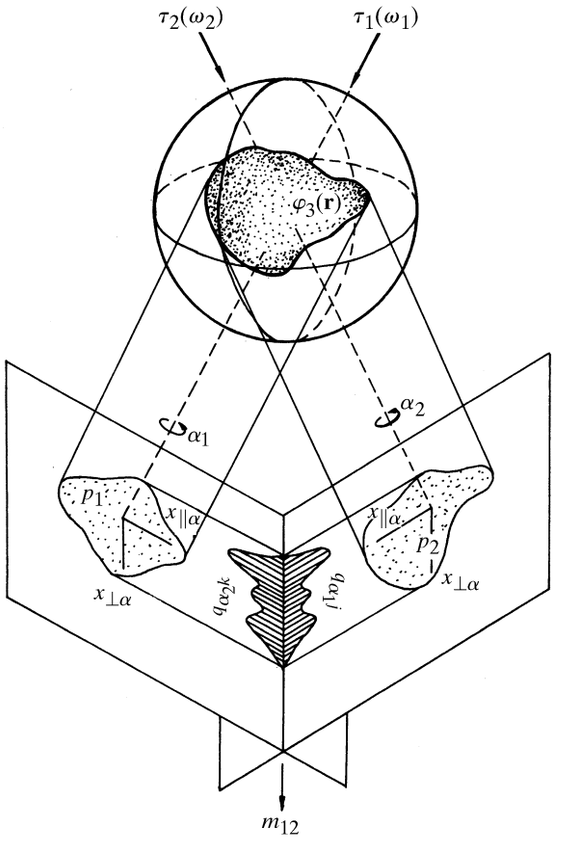

Fig. 2.5.6.6. Relative position of the particle and planes of projection.

accordance with *Lemma* 1, there exists a one-dimensional projection, common for both p_1 and p_2, which determines angles α_{1j} and α_{2k} along which p_1 and p_2 should be projected for obtaining the identical projection q_{12} (Fig. 2.5.6.5). Comparing $q_{1,\,\alpha_1 j}$ and $q_{2,\,\alpha_2 k}$ and using the minimizing function

$$D(1,2) = |q_{1,\,\alpha_1 j} - q_{2,\,\alpha_2 k}|^2 \qquad (2.5.6.30)$$

it is possible to find such a common projection q_{12}. (A similar consideration in Fourier space yields Q_{12}.)

The mutual spatial orientations of any three non-coplanar projection vectors $\boldsymbol{\tau}_1$, $\boldsymbol{\tau}_2$, $\boldsymbol{\tau}_3$ can be found from three different two-dimensional projections p_1, p_2 and p_3 by comparing the following pairs of projections: p_1 and p_2, p_1 and p_3, and p_2 and

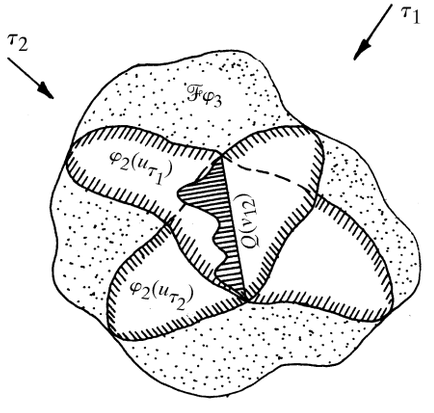

Fig. 2.5.6.7. Section of a three-dimensional Fourier transform of the density of the particles, corresponding to plane projections of this density.

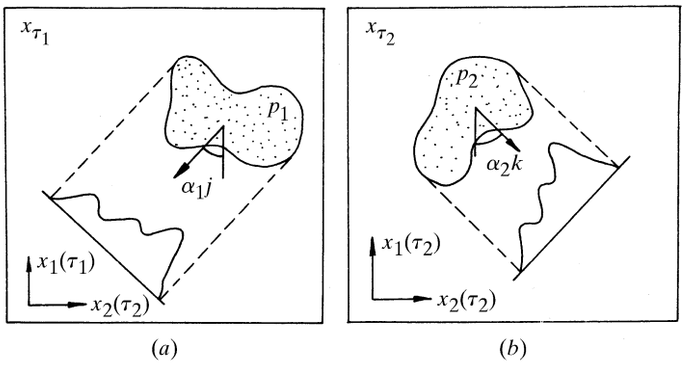

Fig. 2.5.6.8. Plane projections of a three-dimensional body. The systems of coordinates in planes (*a*) and (*b*) are chosen independently of one another.

p_3, and by determining the corresponding q_{12}, q_{13} and q_{23}. The determination of angles ω_1, ω_2 and ω_3 reduces to the construction of a trihedral angle formed by planes h_{12}, h_{13} and h_{23}. Then the projections $p_i(\omega_i)$ with the known ω_i $(i = 1, 2, 3)$ can be complemented with other projections $(i = 4, 5, \ldots)$ and the corresponding values of ω can be determined. Having a sufficient number of projections and knowing the orientations ω_i, it is possible to carry out the 3D reconstruction of the object [see (2.5.6.27); Orlov, 1975; Vainshtein & Goncharov, 1986*a*; Goncharov *et al.*, 1987].

2.5.7. Direct phase determination in electron crystallography (D. L. DORSET)

2.5.7.1. *Problems with 'traditional' phasing techniques*

The concept of using experimental electron-diffraction intensities for quantitative crystal structure analyses has already been presented in Section 2.5.4. Another aspect of quantitative structure analysis, employing high-resolution images, has been presented in Sections 2.5.5 and 2.5.6. That is to say, electron micrographs can be regarded as an independent source of crystallographic phases.

Before direct methods (Chapter 2.2) were developed as the standard technique for structure determination in small-molecule X-ray crystallography, there were two principal approaches to solving the crystallographic phase problem. First, 'trial and error' was used, finding some means to construct a reasonable model for the crystal structure *a priori*, *e.g.* by matching symmetry properties shared by the point group of the molecule or atomic cluster and the unit-cell space group. Secondly, the autocorrelation function of the crystal, known as the Patterson function (Chapter 2.3), was calculated (by the direct Fourier transform of the available intensity data) to locate salient interatomic vectors within the unit cell.

The same techniques had been used for electron-diffraction structure analysis (nowadays known as *electron crystallography*). In fact, advocacy of the first method persists. Because of the perturbations of diffracted intensities by multiple-beam dynamical scattering (Chapter 5.2), it has often been suggested that trial and error be used to construct the scattering model for the unit crystal in order to test its convergence to observed data after simulation of the scattering events through the crystal. This indirect approach assumes that no information about the crystal structure can be obtained directly from observed intensity data. Under more favourable scattering conditions nearer to the kinematical approximation, *i.e.* for experimental data from thin crystals made up of light atoms, trial and error modelling, simultaneously minimizing an atom–atom nonbonded potential function with the crystal-

lographic residual, has enjoyed widespread use in electron crystallography, especially for the determination of linear polymer structures (Brisse, 1989; Pérez & Chanzy, 1989).

Interpretation of Patterson maps has also been important for structure analysis in electron crystallography. Applications have been discussed by Vainshtein (1964), Zvyagin (1967) and Dorset (1994*a*). In face of the dynamical scattering effects for electron scattering from heavy-atom crystals realized later (*e.g.* Cowley & Moodie, 1959), attempts had also been made to modify this autocorrelation function by using a power series in $|F_{\mathbf{h}}|$ to sharpen the peaks (Cowley, 1956). (Here $F_{\mathbf{h}} \equiv \Phi_{\mathbf{h}}$, replacing the notation for the kinematical electron-diffraction structure factor employed in Section 2.5.4.) More recently, Vincent and co-workers have selected first-order-Laue-zone data from inorganics to minimize the effect of dynamical scattering on the interpretability of their Patterson maps (Vincent & Exelby, 1991, 1993; Vincent & Midgley, 1994). Vainshtein & Klechkovskaya (1993) have also reported use of the Patterson function to solve the crystal structure of a lead soap from texture electron-diffraction intensity data.

It is apparent that trial-and-error techniques are most appropriate for *ab initio* structure analysis when the underlying crystal structures are reasonably easy to model. The requisite positioning of molecular (or atomic) groups within the unit cell may be facilitated by finding atoms that fit a special symmetry position [see *IT* A (1995)]. Alternatively, it is helpful to know the molecular orientation within the unit cell (*e.g.* provided by the Patterson function) to allow the model to be positioned for a conformational or translational search. [Examples would include the polymer-structure analyses cited above, as well as the layer-packing analysis of some phospholipids (Dorset, 1987).] While attempts at *ab initio* modelling of three-dimensional crystal structures, by searching an n-dimensional parameter space and seeking a global internal energy minimum, has remained an active research area, most success so far seems to have been realized with the prediction of two-dimensional layers (Scaringe, 1992). In general, for complicated unit cells, determination of a structure by trial and error is very difficult unless adequate constraints can be placed on the search.

Although Patterson techniques have been very useful in electron crystallography, there are also inherent difficulties in their use, particularly for locating heavy atoms. As will be appreciated from comparison of scattering-factor tables for X-rays [*IT* C (1999) Chapter 6.1] with those for electrons, [*IT* C (1999) Chapter 4.3] the relative values of the electron form factors are more compressed with respect to atomic number than are those for X-ray scattering. As discussed in Chapter 2.3, it is desirable that the ratio of summed scattering factor terms, $r = \sum_{\text{heavy}} Z^2 / \sum_{\text{light}} Z^2$, where Z is the scattering factor value at $\sin\theta/\lambda = 0$, be near unity. A practical comparison would be the value of r for copper (DL-alaninate) solved from electron-diffraction data by Vainshtein *et al.* (1971). For electron diffraction, $r = 0.47$ compared to the value 2.36 for X-ray diffraction. Orientation of salient structural features, such as chains and rings, would be equally useful for light-atom moieties in electron or X-ray crystallography with Patterson techniques. As structures become more complicated, interpretation of Patterson maps becomes more and more difficult unless an automated search can be carried out against a known structural fragment (Chapter 2.3).

2.5.7.2. *Direct phase determination from electron micrographs*

The 'direct method' most familiar to the electron microscopist is the high-resolution electron micrograph of a crystalline lattice. Retrieval of an average structure from such a micrograph assumes that the experimental image conforms adequately to the 'weak phase object' approximation, as discussed in Section 2.5.5. If this is so, the use of image-averaging techniques, *e.g.* Fourier filtration or correlational alignment, will allow the unit-cell contents to be visualized after the electron-microscope phase contrast transfer function is deconvoluted from the average image, also discussed in Section 2.5.5. Image analyses can also be extended to three dimensions, as discussed in Section 2.5.6, basically by employing tomographic reconstruction techniques to combine information from the several tilt projections taken from the crystalline object. The potential distribution of the unit cell to the resolution of the imaging experiment can then be used, *via* the Fourier transform, to obtain crystallographic phases for the electron-diffraction amplitudes recorded at the same resolution. This method for phase determination has been the mainstay of protein electron crystallography.

Once a set of phases is obtained from the Fourier transform of the deconvoluted image, they must, however, be referred to an allowed crystallographic origin. For many crystallographic space groups, this choice of origin may coincide with the location of a major symmetry element in the unit cell [see *IT* A (1995)]. Hence, since the Fourier transform of translation is a phase term, if an image shift $[\delta(\mathbf{r} + \mathbf{r}_0)]$ is required to translate the origin of the repeating mass unit $\varphi(\mathbf{r})$ from the arbitrary position in the image to a specific site allowed by the space group,

$$\mathrm{g}(\mathbf{r}) = \varphi(\mathbf{r}) \otimes \delta(\mathbf{r} + \mathbf{r}_0) = \varphi(\mathbf{r} + \mathbf{r}_0),$$

where the operation '$\otimes$' denotes convolution. The Fourier transform of this shifted density function will be

$$G(\mathbf{s}) = F(\mathbf{s}) \exp(2\pi i \mathbf{s} \cdot \mathbf{r}_0) = |F(\mathbf{s})| \exp[i(\phi_s + 2\pi i \mathbf{s} \cdot \mathbf{r}_0)].$$

In addition to the crystallographic phases ϕ_s, it will, therefore, be necessary to find the additional phase-shift term $2\pi i \mathbf{s} \cdot \mathbf{r}_0$ that will access an allowed unit-cell origin. Such origin searches are carried out automatically by some commercial image-averaging computer-software packages.

In addition to applications to thin protein crystals (*e.g.* Henderson *et al.*, 1990; Jap *et al.*, 1991; Kühlbrandt *et al.*, 1994), there are numerous examples of molecular crystals that have been imaged to a resolution of 3–4 Å, many of which have been discussed by Fryer (1993). For π-delocalized compounds, which are the most stable in the electron beam against radiation damage, the best results (2 Å resolution) have been obtained at 500 kV from copper perchlorophthalocyanine epitaxically crystallized onto KCl. As shown by Uyeda *et al.* (1978–1979), the averaged images clearly depict the positions of the heavy Cu and Cl atoms, while the positions of the light atoms in the organic residue are not resolved. (The utility of image-derived phases as a basis set for phase extension will be discussed below.) A number of aromatic polymer crystals have also been imaged to about 3 Å resolution, as reviewed recently (Tsuji, 1989; Dorset, 1994*b*).

Aliphatic molecular crystals are much more difficult to study because of their increased radiation sensitivity. Nevertheless, monolamellar crystals of the paraffin n-$C_{44}H_{90}$ have been imaged to 2.5 Å resolution with a liquid-helium cryomicroscope (Zemlin *et al.*, 1985). Similar images have been obtained at room temperature from polyethylene (Revol & Manley, 1986) and also a number of other aliphatic polymer crystals (Revol, 1991).

As noted by J. M. Cowley in Section 2.5.1, dynamical scattering can pose a significant barrier to the direct interpretation of high-resolution images from many inorganic materials. Nevertheless, with adequate control of experimental conditions (limiting crystal thickness, use of high-voltage electrons) some progress has been made. Pan & Crozier (1993) have described 2.0 Å images from zeolites in terms of the phase-grating approximation. A three-dimensional structural study has been carried out on an aluminosilicate by Wenk *et al.* (1992) with thin samples that

conform to the weak-phase-object approximation at the 800 kV used for the imaging experiment. Heavy and light (*e.g.* oxygen) atoms were located in the micrographs in good agreement with an X-ray crystal structure. Heavy-atom positions from electron microscopic and X-ray structure analyses have also been favourably compared for two heavy-metal oxides (Hovmöller *et al.*, 1984; Li & Hovmöller, 1988).

2.5.7.3. *Probabilistic estimate of phase invariant sums*

Conventional direct phasing techniques, as commonly employed in X-ray crystallography (*e.g.* see Chapter 2.2), have also been used for *ab initio* electron-crystallographic analyses. As in X-ray crystallography, probabilistic estimates of a linear combination of phases (Hauptman & Karle, 1953; Hauptman, 1972) are made after normalized structure factors are calculated *via* electron form factors, *i.e.*

$$|E_{\mathbf{h}}^2| = I_{\rm obs}/\varepsilon\sum_i f_i^2, \text{ where } \langle|E|^2\rangle = 1.000.$$

(Here, an overall temperature factor can be found from a Wilson plot. Because of multiple scattering, the value of B may be found occasionally to lie close to 0.0 Å^2.) The phase invariant sums

$$\psi = \phi_{\mathbf{h}_1} + \phi_{\mathbf{h}_2} + \phi_{\mathbf{h}_3} + \ldots$$

can be particularly effective for structure analysis. Of particular importance historically have been the Σ_2-triple invariants where $\mathbf{h}_1 + \mathbf{h}_2 + \mathbf{h}_3 = 0$ and $\mathbf{h}_1 \neq \mathbf{h}_2 \neq \mathbf{h}_3$. The probability of predicting $\psi = 0$ is directly related to the value of

$$A = (2\sigma_3/\sigma_2^{3/2})|E_{\mathbf{h}_1}E_{\mathbf{h}_2}E_{\mathbf{h}_3}|,$$

where $\sigma_{\mathbf{h}} = \sum_{j=1}^{N} Z_j^n$ and Z is the value of the scattering factor at $\sin\theta/\lambda = 0$. Thus, the values of the phases are related to the measured structure factors, just as they are found to be in X-ray crystallography. The normalization described above imposes the point-atom structure (compensating for the fall-off of an approximately Gaussian form factor) often assumed in deriving the joint probability distributions. Especially for van der Waals structures, the constraint of positivity also holds in electron crystallography. (It is also quite useful for charged atoms so long as the reflections are not measured at very low angles.) Other useful phase invariant sums are the Σ_1 triples, where $\mathbf{h}_1 = \mathbf{h}_2 = -1/2\mathbf{h}_3$, and the quartets, where $\mathbf{h}_1 + \mathbf{h}_2 + \mathbf{h}_3 + \mathbf{h}_4 = 0$ and $\mathbf{h}_1 \neq \mathbf{h}_2 \neq \mathbf{h}_3 \neq \mathbf{h}_4$. The prediction of a correct phase for an invariant is related in each case to the normalized structure-factor magnitudes.

The procedure for phase determination, therefore, is identical to the one used in X-ray crystallography (see Chapter 2.2). Using vectorial combinations of Miller indices, one generates triple and quartet invariants from available measured data and ranks them according to parameters such as A, defined above, which, as shown in Chapter 2.2, are arguments of the Cochran formula. The invariants are thus listed in order of their reliability. This, in fact, generates a set of simultaneous equations in crystallographic phase. In order to begin solving these equations, it is permissible to define arbitrarily the phase values of a limited number of reflections (three for a three-dimensional primitive unit cell) for reflections with Miller-index parity $hkl \neq ggg$ and $\sum_i h_i k_i l_i \neq ggg$, where g is an even number. This defines the origin of a unit cell. For noncentrosymmetric unit cells, the condition for defining the origin, which depends on the space group, is somewhat more complicated and an enantiomorph-defining reflection must be added.

In the evaluation of phase-invariant sums above a certain probability threshold, phase values are determined algebraically after origin (and enantiomorph) definition until a large enough set is obtained to permit calculation of an interpretable potential map (*i.e.* where atomic positions can be seen). There may be a few invariant phase sums above this threshold probability value which are incorrectly predicted, leading either to false phase assignments or at least to phase assignments inconsistent with those found from other invariants. A small number of such errors can generally be tolerated. Another problem arises when an insufficient quantity of new phase values is assigned directly from the phase invariants after the origin-defining phases are defined. This difficulty may occur for small data sets, for example. If this is the case, it is possible that a new reflection of proper index parity can be used to define the origin. Alternatively, $\phi_n = a, b, c \ldots$ algebraic unknowns can be used to establish the phase linkage among certain reflections. If the structure is centrosymmetric, and when enough reflections are given at least symbolic phase assignments, 2^n maps are calculated and the correct structure is identified by inspection of the potential maps. When all goes well in this so-called 'symbolic addition' procedure, the symbols are uniquely determined and there is no need to calculate more than a single map. If algebraic values are retained for certain phases because of limited vectorial connections in the data set, then a few maps may need to be generated so that the correct structure can be identified using the chemical knowledge of the investigator. The atomic positions identified can then be used to calculate phases for all observed data (*via* the structure-factor calculation) and the structure can be refined by Fourier (or, sometimes, least-squares) techniques to minimize the crystallographic R factor.

The first actual application of direct phasing techniques to experimental electron-diffraction data, based on symbolic addition procedures, was to two methylene subcell structures (an *n*-paraffin and a phospholipid; Dorset & Hauptman, 1976). Since then, evaluation of phase invariants has led to numerous other structures. For example, early texture electron-diffraction data sets obtained in Moscow (Vainshtein, 1964) were shown to be suitable for direct analysis. The structure of diketopiperazine (Dorset, 1991*a*) was determined from these electron-diffraction data (Vainshtein, 1955) when directly determined phases allowed computation of potential maps such as the one shown in Fig. 2.5.7.1. Bond distances and angles are in good agreement with the X-ray structure, particularly after least-squares refinement (Dorset & McCourt, 1994*a*). In addition, the structures of urea (Dorset, 1991*b*), using data published by Lobachev & Vainshtein (1961), paraelectric thiourea (Dorset, 1991*b*), using data published by Dvoryankin & Vainshtein (1960), and three mineral structures (Dorset, 1992*a*), from data published by Zvyagin (1967), have been determined, all using the original texture (or mosaic single-crystal) diffraction data. The most recent determination based on such texture diffraction data is that of basic copper chloride (Voronova & Vainshtein, 1958; Dorset, 1994*c*).

Symbolic addition has also been used to assign phases to selected-area diffraction data. The crystal structure of boric acid (Cowley, 1953) has been redetermined, adding an independent low-temperature analysis (Dorset, 1992*b*). Additionally, a direct structure analysis has been reported for graphite, based on high-voltage intensity data (Ogawa *et al.*, 1994). Two-dimensional data from several polymer structures have also been analysed successfully (Dorset, 1992*c*) as have three-dimensional intensity data (Dorset, 1991*c*,*d*; Dorset & McCourt, 1993).

Phase information from electron micrographs has also been used to aid phase determination by symbolic addition. Examples include the epitaxically oriented paraffins *n*-hexatriacontane (Dorset & Zemlin, 1990), *n*-tritriacontane (Dorset & Zhang, 1991) and a 1:1 solid solution of *n*-$C_{32}H_{66}$/*n*-$C_{36}H_{74}$ (Dorset, 1990*a*). Similarly, lamellar electron-diffraction data to *ca* 3 Å resolution from epitaxically oriented phospholipids have been phased by analysis of Σ_1 and Σ_2-triplet invariants (Dorset, 1990*b*, 1991*e*,*f*), in one case combined with values from a 6 Å resolution electron

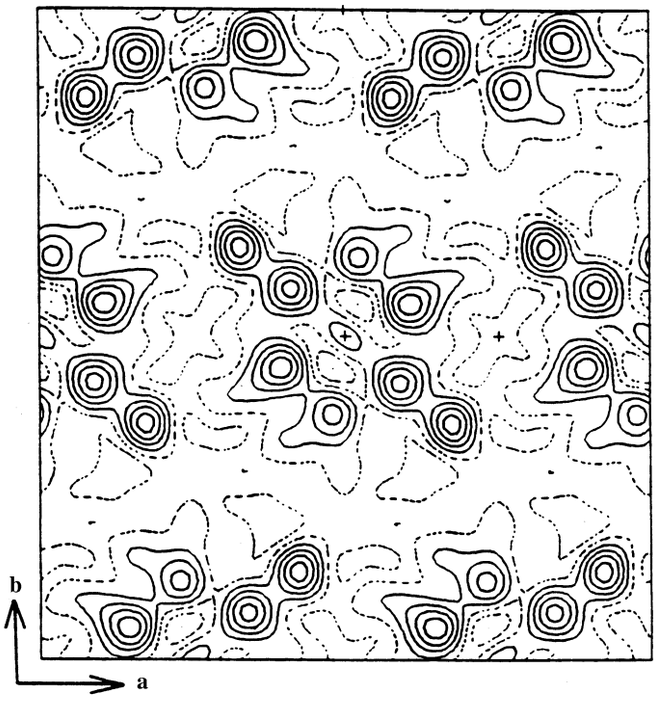

Fig. 2.5.7.1. Potential map for diketopiperazine ([001] projection) after a direct phase determination with texture electron-diffraction intensity data obtained originally by Vainshtein (1955).

microscope image (Dorset *et al.*, 1990, 1993). Most recently, such data have been used to determine the layer packing of a phospholipid binary solid solution (Dorset, 1994*d*).

An *ab initio* direct phase analysis was carried out with zonal electron-diffraction data from copper perchlorophthalocyanine. Using intensities from a *ca* 100 Å thick sample collected at 1.2 MeV, the best map from a phase set with symbolic unknowns retrieves the positions of all the heavy atoms, equivalent to the results of the best images (Uyeda *et al.*, 1978–1979). Using these positions to calculate an initial phase set, the positions of the remaining light C, N atoms were found by Fourier refinement so that the final bond distances and angles were in good agreement with those from X-ray structures of similar compounds (Dorset *et al.*, 1991). A similar analysis has been carried out for the perbromo analogue (Dorset *et al.*, 1992). Although dynamical scattering and secondary scattering significantly perturb the observed intensity data, the total molecular structure can be visualized after a Fourier refinement. Most recently, a three-dimensional structure determination was reported for C_{60} buckminsterfullerene based on symbolic addition with results most in accord with a rotationally disordered molecular packing (Dorset & McCourt, 1994*b*).

2.5.7.4. *The tangent formula*

Given a triple phase relationship

$$\phi_{\mathbf{h}} \simeq \phi_{\mathbf{k}} + \phi_{\mathbf{h}-\mathbf{k}},$$

where $\mathbf{h}$, $\mathbf{k}$ and $\mathbf{h}-\mathbf{k}$ form a vector sum, it is often possible to find a more reliable estimate of $\phi_{\mathbf{h}}$ when all the possible vectorial contributions to it within the observed data set $\mathbf{k}_{\mathbf{r}}$ are considered as an average, *viz:*

$$\phi_{\mathbf{h}} \simeq \langle \phi_{\mathbf{k}} + \phi_{\mathbf{h}-\mathbf{k}} \rangle_{\mathbf{k}_{\mathbf{r}}}.$$

For actual phase determination, this can be formalized as follows. After calculating normalized structure-factor magnitudes $|E_{\mathbf{h}}|$ from the observed $|F_{\mathbf{h}}|$ to generate all possible phase triples within a reasonably high $A_{\mathbf{h}}$ threshold, new phase values can be estimated after origin definition by use of the tangent formula (Karle & Hauptman, 1956):

$$\tan \phi_{\mathbf{h}} = \frac{\sum_{\mathbf{k}_{\mathbf{r}}} W_{\mathbf{h}} |E_{\mathbf{k}}||E_{\mathbf{h}-\mathbf{k}}| \sin(\phi_{\mathbf{k}} + \phi_{\mathbf{h}-\mathbf{k}})}{\sum_{\mathbf{k}_{\mathbf{r}}} W_{\mathbf{h}} |E_{\mathbf{k}}||E_{\mathbf{h}-\mathbf{k}}| \cos(\phi_{\mathbf{k}} + \phi_{\mathbf{h}-\mathbf{k}})}.$$

The reliability of the phase estimate depends on the variance $V(\phi_{\mathbf{h}})$, which is directly related to the magnitude of $\alpha_{\mathbf{h}}$, *i.e.*

$$\alpha_{\mathbf{h}}^2 = \left[\sum_{\mathbf{k}_{\mathbf{r}}} A_{\mathbf{h},\,\mathbf{k}} \cos(\phi_{\mathbf{k}} + \phi_{\mathbf{h}-\mathbf{k}})\right]^2 + \left[\sum_{\mathbf{k}_{\mathbf{r}}} A_{\mathbf{h},\,\mathbf{k}} \sin(\phi_{\mathbf{k}} + \phi_{\mathbf{h}-\mathbf{k}})\right]^2;$$

$A_{\mathbf{h},\,\mathbf{k}}$ is identical to the A value defined in the previous section. In the initial stages of phase determination $\alpha_{\mathbf{h}}$ is replaced by an expectation value α_E until enough phases are available to permit its calculation.

The phase solutions indicated by the tangent formula can thus be ranked according to the phase variance and the determination of phases can be made symbolically from the most probable triple-product relationships. This procedure is equivalent to the one described above for the evaluation of phase-invariant sums by symbolic addition. This procedure may allow determination of a large enough basis phase set to produce an interpretable map.

An alternative procedure is to use an automatic version of the tangent formula in a multisolution process. This procedure is described in Chapter 2.2. After origin definition, enough algebraic unknowns are defined (two values if centrosymmetric and four values, cycling through phase quadrants, if noncentrosymmetric) to access as many of the unknown phases as possible. These are used to generate a number of trial phase sets and the likelihood of identifying the correct solution is based on the use of some figure of merit.

Multisolution approaches employing the tangent formula include *MULTAN* (Germain *et al.*, 1971), *QTAN* (Langs & DeTitta, 1975) and *RANTAN* (Yao, 1981). *RANTAN* is a version of *MULTAN* that allows for a larger initial random phase set (with suitable control of weights in the tangent formula). *QTAN* utilizes the $\alpha_{\mathbf{h}_{\rm est}}$ definition, where

$$\alpha_{\mathbf{h}_{\rm est}} = \left\{\sum_{\mathbf{k}} A_{\mathbf{h},\,\mathbf{k}}^2 + 2\sum_{\mathbf{k}\neq\mathbf{k}'}\sum A_{\mathbf{h},\,\mathbf{k}} A'_{\mathbf{h},\,\mathbf{k}} \frac{I_1(A_{\mathbf{h},\,\mathbf{k}}) I_1(A'_{\mathbf{h},\,\mathbf{k}})}{I_0(A_{\mathbf{h},\,\mathbf{k}}) I_0(A'_{\mathbf{h},\,\mathbf{k}})}\right\}^{1/2},$$

for evaluating the phase variance. (Here I_0, I_1 are modified Bessel functions.) After multiple solutions are generated, it is desirable to locate the structurally most relevant phase sets by some figure of merit. There are many that have been suggested (Chapter 2.2). The most useful figure of merit in *QTAN* has been the NQEST (De Titta *et al.*, 1975) estimate of negative quartet invariants (see Chapter 2.2). More recently, this has been superseded by the minimal function (Hauptman, 1993):

$$R(\phi) = \frac{\sum_{\mathbf{h},\,\mathbf{k}} A_{\mathbf{h},\,\mathbf{k}} (\cos\phi_{\mathbf{h},\,\mathbf{k}} - t_{\mathbf{h},\,\mathbf{k}})^2}{\sum_{\mathbf{h},\,\mathbf{k}} A_{\mathbf{h},\,\mathbf{k}}},$$

where $t_{\mathbf{h},\,\mathbf{k}} = I_1(A_{\mathbf{h},\,\mathbf{k}})/I_0(A_{\mathbf{h},\,\mathbf{k}})$ and $\phi_{\mathbf{h},\,\mathbf{k}} = \phi_{\mathbf{h}} + \phi_{\mathbf{k}} + \phi_{-\mathbf{h}-\mathbf{k}}$.

In the first application (Dorset *et al.*, 1979) of multisolution phasing to electron-diffraction data (using the program *QTAN*), n-beam dynamical structure factors generated for cytosine and disodium 4-oxypyrimidine-2-sulfinate were used to assess the effect of increasing crystal thickness and electron accelerating voltage on the success of the structure determination. At 100 kV samples at least 80 Å thickness were usable for data collection and at 1000 kV this sample thickness limit could be pushed to 300 Å – or, perhaps, 610 Å if a partial structure were accepted for later Fourier

refinement. NQEST identified the best phase solutions. Later *QTAN* was used to evaluate the effect of elastic crystal bend on the structure analysis of cytosine (Moss & Dorset, 1982).

In actual experimental applications, two forms of thiourea were investigated with *QTAN* (Dorset, 1992*d*), using published three-dimensional electron-diffraction intensities (Dvoryankin & Vainshtein, 1960, 1962). Analysis of the centrosymmetric paraelectric structure yielded results equivalent to those found earlier by symbolic addition (Dorset, 1991*b*). Analysis of the noncentrosymmetric ferroelectric form was also quite successful (Dorset, 1992*d*). In both cases, the correct structure was found at the lowest value of NQEST. Re-analysis of the diketopiperazine structure with *QTAN* also found the correct structure (Dorset & McCourt, 1994*a*) within the four lowest values of NQEST, but not the one at the lowest value. The effectiveness of this figure of merit became more questionable when *QTAN* was used to solve the noncentrosymmetric crystal structure of a polymer (Dorset, McCourt, Kopp *et al.*, 1994). The solution could not be found readily when *NQEST* was used but was easily identified when the minimal function $R(\phi)$ was employed instead.

MULTAN has been used to phase simulated data from copper perchlorophthalocyanine (Fan *et al.*, 1985). Within the 2 Å resolution of the electron-microscope image, if one seeks phases for diffraction data in reciprocal-space regions where the objective lens phase contrast transfer function $|C(s)| \leq 0.2$, the method proves to be successful. The method is also quite effective for phase extension from 2 Å to 1 Å diffraction resolution, where the low-angle data serve as a large initial phase set for the tangent formula. However, no useful results were found from an *ab initio* phase determination carried out solely with the electron-diffraction structure-factor magnitudes. Similar results were obtained when *RANTAN* was used to phase experimental data from this compound (Fan *et al.*, 1991), *i.e.* the multisolution approach worked well for phase extension but not for *ab initio* phase determination. Additional tests were subsequently carried out with *QTAN* on an experimental *hk*0 electron-diffraction data set collected at 1200 kV (Dorset, McCourt, Fryer *et al.*, 1994). Again, *ab initio* phase determination is not possible by this technique. However, if a basis set was constructed from the Fourier transform of a 2.4 Å image, a correct solution could be found, but not at the lowest value of NQEST. This figure of merit was useful, however, when the basis set was taken from the symbolic addition determination mentioned in the previous section.

2.5.7.5. *Density modification*

Another method of phase determination, which is best suited to refining or extending a partial phase set, is the Hoppe–Gassmann density modification procedure (Hoppe & Gassmann, 1968; Gassmann & Zechmeister, 1972; Gassmann, 1976). The procedure is very simple but also very computer-intensive. Starting with a small set of (phased) $F_{\mathbf{h}}$, an initial potential map $\varphi(\mathbf{r})$ is calculated by Fourier transformation. This map is then modified by some real-space function, which restricts peak sizes to a maximum value and removes all negative density regions. The modified map $\varphi'(\mathbf{r})$ is then Fourier-transformed to produce a set of phased structure factors. Phase values are accepted *via* another modification function in reciprocal space, *e.g.* $E_{\rm calc}/E_{\rm obs} \geq p$, where p is a threshold quantity. The new set is then transformed to obtain a new $\varphi(\mathbf{r})$ and the phase refinement continues iteratively until the phase solution converges (judged by lower crystallographic R values).

The application of density modification procedures to electron-crystallographic problems was assessed by Ishizuka *et al.* (1982), who used simulated data from copper perchlorophthalocyanine within the resolution of the electron-microscope image. The method was useful for finding phase values in reciprocal-space regions where the transfer function $|C(s)| \leq 0.2$. As a technique for phase extension, density modification was acceptable for test cases where the resolution was extended from 1.67 to 1.0 Å, or 2.01 to 1.21 Å, but it was not very satisfactory for a resolution enhancement from 2.5 to 1.67 Å. There appear to have been no tests of this method yet with experimental data. However, the philosophy of this technique will be met again below in the description of the the maximum entropy and likelihood procedure.

2.5.7.6. *Convolution techniques*

One of the first relationships ever derived for phase determination is the Sayre (1952) equation:

$$F_{\mathbf{h}} = \frac{\theta}{V} \sum_{\mathbf{k}} F_{\mathbf{k}} F_{\mathbf{h}-\mathbf{k}},$$

which is a simple convolution of phased structure factors multiplied by a function of the atomic scattering factors. For structures with non-overlapping atoms, consisting of one atomic species, it is an exact expression. Although the convolution term resembles part of the tangent formula above, no statistical averaging is implied (Sayre, 1980). In X-ray crystallography this relationship has not been used very often, despite its accuracy. Part of the reason for this is that it requires relatively high resolution data for it to be useful. It can also fail for structures comprised of different atomic species.

Since, relative to X-ray scattering factors, electron scattering factors span a narrower range of magnitudes at $\sin\theta/\lambda = 0$, it might be thought that the Sayre equation would be particularly useful in electron crystallography. In fact, Liu *et al.* (1988) were able to extend phases for simulated data from copper perchlorophthalocyanine starting at the image resolution of 2 Å and reaching the 1 Å limit of an electron-diffraction data set. This analysis has been improved with a 2.4 Å basis set obtained from the Fourier transform of an electron micrograph of this material at 500 kV and extended to the 1.0 Å limit of a 1200 kV electron-diffraction pattern (Dorset *et al.*, 1995). Using the partial phase sets for zonal diffraction data from several polymers by symbolic addition (see above), the Sayre equation has been useful for extending into the whole *hk*0 set, often with great accuracy. The size of the basis set is critical but the connectivity to access all reflections is more so. Fan and co-workers have had considerable success with the analysis of incommensurately modulated structures. The average structure (basis set) is found by high-resolution electron microscopy and the 'superlattice' reflections, corresponding to the incommensurate modulation, are assigned phases in hyperspace by the Sayre convolution. Examples include a high T_c superconductor (Mo *et al.*, 1992) and the mineral ankangite (Xiang *et al.*, 1990). Phases of regular inorganic crystals have also been extended from the electron micrograph to the electron-diffraction resolution by this technique (Hu *et al.*, 1992).

In an investigation of how direct methods might be used for phase extension in protein electron crystallography, low-resolution phases from two proteins, bacteriorhodopsin (Henderson *et al.*, 1986) and halorhodopsin (Havelka *et al.*, 1993) were extended to higher resolution with the Sayre equation (Dorset *et al.*, 1995). For the noncentrosymmetric bacteriorhodopsin *hk*0 projection a 10 Å basis set was used, whereas a 15 Å set was accepted for the centrosymmetric halorhodopsin projection. In both cases, extensions to 6 Å resolution were reasonably successful. For bacteriorhodopsin, for which data were available to 3.5 Å, problems with the extension were encountered near 5 Å, corresponding to a minimum in a plot of average intensity *versus* resolution. Suggestions were made on how a multisolution procedure might be successful beyond this point.

2.5.7.7. *Maximum entropy and likelihood*

Maximum entropy has been applied to electron crystallography in several ways. In the sense that images are optimized, the entropy term

$$S = -\sum_i P_i \ln P_i,$$

where $P_i = p_i / \sum_i p_i$ and p_i is a pixel density, has been evaluated for various test electron-microscope images. For crystals, the true projected potential distribution function is thought to have the maximum value of S. If the phase contrast transfer function used to obtain a micrograph is unknown, test images (*i.e.* trial potential maps) can be calculated for different values of $\Delta f_{\rm trial}$. The value that corresponds to the maximum entropy would be near the true defocus. In this way, the actual objective lens transfer function can be found for a single image (Li, 1991) in addition to the other techniques suggested by this group.

Another use of the maximum-entropy concept is to guide the progress of a direct phase determination (Bricogne & Gilmore, 1990; Gilmore *et al.*, 1990). Suppose that there is a small set H of known phases $\phi_{\mathbf{h}\in H}$ (corresponding either to origin definition, or the Fourier transform of an electron micrograph, or both) with associated unitary structure-factor amplitudes $|U_{\mathbf{h}\in H}|$. [The unitary structure factor is defined as $|U_{\mathbf{h}}| = |E_{\mathbf{h}}|/(N)^{1/2}$.] As usual, the task is to expand into the unknown phase set K to solve the crystal structure. From Bayes' theorem, the procedure is based on an operation where $p(\text{map}|\text{data}) \propto p(\text{map})p(\text{data}|\text{map})$. This means that the probability of successfully deriving a potential map, given diffraction data, is estimated. This so-called posterior probability is approximately proportional to the product of the probability of generating the map (known as the prior) and the probability of generating the data, given the map (known as the likelihood). The latter probability consults the observed data and can be used as a figure of merit.

Beginning with the basis set H, a trial map is generated from the limited number of phased structure factors. As discussed above, the map can be immediately improved by removing all negative density. The map can be improved further if its entropy is maximized using the equation given above for S. This produces the so-called maximum-entropy prior $q^{\rm ME}(X)$.

So far, it has been assumed that all $|U_{\mathbf{h}\in K}| = 0$. If large reflections from the K set are now added and their phase values are permuted, then a number of new maps can be generated and their entropies can be maximized as before. This creates a phasing 'tree' with many possible solutions; individual branch points can have further reflections added *via* permutations to produce further sub-branches, and so on. Obviously, some figure of merit is needed to 'prune' the tree, *i.e.* to find likely paths to a solution.

The desired figure of merit is the likelihood $L(H)$. First a quantity

$$\Lambda_{\mathbf{h}} = 2NR \exp[-N(r^2 + R^2)] I_o(2NrR),$$

where $r = |^{\rm ME}U_{\mathbf{h}}|$ (the calculated unitary structure factors) and $R = |^{o}U_{\mathbf{h}}|$ (the observed unitary structure factors), is defined. From this one can calculate

$$L(H) = \sum_{\mathbf{h}\notin H} \ln \Lambda_{\mathbf{h}}.$$

The null hypothesis $L(H_o)$ can also be calculated from the above when $r = 0$, so that the likelihood gain

$$LLg = L(H) - L(H_o)$$

ranks the nodes of the phasing tree in order of the best solutions.

Applications have been made to experimental electron-crystallographic data. A small-molecule structure starting with phases from an electron micrograph and extending to electron-diffraction resolution has been reported (Dong *et al.*, 1992). Other experimental electron-diffraction data sets used in other direct phasing approaches (see above) also have been assigned phases by this technique (Gilmore, Shankland & Bricogne, 1993). These include intensities from diketopiperazine and basic copper chloride. An application of this procedure in protein structure analysis has been published by Gilmore *et al.* (1992) and Gilmore, Shankland & Fryer (1993). Starting with 15 Å phases, it was possible to extend phases for bacteriorhodopsin to the limits of the electron-diffraction pattern, apparently with greater accuracy than possible with the Sayre equation (see above).

2.5.7.8. *Influence of multiple scattering on direct electron crystallographic structure analysis*

The aim of electron-crystallographic data collection is to minimize the effect of dynamical scattering, so that the unit-cell potential distribution or its Fourier transform is represented significantly in the recorded signal. It would be a mistake, however, to presume that these data ever conform strictly to the kinematical approximation, for there is always some deviation from this ideal scattering condition that can affect the structure analysis. Despite this fact, some direct phasing procedures have been particularly 'robust', even when multiple scattering perturbations to the data are quite obvious (*e.g.* as evidenced by large crystallographic residuals).

The most effective direct phasing procedures seem to be those based on the Σ_2 triple invariants. These phase relationships will not only include the symbolic addition procedure, as it is normally carried out, but also the tangent formula and the Sayre equation (since it is well known that this convolution can be used to derive the functional form of the three-phase invariant). The strict ordering of $|E_{\mathbf{h}}|$ magnitudes is, therefore, not critically important so long as there are no major changes from large to small values (or *vice versa*). This was demonstrated in direct phase determinations of simulated n-beam dynamical diffraction data from a sulfur-containing polymer (Dorset & McCourt, 1992). Nevertheless, there is a point where measured data cannot be used. For example, intensities from *ca* 100 Å-thick epitaxically oriented copper perchlorophthalocyanine crystals become less and less representative of the unit-cell transform at lower electron-beam energies (Tivol *et al.*, 1993) and, accordingly, the success of the phase determination is compromised (Dorset, McCourt, Fryer *et al.*, 1994). The similarity between the Sayre convolution and the interactions of structure-factor terms in, *e.g.*, the multislice formulation of n-beam dynamical scattering was noted by Moodie (1965). It is interesting to note that dynamical scattering interactions observed by direct excitation of Σ_2 and Σ_1 triples in convergent-beam diffraction experiments can actually be exploited to determine crystallographic phases to very high precision (Spence & Zuo, 1992, pp. 56–63).

While the evaluation of positive quartet invariant sums (see Chapter 2.2) seems to be almost as favourable in the electron diffraction case as is the evaluation of Σ_2 triples, negative quartet invariants seem to be particularly sensitive to dynamical diffraction. If dynamical scattering can be modelled crudely by a convolutional smearing of the diffraction intensities, then the lowest structure-factor amplitudes, and hence the estimates of lowest $|E_{\mathbf{h}}|$ values, will be the ones most compromised. Since the negative-quartet relationships require an accurate prediction of small 'cross-term' $|E_{\mathbf{h}}|$ values, multiple scattering can, therefore, limit the efficacy of this invariant for phase determination. In initial work, negative quartets have been mostly employed in the NQEST figure of merit, and analyses (Dorset, McCourt, Fryer *et al.*, 1994; Dorset & McCourt, 1994*a*) have shown how the degradation of weak kinematical $|E_{\mathbf{h}}|$ terms effectively reduced its effectiveness for

locating correct structure solutions *via* the tangent formula, even though the tangent formula itself (based on triple phase estimates) was quite effective for phase determination. Substitution of the minimal function $R(\phi)$ for NQEST seems to have overcome this difficulty. [It should be pointed out, though, that only the Σ_2-triple contribution to $R(\phi)$ is considered.]

Structure refinement is another area where the effects of dynamical scattering are also problematic. For example, in the analysis of the paraelectric thiourea structure (Dorset, 1991*b*) from published texture diffraction data (Dvoryankin & Vainshtein, 1960), it was virtually impossible to find a chemically reasonable structure geometry by Fourier refinement, even though the direct phase determination itself was quite successful. The best structure was found only when higher-angle intensities (*i.e.* those least affected by dynamical scattering) were used to generate the potential map. Later analyses on heavy-atom-containing organics (Dorset *et al.*, 1992) found that the lowest kinematical *R*-factor value did not correspond to the chemically correct structure geometry. This observation was also made in the least-squares refinement of diketopiperazine (Dorset & McCourt, 1994*a*). It is obvious that, if a global minimum is sought for the crystallographic residual, then dynamical structure factors, rather than kinematical values, should be compared to the observed values (Dorset *et al.*, 1992). Ways of integrating such calculations into the refinement process have been suggested (Sha *et al.*, 1993). Otherwise one must constrain the refinement to chemically reasonable bonding geometry in a search for a local *R*-factor minimum.

Corrections for such deviations from the kinematical approximation are complicated by the presence of other possible data perturbations, especially if microareas are being sampled, *e.g.* in typical selected-area diffraction experiments. Significant complications can arise from the diffraction incoherence observed from elastically deformed crystals (Cowley, 1961) as well as secondary scattering (Cowley *et al.*, 1951). These complications were also considered for the larger (*e.g.* millimeter diameter) areas sampled in an electron-diffraction camera when recording texture diffraction patterns (Turner & Cowley, 1969), but, because of the crystallite distributions, it is sometimes found that the two-beam dynamical approximation is useful (accounting for a number of successful structure analyses carried out in Moscow).

References

2.1

Abramowitz, M. & Stegun, I. A. (1972). *Handbook of mathematical functions.* New York: Dover.

Barakat, R. (1974). *First-order statistics of combined random sinusoidal waves with application to laser speckle patterns. Opt. Acta*, **21**, 903–921.

Bernstein, S. (1922). *Sur la théorème limite du calcul des probabilités. Math. Ann.* **85**, 237–241.

Bernstein, S. (1927). *Sur l'extension du théorème limite du calcul des probabilités aux sommes de quantités dépendantes. Math. Ann.* **97**, 1–59.

Cramér, H. (1951). *Mathematical methods of statistics.* Princeton University Press.

Faggiani, R., Lippert, B. & Lock, C. J. L. (1980). *Heavy transition metal complexes of biologically important molecules. 4. Crystal and molecular structure of pentahydroxonium chloro(uracilato-N(1))(ethylenediamine)platinum(II)chloride* $(H_5O_2)[PtCl(NH_2CH_2CH_2NH_2)(C_4H_5N_2O_2)]Cl$, *and chloro(thyminato-N(1))(ethylenediamine)platinum(II),* $PtCl(NH_2CH_2CH_2NH_2)(C_5H_5N_2O_2)$. *Inorg. Chem.* **19**, 295–300.

French, S. & Wilson, K. (1978). *On the treatment of negative intensity observations. Acta Cryst.* A**34**, 517–525.

Gerhard, O. E. (1993). *Line-of-sight velocity profiles in spherical galaxies: breaking the degeneracy between anisotropy and mass. Mon. Not. R. Astron. Soc.* **265**, 213–230.

Giacovazzo, C. (1977). *On different probabilistic approaches to quartet theory. Acta Cryst.* A**33**, 50–54.

Giacovazzo, C. (1980). *Direct methods in crystallography.* London: Academic Press.

Harker, D. (1953). *The meaning of the average of* $|F|^2$ *for large values of interplanar spacing. Acta Cryst.* **6**, 731–736.

Hauptman, H. & Karle, J. (1953). *Solution of the phase problem. I. The centrosymmetric crystal.* Am. Crystallogr. Assoc. Monograph No. 3. Dayton, Ohio: Polycrystal Book Service.

Howells, E. R., Phillips, D. C. & Rogers, D. (1950). *The probability distribution of X-ray intensities. II. Experimental investigation and the X-ray detection of centers of symmetry. Acta Cryst.* **3**, 210–214.

International Tables for Crystallography (1983). Vol. A. *Space-group symmetry*, edited by T. Hahn. Dordrecht: Kluwer Academic Publishers.

International Tables for Crystallography (1999). Vol. C. *Mathematical, physical and chemical tables*, edited by A. J. C. Wilson & E. Prince. Dordrecht: Kluwer Academic Publishers.

Kendall, M. & Stuart, A. (1977). *The advanced theory of statistics*, Vol. 1, 4th ed. London: Griffin.

Lipson, H. & Woolfson, M. M. (1952). *An extension of the use of intensity statistics. Acta Cryst.* **5**, 680–682.

Lomer, T. R. & Wilson, A. J. C. (1975). *Scaling of intensities. Acta Cryst.* B**31**, 646–647.

Marel, R. P. van der & Franx, M. (1993). *A new method for the identification of non-Gaussian line profiles in elliptical galaxies. Astrophys. J.* **407**, 525–539.

Myller-Lebedeff, W. (1907). *Die Theorie der Integralgleichungen in Anwendung auf einige Reihenentwicklungen. Math. Ann.* **64**, 388–416.

Nigam, G. D. (1972). *On the compensation of X-ray intensity. Indian J. Pure Appl. Phys.* **10**, 655–656.

Nigam, G. D. & Wilson, A. J. C. (1980). *Compensation of excess intensity in space group P2. Acta Cryst.* A**36**, 832–833.

Rabinovich, D. & Shakked, Z. (1984). *A new approach to structure determination of large molecules by multi-dimensional search methods. Acta Cryst.* A**40**, 195–200.

Rabinovich, S., Shmueli, U., Stein, Z., Shashua, R. & Weiss, G. H. (1991*a*). *Exact random-walk models in crystallographic statistics. VI. P.d.f.'s of* $|E|$ *for all plane groups and most space groups. Acta Cryst.* A**47**, 328–335.

Rabinovich, S., Shmueli, U., Stein, Z., Shashua, R. & Weiss, G. H. (1991*b*). *Exact random-walk models in crystallographic statistics. VII. An all-space-group study of the effects of atomic heterogeneity on the p.d.f.'s of* $|E|$. *Acta Cryst.* A**47**, 336–340.

Rayleigh, Lord (1879). *Investigations in optics with special reference to the spectroscope. Philos. Mag.* **8**, 261–274.

Rogers, D. (1950). *The probability distribution of X-ray intensities. IV. New methods of determining crystal classes and space groups. Acta Cryst.* **3**, 455–464.

Rogers, D. & Wilson, A. J. C. (1953). *The probability distribution of X-ray intensities. V. A note on some hypersymmetric distributions. Acta Cryst.* **6**, 439–449.

Shmueli, U. (1979). *Symmetry- and composition-dependent cumulative distributions of the normalized structure amplitude for use in intensity statistics. Acta Cryst.* A**35**, 282–286.

Shmueli, U. (1982). *A study of generalized intensity statistics: extension of the theory and practical examples. Acta Cryst.* A**38**, 362–371.

Shmueli, U. & Kaldor, U. (1981). *Calculation of even moments of the trigonometric structure factor. Methods and results. Acta Cryst.* A**37**, 76–80.

Shmueli, U. & Kaldor, U. (1983). *Moments of the trigonometric structure factor. Acta Cryst.* A**39**, 615–621.

Shmueli, U., Rabinovich, S. & Weiss, G. H. (1989). *Exact conditional distribution of a three-phase invariant in the space group P1. I. Derivation and simplification of the Fourier series. Acta Cryst.* A**45**, 361–367.

Shmueli, U., Rabinovich, S. & Weiss, G. H. (1990). *Exact random-walk models in crystallographic statistics. V. Non-symmetrically bounded distributions of structure-factor magnitudes. Acta Cryst.* A**46**, 241–246.

Shmueli, U. & Weiss, G. H. (1985*a*). *Centric, bicentric and partially bicentric intensity statistics. Structure and statistics in crystallography*, edited by A. J. C. Wilson, pp. 53–66. Guilderland: Adenine Press.

Shmueli, U. & Weiss, G. H. (1985*b*). *Exact joint probability distributions for centrosymmetric structure factors. Derivation and application to the* Σ_1 *relationship in the space group* $P\bar{1}$. *Acta Cryst.* A**41**, 401–408.

Shmueli, U. & Weiss, G. H. (1986). *Exact joint distribution of* $E_{\mathbf{h}}$, $E_{\mathbf{k}}$ *and* $E_{\mathbf{h+k}}$, *and the probability for the positive sign of the triple product in the space group* $P\bar{1}$. *Acta Cryst.* A**42**, 240–246.

Shmueli, U. & Weiss, G. H. (1987). *Exact random-walk models in crystallographic statistics. III. Distributions of* $|E|$ *for space groups of low symmetry. Acta Cryst.* A**43**, 93–98.

Shmueli, U. & Weiss, G. H. (1988). *Exact random-walk models in crystallographic statistics. IV. P.d.f.'s of* $|E|$ *allowing for atoms in special positions. Acta Cryst.* A**44**, 413–417.

Shmueli, U., Weiss, G. H. & Kiefer, J. E. (1985). *Exact random-walk models in crystallographic statistics. II. The bicentric distribution in the space group* $P\bar{1}$. *Acta Cryst.* A**41**, 55–59.

Shmueli, U., Weiss, G. H., Kiefer, J. E. & Wilson, A. J. C. (1984). *Exact random-walk models in crystallographic statistics. I. Space groups* $P\bar{1}$ *and P1. Acta Cryst.* A**40**, 651–660.

Shmueli, U., Weiss, G. H. & Wilson, A. J. C. (1989). *Explicit Fourier representations of non-ideal hypercentric p.d.f.'s of* $|E|$. *Acta Cryst.* A**45**, 213–217.

Shmueli, U. & Wilson, A. J. C. (1981). *Effects of space-group symmetry and atomic heterogeneity on intensity statistics. Acta Cryst.* A**37**, 342–353.

Shmueli, U. & Wilson, A. J. C. (1982). *Intensity statistics: non-ideal distributions in theory and practice.* In *Crystallographic statistics: progress and problems*, edited by S. Ramaseshan, M. F. Richardson & A. J. C. Wilson, pp. 83–97. Bangalore: Indian Academy of Sciences.

Shmueli, U. & Wilson, A. J. C. (1983). *Generalized intensity statistics: the subcentric distribution and effects of dispersion. Acta Cryst.* A**39**, 225–233.

Spiegel, M. R. (1974). *Theory and problems of Fourier analysis.* Schaum's Outline Series. New York: McGraw-Hill.

2.1 (*cont.*)

Srinivasan, R. & Parthasarathy, S. (1976). *Some statistical applications in X-ray crystallography*. Oxford: Pergamon Press.

Stuart, A. & Ord, K. (1994). *Kendall's advanced theory of statistics.* Vol. 1. *Distribution theory*, 6th ed. London: Edward Arnold.

Weiss, G. H. & Kiefer, J. E. (1983). *The Pearson random walk with unequal step sizes. J. Phys. A*, **16**, 489–495.

Wilson, A. J. C. (1942). *Determination of absolute from relative intensity data. Nature (London)*, **150**, 151–152.

Wilson, A. J. C. (1949). *The probability distribution of X-ray intensities. Acta Cryst.* **2**, 318–320.

Wilson, A. J. C. (1950). *The probability distribution of X-ray intensities. III. Effects of symmetry elements on zones and rows. Acta Cryst.* **3**, 258–261.

Wilson, A. J. C. (1952). *Hypercentric and hyperparallel distributions of X-ray intensities. Research (London)*, **5**, 588–589.

Wilson, A. J. C. (1956). *The probability distribution of X-ray intensities. VII. Some sesquicentric distributions. Acta Cryst.* **9**, 143–144.

Wilson, A. J. C. (1964). *The probability distribution of X-ray intensities. VIII. A note on compensation for excess average intensity. Acta Cryst.* **17**, 1591–1592.

Wilson, A. J. C. (1975). *Effect of neglect of dispersion on apparent scale and temperature factors.* In *Anomalous scattering*, edited by S. Ramaseshan & S. C. Abrahams, pp. 325–332. Copenhagen: Munksgaard.

Wilson, A. J. C. (1976). *Statistical bias in least-squares refinement. Acta Cryst.* A**32**, 994–996.

Wilson, A. J. C. (1978*a*). *On the probability of measuring the intensity of a reflection as negative. Acta Cryst.* A**34**, 474–475.

Wilson, A. J. C. (1978*b*). *Variance of X-ray intensities: effect of dispersion and higher symmetries. Acta Cryst.* A**34**, 986–994.

Wilson, A. J. C. (1978*c*). *Statistical bias in scaling factors: Erratum. Acta Cryst*. B**34**, 1749.

Wilson, A. J. C. (1979). *Problems of resolution and bias in the experimental determination of the electron density and other densities in crystals. Acta Cryst.* A**35**, 122–130.

Wilson, A. J. C. (1980*a*). *Relationship between 'observed' and 'true' intensity: effects of various counting modes. Acta Cryst.* A**36**, 929–936.

Wilson, A. J. C. (1980*b*). *Effect of dispersion on the probability distribution of X-ray reflections. Acta Cryst.* A**36**, 945–946.

Wilson, A. J. C. (1981). *Can intensity statistics accommodate stereochemistry? Acta Cryst.* A**37**, 808–810.

Wilson, A. J. C. (1986*a*). *Distributions of sums and ratios of sums of intensities. Acta Cryst.* A**42**, 334–339.

Wilson, A. J. C. (1986*b*). *Fourier versus Hermite representations of probability distributions. Acta Cryst.* A**42**, 81–83.

Wilson, A. J. C. (1987*a*). *Treatment of enhanced zones and rows in normalizing intensities. Acta Cryst.* A**43**, 250–252.

Wilson, A. J. C. (1987*b*). *Functional form of the ideal hypersymmetric distributions of structure factors. Acta Cryst.* A**43**, 554–556.

Wilson, A. J. C. (1993). *Space groups rare for organic structures. III. Symmorphism and inherent symmetry. Acta Cryst.* A**49**, 795–806.

2.2

Allegra, G. (1979). *Derivation of three-phase invariants from the Patterson function. Acta Cryst.* A**35**, 213–220.

Altomare, A., Burla, M. C., Camalli, M., Cascarano, G. L., Giacovazzo, C., Guagliardi, A., Moliterni, A. G. G., Polidori, G. & Spagna, R. (1999). *SIR97: a new tool for crystal structure determination and refinement. J. Appl. Cryst.* **32**, 115–119.

Anzenhofer, K. & Hoppe, W. (1962). *Phys. Verh. Mosbach.* **13**, 119.

Ardito, G., Cascarano, G., Giacovazzo, C. & Luić, M. (1985). *1-Phase seminvariants and Harker sections. Z. Kristallogr.* **172**, 25–34.

Argos, P. & Rossmann, M. G. (1980). *Molecular replacement method.* In *Theory and practice of direct methods in crystallography,* edited by M. F. C. Ladd & R. A. Palmer, pp. 381–389. New York: Plenum.

Avrami, M. (1938). *Direct determination of crystal structure from X-ray data. Phys. Rev.* **54**, 300–303.

Baggio, R., Woolfson, M. M., Declercq, J.-P. & Germain, G. (1978). *On the application of phase relationships to complex structures. XVI. A random approach to structure determination. Acta Cryst.* A**34**, 883–892.

Banerjee, K. (1933). *Determination of the signs of the Fourier terms in complete crystal structure analysis. Proc. R. Soc. London Ser. A*, **141**, 188–193.

Bertaut, E. F. (1955*a*). *La méthode statistique en cristallographie. I. Acta Cryst*. **8**, 537–543.

Bertaut, E. F. (1955*b*). *La méthode statistique en cristallographie. II. Quelques applications. Acta Cryst*. **8**, 544–548.

Bertaut, E. F. (1960). *Ordre logarithmique des densités de répartition. I. Acta Cryst*. **13**, 546–552.

Beurskens, P. T., Beurskens, G., de Gelder, R., Garcia-Granda, S., Gould, R. O., Israel, R. & Smits, J. M. M. (1999). *The DIRDIF-99 program system.* Crystallography Laboratory, University of Nijmegen, The Netherlands.

Beurskens, P. T., Gould, R. O., Bruins Slot, H. J. & Bosman, W. P. (1987). *Translation functions for the positioning of a well oriented molecular fragment. Z. Kristallogr.* **179**, 127–159.

Beurskens, P. T., Prick, A. J., Doesburg, H. M. & Gould, R. O. (1979). *Statistical properties of normalized difference-structure factors for non-centrosymmetric structures. Acta Cryst.* A**35**, 765–772.

Böhme, R. (1982). *Direkte Methoden für Strukturen mit Uberstruktureffekten. Acta Cryst.* A**38**, 318–326.

Bouman, J. (1956). *A general theory of inequalities. Acta Cryst.* **9**, 777–780.

Bricogne, G. (1984). *Maximum entropy and the foundation of direct methods. Acta Cryst.* A**40**, 410–415.

Britten, P. L. & Collins, D. M. (1982). *Information theory as a basis for the maximum determinant. Acta Cryst.* A**38**, 129–132.

Buerger, M. J. (1959). *Vector space and its applications in crystal structure investigation.* New York: John Wiley.

Burla, M. C., Camalli, M., Carrozzini, B., Cascarano, G. L., Giacovazzo, C., Polidori, G. & Spagna, R. (1999). *SIR99, a program for the automatic solution of small and large crystal structures. Acta Cryst.* A**55**, 991–999.

Burla, M. C., Cascarano, G., Giacovazzo, C., Nunzi, A. & Polidori, G. (1987). *A weighting scheme for tangent formula development. III. The weighting scheme of the SIR program. Acta Cryst.* A**43**, 370–374.

Busetta, B. (1976). *An example of the use of quartet and triplet structure invariants when enantiomorph discrimination is difficult. Acta Cryst.* A**32**, 139–143.

Busetta, B., Giacovazzo, C., Burla, M. C., Nunzi, A., Polidori, G. & Viterbo, D. (1980). *The SIR program. I. Use of negative quartets. Acta Cryst.* A**36**, 68–74.

Camalli, M., Giacovazzo, C. & Spagna, R. (1985). *From a partial to the complete crystal structure. II. The procedure and its applications. Acta Cryst.* A**41**, 605–613.

Cascarano, G. & Giacovazzo, C. (1983). *One-phase seminvariants of first rank. I. Algebraic considerations. Z. Kristallogr.* **165**, 169–174.

Cascarano, G. & Giacovazzo, C. (1985). *One-wavelength technique: some probabilistic formulas using the anomalous dispersion effect. Acta Cryst.* A**41**, 408–413.

Cascarano, G., Giacovazzo, C., Burla, M. C., Nunzi, A. & Polidori, G. (1984). *The distribution of* $\alpha_{\mathbf{h}}$. *Acta Cryst.* A**40**, 389–394.

Cascarano, G., Giacovazzo, C., Calabrese, G., Burla, M. C., Nunzi, A., Polidori, G. & Viterbo, D. (1984). *One-phase seminvariants of first rank. II. Probabilistic considerations. Z. Kristallogr.* **167**, 37–47.

2.2 (*cont.*)

Cascarano, G., Giacovazzo, C., Camalli, M., Spagna, R., Burla, M. C., Nunzi, A. & Polidori, G. (1984). *The method of representations of structure seminvariants. The strengthening of triplet relationships. Acta Cryst.* A**40**, 278–283.

Cascarano, G., Giacovazzo, C. & Luić, M. (1985*a*). *Non-crystallographic translational symmetry: effects on diffraction-intensity statistics.* In *Structure and statistics in crystallography*, edited by A. J. C. Wilson, pp. 67–77. Guilderland, USA: Adenine Press.

Cascarano, G., Giacovazzo, C. & Luić, M. (1985*b*). *Direct methods and superstructures. I. Effects of the pseudotranslation on the reciprocal space. Acta Cryst.* A**41**, 544–551.

Cascarano, G., Giacovazzo, C. & Luić, M. (1987). *Direct methods and structures showing superstructure effects. II. A probabilistic theory of triplet invariants. Acta Cryst.* A**43**, 14–22.

Cascarano, G., Giacovazzo, C. & Luić, M. (1988*a*). *Direct methods and structures showing superstructure effects. III. A general mathematical model. Acta Cryst.* A**44**, 176–183.

Cascarano, G., Giacovazzo, C. & Luić, M. (1988*b*). *Direct methods and structures showing superstructure effects. IV. A new approach for phase solution. Acta Cryst.* A**44**, 183–188.

Cascarano, G., Giacovazzo, C., Luić, M., Pifferi, A. & Spagna, R. (1987). *1-Phase seminvariants and Harker sections. II. A new procedure. Z. Kristallogr.* **179**, 113–125.

Cascarano, G., Giacovazzo, C. & Viterbo, D. (1987). *Figures of merit in direct methods: a new point of view. Acta Cryst.* A**43**, 22–29.

Castellano, E. E., Podjarny, A. D. & Navaza, J. (1973). *A multivariate joint probability distribution of phase determination. Acta Cryst.* A**29**, 609–615.

Cochran, W. (1955). *Relations between the phases of structure factors. Acta Cryst.* **8**, 473–478.

Cochran, W. & Douglas, A. S. (1957). *The use of a high-speed digital computer for the direct determination of crystal structure. II. Proc. R. Soc. London Ser. A*, **243**, 281–288.

Cochran, W. & Woolfson, M. M. (1955). *The theory of sign relations between structure factors. Acta Cryst.* **8**, 1–12.

Coulter, C. L. & Dewar, R. B. K. (1971). *Tangent formula applications in protein crystallography: an evaluation. Acta Cryst.* B**27**, 1730–1740.

Crowther, R. A. & Blow, D. M. (1967). *A method of positioning of a known molecule in an unknown crystal structure. Acta Cryst.* **23**, 544–548.

Cutfield, J. F., Dodson, E. J., Dodson, G. G., Hodgkin, D. C., Isaacs, N. W., Sakabe, K. & Sakabe, N. (1975). *The high resolution structure of insulin: a comparison of results obtained from least-squares phase refinement and difference Fourier refinement. Acta Cryst.* A**31**, S21.

Debaerdemaeker, T., Tate, C. & Woolfson, M. M. (1985). *On the application of phase relationships to complex structures. XXIV. The Sayre tangent formula. Acta Cryst.* A**41**, 286–290.

Debaerdemaeker, T. & Woolfson, M. M. (1972). *On the application of phase relationships to complex structures. IV. The coincidence method applied to general phases. Acta Cryst.* A**28**, 477–481.

Debaerdemaeker, T. & Woolfson, M. M. (1983). *On the application of phase relationships to complex structures. XXII. Techniques for random refinement. Acta Cryst.* A**39**, 193–196.

Declercq, J.-P., Germain, G., Main, P. & Woolfson, M. M. (1973). *On the application of phase relationships to complex structures. V. Finding the solution. Acta Cryst.* A**29**, 231–234.

Declercq, J.-P., Germain, G. & Woolfson, M. M. (1975). *On the application of phase relationships to complex structures. VIII. Extension of the magic-integer approach. Acta Cryst.* A**31**, 367–372.

De Titta, G. T., Edmonds, J. W., Langs, D. A. & Hauptman, H. (1975). *Use of the negative quartet cosine invariants as a phasing figure of merit: NQEST. Acta Cryst.* A**31**, 472–479.

DeTitta, G. T., Weeks, C. M., Thuman, P., Miller, R. & Hauptman, H. A. (1994). *Structure solution by minimal-function phase refinement and Fourier filtering. I. Theoretical basis. Acta Cryst.* A**50**, 203–210.

Egert, E. (1983). *Patterson search – an alternative to direct methods. Acta Cryst.* A**39**, 936–940.

Egert, E. & Sheldrick, G. M. (1985). *Search for a fragment of known geometry by integrated Patterson and direct methods. Acta Cryst.* A**41**, 262–268.

Eller, G. von (1973). *Génération de formules statistiques entre facteurs de structure: la méthode du polynome. Acta Cryst*. A**29**, 63–67.

Fan, H.-F. (1999). *Crystallographic software: teXsan for Windows.* http://www.msc.com/brochures/teXsan/wintex.html.

Fan, H.-F. & Gu, Y.-X. (1985). *Combining direct methods with isomorphous replacement or anomalous scattering data. III. The incorporation of partial structure information. Acta Cryst.* A**41**, 280–284.

Fan, H. F., Hao, Q. & Woolfson, M. M. (1991). *Proteins and direct methods. Z. Kristallogr.* **197**, 197–208.

Fan, H.-F., Yao, J.-X., Main, P. & Woolfson, M. M. (1983). *On the application of phase relationships to complex structures. XXIII. Automatic determination of crystal structures having pseudo-translational symmetry by a modified MULTAN procedure. Acta Cryst.* A**39**, 566–569.

Fortier, S. & Hauptman, H. (1977). *Quintets in $P\bar{1}$: probabilistic theory of the five-phase structure invariant in the space group $P\bar{1}$. Acta Cryst.* A**33**, 829–833.

Fortier, S., Weeks, C. M. & Hauptman, H. (1984). *On integrating the techniques of direct methods and isomorphous replacement. III. The three-phase invariant for the native and two-derivative case. Acta Cryst.* A**40**, 646–651.

Freer, A. A. & Gilmore, C. J. (1980). *The use of higher invariants in MULTAN. Acta Cryst.* A**36**, 470–475.

French, S. & Wilson, K. (1978). *On the treatment of negative intensity observations. Acta Cryst.* A**34**, 517–525.

Gelder, R. de (1992). Thesis. University of Leiden, The Netherlands.

Gelder, R. de, de Graaff, R. A. G. & Schenk, H. (1990). *On the construction of Karle–Hauptman matrices. Acta Cryst.* A**46**, 688–692.

Gelder, R. de, de Graaff, R. A. G. & Schenk, H. (1993). *Automatic determination of crystal structures using Karle–Hauptman matrices. Acta Cryst.* A**49**, 287–293.

Germain, G., Main, P. & Woolfson, M. M. (1970). *On the application of phase relationships to complex structures. II. Getting a good start. Acta Cryst.* B**26**, 274–285.

Germain, G., Main, P. & Woolfson, M. M. (1971). *The application of phase relationships to complex structures. III. The optimum use of phase relationships. Acta Cryst.* A**27**, 368–376.

Giacovazzo, C. (1974). *A new scheme for seminvariant tables in all space groups. Acta Cryst.* A**30**, 390–395.

Giacovazzo, C. (1975). *A probabilistic theory in $P\bar{1}$ of the invariant $E_{\mathbf{h}}E_{\mathbf{k}}E_{\mathbf{l}}E_{\mathbf{h+k+l}}$. Acta Cryst.* A**31**, 252–259.

Giacovazzo, C. (1976). *A probabilistic theory of the cosine invariant* $\cos(\varphi_{\mathbf{h}} + \varphi_{\mathbf{k}} + \varphi_{\mathbf{l}} - \varphi_{\mathbf{h+k+l}})$. *Acta Cryst.* A**32**, 91–99.

Giacovazzo, C. (1977*a*). *A general approach to phase relationships: the method of representations. Acta Cryst.* A**33**, 933–944.

Giacovazzo, C. (1977*b*). *Strengthening of the triplet relationships. II. A new probabilistic approach in $P\bar{1}$. Acta Cryst.* A**33**, 527–531.

Giacovazzo, C. (1977*c*). *On different probabilistic approaches to quartet theory. Acta Cryst.* A**33**, 50–54.

Giacovazzo, C. (1977*d*). *Quintets in $P\bar{1}$ and related phase relationships: a probabilistic approach. Acta Cryst.* A**33**, 944–948.

Giacovazzo, C. (1977*e*). *A probabilistic theory of the coincidence method. I. Centrosymmetric space groups. Acta Cryst.* A**33**, 531–538.

Giacovazzo, C. (1977*f*). *A probabilistic theory of the coincidence method. II. Non-centrosymmetric space groups. Acta Cryst.* A**33**, 539–547.

Giacovazzo, C. (1978). *The estimation of the one-phase structure seminvariants of first rank by means of their first and second representation. Acta Cryst.* A**34**, 562–574.

Giacovazzo, C. (1979*a*). *A probabilistic theory of two-phase seminvariants of first rank via the method of representations. III. Acta Cryst.* A**35**, 296–305.

2.2 (*cont.*)

Giacovazzo, C. (1979*b*). *A theoretical weighting scheme for tangent-formula development and refinement and Fourier synthesis. Acta Cryst.* A**35**, 757–764.

Giacovazzo, C. (1980*a*). *Direct methods in crystallography.* London: Academic Press.

Giacovazzo, C. (1980*b*). *The method of representations of structure seminvariants. II. New theoretical and practical aspects. Acta Cryst.* A**36**, 362–372.

Giacovazzo, C. (1980*c*). *Triplet and quartet relations: their use in direct procedures. Acta Cryst.* A**36**, 74–82.

Giacovazzo, C. (1983*a*). *From a partial to the complete crystal structure. Acta Cryst.* A**39**, 685–692.

Giacovazzo, C. (1983*b*). *The estimation of two-phase invariants in $P\bar{1}$ when anomalous scatterers are present. Acta Cryst.* A**39**, 585–592.

Giacovazzo, C. (1987). *One wavelength technique: estimation of centrosymmetrical two-phase invariants in dispersive structures. Acta Cryst.* A**43**, 73–75.

Giacovazzo, C. (1988). *New probabilistic formulas for finding the positions of correctly oriented atomic groups. Acta Cryst.* A**44**, 294–300.

Giacovazzo, C. (1998). *Direct phasing in crystallography*. New York: IUCr, Oxford University Press.

Giacovazzo, C., Cascarano, G. & Zheng, C.-D. (1988). *On integrating the techniques of direct methods and isomorphous replacement. A new probabilistic formula for triplet invariants. Acta Cryst.* A**44**, 45–51.

Giacovazzo, C., Guagliardi, A., Ravelli, R. & Siliqi, D. (1994). *Ab initio direct phasing of proteins: the limits. Z. Kristallogr.* **209**, 136–142.

Giacovazzo, C., Siliqi, D. & Platas, J. G. (1995). *The ab initio crystal structure solution of proteins by direct methods. V. A new normalizing procedure. Acta Cryst.* A**51**, 811–820.

Giacovazzo, C., Siliqi, D., Platas, J. G., Hecht, H.-J., Zanotti, G. & York, B. (1996). *The ab initio crystal structure solution of proteins by direct methods. VI. Complete phasing up to derivative resolution. Acta Cryst.* D**52**, 813–825.

Giacovazzo, C., Siliqi, D. & Ralph, A. (1994). *The ab initio crystal structure solution of proteins by direct methods. I. Feasibility. Acta Cryst.* A**50**, 503–510.

Giacovazzo, C., Siliqi, D. & Spagna, R. (1994). *The ab initio crystal structure solution of proteins by direct methods. II. The procedure and its first applications. Acta Cryst.* A**50**, 609–621.

Giacovazzo, C., Siliqi, D. & Zanotti, G. (1995). *The ab initio crystal structure solution of proteins by direct methods. III. The phase extension process. Acta Cryst.* A**51**, 177–188.

Gillis, J. (1948). *Structure factor relations and phase determination. Acta Cryst.* **1**, 76–80.

Gilmore, C. J. (1984). *MITHRIL. An integrated direct-methods computer program. J. Appl. Cryst.* **17**, 42–46.

Goedkoop, J. A. (1950). *Remarks on the theory of phase limiting inequalities and equalities. Acta Cryst.* **3**, 374–378.

Gramlich, V. (1984). *The influence of rational dependence on the probability distribution of structure factors. Acta Cryst.* A**40**, 610–616.

Grant, D. F., Howells, R. G. & Rogers, D. (1957). *A method for the systematic application of sign relations. Acta Cryst.* **10**, 489–497.

Hall, S. R., du Boulay, D. J. & Olthof-Hazekamp, R. (1999). *Xtal3.6 crystallographic software.* http://www.crystal.uwa.edu.au/Crystal/xtal.

Hao, Q. & Woolfson, M. M. (1989). *Application of the P_s -function method to macromolecular structure determination. Acta Cryst.* A**45**, 794–797.

Harker, D. & Kasper, J. S. (1948). *Phases of Fourier coefficients directly from crystal diffraction data. Acta Cryst.* **1**, 70–75.

Hauptman, H. (1964). *The role of molecular structure in the direct determination of phase. Acta Cryst.* **17**, 1421–1433.

Hauptman, H. (1965). *The average value of* $\exp\{2\pi i(\mathbf{h}\cdot\mathbf{r}+\mathbf{h}'\cdot\mathbf{r}')\}$. *Z. Kristallogr.* **121**, 1–8.

Hauptman, H. (1970). Communication at New Orleans Meeting of Am. Crystallogr. Assoc.

Hauptman, H. (1974). *On the identity and estimation of those cosine invariants,* $\cos(\varphi_{\mathbf{m}}+\varphi_{\mathbf{n}}+\varphi_{\mathbf{p}}+\varphi_{\mathbf{q}})$*, which are probably negative. Acta Cryst.* A**30**, 472–476.

Hauptman, H. (1975). *A new method in the probabilistic theory of the structure invariants. Acta Cryst.* A**31**, 680–687.

Hauptman, H. (1982*a*). *On integrating the techniques of direct methods and isomorphous replacement. I. The theoretical basis. Acta Cryst.* A**38**, 289–294.

Hauptman, H. (1982*b*). *On integrating the techniques of direct methods with anomalous dispersion. I. The theoretical basis. Acta Cryst.* A**38**, 632–641.

Hauptman, H. (1995). *Looking ahead. Acta Cryst.* B**51**, 416–422.

Hauptman, H., Fisher, J., Hancock, H. & Norton, D. A. (1969). *Phase determination for the estriol structure. Acta Cryst.* B**25**, 811–814.

Hauptman, H. & Green, E. A. (1976). *Conditional probability distributions of the four-phase structure invariant* $\varphi_{\mathbf{h}}+\varphi_{\mathbf{k}}+\varphi_{\mathbf{l}}+\varphi_{\mathbf{m}}$ *in $P\bar{1}$. Acta Cryst.* A**32**, 45–49.

Hauptman, H. & Green, E. A. (1978). *Pairs in $P2_1$: probability distributions which lead to estimates of the two-phase structure seminvariants in the vicinity of $\pi/2$. Acta Cryst.* A**34**, 224–229.

Hauptman, H. & Karle, J. (1953). *Solution of the phase problem. I. The centrosymmetric crystal.* Am. Crystallogr. Assoc. Monograph No. 3. Dayton, Ohio: Polycrystal Book Service.

Hauptman, H. & Karle, J. (1956). *Structure invariants and seminvariants for non-centrosymmetric space groups. Acta Cryst.* **9**, 45–55.

Hauptman, H. & Karle, J. (1958). *Phase determination from new joint probability distributions: space group $P\bar{1}$. Acta Cryst.* **11**, 149–157.

Hauptman, H. & Karle, J. (1959). *Table 2. Equivalence classes, seminvariant vectors and seminvariant moduli for the centered centrosymmetric space groups, referred to a primitive unit cell. Acta Cryst.* **12**, 93–97.

Heinermann, J. J. L. (1977*a*). *The use of structural information in the phase probability of a triple product. Acta Cryst.* A**33**, 100–106.

Heinermann, J. J. L. (1977*b*). Thesis. University of Utrecht.

Heinermann, J. J. L., Krabbendam, H. & Kroon, J. (1979). *The joint probability distribution of the structure factors in a Karle–Hauptman matrix. Acta Cryst.* A**35**, 101–105.

Heinermann, J. J. L., Krabbendam, H., Kroon, J. & Spek, A. L. (1978). *Direct phase determination of triple products from Bijvoet inequalities. II. A probabilistic approach. Acta Cryst.* A**34**, 447–450.

Hendrickson, W. A., Love, W. E. & Karle, J. (1973). *Crystal structure analysis of sea lamprey hemoglobin at 2 Å resolution. J. Mol. Biol.* **74**, 331–361.

Hendrickson, W. A. & Ogata, C. M. (1997). *Phase determination from multiwavelength anomalous diffraction measurements. Methods Enzymol.* **276**, 494–523.

Hoppe, W. (1963). *Phase determination and zero points in the Patterson function. Acta Cryst.* **16**, 1056–1057.

Hughes, E. W. (1953). *The signs of products of structure factors. Acta Cryst.* **6**, 871.

Hull, S. E. & Irwin, M. J. (1978). *On the application of phase relationships to complex structures. XIV. The additional use of statistical information in tangent-formula refinement. Acta Cryst.* A**34**, 863–870.

Hull, S. E., Viterbo, D., Woolfson, M. M. & Shao-Hui, Z. (1981). *On the application of phase relationships to complex structures. XIX. Magic-integer representation of a large set of phases: the MAGEX procedure. Acta Cryst.* A**37**, 566–572.

International Tables for Crystallography (2001). Vol. F. *Macromolecular crystallography*, edited by M. G. Rossmann & E. Arnold. In the press.

Jaynes, E. T. (1957). *Information theory and statistical mechanics. Phys. Rev.* **106**, 620–630.

Karle, J. (1970*a*). *An alternative form for $B_{3.0}$, a phase determining formula. Acta Cryst.* B**26**, 1614–1617.

2.2 (*cont.*)

Karle, J. (1970*b*). *Partial structures and use of the tangent formula and translation functions.* In *Crystallographic computing*, pp. 155–164. Copenhagen: Munksgaard.

Karle, J. (1972). *Translation functions and direct methods. Acta Cryst.* B**28**, 820–824.

Karle, J. (1979). *Triple phase invariants: formula for centric case from fourth-order determinantal joint probability distributions. Proc. Natl Acad. Sci. USA*, **76**, 2089–2093.

Karle, J. (1980). *Triplet phase invariants: formula for acentric case from fourth-order determinantal joint probability distributions. Proc. Natl Acad. Sci. USA*, **77**, 5–9.

Karle, J. (1983). *A simple rule for finding and distinguishing triplet phase invariants with values near 0 or* π *with isomorphous replacement data. Acta Cryst.* A**39**, 800–805.

Karle, J. (1984). *Rules for evaluating triplet phase invariants by use of anomalous dispersion data. Acta Cryst.* A**40**, 4–11.

Karle, J. (1985). *Many algebraic formulas for the evaluation of triplet phase invariants from isomorphous replacement and anomalous dispersion data. Acta Cryst.* A**41**, 182–189.

Karle, J. & Hauptman, H. (1950). *The phases and magnitudes of the structure factors. Acta Cryst.* **3**, 181–187.

Karle, J. & Hauptman, H. (1956). *A theory of phase determination for the four types of non-centrosymmetric space groups* $1P222$, $2P22$, $3P_12$, $3P_22$. *Acta Cryst.* **9**, 635–651.

Karle, J. & Hauptman, H. (1958). *Phase determination from new joint probability distributions: space group* $P1$. *Acta Cryst.* **11**, 264–269.

Karle, J. & Hauptman, H. (1961). *Seminvariants for non-centrosymmetric space groups with conventional centered cells. Acta Cryst.* **14**, 217–223.

Karle, J. & Karle, I. L. (1966). *The symbolic addition procedure for phase determination for centrosymmetric and non-centrosymmetric crystals. Acta Cryst.* **21**, 849–859.

Klug, A. (1958). *Joint probability distributions of structure factors and the phase problem. Acta Cryst.* **11**, 515–543.

Koch, M. H. J. (1974). *On the application of phase relationships to complex structures. IV. Automatic interpretation of electron-density maps for organic structures. Acta Cryst.* A**30**, 67–70.

Krabbendam, H. & Kroon, J. (1971). *A relation between structure factor, triple products and a single Patterson vector, and its application to sign determination. Acta Cryst.* A**27**, 362–367.

Kroon, J., Spek, A. L. & Krabbendam, H. (1977). *Direct phase determination of triple products from Bijvoet inequalities. Acta Cryst.* A**33**, 382–385.

Lajzérowicz, J. & Lajzérowicz, J. (1966). *Loi de distribution des facteurs de structure pour un répartition non uniforme des atomes. Acta Cryst*. **21**, 8–12.

Langs, D. A. (1985). *Translation functions: the elimination of structure-dependent spurious maxima. Acta Cryst.* A**41**, 305–308.

Lessinger, L. & Wondratschek, H. (1975). *Seminvariants for space groups* $I\bar{4}2m$ *and* $I\bar{4}d$. *Acta Cryst.* A**31**, 521.

Mackay, A. L. (1953). *A statistical treatment of superlattice reflexions. Acta Cryst.* **6**, 214–215.

Main, P. (1976). *Recent developments in the MULTAN system. The use of molecular structure.* In *Crystallographic computing techniques*, edited by F. R. Ahmed, pp. 97–105. Copenhagen: Munksgaard.

Main, P. (1977). *On the application of phase relationships to complex structures. XI. A theory of magic integers. Acta Cryst.* A**33**, 750–757.

Main, P., Fiske, S. J., Germain, G., Hull, S. E., Declercq, J.-P., Lessinger, L. & Woolfson, M. M. (1999). *Crystallographic software: teXsan for Windows.* http://www.msc.com/brochures/teXsan/wintex.html.

Main, P. & Hull, S. E. (1978). *The recognition of molecular fragments in E maps and electron density maps. Acta Cryst.* A**34**, 353–361.

Moncrief, J. W. & Lipscomb, W. N. (1966). *Structure of leurocristine methiodide dihydrate by anomalous scattering methods; relation to leurocristine (vincristine) and vincaleukoblastine (vinblastine). Acta Cryst.* A**21**, 322–331.

Mukherjee, A. K., Helliwell, J. R. & Main, P. (1989). *The use of MULTAN to locate the positions of anomalous scatterers. Acta Cryst.* A**45**, 715–718.

Narayan, R. & Nityananda, R. (1982). *The maximum determinant method and the maximum entropy method. Acta Cryst.* A**38**, 122–128.

Navaza, J. (1985). *On the maximum-entropy estimate of the electron density function. Acta Cryst.* A**41**, 232–244.

Navaza, J., Castellano, E. E. & Tsoucaris, G. (1983). *Constrained density modifications by variational techniques. Acta Cryst.* A**39**, 622–631.

Naya, S., Nitta, I. & Oda, T. (1964). *A study on the statistical method for determination of signs of structure factors. Acta Cryst.* **17**, 421–433.

Naya, S., Nitta, I. & Oda, T. (1965). *Affinement tridimensional du sulfanilamide* β. *Acta Cryst.* **19**, 734–747.

Nordman, C. E. (1985). *Introduction to Patterson search methods.* In *Crystallographic computing 3. Data collection, structure determination, proteins and databases*, edited by G. M. Sheldrick, G. Kruger & R. Goddard, pp. 232–244. Oxford: Clarendon Press.

Oda, T., Naya, S. & Taguchi, I. (1961). *Matrix theoretical derivation of inequalities. II. Acta Cryst.* **14**, 456–458.

Okaya, J. & Nitta, I. (1952). *Linear structure factor inequalities and the application to the structure determination of tetragonal ethylenediamine sulphate. Acta Cryst.* **5**, 564–570.

Okaya, Y. & Pepinsky, R. (1956). *New formulation and solution of the phase problem in X-ray analysis of non-centric crystals containing anomalous scatterers. Phys. Rev.* **103**, 1645–1647.

Ott, H. (1927). *Zur Methodik der Struckturanalyse. Z. Kristallogr.* **66**, 136–153.

Parthasarathy, S. & Srinivasan, R. (1964). *The probability distribution of Bijvoet differences. Acta Cryst.* **17**, 1400–1407.

Peerdeman, A. F. & Bijvoet, J. M. (1956). *The indexing of reflexions in investigations involving the use of the anomalous scattering effect. Acta Cryst.* **9**, 1012–1015.

Piro, O. E. (1983). *Information theory and the phase problem in crystallography. Acta Cryst.* A**39**, 61–68.

Podjarny, A. D., Schevitz, R. W. & Sigler, P. B. (1981). *Phasing low-resolution macromolecular structure factors by matricial direct methods. Acta Cryst.* A**37**, 662–668.

Podjarny, A. D., Yonath, A. & Traub, W. (1976). *Application of multivariate distribution theory to phase extension for a crystalline protein. Acta Cryst.* A**32**, 281–292.

Rae, A. D. (1977). *The use of structure factors to find the origin of an oriented molecular fragment. Acta Cryst.* A**33**, 423–425.

Ralph, A. C. & Woolfson, M. M. (1991). *On the application of one-wavelength anomalous scattering. III. The Wilson-distribution and MPS methods. Acta Cryst.* A**47**, 533–537.

Ramachandran, G. N. & Raman, S. (1956). *A new method for the structure analysis of non-centrosymmetric crystals. Curr. Sci. (India)*, **25**, 348.

Raman, S. (1959). *Syntheses for the deconvolution of the Patterson function. Part II. Detailed theory for non-centrosymmetric crystals. Acta Cryst.* **12**, 964–975.

Rango, C. de (1969). Thesis. Paris.

Rango, C. de, Mauguen, Y. & Tsoucaris, G. (1975). *Use of high-order probability laws in phase refinement and extension of protein structures. Acta Cryst.* A**31**, 227–233.

Rango, C. de, Mauguen, Y., Tsoucaris, G., Dodson, E. J., Dodson, G. G. & Taylor, D. J. (1985). *The extension and refinement of the 1.9 Å spacing isomorphous phases to 1.5 Å spacing in 2Zn insulin by determinantal methods. Acta Cryst.* A**41**, 3–17.

Rango, C. de, Tsoucaris, G. & Zelwer, C. (1974). *Phase determination from the Karle–Hauptman determinant. II. Connexion between inequalities and probabilities. Acta Cryst.* A**30**, 342–353.

Rogers, D., Stanley, E. & Wilson, A. J. C. (1955). *The probability distribution of intensities. VI. The influence of intensity errors on the statistical tests. Acta Cryst.* **8**, 383–393.

2.2 (*cont.*)

Rogers, D. & Wilson, A. J. C. (1953). *The probability distribution of X-ray intensities. V. A note on some hypersymmetric distributions. Acta Cryst.* **6**, 439–449.

Rossmann, M. G., Blow, D. M., Harding, M. M. & Coller, E. (1964). *The relative positions of independent molecules within the same asymmetric unit. Acta Cryst.* **17**, 338–342.

Sayre, D. (1952). *The squaring method: a new method for phase determination. Acta Cryst.* **5**, 60–65.

Sayre, D. (1953). *Double Patterson function. Acta Cryst.* **6**, 430–431.

Sayre, D. (1972). *On least-squares refinement of the phases of crystallographic structure factors. Acta Cryst.* A**28**, 210–212.

Sayre, D. & Toupin, R. (1975). *Major increase in speed of least-squares phase refinement. Acta Cryst.* A**31**, S20.

Schenk, H. (1973*a*). *Direct structure determination in P*1 *and other non-centrosymmetric symmorphic space groups. Acta Cryst.* A**29**, 480–481.

Schenk, H. (1973*b*). *The use of phase relationships between quartets of reflexions. Acta Cryst.* A**29**, 77–82.

Sheldrick, G. M. (1990). *Phase annealing in SHELX-90: direct methods for larger structures. Acta Cryst.* A**46**, 467–473.

Sheldrick, G. M. (1997). In *Direct methods for solving macromolecular structures.* NATO Advanced Study Institute, Erice, Italy.

Sheldrick, G. M. (2000*a*). *The SHELX home page.* http://shelx.uni-ac.gwdg.de/SHELX/.

Sheldrick, G. M. (2000*b*). *SHELX.* http://www.ucg.ie/cryst/shelx.htm.

Sheldrick, G. M. & Gould, R. O. (1995). *Structure solution by iterative peaklist optimization and tangent expansion in space group P*1. *Acta Cryst.* B**51**, 423–431.

Sim, G. A. (1959). *The distribution of phase angles for structures containing heavy atoms. II. A modification of the normal heavy-atoms method for non-centrosymmetrical structures. Acta Cryst.* **12**, 813–815.

Simerska, M. (1956). *Czech. J. Phys.* **6**, 1.

Simonov, V. I. & Weissberg, A. M. (1970). *Calculation of the signs of structure amplitudes by a binary function section of interatomic vectors. Sov. Phys. Dokl.* **15**, 321–323. [Translated from *Dokl. Akad. Nauk SSSR*, **191**, 1050–1052.]

Sint, L. & Schenk, H. (1975). *Phase extension and refinement in non-centrosymmetric structures containing large molecules. Acta Cryst.* A**31**, S22.

Smith, J. L. (1998). *Multiwavelength anomalous diffraction in macromolecular crystallography*. In *Direct methods for solving macromolecular structures*, edited by S. Fortier, pp. 221–225. Dordrecht: Kluwer Academic Publishers.

Srinivasan, R. & Parthasarathy, S. (1976). *Some statistical applications in X-ray crystallography.* Oxford: Pergamon Press.

Taylor, D. J., Woolfson, M. M. & Main, P. (1978). *On the application of phase relationships to complex structures. XV. Magic determinants. Acta Cryst.* A**34**, 870–883.

Tsoucaris, G. (1970). *A new method for phase determination. The maximum determinant rule. Acta Cryst.* A**26**, 492–499.

Van der Putten, N. & Schenk, H. (1977). *On the conditional probability of quintets. Acta Cryst.* A**33**, 856–858.

Vaughan, P. A. (1958). *A phase-determining procedure related to the vector-coincidence method. Acta Cryst.* **11**, 111–115.

Vermin, W. J. & de Graaff, R. A. G. (1978). *The use of Karle–Hauptman determinants in small-structure determinations. Acta Cryst.* A**34**, 892–894.

Vicković, I. & Viterbo, D. (1979). *A simple statistical treatment of unobserved reflexions. Application to two organic substances. Acta Cryst.* A**35**, 500–501.

Weeks, C. M., DeTitta, G. T., Hauptman, H. A., Thuman, P. & Miller, R. (1994). *Structure solution by minimal-function phase refinement and Fourier filtering. II. Implementation and applications. Acta Cryst.* A**50**, 210–220.

Weeks, C. M. & Miller, R. (1999). *The design and implementation of SnB version 2.0. J. Appl. Cryst.* **32**, 120–124.

Weinzierl, J. E., Eisenberg, D. & Dickerson, R. E. (1969). *Refinement of protein phases with the Karle–Hauptman tangent fomula. Acta Cryst.* B**25**, 380–387.

White, P. & Woolfson, M. M. (1975). *The application of phase relationships to complex structures. VII. Magic integers. Acta Cryst.* A**31**, 53–56.

Wilkins, S. W., Varghese, J. N. & Lehmann, M. S. (1983). *Statistical geometry. I. A self-consistent approach to the crystallographic inversion problem based on information theory. Acta Cryst.* A**39**, 47–60.

Wilson, A. J. C. (1942). *Determination of absolute from relative X-ray intensity data. Nature (London)*, **150**, 151–152.

Wilson, K. S. (1978). *The application of MULTAN to the analysis of isomorphous derivatives in protein crystallography. Acta Cryst.* B**34**, 1599–1608.

Wolff, P. M. de & Bouman, J. (1954). *A fundamental set of structure factor inequalities. Acta Cryst.* **7**, 328–333.

Woolfson, M. M. (1958). *Crystal and molecular structure of p,p′-dimethoxybenzophenone by the direct probability method. Acta Cryst.* **11**, 277–283.

Woolfson, M. M. (1977). *On the application of phase relationships to complex structures. X. MAGLIN – a successor to MULTAN. Acta Cryst.* A**33**, 219–225.

Woolfson, M. & Fan, H.-F. (1995). *Physical and non-physical methods of solving crystal structures.* Cambridge University Press.

Yao, J.-X. (1981). *On the application of phase relationships to complex structures. XVIII. RANTAN – random MULTAN. Acta Cryst.* A**37**, 642–664.

2.3

Abad-Zapatero, C., Abdel-Meguid, S. S., Johnson, J. E., Leslie, A. G. W., Rayment, I., Rossmann, M. G., Suck, D. & Tsukihara, T. (1980). *Structure of southern bean mosaic virus at 2.8 Å resolution. Nature (London)*, **286**, 33–39.

Acharya, R., Fry, E., Stuart, D., Fox, G., Rowlands, D. & Brown, F. (1989). *The three-dimensional structure of foot-and-mouth disease virus at 2.9 Å resolution. Nature (London)*, **337**, 709–716.

Adams, M. J., Blundell, T. L., Dodson, E. J., Dodson, G. G., Vijayan, M., Baker, E. N., Harding, M. M., Hodgkin, D. C., Rimmer, B. & Sheat, S. (1969). *Structure of rhombohedral 2 zinc insulin crystals. Nature (London)*, **224**, 491–495.

Åkervall, K., Strandberg, B., Rossmann, M. G., Bengtsson, U., Fridborg, K., Johannisen, H., Kannan, K. K., Lövgren, S., Petef, G., Öberg, B., Eaker, D., Hjertén, S., Rydén, L. & Moring, I. (1972). *X-ray diffraction studies of the structure of satellite tobacco necrosis virus. Cold Spring Harbor Symp. Quant. Biol.* **36**, 469–488.

Argos, P., Ford, G. C. & Rossmann, M. G. (1975). *An application of the molecular replacement technique in direct space to a known protein structure. Acta Cryst.* A**31**, 499–506.

Argos, P. & Rossmann, M. G. (1974). *Determining heavy-atom positions using non-crystallographic symmetry. Acta Cryst.* A**30**, 672–677.

Argos, P. & Rossmann, M. G. (1976). *A method to determine heavy-atom positions for virus structures. Acta Cryst.* B**32**, 2975–2979.

Argos, P. & Rossmann, M. G. (1980). *Molecular replacement methods.* In *Theory and practice of direct methods in crystallography*, edited by M. F. C. Ladd & R. A. Palmer, pp. 361–417. New York: Plenum.

Arnold, E., Erickson, J. W., Fout, G. S., Frankenberger, E. A., Hecht, H. J., Luo, M., Rossmann, M. G. & Rueckert, R. R. (1984). *Virion orientation in cubic crystals of the human common cold virus HRV14. J. Mol. Biol.* **177**, 417–430.

Arnold, E. & Rossmann, M. G. (1986). *Effect of errors, redundancy, and solvent content in the molecular replacement procedure for the structure determination of biological macromolecules. Proc. Natl Acad. Sci. USA*, **83**, 5489–5493.

2.3 (*cont.*)

Arnold, E., Vriend, G., Luo, M., Griffith, J. P., Kamer, G., Erickson, J. W., Johnson, J. E. & Rossmann, M. G. (1987). *The structure determination of a common cold virus, human rhinovirus 14. Acta Cryst.* A**43**, 346–361.

Beevers, C. A. & Robertson, J. M. (1950). *Interpretation of the Patterson synthesis. Acta Cryst.* **3**, 164.

Beurskens, P. T. (1981). *A statistical interpretation of rotation and translation functions in reciprocal space. Acta Cryst.* A**37**, 426–430.

Bhat, T. N. & Blow, D. M. (1982). *A density-modification method for the improvement of poorly resolved protein electron-density maps. Acta Cryst.* A**38**, 21–29.

Bijvoet, J. M. (1954). *Structure of optically active compounds in the solid state. Nature (London)*, **173**, 888–891.

Bijvoet, J. M., Peerdeman, A. F. & van Bommel, A. J. (1951). *Determination of the absolute configuration of optically active compounds by means of X-rays. Nature (London)*, **168**, 271–272.

Bloomer, A. C., Champness, J. N., Bricogne, G., Staden, R. & Klug, A. (1978). *Protein disk of tobacco mosaic virus at 2.8 Å resolution showing the interactions within and between subunits. Nature (London)*, **276**, 362–368.

Blow, D. M. (1958). *The structure of haemoglobin. VII. Determination of phase angles in the noncentrosymmetric [100] zone. Proc. R. Soc. London Ser. A*, **247**, 302–336.

Blow, D. M. & Crick, F. H. C. (1959). *The treatment of errors in the isomorphous replacement method. Acta Cryst.* **12**, 794–802.

Blow, D. M. & Rossmann, M. G. (1961). *The single isomorphous replacement method. Acta Cryst.* **14**, 1195–1202.

Blow, D. M., Rossmann, M. G. & Jeffery, B. A. (1964). *The arrangement of α-chymotrypsin molecules in the monoclinic crystal form. J. Mol. Biol.* **8**, 65–78.

Bluhm, M. M., Bodo, G., Dintzis, H. M. & Kendrew, J. C. (1958). *The crystal structure of myoglobin. IV. A Fourier projection of sperm-whale myoglobin by the method of isomorphous replacement. Proc. R. Soc. London Ser. A*, **246**, 369–389.

Blundell, T. L. & Johnson, L. N. (1976). *Protein crystallography.* New York: Academic Press.

Bodo, G., Dintzis, H. M., Kendrew, J. C. & Wyckoff, H. W. (1959). *The crystal structure of myoglobin. V. A low-resolution three-dimensional Fourier synthesis of sperm-whale myoglobin crystals. Proc. R. Soc. London Ser. A*, **253**, 70–102.

Bragg, W. L. (1958). *The determination of the coordinates of heavy atoms in protein crystals. Acta Cryst.* **11**, 70–75.

Bragg, W. L. & Perutz, M. F. (1954). *The structure of haemoglobin. VI. Fourier projections on the 010 plane. Proc. R. Soc. London Ser. A*, **225**, 315–329.

Braun, P. B., Hornstra, J. & Leenhouts, J. I. (1969). *Automated crystal-structure determination by Patterson search using a known part of the molecule. Philips Res. Rep.* **24**, 85–118.

Bricogne, G. (1974). *Geometric sources of redundancy in intensity data and their use for phase determination. Acta Cryst.* A**30**, 395–405.

Bricogne, G. (1976). *Methods and programs for the direct space exploitation of geometric redundancies. Acta Cryst.* A**32**, 832–847.

Buehner, M., Ford, G. C., Moras, D., Olsen, K. W. & Rossmann, M. G. (1974). *Structure determination of crystalline lobster D-glyceraldehyde-3-phosphate dehydrogenase. J. Mol. Biol.* **82**, 563–585.

Buerger, M. J. (1946). *The interpretation of Harker syntheses. J. Appl. Phys.* **17**, 579–595.

Buerger, M. J. (1950*a*). *Some new functions of interest in X-ray crystallography. Proc. Natl Acad. Sci. USA*, **36**, 376–382.

Buerger, M. J. (1950*b*). *Limitation of electron density by the Patterson function. Proc. Natl Acad. Sci. USA*, **36**, 738–742.

Buerger, M. J. (1951). *A new approach to crystal-structure analysis. Acta Cryst.* **4**, 531–544.

Buerger, M. J. (1953*a*). *Image theory of superposed vector sets. Proc. Natl Acad. Sci. USA*, **39**, 669–673.

Buerger, M. J. (1953*b*). *Solution functions for solving superposed Patterson syntheses. Proc. Natl Acad. Sci. USA*, **39**, 674–678.

Buerger, M. J. (1953*c*). *An intersection function and its relations to the minimum function of X-ray crystallography. Proc. Natl Acad. Sci. USA*, **39**, 678–680.

Buerger, M. J. (1959). *Vector space and its application in crystal-structure investigation.* New York: John Wiley.

Buerger, M. J. (1966). *Background for the use of image-seeking functions. Trans. Am. Crystallogr. Assoc.* **2**, 1–9.

Bullough, R. K. (1961). *On homometric sets. I. Some general theorems. Acta Cryst.* **14**, 257–269.

Bullough, R. K. (1964). *On homometric sets. II. Sets obtained by singular transformations. Acta Cryst.* **17**, 295–308.

Burdina, V. I. (1970). *Symmetry of the rotation function. Kristallografiya*, **15**, 623–630.

Burdina, V. I. (1971). *Symmetry of the rotation function. Sov. Phys. Crystallogr.* **15**, 545–550.

Burdina, V. I. (1973). *Primitive rotation regions of two Patterson syntheses. Kristallografiya*, **18**, 694–700.

Burnett, R. M. & Rossmann, M. G. (1971). *The determination of the crystal structure of trans-2,4-dihydroxy-2,4-dimethylcyclohexane-trans-1-acetic acid γ-lactone, $C_{10}H_{16}O_3$, using rotation and translation functions in reciprocal space. Acta Cryst.* B**27**, 1378–1387.

Carlisle, C. H. & Crowfoot, D. (1945). *The crystal structure of cholesteryl iodide. Proc. R. Soc. London Ser. A*, **184**, 64–83.

Caspar, D. L. D. & Klug, A. (1962). *Physical principles in the construction of regular viruses. Cold Spring Harbor Symp. Quant. Biol.* **27**, 1–24.

Clastre, J. & Gay, R. (1950). *La détermination des structures cristallines à partir du diagramme de Patterson. Compt. Rend.* **230**, 1876–1877.

Collins, D. M. (1975). *Efficiency in Fourier phase refinement for protein crystal structures. Acta Cryst.* A**31**, 388–389.

Colman, P. M. (1974). *Noncrystallographic symmetry and the sampling theorem. Z. Kristallogr.* **140**, 344–349.

Colman, P. M. & Fehlhammer, H. (1976). *Appendix: the use of rotation and translation functions in the interpretation of low resolution electron density maps. J. Mol. Biol.* **100**, 278–282.

Colman, P. M., Fehlhammer, H. & Bartels, K. (1976). *Patterson search methods in protein structure determination: β-trypsin and immunoglobulin fragments.* In *Crystallographic computing techniques*, edited by F. R. Ahmed, K. Huml & B. Sedlacek, pp. 248–258. Copenhagen: Munksgaard.

Corfield, P. W. R. & Rosenstein, R. D. (1966). *Maximum information from the minimum function. Trans. Am. Crystallogr. Assoc.* **2**, 17–28.

Crick, F. H. C. & Magdoff, B. S. (1956). *The theory of the method of isomorphous replacement for protein crystals. I. Acta Cryst.* **9**, 901–908.

Cromer, D. T. (1974). *Dispersion corrections for X-ray atomic scattering factors.* In *International tables for X-ray crystallography*, Vol. IV, edited by J. A. Ibers & W. C. Hamilton, pp. 148–151. Birmingham: Kynoch Press. (Present distributor Kluwer Academic Publishers, Dordrecht.)

Crowther, R. A. (1967). *A linear analysis of the non-crystallographic symmetry problem. Acta Cryst.* **22**, 758–764.

Crowther, R. A. (1969). *The use of non-crystallographic symmetry for phase determination. Acta Cryst.* B**25**, 2571–2580.

Crowther, R. A. (1972). *The fast rotation function.* In *The molecular replacement method*, edited by M. G. Rossmann, pp. 173–178. New York: Gordon & Breach.

Crowther, R. A. & Blow, D. M. (1967). *A method of positioning a known molecule in an unknown crystal structure. Acta Cryst.* **23**, 544–548.

Cullis, A. F., Muirhead, H., Perutz, M. F., Rossmann, M. G. & North, A. C. T. (1962). *The structure of haemoglobin. IX. A three-dimensional Fourier synthesis at 5.5 Å resolution: description of the structure. Proc. R. Soc. London Ser. A*, **265**, 161–187.

2.3 (*cont.*)

Dickerson, R. E., Kendrew, J. C. & Strandberg, B. E. (1961). *The crystal structure of myoglobin: phase determination to a resolution of 2 Å by the method of isomorphous replacement. Acta Cryst.* **14**, 1188–1195.

Dickerson, R. E., Kopka, M. L., Varnum, J. C. & Weinzierl, J. E. (1967). *Bias, feedback and reliability in isomorphous phase analysis. Acta Cryst.* **23**, 511–522.

Dickerson, R. E., Weinzierl, J. E. & Palmer, R. A. (1968). *A least-squares refinement method for isomorphous replacement. Acta Cryst.* B**24**, 997–1003.

Dodson, E., Harding, M. M., Hodgkin, D. C. & Rossmann, M. G. (1966). *The crystal structure of insulin. III. Evidence for a 2-fold axis in rhombohedral zinc insulin. J. Mol. Biol.* **16**, 227–241.

Egert, E. (1983). *Patterson search – an alternative to direct methods. Acta Cryst.* A**39**, 936–940.

Egert, E. & Sheldrick, G. M. (1985). *Search for a fragment of known geometry by integrated Patterson and direct methods. Acta Cryst.* A**41**, 262–268.

Eisenberg, D. (1970). *X-ray crystallography and enzyme structure.* In *The enzymes*, edited by P. D. Boyer, Vol. I, 3rd ed., pp. 1–89. New York: Academic Press.

Fitzgerald, P. M. D. (1988). *MERLOT, an integrated package of computer programs for the determination of crystal structures by molecular replacement. J. Appl. Cryst.* **21**, 273–278.

Fletterick, R. J. & Steitz, T. A. (1976). *The combination of independent phase information obtained from separate protein structure determinations of yeast hexokinase. Acta Cryst.* A**32**, 125–132.

Fridrichsons, J. & Mathieson, A. McL. (1962). *Image-seeking. A brief study of its scope and comments on certain limitations. Acta Cryst.* **15**, 1065–1074.

Fujinaga, M. & Read, R. J. (1987). *Experiences with a new translation-function program. J. Appl. Cryst.* **20**, 517–521.

Fukuyama, K., Abdel-Meguid, S. S., Johnson, J. E. & Rossmann, M. G. (1983). *Structure of a $T = 1$ aggregate of alfalfa mosaic virus coat protein seen at 4.5 Å resolution. J. Mol. Biol.* **167**, 873–894.

Garrido, J. (1950*a*). *Sur la détermination des structures cristallines au moyen de la transformée de Patterson. Compt. Rend.* **230**, 1878–1879.

Garrido, J. (1950*b*). *Les coincidences fortuites dans la méthode des différences vectorielles. Compt. Rend.* **231**, 297–298.

Gaykema, W. P. J., Hol, W. G. J., Vereijken, J. M., Soeter, N. M., Bak, H. J. & Beintema, J. J. (1984). *3.2 Å structure of the copper-containing, oxygen-carrying protein Panulirus interruptus haemocyanin. Nature (London)*, **309**, 23–29.

Gibbs, J. W. (1898). *Remarks regarding Michelson's letter. Nature (London)*, **59**, 200.

Grau, U. M., Rossmann, M. G. & Trommer, W. E. (1981). *The crystallization and structure determination of an active ternary complex of pig heart lactate dehydrogenase. Acta Cryst.* B**37**, 2019–2026.

Green, D. W., Ingram, V. M. & Perutz, M. F. (1954). *The structure of haemoglobin. IV. Sign determination by the isomorphous replacement method. Proc. R. Soc. London Ser. A*, **225**, 287–307.

Hamilton, W. C. (1965). *The crystal structure of orthorhombic acetamide. Acta Cryst.* **18**, 866–870.

Harada, Y., Lifchitz, A., Berthou, J. & Jolles, P. (1981). *A translation function combining packing and diffraction information: an application to lysozyme (high-temperature form). Acta Cryst.* A**37**, 398–406.

Harker, D. (1936). *The application of the three-dimensional Patterson method and the crystal structures of proustite, Ag_3AsS_3, and pyrargyrite, Ag_3SbS_3. J. Chem. Phys.* **4**, 381–390.

Harker, D. (1956). *The determination of the phases of the structure factors of non-centrosymmetric crystals by the method of double isomorphous replacement. Acta Cryst.* **9**, 1–9.

Harrison, S. C., Olson, A. J., Schutt, C. E., Winkler, F. K. & Bricogne, G. (1978). *Tomato bushy stunt virus at 2.9 Å resolution. Nature (London)*, **276**, 368–373.

Hendrickson, W. A. & Lattman, E. E. (1970). *Representation of phase probability distributions for simplified combination of independent phase information. Acta Cryst.* B**26**, 136–143.

Hendrickson, W. A. & Teeter, M. M. (1981). *Structure of the hydrophobic protein crambin determined directly from the anomalous scattering of sulphur. Nature (London)*, **290**, 107–113.

Hendrickson, W. A. & Ward, K. B. (1976). *A packing function for delimiting the allowable locations of crystallized macromolecules. Acta Cryst.* A**32**, 778–780.

High, D. F. & Kraut, J. (1966). *The crystal structure of androsterone. Acta Cryst.* **21**, 88–96.

Hirshfeld, F. L. (1968). *Symmetry in the generation of trial structures. Acta Cryst.* A**24**, 301–311.

Hodgkin, D. C., Kamper, J., Lindsey, J., MacKay, M., Pickworth, J., Robertson, J. H., Shoemaker, C. B., White, J. G., Prosen, R. J. & Trueblood, K. N. (1957). *The structure of vitamin B_{12}. I. An outline of the crystallographic investigation of vitamin B_{12}. Proc. R. Soc. London Ser. A*, **242**, 228–263.

Hogle, J. M., Chow, M. & Filman, D. J. (1985). *Three-dimensional structure of poliovirus at 2.9 Å resolution. Science*, **229**, 1358–1365.

Hoppe, W. (1957*a*). *Die Faltmolekülmethode und ihre anwendung in der Röntgenographischen Konstitutionsanalyse von Biflorin ($C_{20}H_{20}O_4$). Z. Elektrochem.* **61**, 1076–1083.

Hoppe, W. (1957*b*). *Die 'Faltmolekülmethode' – eine neue Methode zur Bestimmung der Kristallstruktur bei ganz oder teilweise bekannter Molekülstruktur. Acta Cryst.* **10**, 750–751.

Hoppe, W. (1959). *Die Bestimmung genauer Schweratom-parameter in isomorphen azentrischen Kristallen. Acta Cryst.* **12**, 665–674.

Hoppe, W. (1962). *'Nahezu-Homometrische Lösungen' und Faltmolekülmethode. Z. Kristallogr.* **117**, 249–258.

Hoppe, W. & Gassmann, J. (1968). *Phase correction, a new method to solve partially known structures. Acta Cryst.* B**24**, 97–107.

Hosemann, R. & Bagchi, S. N. (1954). *On homometric structures. Acta Cryst.* **7**, 237–241.

Hosur, M. V., Schmidt, T., Tucker, R. C., Johnson, J. E., Gallagher, T. M., Selling, B. H. & Rueckert, R. R. (1987). *Structure of an insect virus at 3.0 Å resolution. Proteins*, **2**, 167–176.

Huber, R. (1965). *Die automatisierte Faltmolekülmethode. Acta Cryst.* **19**, 353–356.

Hughes, E. W. (1940). *The crystal structure of dicyandiamide. J. Am. Chem. Soc.* **62**, 1258–1267.

International Tables for Crystallography (1983). Vol. A. *Space-group symmetry*, edited by Th. Hahn. Dordrecht: Kluwer Academic Publishers.

Jacobson, R. A., Wunderlich, J. A. & Lipscomb, W. N. (1961). *The crystal and molecular structure of cellobiose. Acta Cryst.* **14**, 598–607.

James, R. W. (1965). *The optical principles of the diffraction of X-rays.* Ithaca: Cornell University Press.

Johnson, J. E. (1978). *Appendix II. Averaging of electron density maps. Acta Cryst.* B**34**, 576–577.

Johnson, J. E., Akimoto, T., Suck, D., Rayment, I. & Rossmann, M. G. (1976). *The structure of southern bean mosaic virus at 22.5 Å resolution. Virology*, **75**, 394–400.

Johnson, J. E., Argos, P. & Rossmann, M. G. (1975). *Rotation function studies of southern bean mosaic virus at 22 Å resolution. Acta Cryst.* B**31**, 2577–2583.

Karle, J. (1976). *Partial structures and use of the tangent formula and translation functions.* In *Crystallographic computing techniques*, edited by F. R. Ahmed, K. Huml & B. Sedlacek, pp. 155–164. Copenhagen: Munksgaard.

Karle, J. & Hauptman, H. (1964). *Positivity, point atoms, and Pattersons. Acta Cryst.* **17**, 392–396.

Kartha, G. (1961). *Isomorphous replacement method in non-centrosymmetric structures. Acta Cryst.* **14**, 680–686.

Kartha, G. & Parthasarathy, R. (1965). *Combination of multiple isomorphous replacement and anomalous dispersion data for protein structure determination. I. Determination of heavy-atom positions in protein derivatives. Acta Cryst.* **18**, 745–749.

2.3 (*cont.*)

Ketelaar, J. A. A. & de Vries, T. A. (1939). *The crystal structure of tetra phosphonitrile chloride*, $P_4N_4Cl_8$. *Recl Trav. Chim.* **58**, 1081–1099.

Kraut, J. (1961). *The crystal structure of 2-amino-ethanol phosphate. Acta Cryst.* **14**, 1146–1152.

Lattman, E. E. (1972). *Optimal sampling of the rotation function. Acta Cryst.* B**28**, 1065–1068.

Lattman, E. E. & Love, W. E. (1970). *A rotational search procedure for detecting a known molecule in a crystal. Acta Cryst.* B**26**, 1854–1857.

Lentz, P. J. Jr, Strandberg, B., Unge, T., Vaara, I., Borell, A., Fridborg, K. & Petef, G. (1976). *The determination of the heavy-atom substitution sites in the satellite tobacco necrosis virus. Acta Cryst.* B**32**, 2979–2983.

Lifchitz, A. (1983). *On the choice of the model cell and the integration volume in the use of the rotation function. Acta Cryst.* A**39**, 130–139.

Liljas, L., Unge, T., Jones, T. A., Fridborg, K., Lövgren, S., Skoglund, U. & Strandberg, B. (1982). *Structure of satellite tobacco necrosis virus at 3.0 Å resolution. J. Mol. Biol.* **159**, 93–108.

Lipson, H. & Cochran, W. (1966). *The determination of crystal structures.* Ithaca: Cornell University Press.

Litvin, D. B. (1975). *The molecular replacement method. I. The rotation function problem, application to bovine liver catalase and STNV. Acta Cryst.* A**31**, 407–416.

Luo, M., Vriend, G., Kamer, G., Minor, I., Arnold, E., Rossmann, M. G., Boege, U., Scraba, D. G., Duke, G. M. & Palmenberg, A. C. (1987). *The atomic structure of Mengo virus at 3.0 Å resolution. Science*, **235**, 182–191.

Luzzati, V. (1953). *Résolution d'une structure cristalline lorsque les positions d'une partie des atomes sont connues: traitement statistique. Acta Cryst.* **6**, 142–152.

McLachlan, D. Jr & Harker, D. (1951). *Finding the signs of the F's from the shifted Patterson product. Proc. Natl Acad. Sci. USA*, **37**, 846–849.

Main, P. (1967). *Phase determination using non-crystallographic symmetry. Acta Cryst.* **23**, 50–54.

Main, P. & Rossmann, M. G. (1966). *Relationships among structure factors due to identical molecules in different crystallographic environments. Acta Cryst.* **21**, 67–72.

Matthews, B. W. (1966). *The determination of the position of anomalously scattering heavy atom groups in protein crystals. Acta Cryst.* **20**, 230–239.

Matthews, B. W. & Czerwinski, E. W. (1975). *Local scaling: a method to reduce systematic errors in isomorphous replacement and anomalous scattering measurements. Acta Cryst.* A**31**, 480–487.

Matthews, B. W., Sigler, P. B., Henderson, R. & Blow, D. M. (1967). *Three-dimensional structure of tosyl-α-chymotrypsin. Nature (London)*, **214**, 652–656.

Menzer, G. (1949). *Über die mehrdeutigkeit der Kristallstrukturbestimmung. Z. Naturforsch. Teil A*, **4**, 11–21.

Mighell, A. D. & Jacobson, R. A. (1963). *Analysis of three-dimensional Patterson maps using vector verification. Acta Cryst.* **16**, 443–445.

Moncrief, J. W. & Lipscomb, W. N. (1966). *Structure of leurocristine methiodide dihydrate by anomalous scattering methods; relation to leurocristine (vincristine) and vincaleukoblastine (vinblastine). Acta Cryst.* **21**, 322–331.

Moras, D., Comarmond, M. B., Fischer, J., Weiss, R., Thierry, J. C., Ebel, J. P. & Giegé, R. (1980). *Crystal structure of yeast* $tRNA^{Asp}$. *Nature (London)*, **288**, 669–674.

Muirhead, H., Cox, J. M., Mazzarella, L. & Perutz, M. F. (1967). *Structure and function of haemoglobin. III. A three-dimensional Fourier synthesis of human deoxyhaemoglobin at 5.5 Å resolution. J. Mol. Biol.* **28**, 117–156.

Murthy, M. R. N., Reid, T. J. III, Sicignano, A., Tanaka, N. & Rossmann, M. G. (1981). *Structure of beef liver catalase. J. Mol. Biol.* **152**, 465–499.

Nixon, P. E. (1978). *Overlapping Patterson peaks and direct methods: the structure of prostratin. Acta Cryst.* A**34**, 450–453.

Nordman, C. E. (1966). *Vector space search and refinement procedures. Trans. Am. Crystallogr. Assoc.* **2**, 29–38.

Nordman, C. E. (1972). *An application of vector space search methods to the Patterson function of myoglobin. Acta Cryst.* A**28**, 134–143.

Nordman, C. E. (1980*a*). *Vector-space Patterson search and other stored-function sampling procedures.* In *Computing in crystallography*, edited by R. Diamond, S. Ramaseshan & K. Venkatesan, pp. 5.01–5.13. Bangalore: Indian Academy of Sciences.

Nordman, C. E. (1980*b*). *Procedures for detection and idealization of non-crystallographic symmetry with application to phase refinement of the satellite tobacco necrosis virus structure. Acta Cryst.* A**36**, 747–754.

Nordman, C. E. & Nakatsu, K. (1963). *Interpretation of the Patterson function of crystals containing a known molecular fragment. The structure of an Alstonia alkaloid. J. Am. Chem. Soc.* **85**, 353–354.

Nordman, C. E. & Schilling, J. W. (1970). *Calculation and use of vector overlap weights in Patterson search and refinement.* In *Crystallographic computing*, edited by F. R. Ahmed, S. R. Hall & C. P. Huber, pp. 110–114. Copenhagen: Munksgaard.

North, A. C. T. (1965). *The combination of isomorphous replacement and anomalous scattering data in phase determination of non-centrosymmetric reflexions. Acta Cryst.* **18**, 212–216.

Okaya, Y., Saito, Y. & Pepinsky, R. (1955). *New method in X-ray crystal structure determination involving the use of anomalous dispersion. Phys. Rev.* **98**, 1857–1858.

Patterson, A. L. (1934*a*). *A Fourier series representation of the average distribution of scattering power in crystals. Phys. Rev.* **45**, 763.

Patterson, A. L. (1934*b*). *A Fourier series method for the determination of the components of interatomic distances in crystals. Phys. Rev.* **46**, 372–376.

Patterson, A. L. (1935). *A direct method for the determination of the components of interatomic distances in crystals. Z. Kristallogr.* **90**, 517–542.

Patterson, A. L. (1939). *Homometric structures. Nature (London)*, **143**, 939–940.

Patterson, A. L. (1944). *Ambiguities in the X-ray analysis of crystal structures. Phys. Rev.* **65**, 195–201.

Patterson, A. L. (1949). *An alternative interpretation for vector maps. Acta Cryst.* **2**, 339–340.

Pauling, L. & Shappell, M. D. (1930). *The crystal structure of bixbyite and the C-modification of the sesquioxides. Z. Kristallogr.* **75**, 128–142.

Pepinsky, R., Okaya, Y. & Takeuchi, Y. (1957). *Theory and application of the* $P_s(u)$ *function and anomalous dispersion in direct determination of structures and absolute configuration in non-centric crystals. Acta Cryst.* **10**, 756.

Perutz, M. F. (1954). *The structure of haemoglobin. III. Direct determination of the molecular transform. Proc. R. Soc. London Ser. A*, **225**, 264–286.

Perutz, M. F. (1956). *Isomorphous replacement and phase determination in non-centrosymmetric space groups. Acta Cryst.* **9**, 867–873.

Phillips, D. C. (1966). *Advances in protein crystallography.* In *Advances in structure research by diffraction methods*, Vol. 2, edited by R. Brill & R. Mason, pp. 75–140. New York: John Wiley.

Poljak, R. J. (1963). *Heavy-atom attachment to crystalline lysozyme. J. Mol. Biol.* **6**, 244–246.

Rabinovich, D. & Shakked, Z. (1984). *A new approach to structure determination of large molecules by multi-dimensional search methods. Acta Cryst.* A**40**, 195–200.

Ramachandran, G. N. & Raman, S. (1959). *Syntheses for the deconvolution of the Patterson function. Part I. General principles. Acta Cryst.* **12**, 957–964.

Raman, S. (1966). *Patterson functions and vector sets. Trans. Am. Crystallogr. Assoc.* **2**, 10–16.

2.3 (*cont.*)

Raman, S. & Lipscomb, W. N. (1961). *Two classes of functions for the location of heavy atoms and for solution of crystal structures. Z. Kristallogr.* **116**, 314–327.

Ramaseshan, S. & Abrahams, S. C. (1975). Editors. *Anomalous scattering.* Copenhagen: Munksgaard.

Rao, S. N., Jih, J. H. & Hartsuck, J. A. (1980). *Rotation-function space groups. Acta Cryst.* A**36**, 878–884.

Rayment, I. (1983). *Molecular replacement method at low resolution: optimum strategy and intrinsic limitations as determined by calculations on icosahedral virus models. Acta Cryst.* A**39**, 102–116.

Rayment, I., Baker, T. S. & Caspar, D. L. D. (1983). *A description of the techniques and application of molecular replacement used to determine the structure of polyoma virus capsid at 22.5 Å resolution. Acta Cryst.* B**39**, 505–516.

Rayment, I., Baker, T. S., Caspar, D. L. D. & Murakami, W. T. (1982). *Polyoma virus capsid structure at 22.5 Å resolution. Nature (London)*, **295**, 110–115.

Rayment, I., Johnson, J. E., Suck, D., Akimoto, T. & Rossmann, M. G. (1978). *An 11 Å resolution electron density map of southern bean mosaic virus. Acta Cryst.* B**34**, 567–578.

Robertson, J. M. (1935). *An X-ray study of the structure of phthalocyanines. Part I. The metal-free, nickel, copper, and platinum compounds. J. Chem. Soc.* pp. 615–621.

Robertson, J. M. (1936). *An X-ray study of the phthalocyanines. Part II. Quantitative structure determination of the metal-free compound. J. Chem. Soc.* pp. 1195–1209.

Robertson, J. M. (1951). *Interpretation of the Patterson synthesis: rubidium benzyl penicillin. Acta Cryst.* **4**, 63–66.

Robertson, J. M. & Woodward, I. (1937). *An X-ray study of the phthalocyanines. Part III. Quantitative structure determination of nickel phthalocyanine. J. Chem. Soc.* pp. 219–230.

Rogers, D. (1951). *New methods of direct structure determination using modified Patterson maps. Research*, **4**, 295–296.

Rossmann, M. G. (1960). *The accurate determination of the position and shape of heavy-atom replacement groups in proteins. Acta Cryst.* **13**, 221–226.

Rossmann, M. G. (1961*a*). *The position of anomalous scatterers in protein crystals. Acta Cryst.* **14**, 383–388.

Rossmann, M. G. (1961*b*). *Application of the Buerger minimum function to protein structures.* In *Computing methods and the phase problem in X-ray crystal analysis*, edited by R. Pepinsky, J. M. Robertson & J. C. Speakman, pp. 252–265. Oxford: Pergamon Press.

Rossmann, M. G. (1972). *The molecular replacement method.* New York: Gordon & Breach.

Rossmann, M. G. (1990). *The molecular replacement method. Acta Cryst.* A**46**, 73–82.

Rossmann, M. G., Arnold, E., Erickson, J. W., Frankenberger, E. A., Griffith, J. P., Hecht, H. J., Johnson, J. E., Kamer, G., Luo, M., Mosser, A. G., Rueckert, R. R., Sherry, B. & Vriend, G. (1985). *Structure of a human common cold virus and functional relationship to other picornaviruses. Nature (London)*, **317**, 145–153.

Rossmann, M. G. & Blow, D. M. (1961). *The refinement of structures partially determined by the isomorphous replacement method. Acta Cryst.* **14**, 641–647.

Rossmann, M. G. & Blow, D. M. (1962). *The detection of sub-units within the crystallographic asymmetric unit. Acta Cryst.* **15**, 24–31.

Rossmann, M. G. & Blow, D. M. (1963). *Determination of phases by the conditions of non-crystallographic symmetry. Acta Cryst.* **16**, 39–45.

Rossmann, M. G., Blow, D. M., Harding, M. M. & Coller, E. (1964). *The relative positions of independent molecules within the same asymmetric unit. Acta Cryst.* **17**, 338–342.

Rossmann, M. G., Ford, G. C., Watson, H. C. & Banaszak, L. J. (1972). *Molecular symmetry of glyceraldehyde-3-phosphate dehydrogenase. J. Mol. Biol.* **64**, 237–249.

Rossmann, M. G. & Henderson, R. (1982). *Phasing electron diffraction amplitudes with the molecular replacement method. Acta Cryst.* A**38**, 13–20.

Sasada, Y. (1964). *The differential rotation function. Acta Cryst.* **17**, 611–612.

Schevitz, R. W., Podjarny, A. D., Zwick, M., Hughes, J. J. & Sigler, P. B. (1981). *Improving and extending the phases of medium- and low-resolution macromolecular structure factors by density modification. Acta Cryst.* A**37**, 669–677.

Shoemaker, D. P., Donohue, J., Schomaker, V. & Corey, R. B. (1950). *The crystal structure of L_8-threonine. J. Am. Chem. Soc.* **72**, 2328–2349.

Sim, G. A. (1961). *Aspects of the heavy-atom method.* In *Computing methods and the phase problem in X-ray crystal analysis*, edited by R. Pepinsky, J. M. Robertson & J. C. Speakman, pp. 227–235. Oxford: Pergamon Press.

Simonov, V. I. (1965). *Calculation of the phases of the structure amplitudes by Fourier transformation of the sum, product and minimum functions. Proc. Indian Acad. Sci.* A**62**, 213–223.

Simpson, P. G., Dobrott, R. D. & Lipscomb, W. N. (1965). *The symmetry minimum function: high order image seeking functions in X-ray crystallography. Acta Cryst.* **18**, 169–179.

Singh, A. K. & Ramaseshan, S. (1966). *The determination of heavy atom positions in protein derivatives. Acta Cryst.* **21**, 279–280.

Smith, J. L., Hendrickson, W. A. & Addison, A. W. (1983). *Structure of trimeric haemerythrin. Nature (London)*, **303**, 86–88.

Speakman, J. C. (1949). *The crystal structures of the acid salts of some monobasic acids. Part I. Potassium hydrogen bisphenylacetate. J. Chem. Soc.* pp. 3357–3365.

Stauffacher, C. V., Usha, R., Harrington, M., Schmidt, T., Hosur, M. V. & Johnson, J. E. (1987). *The structure of cowpea mosaic virus at 3.5 Å resolution.* In *Crystallography in molecular biology*, edited by D. Moras, J. Drenth, B. Strandberg, D. Suck & K. Wilson, pp. 293–308. New York, London: Plenum.

Steinrauf, L. K. (1963). *Two Fourier functions for use in protein crystallography. Acta Cryst.* **16**, 317–319.

Stout, G. H. & Jensen, L. H. (1968). *X-ray structure determination.* New York: Macmillan.

Strahs, G. & Kraut, J. (1968). *Low-resolution electron-density and anomalous-scattering-density maps of Chromatium high-potential iron protein. J. Mol. Biol.* **35**, 503–512.

Tanaka, N. (1977). *Representation of the fast-rotation function in a polar coordinate system. Acta Cryst.* A**33**, 191–193.

Taylor, W. J. (1953). *Fourier representation of Buerger's image-seeking minimum function. J. Appl. Phys.* **24**, 662–663.

Terwilliger, T. C. & Eisenberg, D. (1983). *Unbiased three-dimensional refinement of heavy-atom parameters by correlation of origin-removed Patterson functions. Acta Cryst.* A**39**, 813–817.

Tollin, P. (1966). *On the determination of molecular location. Acta Cryst.* **21**, 613–614.

Tollin, P. (1969). *A comparison of the Q-functions and the translation function of Crowther and Blow. Acta Cryst.* A**25**, 376–377.

Tollin, P. & Cochran, W. (1964). *Patterson function interpretation for molecules containing planar groups. Acta Cryst.* **17**, 1322–1324.

Tollin, P., Main, P. & Rossmann, M. G. (1966). *The symmetry of the rotation function. Acta Cryst.* **20**, 404–407.

Tollin, P. & Rossmann, M. G. (1966). *A description of various rotation function programs. Acta Cryst.* **21**, 872–876.

Tong, L. & Rossmann, M. G. (1990). *The locked rotation function. Acta Cryst.* A**46**, 783–792.

Wang, B. C. (1985). *Resolution of phase ambiguity in macromolecular crystallography. Methods Enzymol.* **115**, 90–112.

Wilson, A. J. C. (1942). *Determination of absolute from relative X-ray intensity data. Nature (London)*, **150**, 151–152.

Wilson, I. A., Skehel, J. J. & Wiley, D. C. (1981). *Structure of the haemagglutinin membrane glycoprotein of influenza virus at 3 Å resolution. Nature (London)*, **289**, 366–373.

Woolfson, M. M. (1956). *An improvement of the 'heavy-atom' method of solving crystal structures. Acta Cryst.* **9**, 804–810.

2.3 (*cont.*)

Woolfson, M. M. (1970). *An introduction to X-ray crystallography*. London: Cambridge University Press.

Wrinch, D. M. (1939). *The geometry of discrete vector maps. Philos. Mag.* **27**, 98–122.

Wunderlich, J. A. (1965). *A new expression for sharpening Patterson functions. Acta Cryst.* **19**, 200–202.

2.4

Adams, M. J. (1968). DPhil thesis, Oxford University, England.

Agard, D. A. & Stroud, R. M. (1982). *α-Bungarotoxin structure revealed by a rapid method for averaging electron density of non-crystallographically translationally related molecules. Acta Cryst.* A**38**, 186–194.

Arndt, U. W. (1986). *X-ray position-sensitive detectors. J. Appl. Cryst.* **19**, 145–163.

Arndt, U. W. & Wonacott, A. J. (1977). *The rotation method in crystallography*. Amsterdam: North-Holland.

Ashida, T. (1976). *Some remarks on the phase angle determination by the isomorphous replacement method*. In *Crystallographic computing techniques*, edited by F. R. Ahmed, pp. 282–284. Copenhagen: Munksgaard.

Bhat, T. N. & Blow, D. M. (1982). *A density-modification method for improvement of poorly resolved protein electron-density maps. Acta Cryst.* A**38**, 21–29.

Bijvoet, J. M. (1949). *Phase determination in direct Fourier-synthesis of crystal structures. Proc. K. Ned. Akad. Wet. (B)*, **52**, 313–314.

Bijvoet, J. M. (1954). *Structure of optically active compounds in the solid state. Nature (London),* **173**, 888–891.

Bijvoet, J. M., Peerdeman, A. F. & van Bommel, A. J. (1951). *Determination of the absolute configuration of optically active compounds by means of X-rays. Nature (London)*, **168**, 271–272.

Blow, D. M. & Crick, F. H. C. (1959). *The treatment of errors in the isomorphous replacement method. Acta Cryst.* **12**, 794–802.

Blow, D. M. & Matthews, B. W. (1973). *Parameter refinement in the multiple isomorphous-replacement method. Acta Cryst.* A**29**, 56–62.

Blow, D. M. & Rossmann, M. G. (1961). *The single isomorphous replacement method. Acta Cryst.* **14**, 1195–1202.

Blundell, T. L. & Johnson, L. N. (1976). *Protein crystallography*. London: Academic Press.

Bokhoven, C., Schoone, J. C. & Bijvoet, J. M. (1951). *The Fourier synthesis of the crystal structure of strychnine sulphate pentahydrate. Acta Cryst.* **4**, 275–280.

Bradley, A. J. & Rodgers, J. W. (1934). *The crystal structure of the Heusler alloys. Proc. R. Soc. London Ser. A*, **144**, 340–359.

Cannillo, E., Oberti, R. & Ungaretti, L. (1983). *Phase extension and refinement by density modification in protein crystallography. Acta Cryst.* A**39**, 68–74.

Chacko, K. K. & Srinivasan, R. (1970). *On the Fourier refinement of anomalous dispersion corrections in X-ray diffraction data. Z. Kristallogr.* **131**, 88–94.

Collins, D. M. (1975). *Efficiency in Fourier phase refinement for protein crystal structures. Acta Cryst.* A**31**, 388–389.

Cork, J. M. (1927). *The crystal structure of some of the alums. Philos. Mag.* **4**, 688–698.

Coster, D., Knol, K. S. & Prins, J. A. (1930). *Unterschiede in der Intensität der Röntgenstrahlenreflexion an den beiden 111-Flachen der Zinkblende. Z. Phys.* **63**, 345–369.

Cromer, D. T. (1965). *Anomalous dispersion corrections computed from self-consistent field relativistic Dirac–Slater wave functions. Acta Cryst.* **18**, 17–23.

Cruickshank, D. W. J. & McDonald, W. S. (1967). *Parameter errors in polar space groups caused by neglect of anomalous scattering. Acta Cryst.* **23**, 9–11.

Cullis, A. F., Muirhead, H., Perutz, M. F., Rossmann, M. G. & North, A. C. T. (1961*a*). *The structure of haemoglobin. VIII. A three-dimensional Fourier synthesis at 5.5 Å resolution: determination of the phase angles. Proc. R. Soc. London Ser. A*, **265**, 15–38.

Cullis, A. F., Muirhead, H., Perutz, M. F., Rossmann, M. G. & North, A. C. T. (1961*b*). *The structure of haemoglobin. IX. A three-dimensional Fourier synthesis at 5.5 Å resolution: description of the structure. Proc. R. Soc. London Ser. A*, **265**, 161–187.

Dale, D., Hodgkin, D. C. & Venkatesan, K. (1963). *The determination of the crystal structure of factor V 1a*. In *Crystallography and crystal perfection*, edited by G. N. Ramachandran, pp. 237–242. New York and London: Academic Press.

Dickerson, R. E., Kendrew, J. C. & Strandberg, B. E. (1961). *The crystal structure of myoglobin: phase determination to a resolution of 2 Å by the method of isomorphous replacement. Acta Cryst.* **14**, 1188–1195.

Dickerson, R. E., Weinzierl, J. E. & Palmer, R. A. (1968). *A least-squares refinement method for isomorphous replacement. Acta Cryst.* B**24**, 997–1003.

Dodson, E., Evans, P. & French, S. (1975). *The use of anomalous scattering in refining heavy atom parameters in proteins.* In *Anomalous scattering*, edited by S. Ramaseshan & S. C. Abrahams, pp. 423–436. Copenhagen: Munksgaard.

Dodson, E. & Vijayan, M. (1971). *The determination and refinement of heavy-atom parameters in protein heavy-atom derivatives. Some model calculations using acentric reflexions. Acta Cryst.* B**27**, 2402–2411.

Einstein, J. E. (1977). *An improved method for combining isomorphous replacement and anomalous scattering diffraction data for macromolecular crystals. Acta Cryst.* A**33**, 75–85.

Flook, R. J., Freeman, H. C. & Scudder, M. L. (1977). *An X-ray and neutron diffraction study of aqua(*L*-glutamato) cadmium(II) hydrate. Acta Cryst.* B**33**, 801–809.

Gilli, G. & Cruickshank, D. W. J. (1973). *Effect of neglect of dispersion in centrosymmetric structures: results for OsO_4. Acta Cryst.* B**29**, 1983–1985.

Green, D. W., Ingram, V. M. & Perutz, M. F. (1954). *The structure of haemoglobin. IV. Sign determination by the isomorphous replacement method. Proc. R. Soc. London Ser A*, **225**, 287–307.

Green, E. A. (1979). *A new statistical model for describing errors in isomorphous replacement data: the case of one derivative. Acta Cryst.* A**35**, 351–359.

Harker, D. (1956). *The determination of the phases of the structure factors of non-centrosymmetric crystals by the method of double isomorphous replacement. Acta Cryst.* **9**, 1–9.

Helliwell, J. R. (1984). *Synchrotron X-radiation protein crystallography: instrumentation, methods and applications. Rep. Prog. Phys.* **47**, 1403–1497.

Helliwell, J. R. (1985). *Protein crystallography with synchrotron radiation. J. Mol. Struct.* **130**, 63–91.

Hendrickson, W. A. (1979). *Phase information from anomalous-scattering measurements. Acta Cryst.* A**35**, 245–247.

Hendrickson, W. A. & Karle, J. (1973). *Carp muscle calcium-binding protein. III. Phase refinement using the tangent formula. J. Biol. Chem.* **248**, 3327–3334.

Hendrickson, W. A. & Konnert, J. H. (1980). *Incorporation of stereochemical information into crystallographic refinement.* In *Computing in crystallography*, edited by R. Diamond, S. Ramaseshan & K. Venkatesan, pp. 13.01–13.23. Bangalore: Indian Academy of Sciences.

Hendrickson, W. A. & Lattman, E. E. (1970). *Representation of phase probability distributions in simplified combinations of independent phase information. Acta Cryst.* B**26**, 136–143.

Hendrickson, W. A. & Sheriff, S. (1987). *General density function corresponding to X-ray diffraction with anomalous scattering included. Acta Cryst.* A**43**, 121–125.

Hendrickson, W. A. & Teeter, M. M. (1981). *Structure of the hydrophobic protein crambin determined directly from the anomalous scattering of sulphur. Nature (London)*, **290**, 107–113.

Hoppe, W. & Gassmann, J. (1968). *Phase correction, a new method to solve partially known structures. Acta Cryst.* B**24**, 97–107.

Huber, R., Kukla, D., Bode, W., Schwager, P., Bartels, K., Deisenhofer, J. & Steigemann, W. (1974). *Structure of the complex formed by bovine trypsin and bovine pancreatic trypsin inhibitor. II. Crystallographic refinement at 1.9 Å resolution. J. Mol. Biol.* **89**, 73–101.

2.4 (*cont.*)

Ibers, J. A. & Hamilton, W. C. (1964). *Dispersion corrections and crystal structure refinements. Acta Cryst.* **17**, 781–782.

International Tables for Crystallography (2001). Vol. F. *Macromolecular crystallography*, edited by M. G. Rossmann & E. Arnold. In the press.

International Tables for X-ray Crystallography (1974). Vol. IV, pp. 148–151. Birmingham: Kynoch Press. (Present distributor Kluwer Academic Publishers, Dordrecht.)

Isaacs, N. W. & Agarwal, R. C. (1978). *Experience with fast Fourier least squares in the refinement of the crystal structure of rhombohedral 2-zinc insulin at 1.5 Å resolution. Acta Cryst.* A**34**, 782–791.

Jack, A. & Levitt, M. (1978). *Refinement of large structures by simultaneous minimization of energy and R factor. Acta Cryst.* A**34**, 931–935.

Karle, J. & Hauptman, H. (1950). *The phases and magnitudes of the structure factors. Acta Cryst.* **3**, 181–187.

Kartha, G. (1961). *Isomorphous replacement in non-centrosymmetric structures. Acta Cryst.* **14**, 680–686.

Kartha, G. (1965). *Combination of multiple isomorphous replacement and anomalous dispersion data for protein structure determination. III. Refinement of heavy atom positions by the least-squares method. Acta Cryst.* **19**, 883–885.

Kartha, G. (1975). *Application of anomalous scattering studies in protein structure analysis.* In *Anomalous scattering*, edited by S. Ramaseshan & S. C. Abrahams, pp. 363–392. Copenhagen: Munksgaard.

Kartha, G. (1976). *Protein phase evaluation: multiple isomorphous series and anomalous scattering methods.* In *Crystallographic computing techniques*, edited by F. R. Ahmed, pp. 269–281. Copenhagen: Munksgaard.

Kartha, G. & Parthasarathy, R. (1965). *Combination of multiple isomorphous replacement and anomalous dispersion data for protein structure determination. I. Determination of heavy-atom positions in protein derivatives. Acta Cryst.* **18**, 745–749.

Kendrew, J. C., Dickerson, R. E., Strandberg, B. E., Hart, R. G., Phillips, D. C. & Shore, V. C. (1960). *Structure of myoglobin. A three-dimensional Fourier synthesis at 2 Å resolution. Nature (London)*, **185**, 422–427.

Kitagawa, Y., Tanaka, N., Hata, Y., Katsube, Y. & Satow, Y. (1987). *Distinction between Cu^{2+} and Zn^{2+} ions in a crystal of spinach superoxide dismutase by use of anomalous dispersion and tuneable synchrotron radiation. Acta Cryst.* B**43**, 272–275.

Koetzle, T. F. & Hamilton, W. C. (1975). *Neutron diffraction study of $NaSmEDTA.8H_2O$: an evaluation of methods of phase determination based on three-wavelength anomalous dispersion data.* In *Anomalous scattering*, edited by S. Ramaseshan & S. C. Abrahams, pp. 489–502. Copenhagen: Munksgaard.

Kraut, J. (1968). *Bijvoet-difference Fourier function. J. Mol. Biol.* **35**, 511–512.

Kraut, J., Sieker, L. C., High, D. F. & Freer, S. T. (1962). *Chymotrypsin: a three-dimensional Fourier synthesis at 5 Å resolution. Proc. Natl Acad. Sci. USA*, **48**, 1417–1424.

McPherson, A. (1982). *Preparation and analysis of protein crystals*. New York: John Wiley.

Mark, H. & Szillard, L. (1925). *Ein einfacher versuch zur auffinclung eines selectiven effecktes bei der zerstrenung von Röntgenstrahlen. Z. Phys.* **33**, 688–691.

Matthews, B. W. (1966). *The determination of the position of anomalously scattering heavy atom groups in protein crystals. Acta Cryst.* **20**, 230–239.

Moon, P. B. (1961). *Developments in gamma-ray optics. Nature (London)*, **185**, 427–429.

Muirhead, H., Cox, J. M., Mazzarella, L. & Perutz, M. F. (1967). *Structure and function of haemoglobin. III. A three-dimensional Fourier synthesis of human deoxyhaemoglobin at 5.5 Å resolution. J. Mol. Biol.* **28**, 156–177.

Narayan, R. & Ramaseshan, S. (1981). *Optimum choice of wavelengths in the anomalous scattering technique with synchrotron radiation. Acta Cryst.* A**37**, 636–641.

Navia, M. A. & Sigler, P. B. (1974). *The application of direct methods to the analysis of heavy-atom derivatives. Acta Cryst.* A**30**, 706–712.

North, A. C. T. (1965). *The combination of isomorphous replacement and anomalous scattering data in phase determination of non-centrosymmetric reflexions. Acta Cryst.* **18**, 212–216.

Okaya, Y. & Pepinsky, R. (1956). *New formulations and solution of the phase problem in X-ray analysis for noncentric crystals containing anomalous scatterers. Phys. Rev.* **103**, 1645–1657.

Parthasarathy, S. (1967). *Expectation value of the Bijvoet ratio. Acta Cryst.* **22**, 98–103.

Parthasarathy, S. & Srinivasan, R. (1964). *The probability distribution of Bijvoet differences. Acta Cryst.* **17**, 1400–1407.

Patterson, A. L. (1963). *Treatment of anomalous dispersion in X-ray diffraction data. Acta Cryst.* **16**, 1255–1256.

Peerdeman, A. F. & Bijvoet, J. M. (1956). *The indexing of reflexions in investigations involving the use of the anomalous scattering effect. Acta Cryst.* **9**, 1012–1015.

Peerdeman, A. F., van Bommel, A. J. & Bijvoet, J. M. (1951). *Determination of the absolute configuration of optically active compounds by means of X-rays. Proc. K. Ned. Akad. Wet. (B)*, **54**, 16–19.

Pepinsky, R., Okaya, Y. & Takeuchi, Y. (1957). *Theory and application of the $P_s(\mathbf{u})$ function and anomalous dispersion in direct determination of structures and absolute configuration in non-centric crystals. Acta Cryst.* **10**, 756.

Phillips, D. C. (1966). *Advances in protein crystallography.* In *Advances in structure research by diffraction methods*, Vol. 2, edited by R. Brill & R. Mason, pp. 75–140. New York and London: Interscience.

Raghavan, N. V. & Tulinsky, A. (1979). *The structure of α-chymotrypsin. II. Fourier phase refinement and extension of the dimeric structure at 1.8 Å resolution by density modification. Acta Cryst.* B**35**, 1776–1785.

Raghavan, R. S. (1961). *On the possibility of a new phase-determining method applying the Mössbauer effect. Proc. Indian Acad. Sci. Sect. A*, **53**, 265–271.

Raiz, V. Sh. & Andreeva, N. S. (1970). *Determining the coefficients of the Fourier series of the electron density function of protein crystals. Sov. Phys. Crystallogr.* **15**, 206–210.

Ramachandran, G. N. & Raman, S. (1956). *A new method for the structure analysis of non-centrosymmetric crystals. Curr. Sci.* **25**, 348–351.

Ramachandran, G. N. & Raman, S. (1959). *Syntheses for the deconvolution of the Patterson function. Part I. General principles. Acta Cryst.* **12**, 957–964.

Ramachandran, G. N. & Srinivasan, R. (1970). *Fourier methods in crystallography*. New York: Wiley–Interscience.

Ramaseshan, S. (1963). *The use of anomalous scattering in crystal structure analysis.* In *Advanced methods of crystallography*, edited by G. N. Ramachandran, pp. 67–95. London and New York: Academic Press.

Ramaseshan, S. (1966). *The use of anomalous scattering of neutrons in the solution of crystal structures containing large molecules. Curr. Sci.* **35**, 87–91.

Ramaseshan, S. (1982). *Use of the multi-wavelength anomalous scattering method in crystallography.* In *Computational crystallography*, edited by D. Sayre, pp. 201–208. Oxford: Clarendon Press.

Ramaseshan, S. & Abrahams, S. C. (1975). *Anomalous scattering*. Copenhagen: Munksgaard.

Ramaseshan, S. & Venkatesan, K. (1957). *The use of anomalous scattering without phase change in crystal structure analysis. Curr. Sci.* **26**, 352–353.

Ramaseshan, S., Venkatesan, K. & Mani, N. V. (1957). *The use of anomalous scattering for the determination of crystal structures – $KMnO_4$. Proc. Indian Acad. Sci.* **46**, 95–111.

Rango, C. de, Mauguen, Y. & Tsoucaris, G. (1975). *Use of high-order probability laws in phase refinement and extension of protein structures. Acta Cryst.* A**31**, 227–233.

2.4 (*cont.*)

Robertson, J. M. (1936). *An X-ray study of the phthalocyanines. Part II. Quantitative structure determination of the metal-free compound. J. Chem. Soc.* pp. 1195–1209.

Robertson, J. M. & Woodward, I. (1937). *An X-ray study of the phthalocyanines. Part III. Quantitative structure determination of nickel phthalocyanine. J. Chem. Soc.* pp. 219–230.

Rossmann, M. G. (1960). *The accurate determination of the position and shape of heavy-atom replacement groups in proteins. Acta Cryst.* **13**, 221–226.

Rossmann, M. G. (1961). *The position of anomalous scatterers in protein crystals. Acta Cryst.* **14**, 383–388.

Rossmann, M. G. & Blow, D. M. (1961). *The refinement of structures partially determined by the isomorphous replacement method. Acta Cryst.* **14**, 641–647.

Sayre, D. (1952). *The squaring method: a new method for phase determination. Acta Cryst.* **5**, 60–65.

Sayre, D. (1974). *Least-squares phase refinement. II. High-resolution phasing of a small protein. Acta Cryst.* A**30**, 180–184.

Schevitz, R. W., Podjarny, A. D., Zwick, M., Hughes, J. J. & Sigler, P. B. (1981). *Improving and extending the phases of medium- and low-resolution macromolecular structure factors by density modification. Acta Cryst.* A**37**, 669–677.

Schoenborn, B. P. (1975). *Phasing of neutron protein data by anomalous dispersion*. In *Anomalous scattering*, edited by S. Ramaseshan & S. C. Abrahams, pp. 407–416, Copenhagen: Munksgaard.

Sheriff, S. & Hendrickson, W. A. (1987). *Location of iron and sulfur atoms in myohemerythrin from anomalous-scattering measurements. Acta Cryst.* B**43**, 209–212.

Sikka, S. K. (1969). *On the application of the symbolic addition procedure in neutron diffraction structure determination. Acta Cryst.* A**25**, 539–543.

Sikka, S. K. & Rajagopal, H. (1975). *Application of neutron anomalous dispersion in the structure determination of cadmium tartrate pentahydrate*. In *Anomalous scattering*, edited by S. Ramaseshan & S. C. Abrahams, pp. 503–514. Copenhagen: Munksgaard.

Singh, A. K. & Ramaseshan, S. (1966). *The determination of heavy atom positions in protein derivatives. Acta Cryst.* **21**, 279–280.

Singh, A. K. & Ramaseshan, S. (1968). *The use of neutron anomalous scattering in crystal structure analysis. I. Noncentrosymmetric structures. Acta Cryst.* B**24**, 35–39.

Srinivasan, R. (1972). *Applications of X-ray anomalous scattering in structural studies*. In *Advances in structure research by diffraction methods*, Vol. 4, edited by W. Hoppe & R. Mason, pp. 105–197. Braunschweig: Freidr. Vieweg & Sohn; and Oxford: Pergamon Press.

Srinivasan, R. & Chacko, K. K. (1970). *On the determination of phases of a noncentrosymmetric crystal by the anomalous dispersion method. Z. Kristallogr.* **131**, 29–39.

Sussman, J. L., Holbrook, S. R., Church, G. M. & Kim, S.-H. (1977). *A structure-factor least-squares refinement procedure for macromolecular structures using constrained and restrained parameters. Acta Cryst.* A**33**, 800–804.

Templeton, D. H., Templeton, L. K., Phillips, J. C. & Hodgson, K. O. (1980). *Anomalous scattering of X-rays by cesium and cobalt measured with synchrotron radiation. Acta Cryst.* A**36**, 436–442.

Templeton, L. K., Templeton, D. H. & Phizackerley, R. P. (1980). *L_3-edge anomalous scattering of X-rays by praseodymium and samarium. J. Am. Chem. Soc.* **102**, 1185–1186.

Templeton, L. K., Templeton, D. H., Phizackerley, R. P. & Hodgson, K. O. (1982). *L_3-edge anomalous scattering by gadolinium and samarium measured at high resolution with synchrotron radiation. Acta Cryst.* A**38**, 74–78.

Terwilliger, T. C. & Eisenberg, D. (1983). *Unbiased three-dimensional refinement of heavy-atom parameters by correlation of origin-removed Patterson functions. Acta Cryst.* A**39**, 813–817.

Ueki, T., Zalkin, A. & Templeton, D. H. (1966). *Crystal structure of thorium nitrate pentahydrate by X-ray diffraction. Acta Cryst.* **20**, 836–841.

Vijayan, M. (1980*a*). *On the Fourier refinement of protein structures. Acta Cryst.* A**36**, 295–298.

Vijayan, M. (1980*b*). *Phase evaluation and some aspects of the Fourier refinement of macromolecules*. In *Computing in crystallography*, edited by R. Diamond, S. Ramaseshan & K. Venkatesan, pp. 19.01–19.25. Bangalore: Indian Academy of Sciences.

Vijayan, M. (1981). *X-ray analysis of 2Zn insulin: some crystallographic problems*. In *Structural studies on molecules of biological interest*, edited by G. Dodson, J. P. Glusker & D. Sayre, pp. 260–273. Oxford: Clarendon Press.

Vijayan, M. (1987). *Anomalous scattering methods.* In *Direct methods, macromolecular crystallography and crystallographic statistics*, edited by H. Schenk, A. J. C. Wilson & S. Parthasarathy, pp. 121–139. Singapore: World Scientific Publishing Co. Pte. Ltd.

Vos, A. (1975). *Anomalous scattering and chemical crystallography*. In *Anomalous scattering*, edited by S. Ramaseshan & S. C. Abrahams, pp. 307–317. Copenhagen: Munksgaard.

Wang, B. C. (1985). *Resolution of phase ambiguity in macromolecular crystallography. Methods Enzymol.* **115**, 90–112.

Watenpaugh, K. D., Sieker, L. C., Herriot, J. R. & Jensen, L. H. (1973). *Refinement of the model of a protein: rubredoxin at 1.5 Å resolution. Acta Cryst.* B**29**, 943–956.

Watenpaugh, K. D., Sieker, L. C. & Jensen, L. H. (1975). *Anomalous scattering in protein structure analysis*. In *Anomalous scattering*, edited by S. Ramaseshan & S. C. Abrahams, pp. 393–405. Copenhagen: Munksgaard.

Wilson, A. J. C. (1942). *Determination of absolute from relative X-ray intensity data. Nature (London)*, **150**, 151–152.

Wilson, A. J. C. (1975). *Effect of neglect of dispersion on apparent scale and temperature parameters*. In *Anomalous scattering*, edited by S. Ramaseshan & S. C. Abrahams, pp. 325–332. Copenhagen: Munksgaard.

Zachariasen, W. H. (1965). *Dispersion in quartz. Acta Cryst.* **18**, 714–716.

2.5

Avilov, A. S. (1979). *Electrical measurement of reflection intensities on electron diffraction from mosaic single crystals. Sov. Phys. Crystallogr.* **24**, 103–104.

Avilov, A. S., Kuligin, A. K., Pietsch, U., Spence, J. C. H., Tsirelson, V. G. & Zuo, J. M. (1999). *Scanning system for high-energy electron diffractometry. J. Appl. Cryst.* **32**, 1033–1038.

Avilov, A. S., Parmon, V. S., Semiletov, S. A. & Sirota, M. I. (1984). *Calculation of reflected intensities in multiple-beam diffraction of fast electrons by polycrystalline specimens. Sov. Phys. Crystallogr.* **29**, 5–7.

Bando, Y. (1981). *Weak asymmetry in β-Si_3N_4 as revealed by convergent beam electron diffraction. Acta Cryst.* B**39**, 185–189.

Bethe, H. A. (1928). *Theorie der Beugung von Elektronen an Kristallen. Ann. Phys. (Leipzig)*, **87**, 55–129.

Bilhorn, D. E., Foldy, L. L., Thaler, R. M. & Tobacman, W. (1964). *Remarks concerning reciprocity in quantum mechanics. J. Math. Phys.* **5**, 435–441.

Blackman, M. (1939). *On the intensities of electron diffraction rings. Proc. R. Soc. London Ser. A*, **173**, 68–82.

Bracewell, B. N. (1956). *Strip integration in radio astronomy. Austr. J. Phys.* **9**, 198–217.

Bricogne, G. & Gilmore, C. J. (1990). *A multisolution method of phase determination by combined maximization of entropy and likelihood. I. Theory, algorithms and strategy. Acta Cryst.* A**46**, 284–297.

Brisse, F. (1989). *Electron diffraction of synthetic polymers: the model compound approach to polymer structure. J. Electron Microsc. Tech.* **11**, 272–279.

Buxton, B., Eades, J. A., Steeds, J. W. & Rackham, G. M. (1976). *The symmetry of electron diffraction zone axis patterns. Philos. Trans. R. Soc. London Ser. A*, **181**, 171–193.

2.5 (*cont.*)

Carpenter, R. W. & Spence, J. C. H. (1982). *Three-dimensional strain-field information in convergent-beam electron diffraction patterns. Acta Cryst.* A**38**, 55–61.

Chou, C. T., Anderson, S. C., Cockayne, D. J. H., Sikorski, A. Z. & Vaughan, M. R. (1994). *Ultramicroscopy*, **55**, 334–347.

Cochran, W., Crick, F. H. C. & Vand, V. (1952). *The structure of synthetic polypeptides. 1. The transform of atoms on a helix. Acta Cryst.* **5**, 581–586.

Cowley, J. M. (1953). *Structure analysis of single crystals by electron diffraction. II. Disordered boric acid structure. Acta Cryst.* **6**, 522–529.

Cowley, J. M. (1956). *A modified Patterson function. Acta Cryst.* **9**, 397–398.

Cowley, J. M. (1961). *Diffraction intensities from bent crystals. Acta Cryst.* **14**, 920–927.

Cowley, J. M. (1969). *Image contrast in transmission scanning electron microscopy. Appl. Phys. Lett.* **15**, 58–59.

Cowley, J. M. (1981). *Diffraction physics*, 2nd ed. Amsterdam: North-Holland.

Cowley, J. M. (1995). *Diffraction physics*, 3rd ed. Amsterdam: North-Holland.

Cowley, J. M. & Au, A. Y. (1978). *Image signals and detector configurations for STEM*. In *Scanning electron microscopy*, Vol. 1, pp. 53–60. AMF O'Hare, Illinois: SEM Inc.

Cowley, J. M. & Moodie, A. F. (1957). *The scattering of electrons by atoms and crystals. I. A new theoretical approach. Acta Cryst.* **10**, 609–619.

Cowley, J. M. & Moodie, A. F. (1959). *The scattering of electrons by atoms and crystals. III. Single-crystal diffraction patterns. Acta Cryst.* **12**, 360–367.

Cowley, J. M. & Moodie, A. F. (1960). *Fourier images. IV. The phase grating. Proc. Phys. Soc. London*, **76**, 378–384.

Cowley, J. M., Moodie, A. F., Miyake, S., Takagi, S. & Fujimoto, F. (1961). *The extinction rules for reflections in symmetrical electron diffraction spot patterns. Acta Cryst.* **14**, 87–88.

Cowley, J. M., Rees, A. L. G. & Spink, J. A. (1951). *Secondary elastic scattering in electron diffraction. Proc. Phys. Soc. London Sect. A*, **64**, 609–619.

Cramér, H. (1954). *Mathematical methods of statistics*. University of Princeton.

Creek, R. C. & Spargo, A. E. C. (1985). *Electron optical study of rutile. J. Appl. Cryst.* **18**, 197–204.

Crowther, R. A. & Amos, L. A. (1971). *Harmonic analysis of electron microscope images with rotational symmetry. J. Mol. Biol.* **60**, 123–130.

Crowther, R. A., Amos, L. A., Finch, J. T., DeRosier, D. J. & Klug, A. (1970). *Three dimensional reconstruction of spherical viruses by Fourier synthesis from electron micrographs. Nature (London)*, **226**, 421–425.

Crowther, R. A., DeRosier, D. J. & Klug, A. (1970). *The reconstruction of a three-dimensional structure from projections and its application to electron microscopy. Proc. R. Soc. London Ser. A*, **317**, 319–340.

Crowther, R. A. & Klug, A. (1974). *Three dimensional image reconstruction on an extended field – a fast, stable algorithm. Nature (London)*, **251**, 490–492.

Dawson, B., Goodman, P., Johnson, A. W. S., Lynch, D. F. & Moodie, A. F. (1974). *Some definitions and units in electron diffraction. Acta Cryst.* A**30**, 297–298.

Deans, S. R. (1983). *The Radon transform and some of its applications*. New York: John Wiley.

DeRosier, D. J. & Klug, A. (1968). *Reconstruction of three dimensional structures from electron micrographs. Nature (London)*, **217**, 130–134.

DeRosier, D. J. & Moore, P. B. (1970). *Reconstruction of three-dimensional images from electron micrographs of structure with helical symmetry. J. Mol. Biol.* **52**, 355–369.

De Titta, G. T., Edmonds, J. W., Langs, D. A. & Hauptman, H. (1975). *Use of negative quartet cosine invariants as a phasing figure of merit: NQEST. Acta Cryst.* A**31**, 472–479.

Dong, W., Baird, T., Fryer, J. R., Gilmore, C. J., MacNicol, D. D., Bricogne, G., Smith, D. J., O'Keefe, M. A. & Hovmöller, S. (1992). *Electron microscopy at 1 Å resolution by entropy maximization and likelihood ranking. Nature (London)*, **355**, 605–609.

Dorset, D. L. (1976). *The interpretation of quasi-kinematical single-crystal electron diffraction intensity data from paraffins. Acta Cryst.* A**32**, 207–215.

Dorset, D. L. (1987). *Electron diffraction structure analysis of phospholipids. J. Electron Microsc. Tech.* **7**, 35–46.

Dorset, D. L. (1990*a*). *Direct structure analysis of a paraffin solid solution. Proc. Natl Acad. Sci. USA*, **87**, 8541–8544.

Dorset, D. L. (1990*b*). *Direct determination of crystallographic phases for diffraction data from phospholipid multilamellar arrays. Biophys. J.* **58**, 1077–1087.

Dorset, D. L. (1991*a*). *Electron diffraction structure analysis of diketopiperazine – a direct phase determination. Acta Cryst.* A**47**, 510–515.

Dorset, D. L. (1991*b*). *Is electron crystallography possible? The direct determination of organic crystal structures. Ultramicroscopy*, **38**, 23–40.

Dorset, D. L. (1991*c*). *Electron diffraction structure analysis of polyethylene. A direct phase determination. Macromolecules*, **24**, 1175–1178.

Dorset, D. L. (1991*d*). *Electron crystallography of linear polymers: direct structure analysis of poly(ε-caprolactone). Proc. Natl Acad. Sci. USA*, **88**, 5499–5502.

Dorset, D. L. (1991*e*). *Direct determination of crystallographic phases for diffraction data from lipid bilayers. I. Reliability and phase refinement. Biophys. J.* **60**, 1356–1365.

Dorset, D. L. (1991*f*). *Direct determination of crystallographic phases for diffraction data from lipid bilayers. II. Refinement of phospholipid structures. Biophys. J.* **60**, 1366–1373.

Dorset, D. L. (1992*a*). *Direct phasing in electron crystallography: determination of layer silicate structures. Ultramicroscopy*, **45**, 5–14.

Dorset, D. L. (1992*b*). *Direct methods in electron crystallography – structure analysis of boric acid. Acta Cryst.* A**48**, 568–574.

Dorset, D. L. (1992*c*). *Electron crystallography of linear polymers: direct phase determination for zonal data sets. Macromolecules*, **25**, 4425–4430.

Dorset, D. L. (1992*d*). *Automated phase determination in electron crystallography: thermotropic phases of thiourea. Ultramicroscopy*, **45**, 357–364.

Dorset, D. L. (1994*a*). *Electron crystallography of organic molecules. Adv. Electron. Electron Phys.* **88**, 111–197.

Dorset, D. L. (1994*b*). *Electron crystallography of linear polymers.* In *Characterization of solid polymers. New techniques and developments*, edited by S. J. Spells, pp. 1–16. London: Chapman and Hall.

Dorset, D. L. (1994*c*). *Electron crystallography of inorganic compounds. Direct determination of the basic copper chloride structure* $CuCl_2 \cdot 3Cu(OH)_2$. *J. Chem. Crystallogr.* **24**, 219–224.

Dorset, D. L. (1994*d*). *Direct determination of layer packing for a phospholipid solid solution at 0.32 nm resolution. Proc. Natl Acad. Sci. USA*, **91**, 4920–4924.

Dorset, D. L., Beckmann, E. & Zemlin, F. (1990). *Direct determination of a phospholipid lamellar structure at 0.34 nm resolution. Proc. Natl Acad. Sci. USA*, **87**, 7570–7573.

Dorset, D. L. & Hauptman, H. A. (1976). *Direct phase determination for quasi-kinematical electron diffraction intensity data from organic microcrystals. Ultramicroscopy*, **1**, 195–201.

Dorset, D. L., Jap, B. K., Ho, M.-H. & Glaeser, R. M. (1979). *Direct phasing of electron diffraction data from organic crystals: the effect of n-beam dynamical scattering. Acta Cryst.* A**35**, 1001–1009.

Dorset, D. L., Kopp, S., Fryer, J. R. & Tivol, W. F. (1995). *The Sayre equation in electron crystallography. Ultramicroscopy*, **57**, 59–89.

Dorset, D. L. & McCourt, M. P. (1992). *Effect of dynamical scattering on successful direct phase determination in electron crystallography – a model study. Trans. Am. Crystallogr. Assoc.* **28**, 105–113.

2.5 (*cont.*)

Dorset, D. L. & McCourt, M. P. (1993). *Electron crystallographic analysis of a polysaccharide structure – direct phase determination and model refinement for mannan I. J. Struct. Biol*. **111**, 118–124.

Dorset, D. L. & McCourt, M. P. (1994*a*). *Automated structure analysis in electron crystallography: phase determination with the tangent formula and least-squares refinement. Acta Cryst*. A**50**, 287–292.

Dorset, D. L. & McCourt, M. P. (1994*b*). *Disorder and molecular packing of C_{60} buckminsterfullerene: a direct electron-crystallographic analysis. Acta Cryst*. A**50**, 344–351.

Dorset, D. L., McCourt, M. P., Fryer, J. R., Tivol, W. F. & Turner, J. N. (1994). *The tangent formula in electron crystallography: phase determination of copper perchlorophthalocyanine. Microsc. Soc. Am. Bull*. **24**, 398–404.

Dorset, D. L., McCourt, M. P., Kopp, S., Wittmann, J.-C. & Lotz, B. (1994). *Direct determination of polymer crystal structures by electron crystallography – isotactic poly(1-butene), form III. Acta Cryst*. B**50**, 201–208.

Dorset, D. L., McCourt, M. P., Tivol, W. F. & Turner, J. N. (1993). *Electron diffraction from phospholipids – an approximate correction for dynamical scattering and tests for a correct phase determination. J. Appl. Cryst*. **26**, 778–786.

Dorset, D. L., Tivol, W. F. & Turner, J. N. (1991). *Electron crystallography at atomic resolution: ab initio structure analysis of copper perchlorophthalocyanine. Ultramicroscopy*, **38**, 41–45.

Dorset, D. L., Tivol, W. F. & Turner, J. N. (1992). *Dynamical scattering and electron crystallography – ab initio structure analysis of copper perbromophthalocyanine. Acta Cryst*. A**48**, 562–568.

Dorset, D. L. & Zemlin, F. (1990). *Direct phase determination in electron crystallography: the crystal structure of an n-paraffin. Ultramicroscopy*, **33**, 227–236.

Dorset, D. L. & Zhang, W. P. (1991). *Electron crystallography at atomic resolution: the structure of the odd-chain paraffin n-tritriacontane. J. Electron Microsc. Tech*. **18**, 142–147.

Dvoryankin, V. F. & Vainshtein, B. K. (1960). *An electron diffraction study of thiourea. Sov. Phys. Crystallogr*. **5**, 564–574.

Dvoryankin, V. F. & Vainshtein, B. K. (1962). *An electron diffraction study of the low-temperature ferroelectric form of thiourea. Sov. Phys. Crystallogr*. **6**, 765–772.

Eades, J. A. (1980). *Another way to form zone axis patterns. Inst. Phys. Conf. Ser*. **52**, 9–12.

Eades, J. A., Shannon, M. D. & Buxton, B. F. (1983). *Crystal symmetry from electron diffraction*. In *Scanning electron microscopy*, 1983/III, pp. 1051–1060. Chicago: SEM Inc.

Erickson, H. P. & Klug, A. (1971). *Measurements and compensation of defocusing and aberrations by Fourier processing of electron micrographs. Philos. Trans. R. Soc. London Ser. B*, **261**, 105–118.

Fan, H. F., Xiang, S. B., Li, F. H., Pan, Q., Uyeda, N. & Fujiyoshi, Y. (1991). *Image resolution enhancement by combining information from electron diffraction pattern and micrograph. Ultramicroscopy*, **36**, 361–365.

Fan, H.-F., Zhong, Z.-Y., Zheng, C.-D. & Li, F.-H. (1985). *Image processing in high-resolution electron microscopy using the direct method. I. Phase extension. Acta Cryst*. A**41**, 163–165.

Frank, J. (1975). *Averaging of low exposure electron micrographs of non-periodic objects. Ultramicroscopy*, **1**, 159–162.

Frank, J. (1980). *The role of correlation techniques in computer image processing*. In *Computer processing of electron microscopy images*, edited by P. W. Hawkes, pp. 187–222. Berlin: Springer-Verlag.

Fraser, H. L., Maher, D. M., Humphreys, C. J., Hetherington, C. J. D., Knoell, R. V. & Bean, J. C. (1985). *The detection of local strains in strained superlattices*. In *Microscopy of semiconducting materials*, pp. 1–5. London: Institute of Physics.

Fryer, J. R. (1993). *Electron crystallography of small organic molecules. Microsc. Soc. Am. Bull*. **23**, 44–56.

Fujimoto, F. (1959). *Dynamical theory of electron diffraction in Laue-case. I. General theory. J. Phys. Soc. Jpn*, **14**(11), 1158–1168.

Fujiwara, K. (1961). *Relativistic dynamical theory of electron diffraction. J. Phys. Soc. Jpn*, **16**, 2226–2238.

Fukuhara, A. (1966). *Many-ray approximations in the dynamical theory of electron diffraction. J. Phys. Soc. Jpn*, **21**, 2645–2662.

Gabor, D. (1949). *Microscopy by reconstructed wavefronts. Proc. R. Soc. London Ser. A*, **197**, 454–487.

Gassmann, J. (1976). *Improvement and extension of approximate phase sets in structure determination*. In *Crystallographic computing techniques*, edited by F. R. Ahmed, pp. 144–154. Copenhagen: Munksgaard.

Gassmann, J. & Zechmeister, K. (1972). *Limits of phase expansion in direct methods. Acta Cryst*. A**28**, 270–280.

Germain, G., Main, P. & Woolfson, M. M. (1971). *The application of phase relationships to complex structures. III. The optimum use of phase relationships. Acta Cryst*. A**27**, 368–376.

Gilbert, P. F. C. (1972*a*). *The reconstruction of a three-dimensional structure from projections and its application to electron microscopy. II. Direct methods. Proc. R. Soc. London Ser. B*, **182**, 89–102.

Gilbert, P. F. C. (1972*b*). *Iterative methods for the three-dimensional reconstruction of an object from projections. J. Theor. Biol*. **36**, 105–117.

Gilmore, C. J., Bricogne, G. & Bannister, C. (1990). *A multisolution method of phase determination by combined maximization of entropy and likelihood. II. Application to small molecules. Acta Cryst*. A**46**, 297–308.

Gilmore, C. J., Shankland, K. & Bricogne, G. (1993). *Applications of the maximum entropy method to powder diffraction and electron crystallography. Proc. R. Soc. London Ser. A*, **442**, 97–111.

Gilmore, C. J., Shankland, K. & Fryer, J. R. (1992). *The application of the maximum entropy method to electron microscopy data for purple membrane. Trans. Am. Crystallogr. Assoc*. **28**, 129–139.

Gilmore, C. J., Shankland, K. & Fryer, J. R. (1993). *Phase extension in electron crystallography using the maximum entropy method and its application to two-dimensional purple membrane data from Halobacterium halobium. Ultramicroscopy*, **49**, 132–146.

Gjønnes, J. & Høier, R. (1971). *The application of non-systematic many-beam dynamic effects to structure-factor determination. Acta Cryst*. A**27**, 313–316.

Gjønnes, J. & Moodie, A. F. (1965). *Extinction conditions in dynamic theory of electron diffraction patterns. Acta Cryst*. **19**, 65–67.

Glauber, R. & Schomaker, V. (1953). *The theory of electron diffraction. Phys. Rev*. **89**, 667–670.

Goncharov, A. B. (1987). *Integral geometry and 3D-reconstruction of arbitrarily oriented identical particles from their electron micrographs. Sov. Phys. Crystallogr*. **32**, 663–666.

Goncharov, A. B., Vainshtein, B. K., Ryskin, A. I. & Vagin, A. A. (1987). *Three-dimensional reconstruction of arbitrarily oriented identical particles from their electron photomicrographs. Sov. Phys. Crystallogr*. **32**, 504–509.

Goodman, P. (1974). *The role of upper layer interactions in electron diffraction. Nature (London)*, **251**, 698–701.

Goodman, P. (1976). *Examination of the graphite structure by CBED. Acta Cryst*. A**32**, 793–798.

Goodman, P. (1984*a*). *A matrix basis for CBED pattern analysis. Acta Cryst*. A**40**, 522–526.

Goodman, P. (1984*b*). *A retabulation of the 80 layer groups for electron diffraction usage. Acta Cryst*. A**40**, 633–642.

Goodman, P., McLean, J. D., Wilson, I. J. & Olsen, A. (1984). *Optical microdiffraction and image analysis of subsymmetries in Nb_2O_5 tunnel structures*. In *Analytical electron microscopy*–1984, pp. 130–134. San Francisco Press.

Goodman, P. & Miller, P. (1993). *Reassessment of the symmetry of the 221 PbBiSrCaCuO structure using LACBED and high-resolution SAD: the relevance of Cowley's theory of disorder scattering to a real-space structural analysis. Ultramicroscopy*, **52**, 549–556.

2.5 (*cont.*)

Goodman, P., Miller, P., White, T. J. & Withers, R. L. (1992). *Symmetry determination and Pb-site ordering analysis for the* $n = 1, 2$ $Pb_xBi_{2-x}Sr_2Ca_{n-1}Cu_nO_{4+2n+\delta}$ *compounds by convergent-beam and selected-area electron diffraction. Acta Cryst.* B**48**, 376–387.

Goodman, P. & Whitfield, H. J. (1980). *The space group determination of GaS and* $Cu_3As_2S_3I$ *by convergent beam electron diffraction. Acta Cryst.* A**36**, 219–228.

Gordon, R. (1974). *A tutorial on ART (algebraic reconstruction techniques). IEEE Trans. Nucl. Sci.* NS-**21**, 78–93.

Gordon, R., Bender, R. & Herman, G. T. (1970). *Algebraic reconstruction techniques (ART) for three-dimensional electron microscopy and X-ray photography. J. Theor. Biol.* **29**, 471–481.

Gordon, R. & Herman, G. T. (1971). *Reconstruction of pictures from their projections. Commun. ACM*, **14**, 759–768.

Grzinic, G. (1985). *Calculation of incommensurate diffraction intensities from disordered crystals. Philos. Mag. A*, **52**, 161–187.

Gunning, J. & Goodman, P. (1992). *Reciprocity in electron diffraction. Acta Cryst.* A**48**, 591–595.

Gurskaya, G. V., Lobanova, G. M. & Vainshtein, B. K. (1971). *X-ray diffraction and electron-microscope study of hexagonal catalase crystal. Sov. Phys. Crystallogr.* **16**, 662–669.

Hashimoto, H., Endoh, H., Tanji, T., Ono, A. & Watanabe, E. (1977). *Direct observation of fine structure within images of atoms in crystals by transmission electron microscopy. J. Phys. Soc. Jpn*, **42**, 1073–1074.

Hashimoto, H., Mannami, M. & Naiki, T. (1961). *Dynamical theory of electron diffraction for the electron microscope image of crystal lattices. I. Image of single crystals. II. Image of superposed crystals (moiré pattern). Philos. Trans. R. Soc. London*, **253**, 459–516.

Hauptman, H. (1972). *Crystal structure determination. The role of the cosine seminvariants*. NY: Plenum Press.

Hauptman, H. (1993). *A minimal principle in X-ray crystallography: starting in a small way. Proc. R. Soc. London Ser. A*, **442**, 3–12.

Hauptman, H. & Karle, J. (1953). *Solution of the phase problem. I. The centrosymmetric crystal*. American Crystallographic Association Monograph No. 3. Ann Arbor, MI: Edwards Brothers.

Havelka, W., Henderson, R., Heymann, J. A. W. & Oesterhelt, D. (1993). *Projection structure of halorhodopsin from Halobacterium halobium at 6 Å resolution obtained by electron cryomicroscopy. J. Mol. Biol.* **234**, 837–846.

Henderson, R., Baldwin, J. M., Ceska, T. A., Zemlin, F., Beckmann, E. & Downing, K. H. (1990). *Model for the structure of bacteriorhodopsin based on high-resolution electron cryomicroscopy. J. Mol. Biol.* **213**, 899–929.

Henderson, R., Baldwin, J. M., Downing, K. H., Lepault, J. & Zemlin, F. (1986). *Structure of purple membrane from Halobacterium halobium: recording, measurement and evaluation of electron micrographs at 3.5 Å resolution. Ultramicroscopy*, **19**, 147–178.

Henderson, R. & Unwin, P. N. T. (1975). *Three-dimensional model of purple membrane obtained by electron microscopy. Nature (London)*, **257**, 28–32.

Herman, G. T. (1980). *Image reconstruction from projection: the fundamentals of computerized tomography*. New York: Academic Press.

Herrmann, K. H., Krahl, D. & Rust, H.-P. (1980). *Low-dose image recording by TV techniques*. In *Electron microscopy at molecular dimensions*, edited by W. Baumeister & W. Vogell, pp. 186–193. Berlin: Springer-Verlag.

Hirsch, P. B., Howie, A., Nicholson, R. B., Pashley, D. W. & Whelan, M. J. (1965). *Electron microscopy of thin crystals*. London: Butterworths.

Hoppe, W. (1971). *Use of zone correction plate and other techniques for structure determination of aperiodic objects at atomic resolution using a conventional electron microscope. Philos. Trans. R. Soc. London Ser. B*, **261**, 71–94.

Hoppe, W., Bussler, P., Feltynowski, A., Hunsmann, N. & Hirt, A. (1973). *Some experience with computerized image reconstruction methods*. In *Image processing and computer-aided design in electron optics*, edited by R. W. Hawkes, pp. 92–126. London: Academic Press.

Hoppe, W. & Gassmann, J. (1968). *Phase correction, a new method to solve partially known structures. Acta Cryst.* B**24**, 97–107.

Hoppe, W. & Typke, D. (1979). *Three-dimensional reconstruction of aperiodic objects in electron microscopy*. In *Advances in structure research by diffraction method*. Oxford: Pergamon Press.

Horstmann, M. & Meyer, G. (1965). *Messung der Elektronenbeugungsintensitaten polykristalliner Aluminium schichten bei tiefer Temperatur und Vergleich mit der dynamischen Theorie. Z. Phys.* **182**, 380–397.

Hovmöller, S., Sjögren, A., Farrants, G., Sundberg, M. & Marinder, B. O. (1984). *Accurate atomic positions from electron microscopy. Nature (London)*, **311**, 238–241.

Hu, H. H., Li, F. H. & Fan, H. F. (1992). *Crystal structure determination of* $K_2O \cdot 7Nb_2O_5$ *by combining high resolution electron microscopy and electron diffraction. Ultramicroscopy*, **41**, 387–397.

Hurley, A. C. & Moodie, A. F. (1980). *The inversion of three-beam intensities for scalar scattering by a general centrosymmetric crystal. Acta Cryst.* A**36**, 737–738.

International Tables for Crystallography (1995). Vol. A. *Space-group symmetry*, edited by Th. Hahn, 4th ed. Dordrecht: Kluwer Academic Publishers.

International Tables for Crystallography (1999). Vol. C. *Mathematical, physical and chemical tables*, edited by A. J. C. Wilson and E. Prince, 2nd ed. Dordrecht: Kluwer Academic Publishers.

International Tables for X-ray Crystallography (1952). Vol. I. *Symmetry groups*. Birmingham: Kynoch Press. (Present distributor Kluwer Academic Publishers, Dordrecht.)

Ishizuka, K., Miyazaki, M. & Uyeda, N. (1982). *Improvement of electron microscope images by the direct phasing method. Acta Cryst.* A**38**, 408–413.

Ishizuka, K. & Taftø, J. (1982). *Kinematically allowed reflections caused by scattering via HOLZ. Proc. Electron Microsc. Soc. Am.* pp. 688–689.

Jap, B. K. & Glaeser, R. M. (1980). *The scattering of high-energy electrons. II. Quantitative validity domains of the single-scattering approximations for organic crystals. Acta Cryst.* A**36**, 57–67.

Jap, B. K., Walian, P. J. & Gehring, K. (1991). *Structural architecture of an outer membrane channel as determined by electron crystallography. Nature (London)*, **350**, 167–170.

Johnson, A. W. S. (1972). *Stacking faults in graphite. Acta Cryst.* A**28**, 89–93.

Johnson, A. W. S. & Preston, A. R. (1994). *Some notes on the selection of structural chirality by CBED. Ultramicroscopy*, **55**, 348–355.

Jones, P. M., Rackham, G. M. & Steeds, J. W. (1977). *Higher order Laue zone effects in electron diffraction and their use in lattice parameter determination. Proc. R. Soc. London Ser. A*, **354**, 197–222.

Kam, Z. (1980). *Three-dimensional reconstruction of aperiodic objects. J. Theor. Biol.* **82**, 15–32.

Kambe, K. (1982). *Visualization of Bloch waves of high energy electrons in high resolution electron microscopy. Ultramicroscopy*, **10**, 223–228.

Karle, J. & Hauptman, H. (1956). *A theory of phase determination for the four types of non-centrosymmetric space groups* 1*P*222, 2*P*22, $3P_12$, $3P_22$. *Acta Cryst.* **9**, 635–651.

Kirkland, E. J., Siegel, B. M., Uyeda, N. & Fujiyoshi, Y. (1980). *Digital reconstruction of bright field phase contrast images from high resolution electron micrographs. Ultramicroscopy*, **5**, 479–503.

Kiselev, N. A., Lerner, F. Ya. & Livanova, N. B. (1971). *Electron microscopy of muscle phosphorylase B. J. Mol. Biol.* **62**, 537–549.

Klug, A. & Berger, J. E. (1964). *An optical method for the analysis of periodicities in electron micrographs and some observations on the mechanism of negative staining. J. Mol. Biol.* **10**, 565–569.

2.5 (*cont.*)

Klug, A. & DeRosier, D. J. (1966). *Optical filtering of electron micrographs: reconstruction of one-sided images. Nature (London)*, **212**, 29–32.

Kossel, W. & Möllenstedt, G. (1938). *Electron interference in a convergent beam. Nature (London)*, **26**, 660.

Kosykh, V. P., Pustovskikh, A. I., Kirichuk, V. S., Kühne, T., Orlova, E. V., Tsuprun, V. L. & Kiselev, N. A. (1983). *Use of digital storage methods to recover images of monocrystalline layers of virus particles. Sov. Phys. Crystallogr.* **28**, 637–643.

Kühlbrandt, W., Wang, D. N. & Fujiyoshi, Y. (1994). *Atomic model of plant light-harvesting complex by electron crystallography. Nature (London)*, **367**, 614–621.

Kuwabara, S. (1978). *Nearly aberration-free crystal images in high voltage electron microscopy. J. Electron Microsc.* **27**, 161–169.

Langer, R., Frank, J., Feltynowski, A. & Hoppe, W. (1970). *Anwendung des Bilddifferenzverfahrens auf die Untersuchung von Strukturänderungen dünner Kohlefolien bei Elektronenbestrahlung. Ber. Bunsenges Phys. Chem.* **74**(11), 1120–1126.

Langs, D. A. & DeTitta, G. T. (1975). *A flexible and rapid phase determination and refinement procedure. Acta Cryst.* A**31**, S16.

Laue, M. von (1935). *Die Fluoreszenzrontgenstrahlung von Einkristallen. Ann. Phys. (Leipzig)*, **23**, 703–726.

Li, D. X. & Hovmöller, S. (1988). *The crystal structure of $Na_3Nb_{12}O_{31}F$ determined by HREM and image processing. J. Solid State Chem.* **73**, 5–10.

Li, F. H. (1991). *Crystal structures from high-resolution electron microscopy*. In *Electron crystallography of organic molecules*, edited by J. R. Fryer & D. L. Dorset, pp. 153–167. Dordrecht: Kluwer Academic Publishers.

Liebman, G. (1955). *A unified representation of magnetic electron lens properties. Proc. Phys. Soc. London Sect. B*, **68**, 737–745.

Liu, Y.-W., Fan, H.-F. & Zheng, C.-D. (1988). *Image processing in high-resolution electron microscopy using the direct method. III. Structure-factor extrapolation. Acta Cryst.* A**44**, 61–63.

Lobachev, A. N. & Vainshtein, B. K. (1961). *An electron diffraction study of urea. Sov. Phys. Crystallogr.* **6**, 313–317.

Lynch, D. F. & Moodie, A. F. (1972). *Numerical evaluation of low energy electron diffraction intensity. I. The perfect crystal with no upper layer lines and no absorption. Surf. Sci.* **32**, 422–438.

Lynch, D. F., Moodie, A. F. & O'Keefe, M. A. (1975). *n-Beam lattice images. V. The use of the charge-density approximation in the interpretation of lattice images. Acta Cryst.* A**31**, 300–307.

McLachlan, D. (1958). *Crystal structure and information theory. Proc. Natl Acad. Sci. USA*, **44**, 948–956.

Mansfield, J. (1984). *Convergent beam electron diffraction of alloy phases by the Bristol Group under the direction of John Steeds*. Bristol: Adam Hilger.

Markham, R., Frey, S. & Hills, G. J. (1963). *Methods for the enhancement of image detail and accentuation of structure in electron microscopy. Virology*, **20**, 88–102.

Matsuda, T., Tonomura, A. & Komada, T. (1978). *Observation of lattice images with a field emission electron microscope. Jpn. J. Appl. Phys.* **17**, 2073–2074.

Mermin, N. D. (1992). *The space groups of icosahedral quasicrystals and cubic, orthorhombic, monoclinic and triclinic crystals. Rev. Mod. Phys.* **64**, 3–49.

Mersereau, R. M. & Oppenheim, A. V. (1974). *Digital reconstruction of multi-dimensional signals from their projections. Proc. IEEE*, **62**(10), 1319–1338.

Miyake, S. & Uyeda, R. (1950). *An exception to Friedel's law in electron diffraction. Acta Cryst.* **3**, 314.

Mo, Y. D., Cheng, T. Z., Fan, H. F., Li, J. Q., Sha, B. D., Zheng, C. D., Li, F. H. & Zhao, Z. X. (1992). *Structural features of the incommensurate modulation in the Pb-doped Bi-2223 high-T_c phase by defect method electron diffraction analysis. Supercond. Sci. Technol.* **5**, 69–72.

Moodie, A. F. (1965). *Some structural implications of n-beam interactions*. International Conference on Electron Diffraction and Crystal Defects, Melbourne, Australia, paper ID-1.

Moodie, A. F. (1972). *Reciprocity and shape function in multiple scattering diagrams. Z. Naturforsch. Teil A*, **27**, 437–440.

Moodie, A. F. & Whitfield, H. J. (1984). *CBED and HREM in the electron microscope. Ultramicroscopy*, **13**, 265–278.

Moss, B. & Dorset, D. L. (1982). *Effect of crystal bending on direct phasing of electron diffraction data from cytosine. Acta Cryst.* A**38**, 207–211.

Ogawa, T., Moriguchi, S., Isoda, S. & Kobayashi, T. (1994). *Application of an imaging plate to electron crystallography at atomic resolution. Polymer*, **35**, 1132–1136.

Orlov, S. S. (1975). *Theory of three-dimensional reconstruction. II. The recovery operator. Sov. Phys. Crystallogr.* **20**, 429–433.

Ottensmeyer, F. P., Andrews, J. W., Basett-Jones, D. P., Chan, A. S. & Hewitt, J. (1977). *Signal to noise enhancement in dark field electron micrographs of vasopressin: filtering of arrays of images in reciprocal space. J. Microsc.* **109**, 256–268.

Pan, M. & Crozier, P. A. (1993). *Quantitative imaging and diffraction of zeolites using a slow-scan CCD camera. Ultramicroscopy*, **52**, 487–498.

Pérez, S. & Chanzy, H. (1989). *Electron crystallography of linear polysaccharides. J. Electron Microsc. Tech.* **11**, 280–285.

Picture Processing and Digital Filtering (1975). Edited by T. S. Huang. Berlin: Springer-Verlag.

Pinsker, Z. G. (1953). *Electron diffraction*. London: Butterworth.

Pinsker, Z. G., Zvyagin, B. B. & Imamov, R. M. (1981). *Principal results of electron-diffraction structural investigations. Sov. Phys. Crystallogr.* **26**, 669–674.

Pogany, A. P. & Turner, P. S. (1968). *Reciprocity in electron diffraction and microscopy. Acta Cryst.* A**24**, 103–109.

Pond, R. C. & Vlachavas, D. S. (1983). *Bicrystallography. Proc. R. Soc. London Ser. A*, **386**, 95–143.

Portier, R. & Gratias, D. (1981). *Diffraction symmetries for elastic scattering*. In *Electron microscopy and analysis. Inst. Phys. Conf. Ser.* No. 61, pp. 275–278. Bristol, London: Institute of Physics.

Radermacher, M., McEwen, B. & Frank, J. (1987). *Three-dimensional reconstruction of asymmetrical object in standard and high voltage electron microscopy*. Proc. Microscop. Soc. Canada, XII Annual Meet., pp. 4–5.

Radi, G. (1970). *Complex lattice potentials in electron diffraction calculated for a number of crystals. Acta Cryst.* A**26**, 41–56.

Radon, J. (1917). *Über die Bestimmung von Funktionen durch ihre Integralwerte längs gewisser Mannigfaltigkeiten. (On the determination of functions from their integrals along certain manifolds). Ber. Verh. Saechs. Akad. Wiss. Leipzig Math. Phys. Kl.* **69**, 262–277.

Ramachandran, G. N. & Lakshminarayanan, A. V. (1971). *Three-dimensional reconstruction from radiographs and electron micrographs: application of convolutions instead of Fourier transforms. Proc. Natl Acad. Sci. USA*, **68**(9), 2236–2240.

Revol, J. F. (1991). *Electron crystallography of radiation-sensitive polymer crystals*. In *Electron crystallography of organic molecules*, edited by J. R. Fryer & D. L. Dorset, pp. 169–187. Dordrecht: Kluwer Academic Publishers.

Revol, J. F. & Manley, R. St. J. (1986). *Lattice imaging in polyethylene single crystals. J. Mater. Sci. Lett.* **5**, 249–251.

Rez, P. (1978). In *Electron diffraction 1927–1977*, edited by P. J. Dobson, J. B. Pendry & C. J. Humphreys, pp. 61–67. *Inst. Phys. Conf. Ser.* No. 41. Bristol, London: Institute of Physics.

Rozenfeld, A. (1969). *Picture processing by computer*. New York: Academic Press.

Sayre, D. (1952). *The squaring method: a new method for phase determination. Acta Cryst.* **5**, 60–65.

Sayre, D. (1980). *Phase extension and refinement using convolutional and related equation systems*. In *Theory and practice of direct methods in crystallography*, edited by M. F. C. Ladd & R. A. Palmer, pp. 271–286. NY: Plenum Press.

Scaringe, R. P. (1992). *Crystallography in two dimensions: comparison of theory and experiment for molecular layers. Trans. Am. Crystallogr. Assoc.* **28**, 11–23.

Schapink, F. W., Forgany, S. K. E. & Buxton, B. F. (1983). *The symmetry of convergent-beam electron diffraction patterns from bicrystals. Acta Cryst.* A**39**, 805–813.

2.5 (*cont.*)

Scherzer, O. (1949). *The theoretical resolution limit of the electron microscope. J. Appl. Phys*. **20**, 20–29.

Schiske, P. (1968). *Zur Frage der Bildrekonstruktion durch Fokusreihen*. 1 *Y Eur. Reg. Conf. Electron Microsc. Rome*, **1**, 145–146.

Schwartzman, A., Goodman, P. & Johnson, A. W. S. (1996). IUCr XVII Congress and General Assembly, Seattle, Washington, USA, August 8–16, Collected Abstracts, p. C-54, Abstract PS02.03.18.

Sha, B.-D., Fan, H.-F. & Li, F.-H. (1993). *Correction for the dynamical electron diffraction effect in crystal structure analysis. Acta Cryst*. A**49**, 877–880.

Shechtman, D., Blech, I., Gratias, D. & Cahn, J. W. (1984). *Metallic phase with long-range orientational order and no translational symmetry. Phys. Rev. Lett*. **53**, 1951–1953.

Shoemaker, V. & Glauber, R. (1952). *The Born approximation in electron diffraction. Nature (London)*, **170**, 290–291.

Spence, J. C. H., O'Keefe, M. A. & Kolar, H. (1977). *Image interpretation in crystalline germanium. Optik (Stuttgart)*, **49**, 307–323.

Spence, J. C. H. & Zuo, J. M. (1992). *Electron microdiffraction*. New York: Plenum Press.

Steeds, J. W. (1979). *Convergent beam electron diffraction*. In *Introduction to analytical electron microscopy*, edited by J. J. Hren, J. I. Goldstein & D. C. Joy, pp. 387–422. New York: Plenum.

Steeds, J. W. (1983). *Developments in convergent beam electron diffraction*. Report to the Commission on Electron Diffraction of the International Union of Crystallography.

Steeds, J. W. & Evans, N. S. (1980). *Practical examples of point and space group determination in convergent beam diffraction. Proc. Electron Microsc. Soc. Am*. pp. 188–191.

Steeds, J. W., Rackham, G. M. & Shannon, M. D. (1978). *On the observation of dynamically forbidden lines in two and three dimensional electron diffraction*. In *Electron diffraction 1927–1977. Inst. Phys. Conf. Ser*. No. 41, pp. 135–139.

Steeds, J. W. & Vincent, R. (1983). *Use of high symmetry zone axes in electron diffraction in determining crystal point and space groups. J. Appl. Cryst*. **16**, 317–324.

Steinkilberg, M. & Schramm, H. J. (1980). *Eine verbesserte Drehkorrelations Methode für die Strukturbestimmung biologischer Macromoleküle durch Mittelung elektronen-mikroskopischer Bilder. Hoppe–Seyler's Z. Physiol. Chem*. **361**, 1363–1369.

Stereochemical Applications of Gas-Phase Electron Diffraction (1988). Part A, edited by I. Hargittai & M. Hargittai. New York: VCH.

Tanaka, M. (1994). *Convergent-beam electron diffraction. Acta Cryst*. A**50**, 261–286.

Tanaka, M., Saito, P., Ueno, K. & Harada, Y. (1980). *Large angle convergent-beam electron diffraction. J. Electron. Microsc*. **29**, 408–412.

Tanaka, M., Sekii, H. & Nagasawa, T. (1983). *Space group determination by dynamic extinction in convergent beam electron diffraction. Acta Cryst*. A**39**, 825–837.

Tanaka, M. & Terauchi, M. (1985). *Convergent-beam electron diffraction*. Tokyo: JEOL Ltd.

Tanaka, M., Terauchi, M. & Tsuda, K. (1994). *Convergent-beam electron diffraction III*. Tokyo: JEOL–Maruzen.

Thon, F. (1966). *On the defocusing dependence of phase contrast in electron microscopical images. Z. Naturforsch. Teil A*, **21**, 476–478.

Tivol, W. F., Dorset, D. L., McCourt, M. P. & Turner, J. N. (1993). *Voltage-dependent effect on dynamical scattering and the electron diffraction structure analysis of organic crystals: copper perchlorophthalocyanine. Microsc. Soc. Am. Bull*. **23**, 91–98.

Tournaire, M. (1962). *Recent developments of the matrical and semi-reciprocal formulation in the field of dynamical theory. J. Phys. Soc. Jpn*, **17**, Suppl. B11, 98–100.

Tsipursky, S. I. & Drits, V. A. (1977). *Efficiency of electronometric intensity registration at electron diffraction structural studies. Izv. Akad. Nauk SSSR Ser. Fiz*. **41**, 2263–2271. (In Russian.)

Tsuji, M. (1989). *Electron microscopy*. In *Comprehensive polymer science*, Vol. 1. *Polymer characterization*, edited by C. Booth & C. Price, pp. 785–840. Oxford: Pergamon Press

Turner, P. S. & Cowley, J. M. (1969). *The effects of n-beam dynamical diffraction on electron diffraction intensities from polycrystalline materials. Acta Cryst*. A**25**, 475–481.

Unwin, P. N. T. & Henderson, R. (1975). *Molecular structure determination by electron microscopy of unstained crystalline specimens. J. Mol. Biol*. **94**, 425–440.

Uyeda, N., Kobayashi, T., Ishizuka, K. & Fujiyoshi, Y. (1978–1979). *High voltage electron microscopy for image discrimination of constituent atoms in crystals and molecules. Chem. Scr*. **14**, 47–61.

Vainshtein, B. K. (1952). *Dependence of electron scattering on the atomic number. Dokl. Akad. Nauk SSSR*, **85**, 1239–1242. (In Russian.)

Vainshtein, B. K. (1954). *On the studies of crystal lattice potential by electron diffraction. Tr. Inst. Krist. Akad. Nauk SSSR*, **9**, 259–276. (In Russian.)

Vainshtein, B. K. (1955). *Elektronograficheskoe issledovanie diketopiperazina. Zh. Fiz. Khim*. **29**, 327–344.

Vainshtein, B. K. (1956). *Structure analysis by electron diffraction*. Moscow: Akad. Sci. USSR. [English edition (1964): Oxford: Pergamon Press.]

Vainshtein, B. K. (1964). *Structure analysis by electron diffraction*. Oxford: Pergamon Press.

Vainshtein, B. K. (1971*a*). *The synthesis of projecting functions. Sov. Phys. Dokl*. **16**, 66–69.

Vainshtein, B. K. (1971*b*). *Finding the structure of objects from projections. Sov. Phys. Crystallogr*. **15**, 781–787.

Vainshtein, B. K. (1978). *Electron microscopical analysis of the three-dimensional structure of biological macromolecules*. In *Advances in optical and electron microscopy*, Vol. 7, edited by V. E. Cosslett & R. Barer, pp. 281–377. London: Academic Press.

Vainshtein, B. K., Barynin, V. V. & Gurskaya, G. V. (1968). *The hexagonal crystalline structure of catalase and its molecular structure. Sov. Phys. Dokl*. **13**, 838–841.

Vainshtein, B. K., D'yakon, I. A. & Ablov, A. V. (1971). *Electron diffraction determination of the structure of copper* DL*-alaninate. Sov. Phys. Dokl*. **15**, 645–647.

Vainshtein, B. K. & Goncharov, A. B. (1986*a*). *Determination of the spatial orientation of arbitrarily arranged identical particles of unknown structure from their projections. Sov. Phys. Dokl*. **287**, 278–283; (1986*b*). Proceedings of the 11th International Congress on Electron Microscopy, Kyoto, Vol. 1, pp. 459–460.

Vainshtein, B. K. & Klechkovskaya, V. V. (1993). *Electron diffraction by Langmuir–Blodgett films. Proc. R. Soc. London Ser. A*, **442**, 73–84.

Vainshtein, B. K. & Orlov, S. S. (1972). *Theory of the recovery of functions from their projections. Sov. Phys. Crystallogr*. **17**, 213–216.

Vainshtein, B. K. & Orlov, S. S. (1974). *General theory of direct 3D reconstruction*. Proceedings of International Workshop, Brookhaven National Laboratory, pp. 158–164.

Van Heel, M. (1984). *Multivariate statistical classification of noisy images (randomly oriented biological macromolecules). Ultramicroscopy*, **13**, 165–184.

Vilkov, L. V., Mastryukov, V. S. & Sadova, N. I. (1978). *Determination of geometrical structure of free molecules*. Leningrad: Khimiya. (In Russian.)

Vincent, R. & Exelby, D. R. (1991). *Structure of metastable Al–Ge phases determined from HOLZ Patterson transforms. Philos. Mag. Lett*. **63**, 31–38.

Vincent, R. & Exelby, D. R. (1993). *Structure of a metastable Al–Ge phase determined from large angle CBED patterns. Philos. Mag. B*, **68**, 513–528.

Vincent, R. & Midgley, P. A. (1994). *Double conical beam rocking system for measurement of integrated electron diffraction intensities. Ultramicroscopy*, **53**, 271–282.

2.5 (*cont.*)

Voronova, A. A. & Vainshtein, B. K. (1958). *An electron diffraction study of $CuCl_2 \cdot 3Cu(OH)_2$. Sov. Phys. Crystallogr.* **3**, 445–451.

Watanabe, D., Uyeda, R. & Kogiso, M. (1968). *An apparent variation of structure factors for electrons with accelerating voltage. An observation through Kikuchi patterns. Acta Cryst.* A**24**, 249–250.

Wenk, H.-R., Downing, K. H., Ho, M.-S. & O'Keefe, M. A. (1992). *3D structure determination from electron-microscope images: electron crystallography of staurolite. Acta Cryst.* A**48**, 700–716.

Wilson, A. J. C. (1949). *The probability distribution of X-ray intensities. Acta Cryst.* **2**, 318–321.

Withers, R. L., Schmid, S. & Thompson, J. G. (1993). *A composite modulated structure approach to the lanthanide oxide fluoride, uranium nitride fluoride and zirconium nitride fluoride solid-solution fields. Acta Cryst.* B**49**, 941–951.

Wolff, P. M. de, Janssen, T. & Janner, A. (1981). *The superspace groups for incommensurate crystal structures with a one-dimensional modulation. Acta Cryst.* A**37**, 625–636.

Xiang, S.-B., Fan, H.-F., Wu, X.-J., Li, F.-H. & Pan, Q. (1990). *Direct methods in superspace. II. The first application to an unknown incommensurate modulated structure. Acta Cryst.* A**46**, 929–934.

Yao, J.-X. (1981). *On the application of phase relationships to complex structures. XVIII. RANTAN – random MULTAN. Acta Cryst.* A**37**, 642–644.

Zemlin, F., Reuber, E., Beckmann, E., Zeitler, E. & Dorset, D. L. (1985). *Molecular resolution electron micrographs of monolamellar paraffin crystal. Science*, **229**, 461–462.

Zhukhlistov, A. P., Avilov, A. S., Ferraris, G., Zvyagin, B. B. & Plotnikov, V. P. (1997). *Statistical distribution of hydrogen over three positions in the brucite $Mg(OH)_2$ structure from electron diffractometry data. Crystallogr. Rep.* **42**, 774–777.

Zhukhlistov, A. P. & Zvyagin, B. B. (1998). *Crystal structure of lizardite 1T from electron diffractometry data. Crystallogr. Rep.* **43**, 950–955.

Zuo, J. M., Gjønnes, K. & Spence, J. C. H. (1989). *A FORTRAN source listing for simulating three-dimensional CBED patterns with absorption by the Bloch wave method. J. Electron Microsc. Tech.* **12**, 29–55.

Zvyagin, B. B. (1967). *Electron-diffraction analysis of clay mineral structures*. New York: Plenum.

Zvyagin, B. B., Vrublevskaya, Z. V., Zhukhlistov, A. P., Sidorenko, S. V., Soboleva, A. F. & Fedotov, A. F. (1979). *High-voltage electron diffraction investigations of layered minerals*. Moscow: Nauka. (In Russian).

Zvyagin, B. B., Zhukhlistov, A. P. & Plotnikov, A. P. (1996). *Development of the electron diffractometry of minerals. Structural studies of crystals*. (Coll. Works 75th Anniversary Acad. B. K. Vainshtein.) *Nauka-Physmathlit*, pp. 225–234. (In Russian.)